AN INTERMEDIATE-COUPLING EXPANSION FOR HAMILTONIAN LATTICE GAUGE THEORY

A thesis
submitted in partial fulfilment
of the requirements for the degree
of
Doctor of Philosophy in Physics
in the
University of Canterbury

by

N. I. Churcher

University of Canterbury
November 1982

ABSTRACT

An intermediate-coupling expansion for the Hamiltonian formulation of lattice gauge theory without matter fields is developed. The expansion is an alternative to the conventional strong-coupling methods and is applicable to both finite and continuous gauge groups. The set of plaquettes of the lattice contains two complementary subsets, which are identified as even and odd plaquettes. In (2+1)-dimensions they are like the black and white squares of a chess board. The even plaquettes include all the links of the lattice and thus all the degrees of freedom. A zero-order Hamiltonian, written in terms of operators which act on single even plaquette states, is defined. It includes both the link terms and the even plaquette terms of the Kogut-Susskind Hamiltonian, and thus all the degrees of freedom, and is separated into terms involving independent even plaquette states. The odd plaquette terms, which are also written in terms of even plaquette operators, are treated as a perturbation. The vacuum energy density, mass gap and string tension of the (2+1)-dimensional Z(2) lattice gauge theory are calculated as an illustration of the expansion. Results are obtained which compare favourably with those of the corresponding strong-coupling expansions. A diagrammatic method for the enumeration and evaluation of the terms of the expansion is presented and a computer program based on this scheme is discussed. A class of models with inhomogeneous coupling strengths is introduced. These models provide a valuable tool for the study of the phase diagram of the homogeneous-coupling model, onto which they may be mapped smoothly. Several applications and extensions are considered.

ACKNOWLEDGEMENTS

This work is dedicated to my parents, for their support, encouragement and understanding. I would like to thank my supervisor, Dr. W.R. Moreau, whose conscientiousness and dogged tenacity in the face of adversity knew no bounds. His courage in introducing the study of lattice gauge theory to the University of Canterbury is to be admired: without it this work would not have been possible. I am grateful to Chris Tomblin for the use of his plotting routines and, together with Mike Reid, for advice on computing. Thanks are also due to Alec Ford, Peter Horn, Bernard Salmon and S.M.G. for getting me through 1977-78. I would like to thank Mesdames J. Warburton and M.E. Boswell for the speed and precision with which they typed this manuscript, the staff of the Physical Sciences Library for their helpfulness (and all those Nucl. Phys. B. interloans!), and my family and friends. Special mention must be made of Mr. and Mrs. W.T. Newburgh, two of the liveliest pensioners I know, for welcoming me into their family and for the hand of their daughter. Finally, thanks to Clare for her love, and all she has done to speed the conclusion of this work.

Partial List of Printing Errors

Page number	Correction
18	eq. 2-24b $\delta_{1,N} \rightarrow \delta_{j,N}$
26	8,3 element of $h_0(\lambda)$ should be 0
37	Table 2-5 energy of γ_{16} is $\sqrt{\lambda^2+16}$
41	Table 2-7b 16,2 element $\rightarrow$ 0, 16,3 element $\rightarrow \rho_+$
52	eq 3-5 RHS 2nd line $\delta_{\underline{p},\underline{m}+\nu} \rightarrow \delta_{\underline{p},\underline{m}+\mu}$
	eq 3-6 RHS 2nd line $-(N-4)\sqrt{\lambda^2+16} - 4\sqrt{\lambda^2+4}$
57	eq 3-11 summations on plaquette indices run from 1 to 16 not 0 to 16
	- see also eq 3-14 etc.
58	eq 3-15 $+ (\varepsilon_a + \varepsilon_b + \varepsilon_c + \varepsilon_d)$
	eq 3-17 $- (\varepsilon_a + \varepsilon_b + \varepsilon_c + \varepsilon_d)$
	(this correction is made in eq. 3-29)
59	eq 32 is not a condition.
p.67	line 3 Fig. 3.5b
78	X is not a subscript
83	Table 3.2 (i) 3rd row L column last factor should be $(L^2 + 4L + 5)$
	(ii) the entries in the k column should be 1,3,5 to correspond with Table 3.1
103	3rd line from bottom dependent $\rightarrow$ independent.
111	following eq 5-2 surely $\lim_{\lambda \rightarrow 0}$ is meant.
128	eq 5-36 LHS the third sum on $\underline{n}$ should not be there.
	There seems to be some confusion between H and H'.

CONTENTS

LIST OF TABLES

CHAPTER 1

INTRODUCTION

Much effort has been devoted in recent years to the study of quantum chromodynamics (Fritzsch et al. 1974, Marciano and Pagels, 1978), commonly referred to as QCD, which is the only currently viable theory of hadron structure (Fritzsch, 1981). The Lagrangian density for this theory is written, in terms of an octet of gauge fields A_μ^α: $\alpha = 1, \ldots 8$ and a (currently unknown) number of "flavours" of coloured quarks q, as

$$L = -\tfrac{1}{4} F_{\mu\nu}^{\alpha} F_{\alpha}^{\mu\nu} + \bar{q}\gamma_\mu(i\partial_\mu + gA_\mu^\alpha \frac{\lambda^\alpha}{2})q + \bar{q}Mq \quad , \qquad (1.1)$$

where

$$F_{\mu\nu}^{\alpha} = \partial_\mu A_\nu^\alpha - \partial_\nu A_\mu^\alpha + gf^{\alpha\beta\gamma} A_\mu^\beta A_\nu^\gamma \qquad (1.2)$$

and M is a mass matrix which is exactly colour invariant but not flavour invariant. There are three colours (and three anti-colours) and the colour symmetry is that of the group SU(3) whose generators, in the quark representation, are the $\frac{\lambda^\alpha}{2}$ and whose structure constants are the $f^{\alpha\beta\gamma}$. The exact flavour symmetry is not known but is approximated in calculations involving a finite number of flavours.

The coupling constant of the theory is denoted by g. As in the case of quantum electrodynamics (QED) the strength of the coupling depends on the length (momentum) scale of the theory. This dependence may be studied by renormalization group techniques (e.g. Wilson and Kogut 1974, Kadanoff 1977).

One of the features of QCD is that the interactions of the quarks become weak at small distances (large momenta). This is called "asymptotic freedom" (e.g. Politzer, 1974). However at large distances (small momenta) the coupling strength increases and the quarks become more tightly bound. This phenomenon, known as "infra-red slavery" or "confinement", is thought to be responsible for the failure of experiments designed to observe free quarks (Marinelli and Morpurgo, 1982).

In order to decide the fundamental question of confinement, which is essential for the success of QCD, or to calculate the properties of hadrons it is necessary to probe the large distance (small momentum) region. It must be shown that the theory does not undergo a transition from a confining phase to a non-confining phase as the distance scale increases. The theory differs significantly from its near relation QED. The perturbative methods which were so successful in the latter case are applicable only to the small distance region of QCD, where they have been used to study the deep inelastic scattering of quarks inside hadrons (e.g. Close 1976, Ellis 1977). New methods, such as the 1/N expansion ('t Hooft 1974) and non-perturbative "instanton" methods (Callan et al. 1978), have been developed in attempts to overcome this difficulty (e.g. Bander, 1981). The problem is extremely complicated and the desired results have not yet been obtained. It is currently believed (e.g. Hasenfratz, 1982) that non-perturbative effects are important even in the small distance region.

Another approach is to try to solve the problem on a discrete space-time lattice, which automatically provides a distance scale (momentum cutoff). Simply replacing the integrals and differentials of the theory by sums and differences spoils its covariance and gauge invariance properties. Lattice field theories of this type have been studied (e.g. Schiff, 1953). In a pioneering paper 1982 Nobel Laureate K.G. Wilson (1974) showed how gauge invariant field theories could be formulated on a space-time lattice. The Russian physicist A.M. Polyakov, in an unpublished work, independently discovered what is now known as lattice gauge theory. A Hamiltonian formulation of the theory was developed almost immediately by Kogut and Susskind (1975).

Although the smooth recovery of continuum physics as the lattice spacing is reduced to zero has not been rigorously established it has become clear that lattice gauge theory provides a practical method for the calculation of the quantities of interest. In addition to perturbation methods based on the weak-coupling (small distance) region, strong-coupling expansions may be performed about the $g^{-1} \to 0$ limit. Although the subject is comparatively recent a number of comprehensive reviews exist. These include those of Kogut (1976), (1979b), Susskind (1976), (1977), Hamer (1982), Drouffe and Itzykson (1978) and Weinstein (1977).

The formulation of the problem on a lattice makes possible comparisons between statistical mechanics and

(Euclidean) field theory. Some of the observed correspondences (e.g. Hamer 1982, Itzykson 1976) are shown in table 1.1.

Statistical Mechanics	Euclidean Field Theory
Partition function	Path integral
Configuration energy x $\frac{1}{kT}$	Action x $1/\hbar$
Free energy density	Vacuum energy density (generating functional for connected Green's functions)
Correlation function	Propagator
(Correlation length)$^{-1}$	Mass gap

Table 1.1: Some correspondences between statistical mechanics and Euclidean field theory.

The advantages of these correspondences are numerous. Many of the techniques of statistical mechanics (Domb and Green 1972-), such as high and low temperature expansions, Monte Carlo simulations and the renormalization group, are immediately applicable (e.g. Kogut 1979b). Many lattice gauge theories may be related to statistical mechanical spin systems by the principle of geometrical duality (Wegner, 1971), while others are self-dual. The phase structure of many spin systems has been extensively studied

and precise values for their transition temperatures and critical indices have been obtained in many cases (e.g. Fisher 1967).

Theories with gauge groups Z(N) are of particular interest since these groups are the centres of the groups SU(N) which appear in QCD. It is believed (e.g. 't Hooft 1978, Mack 1980) that the phase structure of the SU(N) groups is determined by their Z(N) centres. The Z(N) groups are among the simplest of all groups and in some cases exact solutions are available. Predictions of their behaviour are testable by "experimental" methods such as Monte Carlo simulations or the study of materials.

Lattice gauge theory has been applied to a wide range of problems, with considerable success. Attempts have been made to calculate particle masses (e.g. Kogut et al., 1976, Banks et al. 1977) and modern ideas, such as the 1/N expansion (e.g. Kogut et al. 1980) and super-symmetry (e.g. Ichinose, 1982), have been studied. However the question of confinement has not been resolved and there are difficulties with the incorporation of fermions (quarks) (e.g. Hasenfratz 1982). The region of QCD which must be probed in order to answer these questions is beyond the radius of convergence of strong-coupling expansions and, at best, is at the very limit of other techniques such as Monte Carlo simulations. The method of Padé approxi-mants (e.g. Baker, 1975) is frequently used to extend the range of convergence of the strong-coupling expansions to the weak-coupling limit (e.g. Kogut et al. 1976), but

there are doubts (e.g. Hamer 1982) about the use of this technique. One of the more promising methods developed recently is the finite-lattice approach (e.g. Hamer and Barber 1981, Irving and Thomas 1982, Martin 1982), in which the hypothesis of "finite-size scaling" is employed. The quantity of interest is calculated exactly on a series of finite lattices of different sizes and the results are extrapolated to the infinite lattice.

The aim of the present work is to develop an alternative to the conventional strong-coupling expansions of the Hamiltonian formulation of lattice gauge theory. The pure gauge field system with no matter fields will be considered. The Hamiltonian, which will be examined in chapter two, is of the general form

$$H = \sum_{\text{links}} H_o + \lambda \sum_{\text{plaquettes}} H' \qquad (1.3)$$

where the parameter λ contains the dependence on the coupling constant. The strong-coupling limit $g \to \infty$ corresponds to the limit $\lambda \to 0$. The conventional strong-coupling expansion arises from the treatment of the term $\lambda \sum_{\text{plaquettes}} H'$ of equation (1.3) as a perturbation on the zero-order Hamiltonian $\sum_{\text{links}} H_o$. The resulting zero-order solutions are thus as far from the weak-coupling limit ($g \to 0 \equiv \lambda \to \infty$) as it is possible to be.

In the present method the set of plaquettes of the lattice is divided into two complementary subsets, the even and odd plaquettes. In the case of two space dimensions these subsets are like the black and white

squares of a chess board. No two members of either subset have any common links and each subset includes all the links of the lattice.

The terms of the Hamiltonian of equation (1.3) are written in terms of operators which act on the degrees of freedom of individual plaquettes. The link terms, which are associated with even plaquettes, and the even plaquette terms are combined to form a new zero-order Hamiltonian $\sum_{\text{even plaquettes}} H_o(\lambda)$. The resulting zero-order problem is solved exactly in terms of independent single (even) plaquette states, for any value of λ. The odd plaquette terms of the Hamiltonian are treated as a perturbation. They mix the zero-order eigenstates of $\sum_{\text{even plaquettes}} H_o(\lambda)$.

The choice of an approximate zero-order Hamiltonian is crucial to the success of any perturbative method. The zero-order problem should be exactly soluble and its solutions should describe the true physical state as closely as is possible. The present method is an attempt to satisfy this aim better than the conventional strong-coupling expansion does. The zero-order solutions on which the perturbative treatment of the odd plaquette terms is based already include some of the quantum fluctuation effects which do not occur until higher orders in the conventional method. The expansion based on the new zero-order Hamiltonian will be termed an "intermediate-coupling" expansion since the zeroth order problem is solved for all intermediate values of the coupling constant.

The method, which is introduced in chapter two, is based on a larger zero-order problem than that of the

conventional strong-coupling method. The even plaquette terms of the Hamiltonian are included as well as the link terms. The technique is applicable to all gauge groups, in integral numbers of space-time dimensions. The example of (2+1)-dimensional Z(2) lattice gauge theory, without matter fields, is treated in detail. This theory was discovered by Wegner (1971) as the geometrical dual to the (2+1)-dimensional Ising spin model. This system has been chosen for its relative simplicity and, because both it and its dual system have been extensively studied, the results obtained may be compared with those of other methods. The solution of the new zero-order problem is also described in chapter two.

Details of the intermediate coupling expansion are presented in chapter three. A diagrammatic method for the enumeration and evaluation of the terms of this expansion is presented. The resulting expressions are considerably more complicated than their conventional strong-coupling counterparts but are suitable for evaluation by computer. It is felt that the advantages of basing the expansion on a zero-order state which is closer to the physical state of the system than is that of the conventional method outweigh the disadvantages of this additional complexity. The application of any lattice gauge theory technique to the problem of QCD will undoubtedly require mechanical assistance and it may be better to work with a complicated series, which may be truncated after a few terms, than a simpler one requiring many terms of higher orders.

In chapter four the method is applied to the calculation of the vacuum energy and the mass gap. The results for the vacuum are very close to those of the conventional strong-coupling method. The conventional method is known to be less successful in the calculation of local excitations, such as the mass gap, than of global excitations, such as the fluctuations of the vacuum. The observed agreement is thus encouraging.

It is found that the first excited state is quasi-degenerate and that the expansion for the mass gap converges poorly as a result. Methods for dealing with this quasi-degeneracy are presented in chapter five. A formulation of degenerate perturbation theory due to Bloch (1958) is used to calculate the mass gap. The result compares favourably with that of the conventional method. It is argued that the occurrence of complex values for the mass gap near the critical point may be overcome by the consideration of higher order terms.

The method is applied to the calculation of the string tension in chapter six. Results indicating the presence of the roughening transition are obtained and are compared with those of the conventional method.

The computer program used to perform these calculations is the subject of chapter seven. A number of extensions and applications are presented in chapter eight. These include results for a family of models for which the odd and even plaquette terms in the Hamiltonian have different coupling strengths.

CHAPTER 2

PLAQUETTE OPERATOR FORMULATION OF Z(2) LATTICE GAUGE THEORY IN (2+1) DIMENSIONS

2.1 HAMILTONIAN FORMULATION OF PURE GAUGE FIELD THEORY ON A CUBIC LATTICE

(a) Yang-Mills Theory on a Lattice

The 2d directions on a d-dimensional space-time lattice are labelled by unit vectors $\pm \hat{n}_i$: $i = 1,2, \ldots d$ and the spacing between lattice sites in the ith direction is denoted by a_i: $i = 1,2, \ldots d$. A site is labelled by a vector $\underline{n}$ which has d integer components. In the case of a hyper-cubic lattice

$$a = a_i = a_j \qquad \forall \quad i,j \tag{2.1}$$

and the position vector of any site is

$$\underline{r} = a\underline{n} \ . \tag{2.2}$$

The directed line elements which join a site to its 2d nearest neighbours are called links. A link is specified by a site $\underline{n}$ and a direction vector $\mu \in \{\hat{n}_i\}$ by

$$\ell = (\underline{n}, \mu) \ . \tag{2.3}$$

There are two possible orientations for the link between any two sites as shown in figure 2.1. Such pairs are called link and antilink.

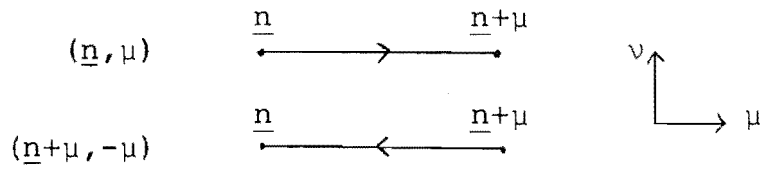

Figure 2.1: A link and its antilink

The degrees of freedom of a pure gauge theory reside in the links and are elements of the gauge group. They are the connections $U(\underline{n},\mu)$ which describe the relative orientation of the colour frames associated with the sites at each end of the link (e.g. Susskind 1976). Because the connection for a particular link is a rotation matrix in colour space, belonging to the fundamental representation of the gauge group, it may be written as

$$U_{ij}(\underline{n},\mu) = \exp[iB(\underline{n},\mu)] \ . \qquad (2.4)$$

The indices i,j label the axes of the colour space and are associated with sites $\underline{n}$ and $\underline{n}+\mu$ respectively as in figure 2.2

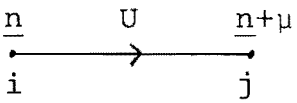

Figure 2.2: The connection $U_{ij}(\underline{n},\mu)$

The connections for a link and its corresponding antilink must be inverses as they describe the same relative orientation of the two frames i.e.

$$U_{ij}(\underline{n},\mu) = U^{-1}_{ij}(\underline{n}+\mu,-\mu) \qquad (2.5)$$

Comparison with the continuum Yang-Mills theory (Yang and Mills 1954) suggests the identification

$$B(\underline{n},\mu) = ag\lambda_k A^k(\underline{n},\mu) \tag{2.6}$$

where g is the coupling constant, $A^k(\underline{n},\mu)$ the gauge vector potential and λ_k the matrix generators of the gauge group. Similarly a local gauge transformation, corresponding to a rotation of the colour frame at a particular site, may be written

$$V_{ij}(\underline{n}) = \exp[-i\lambda_k X^k(\underline{n})] \ . \tag{2.7}$$

The indices i,j are both associated with site $\underline{n}$.
Under a local gauge transformation the connection transforms as

$$U(\underline{n},\mu) \rightarrow V(\underline{n})U(\underline{n},\mu)V^{-1}(\underline{n}+\mu) \ . \tag{2.8}$$

A locally gauge invariant action constructed from the $U(\underline{n},\mu)$ must have the colour indices associated with each site contracted to form a local colour singlet. Thus $U_{ij}(\underline{n},\mu)$ itself is not locally gauge invariant as it has two uncontracted indices. The smallest locally gauge invariant object that can be formed from the $U(\underline{n},\mu)$ is the product of the four connections around a unit square or "plaquette". Using the notation of figure 2.3 it is clear that the quantity

$$U_{\underline{n}} = U_{ij}(\underline{n},\mu)U_{jk}(\underline{n}+\mu,\nu)U_{k\ell}(\underline{n}+\mu+\nu,-\mu)U_{\ell i}(\underline{n}+\nu,-\nu) \tag{2.9}$$

has no uncontracted indices and is therefore locally gauge invariant.

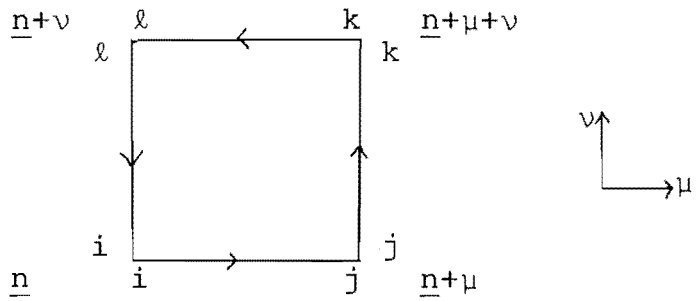

Figure 2.3: An elementary Plaquette.

The product of the $U(\underline{n},\mu)$ around any closed path on the lattice is also locally gauge invariant. The usual choice of action (e.g. Kogut 1979b, Fradkin and Susskind 1978, Wilson 1974) is the Wilson action

$$S = - \frac{1}{2g^2} \sum_{\underline{n}} \mathrm{Tr}(U_{\underline{n}} + U_{\underline{n}}^{\dagger}) \qquad (2.10)$$

where the hermitian conjugate term represents the contribution from plaquettes whose orientation is opposite to that suggested by the arrows in figure 2.3.

Other possible actions have been investigated. Kogut (1979a) has considered products of the connections around closed loops of six links. A somewhat different approach, based on the parameter space of the gauge group, has been suggested by Manton (1980).

The Wilson action equation (2.10) may be shown (e.g. Kogut 1979b) to be the lattice analogue of the pure Yang-Mills action

$$S_{ym} = - \tfrac{1}{4} \int d^4x \, (F_{\mu\nu})^2 . \qquad (2.11)$$

(b) Hamiltonian Formulation for continuous Gauge Group

A Hamiltonian formulation of lattice gauge theory, based on analogy with the rigid rotator, was presented by Kogut and Susskind (1975) only a few months after the publication of Wilson (1974). Later derivations of the Hamiltonian for continuous gauge groups (e.g. Susskind 1976) use the temporal gauge, for which the connections on time-like links are unity, and the conventional canonical procedure. In the limit $a_o \to 0$ the lattice spacing in the time direction becomes infinitesimal and the resulting Hamiltonian is

$$H = \frac{g^2}{2a} \sum_{\ell} E^{\alpha} E^{\alpha} - \frac{1}{4ag^2} \sum_{p} \mathrm{Tr}(\hat{U}_p + \hat{U}_p^{\dagger}) \quad . \tag{2.12}$$

The indices ℓ and p are summed over links and plaquettes respectively and a is the lattice spacing in the spatial directions. The E^{α} are the generators of infinitesimal local gauge transformations and the combination $E^{\alpha}E^{\alpha}$ is the quadratic Casimir operator for the gauge group. The $\hat{U}_p$ are the operators corresponding to U_p.

The space of states in which this Hamiltonian acts is a tensor product with a factor for each link i.e.

$$|\Psi\rangle = \otimes \prod_{\ell} |\psi_{\ell}\rangle . \tag{2.13}$$

Under a local gauge transformation $V(\underline{n})$ at a given site of a cubic lattice the connections on the 2d links emanating from $\underline{n}$ are transformed and any arbitrary gauge transformation may be constructed from the $V(\underline{n})$. The states of interest are the "physical" states which satisfy

$$V(\underline{n})\,|\Psi\rangle = |\Psi\rangle \qquad \forall \quad \underline{n} \tag{2.14}$$

and are thus gauge invariant states. The consideration of only gauge invariant states leads to relations analogous to Gauss' Law (Kogut 1979b, Kogut and Susskind 1975).

In the strong coupling limit $g \to \infty$ the first term in equation (2.12) is dominant. The definition of the reduced Hamiltonian

$$W = \frac{2a}{g^2} H = \sum_{\ell} E^{\alpha}E^{\alpha} - \frac{1}{2g^4} \sum_{p} \mathrm{Tr}(\hat{U}_p + \hat{U}_p^{\dagger}) \tag{2.15}$$

allows the development of strong coupling perturbation expansions (e.g. Kogut et al. 1976).

(c) Hamiltonian formulation for Z(N)

In the case of finite gauge groups it is not possible to obtain the Hamiltonian by the canonical procedure as was the case for the continuous groups of the previous section. The introduction of the transfer matrix (Schultz et al 1964) allows the construction of Hamiltonians for finite groups (e.g. Fradkin and Susskind 1978, Kogut 1979b) including the Z(N) groups which are of special interest.

The gauge field degrees of freedom again reside on the links and are denoted by $q(\underline{n},\mu)$. They take the values

$$q(\underline{n},\mu) \;\varepsilon\; \{e^{i\frac{2\pi k}{N}},\ k = 0,1,\ \ldots\ N-1\}, \tag{2.15}$$

The action is constructed as in the previous section and the counterpart of equation (2.10) is

$$S = -\beta \sum_{n} \mathrm{Tr}(q_n + q_n^\dagger) \tag{2.16}$$

where q_n is the product of the $q(\underline{n},\mu)$ around the elementary plaquette specified by $\underline{n}$. It is customary to use the symbol β for the coupling constant, suggesting identification with the quantity $\beta = \frac{1}{kT}$ of statistical mechanics. Since the formation of the Hamiltonian involves "shrinking" the lattice spacing in the true direction to zero and allowing the coupling in the time direction to become large the action, equation (2.16), is written with anisotropic couplings as

$$S = -\beta_\tau \sum_{p_\tau} (q_{p_\tau} + q_{p_\tau}^\dagger) - \beta_s \sum_{p_s} (q_{p_s} + q_{p_s}^\dagger) \quad . \tag{2.17}$$

Plaquettes containing any time links are included in the first summation and purely spatial plaquettes in the second. The temporal gauge is again used. The transfer matrix method then gives the Hamiltonian which is

$$H = -\tfrac{1}{2} \sum_{\ell} (P(\ell) + P^\dagger(\ell)) - \frac{\lambda}{2} \sum_{p} (Q_p + Q_p^\dagger). \tag{2.18}$$

The Hamiltonian is constructed from unitary link operators $P(\underline{n},\mu)$, $Q(\underline{n},\mu)$ whose eigenvalues are the possible values of the degrees of freedom $q(\underline{n},\mu)$ associated with the link $\ell = (\underline{n},\mu)$. The P operators are like the spin flip operators for $Z(2)$. The Q operators appear in the Hamiltonian as the operator

$$Q_p = \otimes \prod_{\ell \epsilon \underline{p}} Q(\ell) = Q(\underline{p},\mu) \otimes Q(\underline{p}+\mu,\nu) \otimes Q(\underline{p}+\mu+\nu,-\mu) \otimes Q(\underline{p}+\nu,-\nu) \quad (2.19)$$

which is the counterpart of the $\hat{U}_p$ of equation (2.12). Although the Hamiltonian equation (2.18) is commonly used (e.g. Omero 1982) a constant is often added to the action (and Hamiltonian) to make the $\lambda \to 0$ vacuum state energy equal to zero (e.g. Horn, Weinstein and Yankielowicz, 1979). The parameter λ contains the Hamiltonian's dependence on the coupling constant.

The link operators $P(\ell)$ and $Q(\ell)$ obey the $Z(N)$ algebra

$$P^N(\ell) \equiv Q^N(\ell) = 1 \quad (2.20a)$$

$$P^\dagger(\ell)P(\ell) \equiv P(\ell)P^\dagger(\ell) \equiv Q^\dagger(\ell)Q(\ell) \equiv Q(\ell)Q^\dagger(\ell) = 1 \quad (2.20b)$$

$$P^\dagger(\ell)Q(\ell)P(\ell) = e^{i\frac{2\pi}{N}} Q(\ell) \, . \quad (2.20c)$$

Operators associated with different links commute.

Since a local gauge transformation at a site flips the spins on all the links attached to that site the Hermitian operator

$$G(\underline{n}) = \otimes \prod_{\ell \epsilon \underline{n}} P(\ell) \quad (2.21)$$

corresponds to a local gauge transformation at site $\underline{n}$. The required local gauge invariance of the Hamiltonian

$$G(\underline{n})HG^{-1}(\underline{n}) = H \qquad \forall \quad \underline{n} \tag{2.22}$$

follows from equations (2.20). The states of the Z(N) Hamiltonian are of the form equation (2.13) and the states of interest are the "physical" states for which

$$G(\underline{n})|\Psi\rangle = |\Psi\rangle. \qquad \forall \quad \underline{n} \tag{2.23}$$

A useful representation for the operators P(ℓ) and Q(ℓ), given by equations (2.24), is the one in which the Q(ℓ) are diagonal.

$$Q_{jk} = \delta_{jk}\, e^{i\frac{2\pi j}{N}} \qquad j,k = 0,1 \ldots N-1 \tag{2.24a}$$

$$P_{jk} = \delta_{k,j+1} + \delta_{1,N}\delta_{1,k} \qquad j,k = 0,1 \ldots N, \tag{2.24b}$$

In the case N = 2 the matrices are

$$Q^{(2)} = \begin{pmatrix} 1 & 0 \\ 0 & -1 \end{pmatrix} \quad , \quad P^{(2)} = \begin{pmatrix} 0 & 1 \\ 1 & 0 \end{pmatrix} \tag{2.25}$$

which are the Pauli spin matrices σ_3 and σ_1 respectively. The corresponding matrices for N = 3 are

$$Q^{(3)} = \begin{pmatrix} 1 & 0 & 0 \\ 0 & e^{i\frac{2\pi}{3}} & 0 \\ 0 & 0 & e^{i\frac{4\pi}{3}} \end{pmatrix} \quad , \quad P^{(3)} = \begin{pmatrix} 0 & 0 & 1 \\ 1 & 0 & 0 \\ 0 & 1 & 0 \end{pmatrix} \tag{2.26}$$

These matrices may be readily shown to obey the Z(N) algebra equation (2.20).

2.2 REFORMULATION OF THE HAMILTONIAN FOR Z(2) LATTICE GAUGE THEORY

(a) Motivation

The Hamiltonian for the Z(2) lattice gauge theory, in generic form, is

$$H = - \sum_{\ell} \sigma_1 - \lambda \sum_{p} \sigma_3\sigma_3\sigma_3\sigma_3 \ . \tag{2.27}$$

Since σ_1 and σ_3 are self-adjoint the Hermitian conjugate terms are not present. In order to calculate such quantities as the mass gap it is necessary to find the eigenstates of H and their energies. The most obvious method for the solution of this problem is perturbation theory in the parameter λ, in which equation (2.27) is interpreted as

$$H = \sum_{\ell} H_o(\ell) + \lambda \sum_{p} H'(p) \tag{2.28}$$

The unperturbed states are gauge invariant tensor products of the eigenvectors $\underline{x}_i$ of σ_1 i.e.

$$|\Psi>^{\circ} = \otimes \prod_{\ell} |x(\ell)> \ . \tag{2.29}$$

Since $\lambda \sim \frac{1}{g^2}$ this is a strong coupling expansion. Duality arguments may generally be used (e.g. Kogut 1979b) to relate the Z(2) gauge model to the Z(2) spin models and establish the correspondence $\lambda \sim \frac{1}{kT}$ which suggests that this expansion is related to the high-temperature expansions of statistical mechanics (e.g. Stanley 1971). For lattices

of certain dimensions, (3+1) for example, the theory is self dual and such relations cannot be found. Many strong coupling calculations have been performed in the Hamiltonian formulation, particularly in the case d = (1+1). The continuum limit, which is the region of ultimate interest in QCD, corresponds to the weak coupling limit $\lambda \to \infty$ and thus is usually beyond the radius of convergence of strong coupling expansions. The phase transitions for theories with finite gauge groups may occur before this limit is reached. Such techniques as Padé approximants (e.g. Kogut et al. 1976) and the renormalization group (e.g. Horn and Yankielowicz 1979) are often used in conjunction with the strong coupling expansion in order to gain information about the theory's phase diagrams. There are few Hamiltonian methods suited to the calculation of the eigenstates and eigenvalues of equation (2.27) in more than (1+1) dimensions. Those that do exist (e.g. Roomany and Wyld 1980) are typically unwieldy and use such hybrid techniques as those mentioned above. The plaquette operator formulation was motivated by the desire to improve the performance and simplicity of Hamiltonian strong coupling perturbation theory.

(b) Plaquette Operator Formulation of (2+1) dimensional Z(2) Hamiltonian Lattice Gauge Theory

The case d = (2+1) is considered for its relative simplicity. It is possible to extend the following methods to higher dimensions. Sites are denoted by

$\underline{n} = (n_1, n_2)$. Links, lattice directions and elementary plaquettes are as shown in figures 2.1 and 2.3.

The sites of the lattice may be classified as odd or even according to the prescription

$$(-)^{n_1+n_2} = \begin{cases} +1 & \underline{n} \text{ even} \\ -1 & \underline{n} \text{ odd} \end{cases} . \qquad (2.30)$$

The elementary plaquettes labelled by $\underline{n}$ as in figure 2.3 may also be classified in this way. If the even plaquettes are shaded the lattice exhibits the pattern of figure 2.4

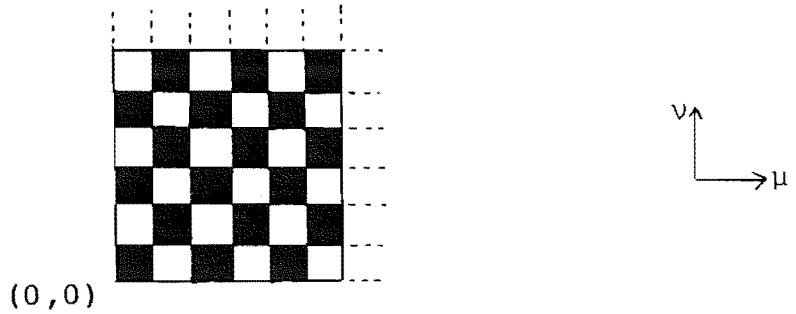

Figure 2.4: Odd and even plaquettes.

In the following a lattice of N odd and N even plaquettes is assumed.

If periodic boundary conditions are imposed so that

$$\underline{n} + L_\mu \mu \equiv \underline{n}, \quad \underline{n} + L_\nu \nu \equiv \underline{n} , \qquad (2.31)$$

or a large lattice is considered so that edge and corner effects are unimportant, then the set of even plaquettes (or the set of odd plaquettes) includes all the links of

the lattice. This suggests that the first term in equation (2.27) may be written in terms of even (or odd) plaquette operators.

Since the Hilbert space E in which the Hamiltonian acts is of the form $E = \otimes \prod_{\ell} E_{\ell}$ the first term of equation (2.27) should be interpreted as

$$- \sum_{\ell} \sigma_1 \equiv -\sum_{\ell} \otimes \prod_{i=1}^{N_{\ell}} [\delta_{i\ell}\sigma_1(\ell) + (1 - \delta_{i\ell})I_2(\ell)]. \qquad (2.32)$$

The contribution to this sum from the four links which bound an even plaquette $\underline{n}$ is

$$\begin{aligned}
\sum_{\ell \in \underline{n}} \sigma_1(\ell) = {} & \sigma_1(\underline{n},\mu) \otimes I_2(\underline{n}+\mu,\nu) \otimes I_2(\underline{n}+\mu+\nu,-\mu) \\
& \otimes I_2(\underline{n}+\nu,-\nu) \\
& + I_2(\underline{n},\mu) \otimes \sigma_1(\underline{n}+\mu,\nu) \otimes I_2(n+\mu+\nu,-\mu) \\
& \otimes I_2(\underline{n}+\nu,-\nu) \\
& + I_2(\underline{n},\mu) \otimes I_2(\underline{n}+\mu,\nu) \otimes \sigma_1(\underline{n}+\mu+\nu,-\mu) \\
& \otimes I_2(\underline{n}+\nu,-\nu) \\
& + I_2(\underline{n},\mu) \otimes I_2(\underline{n}+\mu,\nu) \otimes I_2(\underline{n}+\mu+\nu,-\mu) \\
& \otimes \sigma_1(\underline{n}+\nu,-\nu) \; . \qquad (2.33)
\end{aligned}$$

The second term of equation (2.27) may be expressed in terms of even and odd plaquette operators as

$$- \lambda \sum_{\underline{p}} \sigma_3\sigma_3\sigma_3\sigma_3 \equiv -\lambda \sum_{\underline{p} \text{ even}} \sigma_3\sigma_3\sigma_3\sigma_3 - \lambda \sum_{\underline{p} \text{ odd}} \sigma_3\sigma_3\sigma_3\sigma_3 \; . \qquad (2.34)$$

By combining the even plaquette operators of equations

(2.33) and (2.34) the Hamiltonian may be written in terms of operators acting on even or odd plaquettes as

$$H = H_o(\lambda) + \lambda H' = - \sum_{p \text{ even}} h_o(\lambda) - \lambda \sum_{p \text{ odd}} \sigma_3\sigma_3\sigma_3\sigma_3 \tag{2.35}$$

where

$$h_o(\lambda) = \sigma_1 \otimes I \otimes I \otimes I + I \otimes \sigma_1 \otimes I \otimes I + I \otimes I \otimes \sigma_1 \otimes I + I \otimes I \otimes I \otimes \sigma_1 + \lambda\sigma_3 \otimes \sigma_3 \otimes \sigma_3 \otimes \sigma_3 \tag{2.36}$$

and

$$H' = \sum_{p \text{ odd}} H'(p). \tag{2.37}$$

The odd plaquette operator $\sum_{p \text{ odd}} \sigma_3\sigma_3\sigma_3\sigma_3$ may be written entirely in terms of operators which act on even plaquettes. Consider the odd plaquette $\underline{n}$ and its four neighbouring even plaquettes $\underline{n}\pm\mu$, $\underline{n}\pm\nu$ shown in figure 2.5.

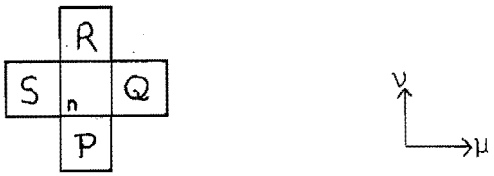

Figure 2.5: An odd plaquette and its neighbouring even plaquettes.

The contribution to equation (2.35) from the odd plaquette at $\underline{n}$ is

$$\sigma_3(\underline{n},\mu) \otimes \sigma_3(\underline{n}+\mu,\nu) \otimes \sigma_3(\underline{n}+\mu+\nu,-\mu) \otimes \sigma_3(\underline{n}+\nu,-\nu) \tag{2.38}$$

which may be written as

$$P(\underline{n}-\nu) \otimes Q(\underline{n}+\mu) \otimes R(\underline{n}+\nu) \otimes S(\underline{n}-\mu) \qquad (2.39)$$

where the even plaquette operators

$$\begin{aligned}
P(\underline{n}-\nu) &= I_2(\underline{n}-\nu,\mu) \otimes I_2(\underline{n}-\nu+\mu,\nu) \otimes \sigma_3(\underline{n}+\mu,-\mu) \otimes I_2(\underline{n},-\nu) \\
Q(\underline{n}+\mu) &= I_2(\underline{n}+\mu,\mu) \otimes I_2(\underline{n}+2\mu,\nu) \otimes I_2(\underline{n}+2\mu+\nu,-u) \\
&\quad \otimes \sigma_3(\underline{n}+\mu+\nu,-\nu) \\
R(\underline{n}+\nu) &= \sigma_3(\underline{n}+\nu,\mu) \otimes I_2(\underline{n}+\mu+\nu,\nu) \otimes I_2(\underline{n}+\mu+2\nu,-\mu) \\
&\quad \otimes I_2(\underline{n}+2\nu,-\nu) \\
S(\underline{n}-\mu) &= I_2(\underline{n}-\mu,\mu) \otimes \sigma_3(\underline{n},\nu) \otimes I_2(\underline{n}+\nu,-\mu) \otimes I_2(\underline{n}+\nu-\mu,-\nu)
\end{aligned} \qquad (2.40)$$

which act on the even plaquettes neighbouring $\underline{n}$ as indicated in figure 2.5 have been defined. Note that the operator given by equation (2.39) includes the operators which act on the anti-links of $\underline{n}$. e.g. $P(\underline{n},-\nu)$ contains $\sigma_3(\underline{n}+\mu,-\mu)$ while equation (2.38) contains $\sigma_3(\underline{n},\mu)$. In the Z(2) case the matrices of equation (2.25) are self-adjoint and the relation $\sigma_3(\underline{n},\mu) = \sigma_3^{\dagger}(\underline{n}+\mu,-\mu)$ holds.

The Hamiltonian may now be written entirely in terms of even plaquette operators as

$$\begin{aligned}
H &= H_o(\lambda) + \lambda H' \\
&= -\sum_{\underline{p}\ \text{even}} [\sigma_1 \otimes I \otimes I \otimes I + I \otimes \sigma_1 \otimes I \otimes I \\
&\quad + I \otimes I \otimes \sigma_1 \otimes I + I \otimes I \otimes I \otimes \sigma_1 + \lambda\sigma_3 \otimes \sigma_3 \otimes \sigma_3 \otimes \sigma_3] \\
&\quad - \lambda \sum_{\underline{p}\ \text{odd}} P(\underline{p}-\nu) \otimes Q(\underline{p}+\mu) \otimes R(\underline{p}+\nu) \otimes S(\underline{p}-\mu).
\end{aligned} \qquad (2.41)$$

Since no even plaquettes have common links the Hilbert space of H may be written as $E = \otimes_{\underline{p}\ \text{even}} E_p$ and the eigenstates, equation (2.13), become

$$|\Psi> = \otimes \prod_{\underline{p}\ \text{even}} |\psi_p> \quad . \tag{2.42}$$

The most significant difference between equations (2.41) and (2.27) is that the first term of the former contains some dependence on the parameter λ. The two forms are equivalent in the strong coupling ($\lambda \to 0$) limit. Equation (2.41) suggests that models may be constructed with different coupling constants for odd and even plaquettes. The Hamiltonians for such models would be of the form

$$H = H_o(\lambda_e) + \lambda_o H' \tag{2.43}$$

where λ_e and λ_o are the coupling strengths for even and odd plaquettes respectively. The case $\lambda_e = \lambda_o = \lambda$ would then correspond to the usual Z(2) gauge model equation (2.27).

(c) Solution of the Zero Order Problem

If the eigenvalues and eigenvectors of $H_o(\lambda)$ can be obtained then they will provide the zero order terms in any perturbative method for obtaining the corresponding quantities for the full Hamiltonian. In the representation (2.24) $H_o(\lambda)$ is a direct sum of single (even) plaquette matrices

SEE ERRATA

$$h_o(\lambda) = \left(\begin{array}{cccc}
\begin{pmatrix}\lambda & 1 & 1 & 0\\ 1 & -\lambda & 0 & 1\\ 1 & 0 & -\lambda & 1\\ 0 & 1 & 1 & \lambda\end{pmatrix} & \begin{pmatrix}1&0&0&0\\0&1&0&0\\0&0&1&0\\0&0&0&1\end{pmatrix} & \begin{pmatrix}1&0&0&0\\0&1&0&0\\0&0&1&0\\0&0&0&1\end{pmatrix} & O_4\\
\begin{pmatrix}1&0&0&0\\0&1&0&0\\0&0&1&0\\0&0&0&-1\end{pmatrix} & \begin{pmatrix}-\lambda & 1 & 1 & 0\\ 1 & \lambda & 0 & 1\\ 1 & 0 & \lambda & 1\\ 0 & 1 & 1 & -\lambda\end{pmatrix} & O_4 & \begin{pmatrix}1&0&0&0\\0&1&0&0\\0&0&1&0\\0&0&0&1\end{pmatrix}\\
\begin{pmatrix}1&0&0&0\\0&1&0&0\\0&0&1&0\\0&0&0&1\end{pmatrix} & O_4 & \begin{pmatrix}-\lambda & 1 & 1 & 0\\ 1 & \lambda & 0 & 1\\ 1 & 0 & \lambda & 1\\ 0 & 1 & 1 & -\lambda\end{pmatrix} & \begin{pmatrix}1&0&0&0\\0&1&0&0\\0&0&1&0\\0&0&0&1\end{pmatrix}\\
O_4 & \begin{pmatrix}1&0&0&0\\0&1&0&0\\0&0&1&0\\0&0&0&1\end{pmatrix} & \begin{pmatrix}1&0&0&0\\0&1&0&0\\0&0&1&0\\0&0&0&1\end{pmatrix} & \begin{pmatrix}\lambda & 1 & 1 & 0\\ 1 & -\lambda & 0 & 1\\ 1 & 0 & -\lambda & 1\\ 0 & 1 & 1 & \lambda\end{pmatrix}
\end{array}\right). \quad (2.44)$$

The dimension of the single plaquette Hamiltonian matrices for Z(N) depends on the order of the group and the number of links per plaquette. Thus in the present case $h_o(\lambda)$ is a $2^4 \times 2^4$ square matrix. Exact algebraic expressions for the eigenvalues and eigenvectors are not necessary in order to begin a strong coupling expansion as their values may be obtained by variational (e.g. Omero 1982) or other numerical methods. Nevertheless they are comforting to have and increase the understanding of the structure of the problem in its present form. Such expressions are obtained in the following sections. In (I) the expected

degeneracy structure is deduced by comparison with the conventional Hamiltonian of equation (2.27). In (II) the eigenvectors are obtained in a basis of direct products of the eigenvectors of σ_1.

(I) The Strong Coupling Limit

In the strong coupling limit $\lambda \to 0$ the eigenvalues and eigenvectors of equation (2.44) should be the same as those of the conventional Hamiltonian, equation (2.27), for a single plaquette.

The eigenvalues of σ_1 are ± 1 and the corresponding normalized eigenvectors are

$$\underline{x}_+ = \frac{1}{\sqrt{2}} \begin{pmatrix} 1 \\ 1 \end{pmatrix} \qquad \underline{x}_- = \frac{1}{\sqrt{2}} \begin{pmatrix} 1 \\ -1 \end{pmatrix} . \tag{2.45}$$

There are 16 linearly independent single plaquette states in the strong coupling limit. These states, together with their energies and degeneracies are shown in table 2.1. Links labelled by + (-) are in link eigenstate $\underline{x}_+$ ($\underline{x}_-$). The corresponding single plaquette eigenvectors are the products

$$|\Psi\rangle_{SC} = |x(\underline{n},\mu)\rangle \otimes |x(\underline{n}+\mu,\nu)\rangle \otimes |x(\underline{n}+\mu+\nu,-\mu)\rangle \otimes |x(\underline{n}+\nu,-\nu)\rangle \tag{2.46}$$

suggested by the plaquette states (table 2.1) and given explicitly in table 2.2.

Energy Λ	Degeneracy g_Λ	Strong Coupling Plaquette States
-4	1	
-2	4	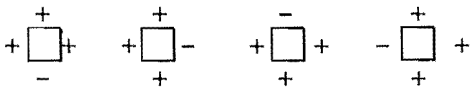
0	6	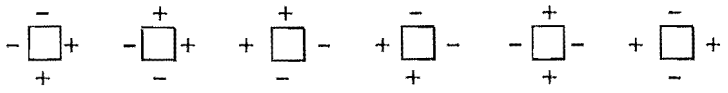
+2	4	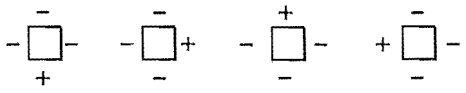
+4	1	
	16	

Table 2.1: Single Plaquette states in the strong coupling limit.

The eigenvalues $\varepsilon_i(\lambda)$ and eigenvectors $\underline{Y}_i(\lambda)$ of equation (2.24) must be related to their strong coupling limit counterparts Λ_i and $\underline{X}_i$ by

$$\varepsilon_i(\lambda) \xrightarrow{\lambda \to 0} \Lambda_i \tag{2.47a}$$

$$\underline{Y}_i(\lambda) \xrightarrow{\lambda \to 0} \sum_{j=0}^{g_\Lambda} C_{ij}\, \underline{X}_j \quad . \tag{2.47b}$$

	$\underline{X}_1$	$\underline{X}_2$	$\underline{X}_3$	$\underline{X}_4$	$\underline{X}_5$	$\underline{X}_6$	$\underline{X}_7$	$\underline{X}_8$	$\underline{X}_9$	$\underline{X}_{10}$	$\underline{X}_{11}$	$\underline{X}_{12}$	$\underline{X}_{13}$	$\underline{X}_{14}$	$\underline{X}_{15}$	$\underline{X}_{16}$
Energy	-4	-2	-2	-2	-2	0	0	0	0	0	0	2	2	2	2	4
Configuration	++++	-+++	+-++	++-+	+++-	++--	+-+-	-++-	+--+	-+-+	--++	+---	-+--	--+-	---+	----
Components	1	1	1	1	1	1	1	1	1	1	1	1	1	1	1	1
	1	1	1	1	-1	-1	-1	-1	1	1	1	-1	-1	-1	1	-1
	1	1	1	-1	1	-1	1	1	-1	-1	1	-1	-1	1	-1	-1
	1	1	1	-1	-1	1	-1	-1	-1	-1	1	1	1	-1	-1	1
	1	1	-1	1	1	1	-1	1	-1	1	-1	-1	1	-1	-1	-1
	1	1	-1	1	-1	-1	1	-1	-1	1	-1	1	-1	1	-1	1
	1	1	-1	-1	1	-1	-1	1	1	-1	-1	1	-1	-1	1	1
	1	1	-1	-1	-1	1	1	-1	1	-1	-1	-1	1	1	1	-1
	1	-1	1	1	1	1	1	-1	1	-1	-1	1	-1	-1	-1	-1
	1	-1	1	1	-1	-1	-1	1	1	-1	-1	-1	1	1	-1	1
	1	-1	1	-1	1	-1	1	-1	-1	1	-1	-1	1	-1	1	1
	1	-1	1	-1	-1	1	-1	1	-1	1	-1	1	-1	1	1	-1
	1	-1	-1	1	1	1	-1	-1	-1	-1	1	-1	-1	1	1	1
	1	-1	-1	1	-1	-1	1	1	-1	-1	1	1	1	-1	1	-1
	1	-1	-1	-1	1	-1	-1	-1	1	1	1	1	1	1	-1	-1
	1	-1	-1	-1	-1	1	1	1	1	1	1	-1	-1	-1	-1	1

Table 2.2: Components of single plaquette strong coupling eigenvectors. The first and second rows are the energies and spin configurations of the plaquette states (see Table 2.1). The vectors require a normalisation factor of $1/\sqrt{16}$.

(II) Direct Product Vector Solution

The eigenvectors of the single plaquette zero-order Hamiltonian $h_o(\lambda)$, and their energies, may be obtained from equation 2.44 by numerical or algebraic methods. The following method, suggested to the author by T. Kalotas (Kalotas 1980), gives the eigenvectors in a basis consisting of direct products of the eigenvectors of σ_1. Comparison with the single plaquette strong coupling eigenvectors of equation (2.46) illustrates the new features introduced by the reformulation of the Hamiltonian. This method is of general applicability and will be applied to the case of Z(3) lattice gauge theory on a (2+1) dimensional triangular lattice in a later section.

The first step is the calculation of the eigenvalues and eigenvectors of σ_1 and σ_3 and the relations between them. The eigenvalues of both σ_1 and σ_3 are ± 1. Write the eigenvalue equation for σ_1 as

$$\sigma_1 \underline{x}_i = \omega_{ij} \underline{x}_j \qquad \omega \equiv \begin{pmatrix} 1 & 0 \\ 0 & -1 \end{pmatrix} \tag{2.48}$$

where summation over repeated indices is understood. The corresponding eigenvectors are

$$\underline{x}_1 = \begin{pmatrix} 1 \\ 1 \end{pmatrix} , \qquad \underline{x}_2 = \begin{pmatrix} 1 \\ -1 \end{pmatrix} . \tag{2.49}$$

Similarly the eigenvalue equation for σ_3 may be written

$$\sigma_3 \underline{y}_i = \mu_{ij} \underline{y}_j \qquad \mu \equiv \begin{pmatrix} 1 & 0 \\ 0 & -1 \end{pmatrix} \tag{2.50}$$

$$\underline{y}_1 = \begin{pmatrix} 1 \\ 0 \end{pmatrix} \qquad \underline{y}_2 = \begin{pmatrix} 0 \\ 1 \end{pmatrix} . \tag{2.51}$$

The eigenvectors of the two operators are related by

$$\underline{x}_i = \alpha_{ij}\underline{y}_j \tag{2.52}$$

where

$$\alpha = 2\alpha^{-1} = \begin{pmatrix} 1 & 1 \\ 1 & -1 \end{pmatrix} . \tag{2.53}$$

The relation

$$\alpha\mu\alpha^{-1} = \sigma_1 \tag{2.54}$$

will be required.

The eigenvectors $\underline{Y}$ of $h_o(\lambda)$, given by the solutions of

$$h_o(\lambda)\ \underline{Y} = \varepsilon\underline{Y} \tag{2.55}$$

are 16-component vectors which may be expanded in any complete set of basis vectors. In order to highlight the relationship of the $\underline{Y}$ to the $\underline{X}$ of table 2.2 the eigenvectors should be written as

$$\underline{Y} = \Gamma_{i'j'k'\ell'}\ \underline{x}_{i'} \otimes \underline{x}_{j'} \otimes \underline{x}_{k'} \otimes \underline{x}_{\ell'} \equiv \Gamma_{i'j'k'\ell'}\ \underline{X}_{i'j'k'\ell'} \tag{2.56}$$

The $\underline{X}$ are a complete orthonormal set. The LHS of equation (2.55) becomes

$$h_o(\lambda)\underline{Y} = \Gamma_{i',j',k',\ell'}[(\sigma_1\underline{x}_{i'}) \otimes (I_2\underline{x}_{j'}) \otimes (I_2\underline{x}_{k'}) \otimes (I_2\underline{x}_{\ell'})$$
$$+ (I_2\underline{x}_{i'}) \otimes (\sigma_1\underline{x}_{j'}) \otimes (I_2\underline{x}_{k'}) \otimes (I_2\underline{x}_{\ell'})$$
$$+ (I_2\underline{x}_{i'}) \otimes (I_2\underline{x}_{j'}) \otimes (\sigma_1\underline{x}_{k'}) \otimes (I_2\underline{x}_{\ell'})$$
$$+ (I_2\underline{x}_{i'}) \otimes (I_2\underline{x}_{j'}) \otimes (I_2\underline{x}_{k'}) \otimes (\sigma_1\underline{x}_{\ell'})$$
$$+ \lambda(\sigma_3\underline{x}_{i'}) \otimes (\sigma_3\underline{x}_{j'}) \otimes (\sigma_3\underline{x}_{k'}) \otimes (\sigma_3\underline{x}_{\ell'})]. \tag{2.57}$$

The last term may also be written in terms of σ_1. We have from equations (2.50) and (2.52)

$$\begin{aligned}\sigma_3\underline{x}_{i'} &= \alpha_{i',j}\sigma_3\underline{Y}_j \\ &= \alpha_{i',j}\mu_{jk}\underline{Y}_k \\ &= \alpha_{i',j}\mu_{jk}(\alpha^{-1})_{ki}\underline{x}_i \\ &= (\alpha\mu\alpha^{-1})_{i',i}\underline{x}_i \end{aligned} \tag{2.58}$$

which may be written using equation (2.55) as

$$\sigma_3 x_{i'} = (\sigma_1)_{i',i}\, x_i \ . \tag{2.59}$$

Equations (2.48) and (2.59) may now be used to write the LHS of the eigenvalue equation (2.55) as

$$\begin{aligned} h_o(\lambda)\underline{Y} &= \Gamma_{i',j',k',\ell'}[\omega_{i',i}\delta_{j',j}\delta_{k',k}\delta_{\ell',\ell} + \delta_{i',i}\omega_{j',j}\delta_{k',k}\delta_{\ell',\ell} \\ &\quad + \delta_{i',i}\delta_{j',j}\omega_{k',k}\delta_{\ell',\ell} + \delta_{i',i}\delta_{j',j}\delta_{k',k}\omega_{\ell',\ell} \\ &\quad + \lambda(\sigma_1)_{i',i}(\sigma_1)_{j',j}(\sigma_1)_{k',k}(\sigma_1)_{\ell',\ell}]\underline{x}_i \otimes \underline{x}_j \otimes \underline{x}_k \otimes \underline{x}_\ell \\ &= \Gamma_{i',j',k',\ell'}[\delta_{i',i}\delta_{j',j}\delta_{k',k}\delta_{\ell',\ell}(\omega_{i',i} + \omega_{j',j} + \omega_{k',k} + \omega_{\ell',\ell}) \\ &\quad + \lambda(\sigma_1)_{i',i}(\sigma_1)_{j',j}(\sigma_1)_{k',k}(\sigma_1)_{\ell',\ell}]\underline{x}_i \otimes \underline{x}_j \otimes \underline{x}_k \otimes \underline{x}_\ell \ . \end{aligned} \tag{2.60}$$

The RHS of equation (2.55) is

$$\varepsilon \underline{Y} = \varepsilon \Gamma_{ijk\ell}\, \underline{x}_i \otimes \underline{x}_j \otimes \underline{x}_k \otimes \underline{x}_\ell \,. \tag{2.61}$$

Equating the coefficients of independent vectors $x_i \otimes x_j \otimes x_k \otimes x_\ell$ of equations (2.60) and (2.61) gives

$$\Gamma_{ijk\ell}(\omega_{ii} + \omega_{jj} + \omega_{kk} + \omega_{\ell\ell})$$

$$- \varepsilon\, \Gamma_{ijk\ell} + \lambda \Gamma_{i'j'k'\ell'}(\sigma_1)_{i'i}(\sigma_1)_{j'j}(\sigma_1)_{k'k}(\sigma_1)_{\ell'\ell} = 0 \,. \tag{2.62}$$

Define the quantity

$$\Sigma_{ijk\ell} \equiv \omega_{ii} + \omega_{jj} + \omega_{kk} + \omega_{\ell\ell} \tag{2.63}$$

which takes the values 0, ±2, ±4 and the four index operators

$$E(ijk\ell) = ijk\ell \equiv E \tag{2.64a}$$

$$Z(ijk\ell) = \overline{ijk\ell} \equiv Z \tag{2.64b}$$

where

$$\bar{i} = \begin{cases} 1 : i = 2 \\ 2 : i = 1 \end{cases} \,. \tag{2.64c}$$

Since the non-zero components of σ_1 are $(\sigma_1)_{12} = (\sigma_1)_{21} = 1$ it is clear that equation (2.62) may be written

$$(\Sigma_E - \varepsilon)\Gamma_E + \lambda \Gamma_Z = 0 \,. \tag{2.65}$$

The operators E,Z form a representation of the Z(2) algebra. Operating on equation (2.65) with E and Z and using the relation

$$\Sigma_Z = \Sigma_{\overline{ijk\ell}} = -\Sigma_{ijk\ell} = -\Sigma_E \tag{2.66}$$

gives two equations for Γ_E and Γ_Z which in matrix form are

$$\begin{pmatrix} \Sigma_E - \varepsilon & \lambda \\ \lambda & -\Sigma_E - \varepsilon \end{pmatrix} \begin{pmatrix} \Gamma_E \\ \Gamma_Z \end{pmatrix} = \begin{pmatrix} 0 \\ 0 \end{pmatrix} . \tag{2.67}$$

Setting the determinant of this matrix to zero gives the expression for the eigenvalues of (2.55)

$$\varepsilon = \pm \sqrt{\lambda^2 + \Sigma_E^2} \quad . \tag{2.68}$$

Substituting the possible values $\Sigma_E = 0, \pm 2, \pm 4$ gives the possible values $\varepsilon = \pm\lambda, \pm\sqrt{\lambda^2+4}, \pm\sqrt{\lambda^2+16}$. Equation (2.65) now becomes

$$\Gamma_Z = \frac{\pm\sqrt{\lambda^2+\Sigma_E^2} - \Sigma_E}{\lambda} \Gamma_E \tag{2.69}$$

and the eigenvectors (2.57) are constructed from its solutions Γ_E. The possible combinations are those of table 2.3.

The number of index combinations in each row reflects the degeneracy of the corresponding eigenvalue ε. The index combination $(\overline{ijk\ell})$ occurs for the same value of Σ_E^2 as $(ijk\ell)$. Such "conjugate pairs" are indicated by the braces in table (2.3). the normalized eigenvectors $\underline{Y}$ are thus superpositions of the form

Σ_E^2	Σ_E	$(ijk\ell)$
16	-4	$\{(2222)$
16	+4	$(1111)\}$
4	-2	$\{(1222)\}$ $\{(2122)\}$ $\{(2212)\}$ $\{(2221)\}$
4	+2	$\{(2111)\}$ $\{(1211)\}$ $\{(1121)\}$ $\{(1112)\}$
0	0	$\{(1122)\}$ $\{(1212)\}$ $\{(1221)\}$
0	0	$\{(2211)\}$ $\{(2121)\}$ $\{(2112)\}$

Table 2.3: Possible index combinations in equation (2.69)

$$\underline{Y} = \frac{1}{\sqrt{K_\varepsilon}} [\Gamma_E \underline{X}_\alpha + \Gamma_Z \underline{X}_{\bar{\alpha}}]$$

$$= \frac{1}{\sqrt{K_\varepsilon}} [\Gamma^{(\varepsilon)}_{ijk\ell}\ \underline{x}_i \otimes \underline{x}_j \otimes \underline{x}_k \otimes \underline{x}_\ell$$

$$+ \Gamma^{(\varepsilon)}_{\bar{i}\bar{j}\bar{k}\bar{\ell}}\ \underline{x}_{\bar{i}} \otimes \underline{x}_{\bar{j}} \otimes \underline{x}_{\bar{k}} \otimes \underline{x}_{\bar{\ell}}] \qquad (2.70)$$

since all the other Γ coefficients are zero (e.g. $\Gamma^{(\sqrt{\lambda^2+4})}_{1111}=0$). In the strong coupling limit one of Γ_E, Γ_Z tends to zero and the other to ± 1. A normalization factor $\frac{1}{\sqrt{K_\varepsilon}}$ has been included in equation (2.70). The components of the eigenvectors $\underline{Y}$ may now be written in terms of the Γ as shown in table 2.4 where the direct products of the eigenvalues of σ_1 have been identified with the $\underline{X}$ of table 2.2.

Solution of eqn (2.70) for the $\Gamma^{(\varepsilon)}(\lambda)$ allows the components of the 16 eigenvectors $\underline{Y}_i$ to be expressed as functions of λ as in table 2.5. The corresponding single plaquette energies ε_i together with their degeneracies

i	ε_i	S.C. Limit	Components of $\underline{Y}_i$ ($\Gamma \equiv \Gamma^{(\varepsilon)}$)
1	$-\sqrt{\lambda^2+16}$	$\underline{X}_1$	$\Gamma_{1111}\underline{X}_1 + \Gamma_{2222}\underline{X}_{16}$
2	$-\sqrt{\lambda^2+4}$	$\underline{X}_4$	$\Gamma_{1121}\underline{X}_4 + \Gamma_{2212}\underline{X}_{14}$
3	"	$\underline{X}_5$	$\Gamma_{1112}\underline{X}_5 + \Gamma_{2221}\underline{X}_{15}$
4	"	$\underline{X}_2$	$\Gamma_{2111}\underline{X}_2 + \Gamma_{1222}\underline{X}_{12}$
5	"	$\underline{X}_3$	$\Gamma_{1211}\underline{X}_3 + \Gamma_{2122}\underline{X}_{13}$
6	$-\lambda$	$\frac{1}{\sqrt{2}}(\underline{X}_6+\underline{X}_{11})$	$\Gamma_{1122}\underline{X}_6 + \Gamma_{2211}\underline{X}_{11}$
7	"	$\frac{1}{\sqrt{2}}(\underline{X}_7+\underline{X}_{10})$	$\Gamma_{1212}\underline{X}_7 + \Gamma_{2121}\underline{X}_{10}$
8	"	$\frac{1}{\sqrt{2}}(\underline{X}_8+\underline{X}_9)$	$\Gamma_{2112}\underline{X}_8 + \Gamma_{1221}\underline{X}_9$
9	$+\lambda$	$\frac{1}{\sqrt{2}}(\underline{X}_9-\underline{X}_8)$	$\Gamma_{2112}\underline{X}_8 + \Gamma_{1221}\underline{X}_9$
10	"	$\frac{1}{\sqrt{2}}(\underline{X}_{10}-\underline{X}_7)$	$\Gamma_{1212}\underline{X}_7 + \Gamma_{2121}\underline{X}_{10}$
11	"	$\frac{1}{\sqrt{2}}(\underline{X}_{11}-\underline{X}_6)$	$\Gamma_{1122}\underline{X}_6 + \Gamma_{2211}\underline{X}_{11}$
12	$+\sqrt{\lambda^2+4}$	$-\underline{X}_{14}$	$\Gamma_{1121}\underline{X}_4 + \Gamma_{2212}\underline{X}_{14}$
13	"	$-\underline{X}_{15}$	$\Gamma_{1112}\underline{X}_5 + \Gamma_{2221}\underline{X}_{15}$
14	"	$-\underline{X}_{12}$	$\Gamma_{2111}\underline{X}_2 + \Gamma_{1222}\underline{X}_{12}$
15	"	$-\underline{X}_{13}$	$\Gamma_{1211}\underline{X}_3 + \Gamma_{2122}\underline{X}_{13}$
16	$+\sqrt{\lambda^2+16}$	$-\underline{X}_{16}$	$\Gamma_{1111}\underline{X}_1 + \Gamma_{2222}\underline{X}_{16}$

Table 2.4: Eigenvectors of $h_o(\lambda)$ in terms of strong coupling eigenstates

	$\underline{Y}_1$	$\underline{Y}_2$	$\underline{Y}_3$	$\underline{Y}_4$	$\underline{Y}_5$	$\underline{Y}_6$	$\underline{Y}_7$	$\underline{Y}_8$	$\underline{Y}_9$	$\underline{Y}_{10}$	$\underline{Y}_{11}$	$\underline{Y}_{12}$	$\underline{Y}_{13}$	$\underline{Y}_{14}$	$\underline{Y}_{15}$	$\underline{Y}_{16}$
Energy	$-\sqrt{\lambda^2+16}$	$-\sqrt{\lambda^2+4}$				$-\lambda$			$+\lambda$			$+\sqrt{\lambda^2+4}$				$4\sqrt{\lambda^2+16}$
Normalization factor	$(\lambda^2+16)^{-\frac{1}{2}}$	$\frac{1}{2}(\lambda^2+4)^{-\frac{1}{2}}$				$\frac{1}{\sqrt{8}}$			$\frac{1}{\sqrt{8}}$			$\frac{1}{2}(\lambda^2+4)^{-\frac{1}{2}}$				$(\lambda^2+16)^{-\frac{1}{2}}$
S.C. limit	$\underline{X}_1$	$\underline{X}_4$	$\underline{X}_5$	$\underline{X}_2$	$\underline{X}_3$	$\frac{1}{\sqrt{2}}(\underline{X}_6+\underline{X}_{11})$	$\frac{1}{\sqrt{2}}(\underline{X}_7+\underline{X}_{10})$	$\frac{1}{\sqrt{2}}(\underline{X}_8+\underline{X}_9)$	$\frac{1}{\sqrt{2}}(\underline{X}_9-\underline{X}_8)$	$\frac{1}{\sqrt{2}}(\underline{X}_{10}-\underline{X}_7)$	$\frac{1}{\sqrt{2}}(\underline{X}_{11}-\underline{X}_6)$	$-\underline{X}_{14}$	$-\underline{X}_{15}$	$-\underline{X}_{11}$	$-\underline{X}_{13}$	$-\underline{X}_{16}$
Components	γ^{-1}	$\alpha/2$	$\alpha/2$	$\alpha/2$	$\alpha/2$	1	1	1	0	0	0	$-\alpha^{-1}$	α^{-1}	$-\alpha^{-1}$	$-\alpha^{-1}$	$-\gamma/4$
	$\gamma/4$	α^{-1}	$-\alpha^{-1}$	α^{-1}	α^{-1}	0	0	0	1	1	1	$\alpha/2$	$\alpha/2$	$\alpha/2$	$\alpha/2$	γ^{-1}
	$\gamma/4$	$-\alpha^{-1}$	α^{-1}	α^{-1}	α^{-1}	0	0	0	-1	-1	1	$-\alpha/2$	$-\alpha/2$	$\alpha/2$	$\alpha/2$	γ^{-1}
	γ^{-1}	$-\alpha/2$	$-\alpha/2$	$\alpha/2$	$\alpha/2$	1	-1	-1	0	0	0	α^{-1}	$-\alpha^{-1}$	$-\alpha^{-1}$	$-\alpha^{-1}$	$-\gamma/4$
	$\gamma/4$	α^{-1}	α^{-1}	α^{-1}	$-\alpha^{-1}$	0	0	0	-1	1	-1	$\alpha/2$	$-\alpha/2$	$\alpha/2$	$-\alpha/2$	γ^{-1}
	γ^{-1}	$\alpha/2$	$-\alpha/2$	$\alpha/2$	$-\alpha/2$	-1	1	-1	0	0	0	$-\alpha^{-1}$	$-\alpha^{-1}$	$-\alpha^{-1}$	α^{-1}	$-\gamma/4$
	γ^{-1}	$-\alpha/2$	$\alpha/2$	$\alpha/2$	$-\alpha/2$	-1	-1	1	0	0	0	α^{-1}	α^{-1}	$-\alpha^{-1}$	α^{-1}	$-\gamma/4$
	$\gamma/4$	$-\alpha^{-1}$	$-\alpha^{-1}$	α^{-1}	$-\alpha^{-1}$	0	0	0	1	-1	-1	$-\alpha/2$	$\alpha/2$	$\alpha/2$	$-\alpha/2$	γ^{-1}
	$\gamma/4$	α^{-1}	α^{-1}	$-\alpha^{-1}$	α^{-1}	0	0	0	1	-1	-1	$\alpha/2$	$-\alpha/2$	$-\alpha/2$	$\alpha/2$	γ^{-1}
	γ^{-1}	$\alpha/2$	$-\alpha/2$	$-\alpha/2$	$\alpha/2$	-1	-1	1	0	0	0	$-\alpha^{-1}$	$-\alpha^{-1}$	α^{-1}	$-\alpha^{-1}$	$-\gamma/4$
	γ^{-1}	$-\alpha/2$	$\alpha/2$	$-\alpha/2$	$\alpha/2$	-1	1	-1	0	0	0	α^{-1}	α^{-1}	α^{-1}	$-\alpha^{-1}$	$-\gamma/4$
	$\gamma/4$	$-\alpha^{-1}$	$-\alpha^{-1}$	$-\alpha^{-1}$	α^{-1}	0	0	0	-1	1	-1	$-\alpha/2$	$\alpha/2$	$-\alpha/2$	$\alpha/2$	γ^{-1}
	γ^{-1}	$\alpha/2$	$\alpha/2$	$-\alpha/2$	$-\alpha/2$	1	-1	-1	0	0	0	$-\alpha^{-1}$	α^{-1}	α^{-1}	α^{-1}	$-\gamma/4$
	$\gamma/4$	α^{-1}	$-\alpha^{-1}$	$-\alpha^{-1}$	$-\alpha^{-1}$	0	0	0	-1	-1	1	$\alpha/2$	$\alpha/2$	$-\alpha/2$	$-\alpha/2$	γ^{-1}
	$\gamma/4$	$-\alpha^{-1}$	α^{-1}	$-\alpha^{-1}$	$-\alpha^{-1}$	0	0	0	1	1	1	$-\alpha/2$	$-\alpha/2$	$-\alpha/2$	$-\alpha/2$	γ^{-1}
	γ^{-1}	$-\alpha/2$	$-\alpha/2$	$\alpha/2$	$-\alpha/2$	1	1	1	0	0	0	α^{-1}	$-\alpha^{-1}$	α^{-1}	α^{-1}	$-\gamma/4$

Table 2.5: Single plaquette eigenvectors $\underline{Y}_i$

$\gamma = (\sqrt{\lambda^2+16} - \lambda)^{\frac{1}{2}}$

$\alpha = (\sqrt{\lambda^2+4} + \lambda)^{\frac{1}{2}}$

$\varepsilon(\lambda)$	$-\sqrt{\lambda^2+16}$	$-\sqrt{\lambda^2+4}$	$-\lambda$	$+\lambda$	$+\sqrt{\lambda^2+4}$	$+\sqrt{\lambda^2+16}$
degeneracy(g_ε)	1	4	3	3	4	1
S.C. limit	-4	-2	0	0	2	4

Table 2.6: Energy structure of zero order plaquette states

and strong coupling limits are those of table 2.6. The dependence of the ε_i on λ is shown in figure 2.6. Note that the degeneracy of the six states whose strong coupling limits are zero has been partially lifted.

(d) Action of Perturbation Hamiltonian

The perturbation Hamiltonian $H' = \sum_{n \text{ odd}} PQRS$ may be expressed in the basis (2.24). The four even plaquette operators then become the diagonal matrices

$$\begin{aligned} P &= \text{Diag}(I_2, -I_2, I_2, -I_2, I_2, -I_2, I_2, -I_2) \\ Q &= \text{Diag}(\sigma_3, \sigma_3, \sigma_3, \sigma_3, \sigma_3, \sigma_3, \sigma_3, \sigma_3) \\ R &= \text{Diag}(I_8, -I_8) \\ S &= \text{Diag}(I_4, -I_4, I_4, -I_4). \end{aligned} \tag{2.71}$$

Since each matrix is real and symmetric the corresponding operator is Hermitian. The corresponding matrix for H' is a sum of diagonal real matrices and therefore is also Hermitian. The action of these operators on the eigenvectors of $h_o(\lambda)$ is given in terms of the coefficients

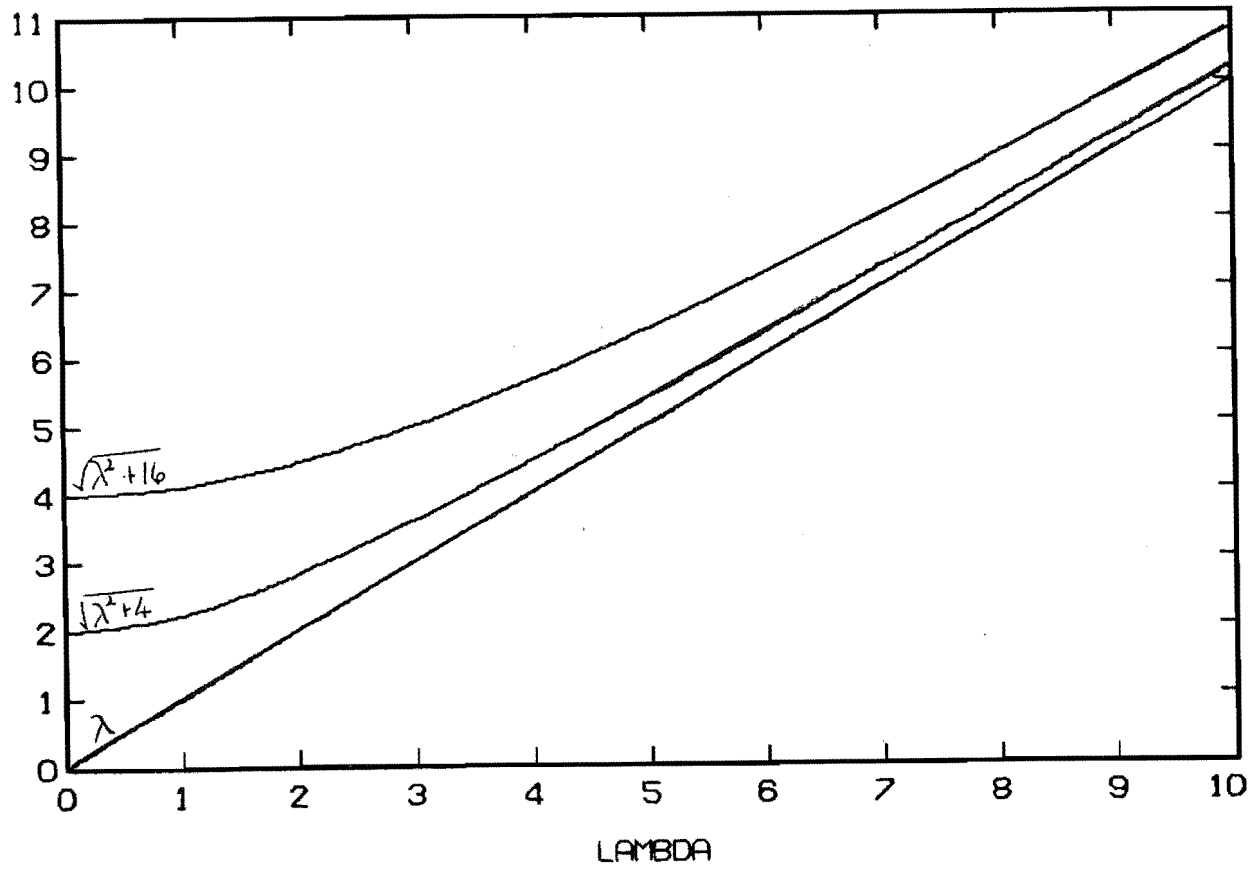

Figure 2.6: The dependence of the energies ε_i on λ.

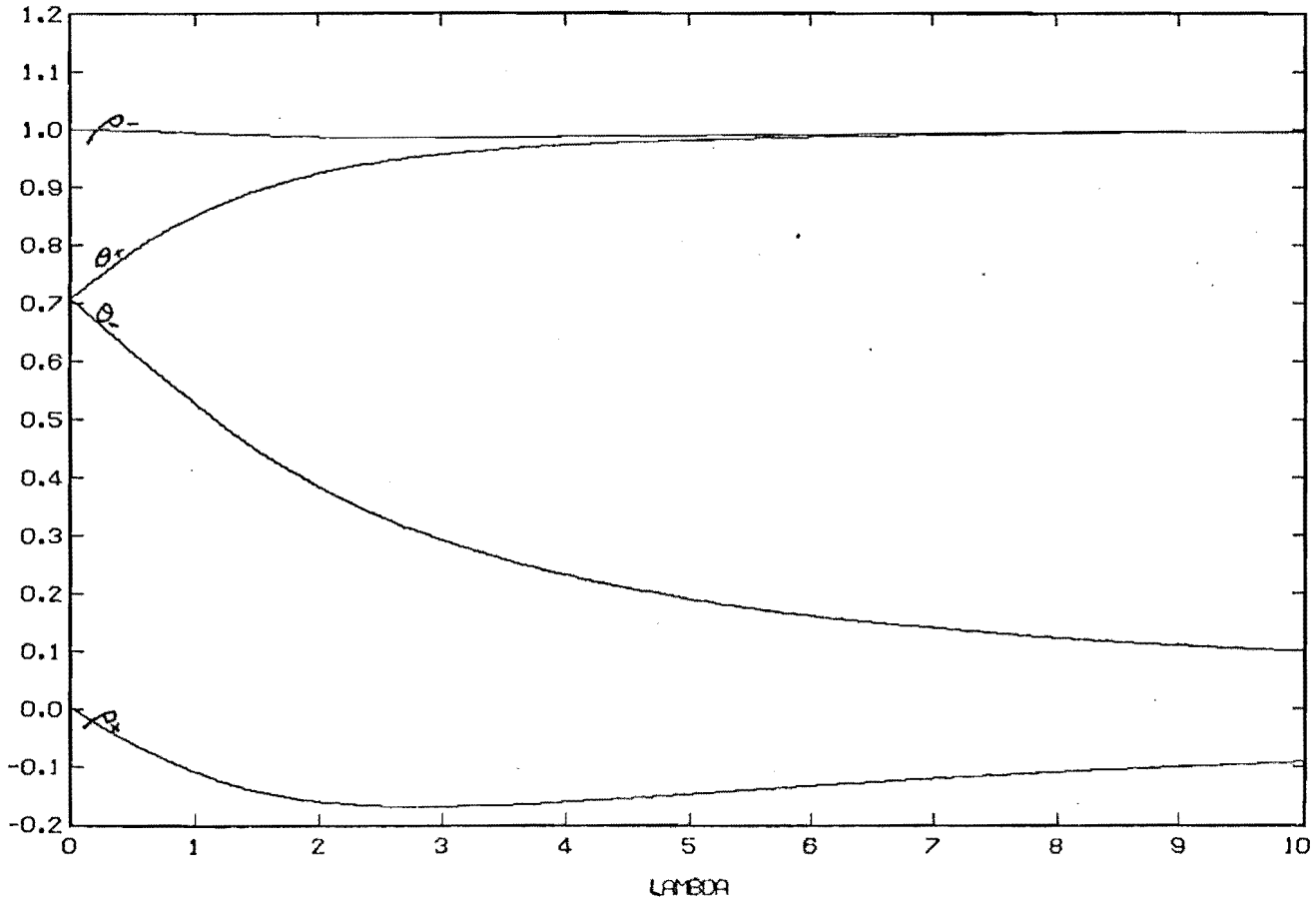

Figure 2.7: The dependence of the coefficients $\rho_{\pm}$, $\theta_{\pm}$ (equations 2.73) on λ.

$$
\begin{aligned}
p_{ij} &= \sum_{j=1}^{16} \underline{Y}_j^T P \underline{Y}_i \\
q_{ij} &= \sum_{j=1}^{16} \underline{Y}_j^T Q \underline{Y}_i \\
r_{ij} &= \sum_{j=1}^{16} \underline{Y}_j^T R \underline{Y}_i \\
s_{ij} &= \sum_{j=1}^{16} \underline{Y}_j^T S \underline{Y}_i
\end{aligned}
\tag{2.72}
$$

which may be obtained from the eigenvectors of table 2.4 or, in terms of the Γ, from table 2.6. The results of this procedure are given in tables 2.7a-d which have several noteworthy features. Only two non-zero entries, corresponding to single plaquette energies ε_j (ε_i) of equal magnitude and opposite sign, occur in any row (column).

Within the subspace E_ε corresponding to each single plaquette energy ε any g_ε orthonormal vectors may be chosen as a basis provided that they span E_ε. The basis choice of equation (2.56) minimizes the number of non-zero coefficients in equation (2.72) and ensures that no state is connected by H' to more than one member of any degenerate subspace. This considerably simplifies the calculation of the matrix elements of H' in the perturbation series of the next chapter. Other methods of solving the eigenvalue problem of equation (2.55) will not automatically produce the correct basis choice for each E_ε. The matrices are symmetric and real. All diagonal entries are zero and none of the $\underline{Y}_j$ belong to the degenerate subspace containing $\underline{Y}_i$. Only four different coefficients appear, namely

Tables 2.7(a-d): Matrices of coefficients p_{ij} etc (equation 2.72) The coefficients $\theta_{\pm}, \rho_{\pm}$ are defined in equations 2.73.

	Y_1	Y_2	Y_3	Y_4	Y_5	Y_6	Y_7	Y_8	Y_9	Y_{10}	Y_{11}	Y_{12}	Y_{13}	Y_{14}	Y_{15}	Y_{16}
Y_1		ρ_-										ρ_+				
Y_2	ρ_-															ρ_+
Y_3						θ_+					$-\theta_-$					
Y_4							θ_+			θ_-						
Y_5								θ_+	θ_-							
Y_6			θ_+										θ_-			
Y_7				θ_+										θ_-		
Y_8					θ_+										θ_-	
Y_9					θ_-										$-\theta_+$	
Y_{10}				θ_-										$-\theta_+$		
Y_{11}			$-\theta_-$										θ_+			
Y_{12}	ρ_+															$-\rho_-$
Y_{13}						θ_-					θ_+					
Y_{14}							θ_-			$-\theta_+$						
Y_{15}								θ_-	$-\theta_+$							
Y_{16}		ρ_+										$-\rho_-$				

Table 2.7a: Action of P on single plaquette states Y_i.

	Y_1	Y_2	Y_3	Y_4	Y_5	Y_6	Y_7	Y_8	Y_9	Y_{10}	Y_{11}	Y_{12}	Y_{13}	Y_{14}	Y_{15}	Y_{16}
Y_1			ρ_-										ρ_+			
Y_2						θ_+					$-\theta_-$					
Y_3	ρ_-															ρ_+
Y_4								θ_+	$-\theta_-$							
Y_5							θ_+			$-\theta_-$						
Y_6		θ_+										θ_-				
Y_7					θ_+										θ_-	
Y_8				θ_+										θ_-		
Y_9			$-\theta_-$											θ_+		
Y_{10}					$-\theta_-$										θ_+	
Y_{11}		$-\theta_-$										θ_+				
Y_{12}						θ_-					θ_+					
Y_{13}	ρ_+															$-\rho_-$
Y_{14}								θ_-	θ_+							
Y_{15}							θ_-			θ_+						
Y_{16}		ρ_+											$-\rho_-$			

Table 2.7b: Action of Q on single plaquette states Y_i.

	Y_1	Y_2	Y_3	Y_4	Y_5	Y_6	Y_7	Y_8	Y_9	Y_{10}	Y_{11}	Y_{12}	Y_{13}	Y_{14}	Y_{15}	Y_{16}
Y_1				ρ_-										ρ_+		
Y_2							θ_+			θ_-						
Y_3								θ_+	$-\theta_-$							
Y_4	ρ_-															ρ_+
Y_5						θ_+					θ_-					
Y_6					θ_+										θ_-	
Y_7		θ_+										θ_-				
Y_8			θ_+										θ_-			
Y_9			$-\theta_-$										θ_+			
Y_{10}		θ_-										$-\theta_+$				
Y_{11}					θ_-										$-\theta_+$	
Y_{12}						θ_-			$-\theta_+$							
Y_{13}								θ_-	θ_+							
Y_{14}	ρ_+															$-\rho_-$
Y_{15}						θ_-					$-\theta_+$					
Y_{16}				ρ_+										$-\rho_-$		

Table 2.7c: Action of R on single plaquette states Y_i.

	Y_1	Y_2	Y_3	Y_4	Y_5	Y_6	Y_7	Y_8	Y_9	Y_{10}	Y_{11}	Y_{12}	Y_{13}	Y_{14}	Y_{15}	Y_{16}
Y_1					ρ_-										ρ_+	
Y_2								θ_+	θ_-							
Y_3							θ_+			$-\theta_-$						
Y_4						θ_+					θ_-					
Y_5	ρ_-															ρ_+
Y_6				θ_+										θ_-		
Y_7			θ_+										θ_-			
Y_8		θ_+										θ_-				
Y_9		θ_-										$-\theta_+$				
Y_{10}			$-\theta_-$										θ_+			
Y_{11}				θ_-										$-\theta_+$		
Y_{12}								θ_-	$-\theta_+$							
Y_{13}							θ_-			θ_+						
Y_{14}						$\theta-$					$-\theta_+$					
Y_{15}	ρ_+															$-\rho_-$
Y_{16}					ρ_+										$-\rho_-$	

Table 2.7d: Action of S on single plaquette states Y_i.

$$\rho_{\pm} = [(\lambda^2+16)(\lambda^2+4)]^{-\frac{1}{4}}[(\sqrt{\lambda^2+16} - \lambda)(\sqrt{\lambda^2+4} \pm \lambda)]^{-\frac{1}{2}}$$

$$[4 \mp\tfrac{1}{2}(\sqrt{\lambda^2+16} - \lambda)(\sqrt{\lambda^2+4} \pm \lambda)] \qquad (2.73a)$$

$$\theta_{\pm} = \frac{2}{\sqrt{8}} (\lambda^2+4)^{-\frac{1}{4}}(\sqrt{\lambda^2+4} \pm \lambda)^{\frac{1}{2}} . \qquad (2.73b)$$

The dependence of these coefficients on λ is shown in figure 2.7.

The relations $P^2 = Q^2 = R^2 = S^2 = I$ imply relations

$$\rho_{\pm}^2 = \theta_{\pm}^2 = 1 \qquad (2.74)$$

which are satisfied by equations (2.73).

(e) Gauge Invariance

The generator of local gauge transformations, equation (2.21), in the representation of equation (2.24) is

$$G(\underline{n}) = G^{+}(\underline{n}) = G^{-1}(\underline{n}) = \otimes \prod_{i\varepsilon\underline{n}} \sigma_1(\underline{n},i) \qquad (2.75)$$

which flips the spins on all links attached to site $\underline{n}$. Any arbitrary gauge transformation may be constructed from the $G(\underline{n})$. The Hamiltonian is required to satisfy the invariance condition equation (2.22) and physical states are to be identified as those satisfying equation (2.23). The effect of equation (2.75) is to flip pairs of spins on each of two nearest neighbour even plaquettes as indicated in figure 2.8.

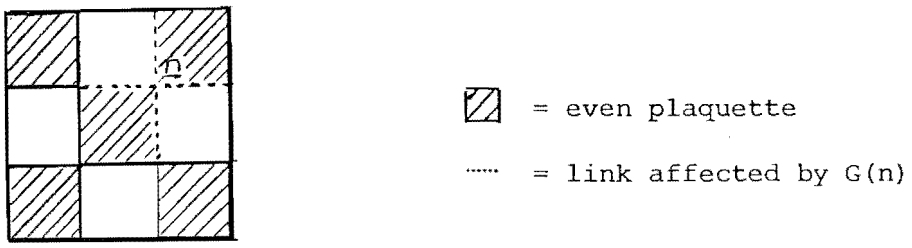

Figure 2.8: Action of local gauge transformation.

The effects of local gauge transformations at the four corners of an even plaquette $\underline{n}$ are

$$
\begin{aligned}
G(\underline{n}) &= \sigma_1(\underline{n},\mu) \otimes I_2(\underline{n}+\mu,\nu) \otimes I_2(\underline{n}+\mu+\nu,-\mu) \\
&\quad \otimes \sigma_1(\underline{n}+\nu,-\nu) \\
G(\underline{n}+\mu) &= \sigma_1(\underline{n},\mu) \otimes \sigma_1(\underline{n}+\mu,\nu) \otimes I_2(\underline{n}+\mu+\nu,-\mu) \\
&\quad \otimes I_2(\underline{n}+\nu,-\nu) \qquad (2.76) \\
G(\underline{n}+\mu+\nu) &= I_2(\underline{n},\mu) \otimes \sigma_1(\underline{n}+\mu,\nu) \otimes \sigma_1(\underline{n}+\mu+\nu,-\mu) \\
&\quad \otimes I_2(\underline{n}+\nu,-\nu) \\
G(\underline{n}+\nu) &= I_2(\underline{n},\mu) \otimes I_2(\underline{n}+\mu,\nu) \otimes \sigma_1(\underline{n}+\mu+\nu,-\mu) \\
&\quad \otimes \sigma_1(\underline{n}+\nu,-\nu) \ .
\end{aligned}
$$

The Hamiltonian has been written as a sum over even plaquettes of even plaquette operators. Each term in this sum will be affected by transformations (2.75) at only four sites. For all other sites the σ_1,σ_3 matrices associated with the gauge transformation and the Hamiltonian act on sets of links with no common members and hence commute,

satisfying equation (2.22) trivially. Substitution of equations (2.76) confirms that the required invariance is also obtained for gauge transformations at the remaining four sites.

The gauge invariance of the single plaquette states $\underline{Y}_i$ is treated similarly. The condition (2.23) becomes

$$G(\underline{n})\underline{Y}_i = \underline{Y}_i \qquad \forall \quad \underline{n} \tag{2.77}$$

which is again trivially satisfied when $\underline{Y}_i$ contains no link attached to $\underline{n}$. The results for the remaining cases $G\underline{Y}_i = \pm\underline{Y}_i$ are summarized in table 2.8. Only the states $\underline{Y}_1$ and $\underline{Y}_{16}$ are invariant under gauge transformations at any site. Each column in table 2.8 occurs twice. There are thus two eigenvectors, one of positive and one of negative energy, which behave in the same way under the action of the gauge transformation (2.75). These pairs (e.g. $\underline{Y}_2$ and $\underline{Y}_{12}$) correspond to the pairs of non-zero entries in tables 2.7. This means that states produced by the action of the perturbation Hamiltonian H' will have identical gauge transformation properties.

(f) Comparison With Conventional Strong Coupling Method

The single plaquette eigenstates for the zero order term in the conventional Hamiltonian (2.27) are the $\underline{X}_i$ of table 2.2. The action of the perturbation part of equation (2.27) $H'_c = \sum_{\text{all } \underline{p}} \sigma_3\sigma_3\sigma_3\sigma_3$ is

	Y_1	Y_2	Y_3	Y_4	Y_5	Y_6	Y_7	Y_8	Y_9	Y_{10}	Y_{11}	Y_{12}	Y_{13}	Y_{14}	Y_{15}	Y_{16}
ε	$-\sqrt{\lambda^2+16}$	$-\sqrt{\lambda^2+4}$				$-\lambda$			$+\lambda$			$+\sqrt{\lambda^2+4}$				$+\sqrt{\lambda^2+16}$
$G(\underline{n})$	+	+	−	−	+	−	−	+	+	−	−	+	−	−	+	+
$G(\underline{n}+\mu)$	+	+	+	−	−	+	−	−	−	−	+	+	+	−	−	+
$G(\underline{n}+\nu)$	+	−	−	+	+	+	−	−	−	−	+	−	−	+	+	+
$G(\underline{n}+\mu+\nu)$	+	−	+	+	−	−	−	+	+	−	−	−	+	+	−	+

Table 2.8: Gauge invariance of the single plaquette eigenstates.

X_i	X_1	X_2	X_3	X_4	X_5	X_6	X_7	X_8	X_9	X_{10}	X_{11}	X_{12}	X_{13}	X_{14}	X_{15}	X_{16}
ε	-4	-2	-2	-2	-2	0	0	0	0	0	0	2	2	2	2	4
X_1																1
X_2															1	
X_3														1		
X_4													1			
X_5												1				
X_6											1					
X_7										1						
X_8									1							
X_9								1								
X_{10}							1									
X_{11}						1										
X_{12}					1											
X_{13}				1												
X_{14}			1													
X_{15}		1														
X_{16}	1															

Table 2.9: Action of H'_c on Strong Coupling eigenstates $\underline{X}_i$.

$$H'_C \underline{X}_i = \sum_{j=1}^{16} \alpha_{ij} \underline{X}_j = \underline{X}_{\bar{i}} \qquad (2.78)$$

where the spins on each link have been flipped. The analogue of equations (2.72) gives the α_{ij} shown in table 2.9. Like tables 2.7 the matrix is real, symmetric and has normalized rows and columns. Each column has a single entry $\alpha_{ij} = \delta_{i\bar{j}}$ and H'_C only connects states where $|\varepsilon_i| = |\varepsilon_j|$.

In this chapter the Hamiltonian for Z(2) Lattice Gauge Theory in (2+1) dimensions has been reformulated so that half of the conventional perturbation term has been included in the zero-order terms. The problem of finding the eigenvalues and eigenvectors of the zero-order Hamiltonian is more complicated than for the conventional case but may be solved in terms of even plaquette states. The single plaquette eigenstates $\underline{Y}_i$ so obtained may be written as linear combinations of pairs of the eigenstates $\underline{X}_i$ of the conventional zero order problem. The relative proportions of the linear combination depend on λ through the relations

$$\underline{Y}_i^{(\varepsilon)}(\lambda) = \frac{1}{\sqrt{K_C}} [\Gamma_\gamma^{(\varepsilon)}(\lambda)\underline{X}_\ell + \Gamma_{\bar{\ell}}^{(\varepsilon)}(\lambda)\underline{X}_{\bar{\ell}}] \qquad (2.80)$$

where

$$H'_C \underline{X}_\ell = \underline{X}_{\bar{\ell}} .$$

The Gauge invariance of the Hamiltonian is retained. The eigenvalues and eigenvectors of the reformulated Hamiltonian reduce to those of the conventional Hamiltonian in the strong coupling limit. The action of the reformulated perturbation

on the eigenstates of the reformulated zero order Hamiltonian has been determined.

In the next chapter perturbation expansions for the energies of the states of the full Hamiltonian will be developed.

CHAPTER 3

PERTURBATION EXPANSIONS

In the previous chapter the Hamiltonian for Z(2) lattice gauge theory was written in terms of operators acting on even and odd plaquettes. A zero order Hamiltonian $H_o(\lambda)$, involving only even plaquette operators, was defined and its eigenstates and their energies were calculated. These tend towards their strong coupling counterparts as $\lambda \to 0$. The odd plaquette operators form the perturbation Hamiltonian and may be rewritten in terms of even plaquette operators. In this chapter perturbative methods for calculating the eigenvalues of the full Hamiltonian as series in the parameter λ are presented.

The eigenstates of the zero-order Hamiltonian $H_o(\lambda)$ are discussed in section 3.1 while section 3.2 introduces the Brillouin-Wigner perturbation series for the energies of the corresponding states of the full Hamiltonian equation (2.41). A method for evaluating the matrix elements which appear in this series in terms of contributions from individual plaquettes is given in section 3.3. Diagrammatic methods for enumerating and evaluating the matrix elements in terms of equivalent plaquettes are the subjects of sections 3.4 and 3.5 respectively.

3.1 ZERO-ORDER EIGENSTATES

The eigenstates for the single-plaquette zero-order problem were obtained in the previous chapter and are listed in tables 2.4 and 2.5. The eigenstates $|\Psi\rangle$ of the total lattice zero-order Hamiltonian H_o are related to these by equation (2.42) and will serve as the zero-order contributions for the perturbation expansions of the next section. In order to obtain the mass gap it is necessary to calculate both the vacuum state and the excited state of lowest energy. The restriction to physical states resulting from the gauge invariance condition of equation (2.23) greatly reduces the number of lattice states which may be constructed from the single plaquette states $\underline{Y}_i$.

(a) Vacuum State

The single-plaquette eigenstate of lowest energy is $\underline{Y}_1$ which is invariant under local gauge transformations, given by equation (2.21), at any site. The lattice state of lowest energy, which is identified as the zero-order vacuum state, is thus

$$|0\rangle = \otimes \prod_{\underline{p} \text{ even}} |\underline{Y}_1\rangle \quad . \tag{3.1}$$

The vacuum is therefore non-degenerate and, since the $\underline{Y}_i$ are normalized, the normalization condition $\langle 0|0\rangle = 1$ is satisfied. The zero order vacuum energy has a contribution of ε_1 from each of the N even plaquettes and is thus

$$E^{(0)}_{|0>} = N\varepsilon_1 = -N\sqrt{\lambda^2+16} \quad . \tag{3.2}$$

(b) Y16 State

The single plaquette state $\underline{Y}_{16}$ has the same gauge invariance properties as $\underline{Y}_1$ as may be seen from table 2.8. Another low energy physical eigenstate of $H_o(\lambda)$ therefore consists of a single even plaquette in state $\underline{Y}_{16}$ with the remainder in state $\underline{Y}_1$. Such a state has an N-fold degeneracy since the single excited plaquette may be located on any one of the N even plaquettes. The usual procedure (e.g. Kogut 1979b) is to define the zero momentum state

$$|\square> = \frac{1}{\sqrt{N}} \sum_{\underline{n}\ \text{even}} \otimes_{\underline{p}\ \text{even}} \prod [\delta_{\underline{n},\underline{p}} |\underline{Y}_{16}> + (1-\delta_{\underline{n},\underline{p}})|\underline{Y}_1> \tag{3.3}$$

which satisfies the normalization condition $<\square|\square> = 1$. The zero-order energy of this state is

$$E^{(0)}_{|\square>} = (N-1)\varepsilon_1 + \varepsilon_{16} = -(N-2)\sqrt{\lambda^2+16} \quad . \tag{3.4}$$

(c) Cross State

The perturbation Hamiltonian $H'(\underline{m})$ acting on the vacuum state of equation (3.1) produces a "cross" consisting of excited states on the four even plaquettes sharing links with odd plaquette $\underline{m}$. There are 16 possible physical states of this type for a given $\underline{m}$ since each of the excited plaquettes may be in one of two excited states.

The one having the lowest energy consists of the four excited states $\underline{Y}_2, \underline{Y}_3, \underline{Y}_4, \underline{Y}_5$ as shown in figure 3.1. All 16 are invariant under equation (2.21) at any site.

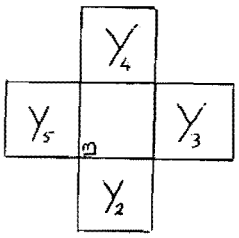

Figure 3.1: The lowest energy cross state.

This state is also N-fold degenerate as it may be centred on any of N odd plaquettes. The "lower cross state" or simply "cross state" is defined as the zero-momentum combination

$$|+\rangle = \frac{1}{\sqrt{N}} \sum_{\underline{m}\ \text{odd}} \otimes \prod_{\underline{p}\ \text{even}} \{[1-(\delta_{\underline{p},\underline{m}-\nu} + \delta_{\underline{p},\underline{m}+\nu} + \delta_{\underline{p},\underline{m}+\nu} + \delta_{\underline{p},\underline{m}-\mu})]|\underline{Y}_1\rangle + \delta_{\underline{p},\underline{m}-\nu}|\underline{Y}_2\rangle + \delta_{\underline{p},\underline{m}+\mu}|\underline{Y}_3\rangle + \delta_{\underline{p},\underline{m}+\nu}|\underline{Y}_4\rangle + \delta_{\underline{p},\underline{m}-\mu}|\underline{Y}_5\rangle\}. \qquad (3.5)$$

This state is also normalized so that $\langle +|+\rangle = 1$ and has zero-order energy

$$E^{(0)}_{|+\rangle} = (N-4)\varepsilon_1 + \varepsilon_2 + \varepsilon_3 + \varepsilon_4 + \varepsilon_5$$

$$= (N-4)\sqrt{\lambda^2+16} - 4\sqrt{\lambda^2+4} \quad . \qquad (3.6)$$

(d) Other States

Table 2.8 may be used to construct a wide variety of states. Some examples are shown in figures 3.2

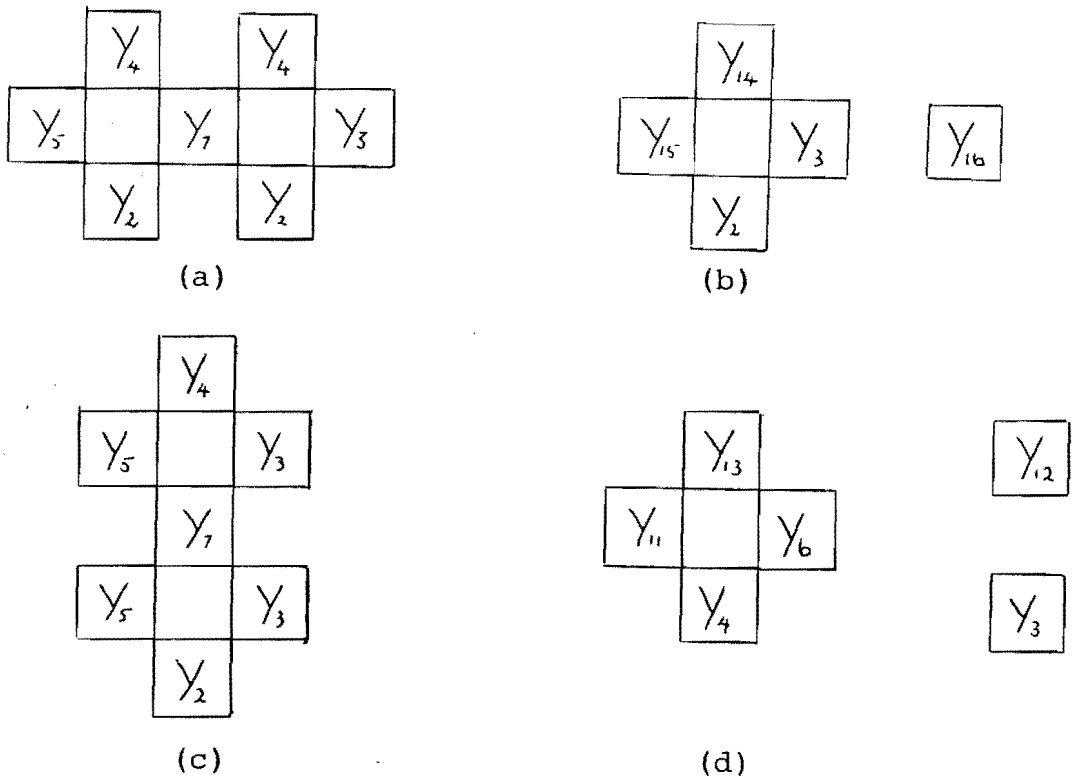

Figure 3.2: Higher energy eigenstates of H_o.

The zero-order energies for the states illustrated in figures 3.2a and 3.2c are $-(N-7)\sqrt{\lambda^2+16} - 6\sqrt{\lambda^2+4} - \lambda$, while those for the states of figures 3.2b and 3.2d are $-(N-6)\sqrt{\lambda^2+16}$. Note that the state of figure 3.2d is not a physical state, as may be confirmed from table 2.8. All four have zero-order energies which are higher than those of the $|+\rangle$ and $|\square\rangle$ states. The degeneracies of these states are greater than those of the $|+\rangle$ and $|\square\rangle$ states because of "rotational" degeneracy (figures 3.2 a,c) or because they consist of more than one group of excited plaquettes (figures 3.2b,d). The state suggested by figure 3.2b consists of a (non-lower)

cross and a single $\underline{Y}_{16}$ which are spatially separated and is thus N(N-4) fold degenerate. Rotational degeneracy will be considered further in section 3.4. It is also possible to define states which may be identified as strings. These are the subject of chapter 6.

3.2 BRILLOUIN-WIGNER PERTURBATION THEORY

The Brillouin-Wigner formulation of perturbation theory (Baym 1969) is a convenient method for obtaining the formulas of Raleigh-Schrodinger perturbation theory, particularly for higher order terms. These formulas allow the energy of an eigenstate $|\Psi>$ of the full Hamiltonian to be written as the power series in λ

$$E_{|\Psi>} = \varepsilon^{(0)} + \varepsilon^{(1)}\lambda + \varepsilon^{(2)}\lambda^2 + \varepsilon^{(3)}\lambda^3 + \varepsilon^{(4)}\lambda^4 + \varepsilon^{(5)}\lambda^5 + \ldots \quad (3.7)$$

The coefficients of this series up to fifth order are

$$\varepsilon^{(0)} = <\Psi|H_o|\Psi> , \quad (3.8a)$$

$$\varepsilon^{(1)} = <\Psi|H'|\Psi> , \quad (3.8b)$$

$$\varepsilon^{(2)} = <\Psi|H' \frac{Q_o}{a} H'|\Psi> , \quad (3.8c)$$

$$\varepsilon^{(3)} = <\Psi|H' \frac{Q_o}{a} H' \frac{Q_o}{a} H'|\Psi> - <\Psi|H'|\Psi><\Psi|H' \frac{Q_o}{a^2} H'|\Psi> , \quad (3.8d)$$

$$\varepsilon^{(4)} = \langle\Psi|H'\frac{Q_o}{a}H'\frac{Q_o}{a}H'\frac{Q_o}{a}H'|\Psi\rangle$$

$$- \langle\Psi|H'\frac{Q_o}{a^2}H'|\Psi\rangle\langle\Psi|H'\frac{Q_o}{a}H'|\Psi\rangle$$

$$+ \langle\Psi|H'|\Psi\rangle\langle\Psi|H'|\Psi\rangle\langle\Psi|H'\frac{Q_o}{a^3}H'|\Psi\rangle \qquad (3.8e)$$

$$- \langle\Psi|H'|\Psi\rangle\langle\Psi|\left(H'\frac{Q_o}{a}H'\frac{Q_o}{a^2}H' + H'\frac{Q_o}{a^2}H'\frac{Q_o}{a}H'\right)|\Psi\rangle \ ,$$

$$\varepsilon^{(5)} = \langle\Psi|H'\frac{Q_o}{a}H'\frac{Q_o}{a}H'\frac{Q_o}{a}H'\frac{Q_o}{a}H'|\Psi\rangle \qquad (3.8f)$$

$$- \langle\Psi|H'|\Psi\rangle\langle\Psi|\left(H'\frac{Q_o}{a}H'\frac{Q_o}{a}H'\frac{Q_o}{a^2}H'\right.$$

$$\left. + H'\frac{Q_o}{a}H'\frac{Q_o}{a^2}H'\frac{Q_o}{a}H' + H'\frac{Q_o}{a^2}H'\frac{Q_o}{a}H'\frac{Q_o}{a}H'\right)|\Psi\rangle$$

$$- \langle\Psi|H'\frac{Q_o}{a}H'|\Psi\rangle\langle\Psi|\left(H'\frac{Q_o}{a}H'\frac{Q_o}{a^2}H'\right.$$

$$\left. + H'\frac{Q_o}{a^2}H'\frac{Q_o}{a}H'\right)|\Psi\rangle$$

$$- \langle\Psi|H'\frac{Q_o}{a}H'\frac{Q_o}{a}H'|\Psi\rangle\langle\Psi|H'\frac{Q_o}{a^2}H'|\Psi\rangle$$

$$+ \langle\Psi|H'|\Psi\rangle\langle\Psi|H'|\Psi\rangle\langle\Psi|\left(H'\frac{Q_o}{a}H'\frac{Q_o}{a^3}H'\right.$$

$$\left. + H'\frac{Q_o}{a^3}H'\frac{Q_o}{a}H' + H'\frac{Q_o}{a^2}H'\frac{Q_o}{a^2}H'\right)|\Psi\rangle$$

$$+ 2\langle\Psi|H'|\Psi\rangle\langle\Psi|H'\frac{Q_o}{a}H'|\Psi\rangle\langle\Psi|H'\frac{Q_o}{a^3}H'|\Psi\rangle$$

$$+ \langle\Psi|H'|\Psi\rangle\langle\Psi|H'\frac{Q_o}{a^2}H'|\Psi\rangle\langle\Psi|H'\frac{Q_o}{a^2}H'|\Psi\rangle$$

$$- \langle\Psi|H'|\Psi\rangle\langle\Psi|H'|\Psi\rangle\langle\Psi|H'|\Psi\rangle\langle\Psi|H'\frac{Q_o}{a^4}H'|\Psi\rangle \ .$$

The operator $\frac{Q_o}{a}$ consists of the idempotent projector

$$Q_o = 1 - |\Psi><\Psi| \tag{3.9}$$

and the energy denominator

$$a^{-1} = \frac{1}{\varepsilon^{(0)} - H_o} \tag{3.10}$$

which involves the zero order energies of the initial and intermediate states. The projector Q_o thus projects out those terms which would have a vanishing denominator. These formulas apply to the case where $|\Psi>$ is non-degenerate.

In order to obtain the mass gap the series (3.7) must be evaluated for the vacuum and first excited states. One difference between the conventional strong coupling series (e.g. Kogut 1979b) and the present case is immediately apparent: in the latter the energy denominators are functions of λ whereas in the former this is not the case.

3.3 INDIVIDUAL PLAQUETTE METHOD OF MATRIX ELEMENT EVALUATION

In order to evaluate the matrix elements contributing to the coefficients given by equations (3.8) the effect of the perturbation Hamiltonian, equation (2.37), on a given state must be calculated. The contribution to H' from the odd plaquette $\underline{n}$ is given by $H'(\underline{n})$, which affects only the four even plaquettes bordering $\underline{n}$. Its action may be written using equations (2.40) and (2.42) as

$$H'(\underline{n})\,|\Psi\rangle = \cdots I_{16} \otimes P(\underline{n}-\nu) \otimes Q(\underline{n}+\mu) \otimes R(\underline{n}+\nu)$$

$$S(\underline{n}-\mu) \otimes I_{16}$$

$$\cdots \otimes \prod_{\underline{p}\ \text{even}} |Y_i\rangle_1 \cdots$$

$$|Y_j\rangle_{\underline{n}-\nu} |Y_k\rangle_{\underline{n}+\mu} |Y_\ell\rangle_{\underline{n}+\nu} |Y_m\rangle_{\underline{n}-\nu} \cdots |Y_z\rangle_N$$

$$= \sum_{a=0}^{16} \sum_{b=0}^{16} \sum_{c=0}^{16} \sum_{d=0}^{16} p_{ja}\, q_{kb}\, r_{\ell c}\, s_{md} \otimes \prod_{\underline{p}\ \text{even}} |Y_i\rangle_1$$

$$\cdots |Y_a\rangle_{\underline{n}-\nu} |Y_b\rangle_{\underline{n}+\mu} |Y_c\rangle_{\underline{n}+\nu} |Y_d\rangle_{\underline{n}-\mu} \cdots |Y_z\rangle_N \qquad (3.11)$$

where the p,q,r,s are given in tables 2.7 a-d. Successive actions of H' may be treated in this manner. Note that, since tables 2.7 contain no non-zero diagonal elements, $\sum_{\underline{n}} \langle\Psi|H'(\underline{n})|\Psi\rangle = \varepsilon^{(1)} = 0$ for all states. The properties of these tables lead to the stronger relation

$$\varepsilon^{(2k+1)} = 0 \quad : \quad k = 0,1,2, \ldots . \qquad (3.12)$$

In order to evaluate the matrix element, the possible intermediate states and their energy denominators must be calculated. Repeated use of equation (3.11) allows these to be calculated in terms of the contributions from individual even plaquettes. Consider the case of the second order vacuum energy, which is given by

$$\varepsilon^{(2)}_{|0\rangle} = \sum_{\underline{n}_2} \sum_{\underline{n}_1} \langle 0|H'(\underline{n}_2)\, \frac{Q_o}{a}\, H'(\underline{n}_1)|0\rangle \ , \qquad (3.13)$$

where the vacuum state $|0\rangle$ is that defined in equation (3.1). The intermediate states obtained from equation (3.11) are

$$H'(\underline{n}_1)|0\rangle = \sum_{abcd=0}^{16} p_{1a}\, q_{1b}\, r_{1c}\, s_{1d}$$

$$\otimes \prod_{\underline{p}\ \text{even}} |Y_1\rangle \cdots |Y_a\rangle_{\underline{n}-\nu} |Y_b\rangle_{\underline{n}+\mu} |Y_c\rangle_{\underline{n}+\nu} |Y_d\rangle_{\underline{n}-\mu} \cdots Y_1\rangle \ . \tag{3.14}$$

These states consist of a single cross of excited plaquettes with the remainder in the $\underline{Y}_1$ state so their energies are given by

$$\varepsilon^{(0)}_{|0\rangle} - \varepsilon_{abcd} = -N\sqrt{\lambda^2+16} - [-(N-4)\sqrt{\lambda^2+16}$$

$$-(\varepsilon_a + \varepsilon_b + \varepsilon_c + \varepsilon_d)] \ . \tag{3.15}$$

If $\varepsilon^{(2)}_{|0\rangle}$ is to be non-zero the $H'(\underline{n}_2)$ must act on the intermediate states of equation (3.14) by returning them to the vacuum state. This implies the requirement

$$\underline{n}_2 = \underline{n}_1 \tag{3.16}$$

which may be used to write

$$\varepsilon^{(2)}_{|0\rangle} = \sum_{\underline{n}_2} \sum_{\underline{n}_1} \delta_{\underline{n}_1\underline{n}_2} \langle 0|H'(\underline{n}_2) \frac{Q_o}{a} H'(\underline{n}_1)|0\rangle$$

$$= N \sum_{a,b,c,d=0}^{16} \frac{(p_{1a}\, q_{1b}\, r_{1c}\, s_{1d})^2}{-4\sqrt{\lambda^2+16} + (\varepsilon_a + \varepsilon_b + \varepsilon_c + \varepsilon_d)} \ . \tag{3.17}$$

The intermediate states are specified by the indices a,b,c,d which label the states of the four even plaquettes excited

by $H'(\underline{n}_1)$. Tables 2.6 and 2.7 and contain the information needed to evaluate equation (3.17). The "counting factor" N appearing in equation (3.17) records the number of ways equation (3.16) may be satisfied.

This method rapidly becomes unwieldy. For example the condition analogous to equation (3.16) for the fourth order vacuum contribution

$$\varepsilon^{(4)}_{|0>} = \sum_{\underline{n}_4} \sum_{\underline{n}_3} \sum_{\underline{n}_2} \sum_{\underline{n}_1} <0| H'(\underline{n}_4) \frac{Q_o}{a} H'(\underline{n}_3) \frac{Q_o}{a} H'(\underline{n}_2) \frac{Q_o}{a} H'(\underline{n}_1) |0> \tag{3.18}$$

is

$$\delta_{\underline{n}_1 \underline{n}_2} + \delta_{\underline{n}_1 \underline{n}_3} + \delta_{\underline{n}_1 \underline{n}_4} + \delta_{\underline{n}_2 \underline{n}_3} + \delta_{\underline{n}_2 \underline{n}_4} + \delta_{\underline{n}_3 \underline{n}_4} \neq 0. \tag{3.19}$$

The individual plaquette treatment leads to the proliferation of p,q,r,s coefficients and lengthy expressions for the energy denominators. The zero-momentum excited states complicate matters further. Consider the cross state of equation (3.5) which may be written

$$|+> = \frac{1}{\sqrt{N}} \sum_{\underline{m} \text{ odd}} |+(\underline{m})> \quad . \tag{3.20}$$

The matrix elements for the second order cross state are

$$\varepsilon^{(2)}_{|+>} = \sum_{\underline{m}'} \sum_{\underline{n}_2} \sum_{\underline{n}_1} \sum_{\underline{m}} \frac{1}{N} <+(\underline{m}')| H'(\underline{n}_2) \frac{Q_o}{a} H'(\underline{n}_1) |+(\underline{m})> , \tag{3.21}$$

with the restriction

$$\delta_{\underline{m}\underline{n}_1} + \delta_{\underline{m}\underline{n}_2} + \delta_{\underline{n}_2\underline{m}'} + \delta_{\underline{m}\underline{m}'} + \delta_{\underline{n}_1\underline{n}_2} + \delta_{\underline{n}_1\underline{m}'} \tag{3.22}$$

which is of comparable complexity to that of equation (3.19) for the fourth order vacuum. As higher order terms, or states of greater complexity, are considered the problem of determining, via the counterparts of equation (3.22), and evaluating the non-zero contributions becomes increasingly difficult, tedious and error prone. A simpler method for the determination of the non-zero matrix elements and their evaluation is required.

(3.4) THE POLYGONAL CLASSIFICATION SCHEME

The examples of the previous section have shown that the relative locations of (1) the sites at which $H'(\underline{n})$ acts and (2) any excited plaquettes present in the initial and final states, determine which matrix elements are non-vanishing and allow the calculation of the counting factor for each of them. The following simple diagrammatical classification scheme allows the different types of matrix elements contributing to particular terms in equations (3.8) to be readily identified and their constituents, together with their counting factors, to be evaluated. Diagram techniques are commonly used for this purpose in the study of lattice gauge theories (e.g. Balian et al. 1975) and spin systems (e.g. Kogut 1979b, Turban 1981). The methods of this section are based on such techniques but are capable of dealing with the additional features introduced by the reformulation of the Hamiltonian.

Matrix elements of order p contribute to $\varepsilon^{(p)}$ and are represented by regular (p+2)-gons whose vertices, when

traversed in a clockwise direction from the upper left, represent the initial state, the p actions of the perturbation Hamiltonian and the final state. Particular initial and final states are denoted by symbols placed at the appropriate vertices. Solid lines joining two vertices indicate that the lattice sites they represent are copunctual. The projector/energy denominator combinations $\frac{Q_o}{a}$ are denoted by dashed lines which perpendicularly bisect the polygon side joining the relevant vertices. Some of the contributions to the fourth order cross state term

$$\varepsilon^{(4)}_{|+>} = \sum_{\underline{m}'\underline{m}} \sum_{\underline{n}_1\underline{n}_2\underline{n}_3\underline{n}_4} <+(\underline{m}')| H'(\underline{n}_4) \frac{Q_o}{a} H'(\underline{n}_3) \frac{Q_o}{a} H'(\underline{n}_2) \frac{Q_o}{a} H'(\underline{n}_1) |+(\underline{m})> \tag{3.23}$$

will be used to illustrate these ideas.

The diagram of figure 3.3 represents the particular case

$$\delta_{\underline{m}\underline{m}'} + \delta_{\underline{n}_1\underline{n}_3} + \delta_{\underline{n}_2\underline{n}_4} = 3 \quad , \tag{3.24}$$

where none of $\underline{m}, \underline{n}_1, \underline{n}_2$ are near neighbours. Plaquette $\underline{q}$ is a near neighbour of plaquette $\underline{p}$ if

$$\underline{q} \in \{\underline{p},\ \underline{p}\pm 2\mu,\ \underline{p}\pm 2\nu,\ \underline{p}\pm\mu\pm\nu\}. \tag{3.25}$$

The figure is based on a hexagon since this is the (4+2)-gon. The three separate solid lines representing the three Kronecker delta functions of equation (3.24) define the

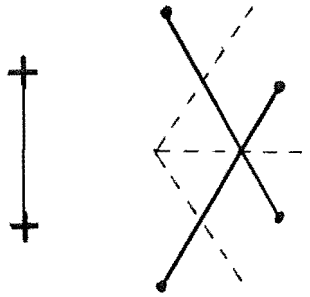

--- sum over states associated with $\frac{Q_o}{a}$

\+ initial and final cross states

—— δ functions on spatial locations

Figure 3.3: Classification polygon for a fourth order cross state matrix element.

particular "type". It is then a simple matter to construct the other diagrams of this type. For a given orientation of the polygon, i.e. with initial and final states specified as above there are

$$\frac{{}^6C_2 \times {}^4C_2 \times 1}{6} = 15$$

ways of joining the three pairs of vertices and hence there are 15 diagrams of this type. The diagram identifies the "active" plaquettes which are those which do not remain in the $\underline{Y}_1$ state. These may be represented by an "active plaquette picture". The three solid lines of figure 3.3 imply that the active plaquettes are confined to 3 separate crosses as shown in figure 3.4.

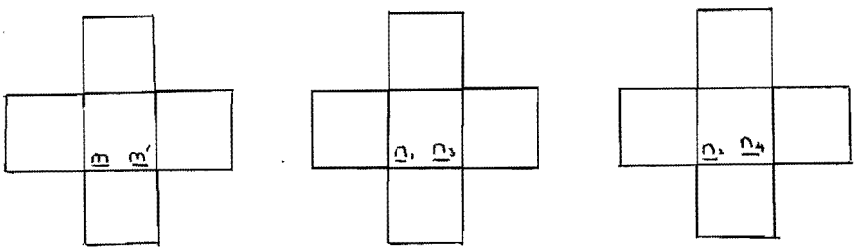

Figure 3.4: Active plaquette picture for figure 3.3.

Each cross is centred on an odd plaquette which is labelled according to figure 3.3. The other diagrams of the same type correspond to different labellings of these central odd plaquettes. The number of ways that these plaquettes may be placed on the lattice, which is the same for all diagrams of the type, is recorded by the counting factor. The counting factor for the matrix elements represented by figures 3.3 and 3.4 is $N^2-27N+194$.

Other types of diagrams arise when the non-near neighbour restriction of equation (3.42) is relaxed. The corresponding active plaquette pictures are obtained by allowing the three separate crosses of figure 3.4 to coalesce or overlap. The polygonal classification scheme allows all the possibilities to be enumerated. There are three basic ways in which active plaquettes may combine, from which all the diagrams may be constructed. These may be illustrated by "dressing" the "skeleton diagram" of figure 3.3.

If one cross of active plaquettes coalesces with another the existing rule for copunctuality leads to the diagram of figure 3.4a whose active plaquette picture is figure 3.4b. There are several equivalent ways of drawing the lines representing the δ functions corresponding to the new restriction

$$\delta_{\underline{m}\underline{m}'} + \delta_{\underline{n}_1\underline{n}_2}\,\delta_{\underline{n}_2\underline{n}_3}\,\delta_{\underline{n}_3\underline{n}_4}\,\delta_{\underline{n}_4\underline{n}_1} = 2$$

$\underline{m},\underline{n}_1$ non-near neighbours. (3.26)

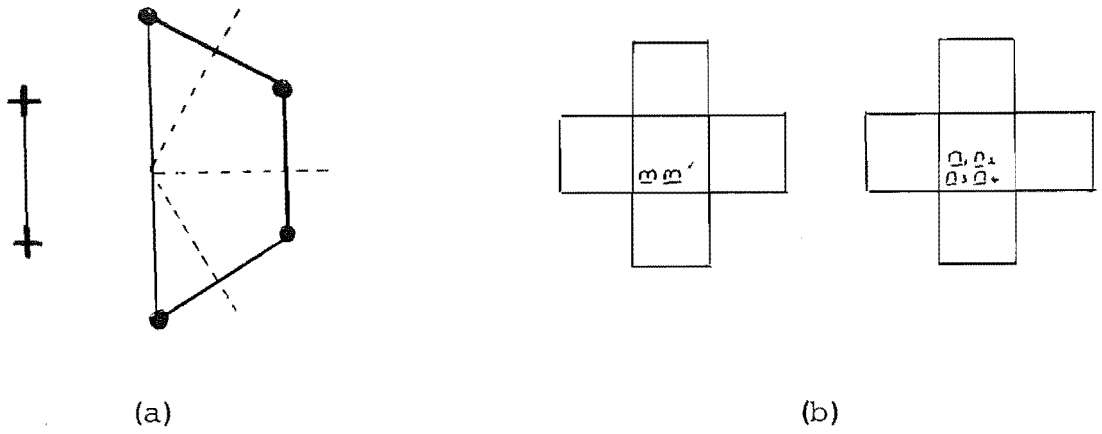

(a) (b)

Figure 3.4: (a) Classification polygon and (b) active plaquette picture for diagram with coalesced crosses of active plaquettes.

If the centres of two crosses of active plaquettes are separated by ±2μ or ±2ν then they will have a single common even plaquette as indicated in figure 3.5b. The single overlap between the crosses is represented by a single curved line connecting the polygon vertices at the centres of the overlapped crosses as shown in figure 3.5a.

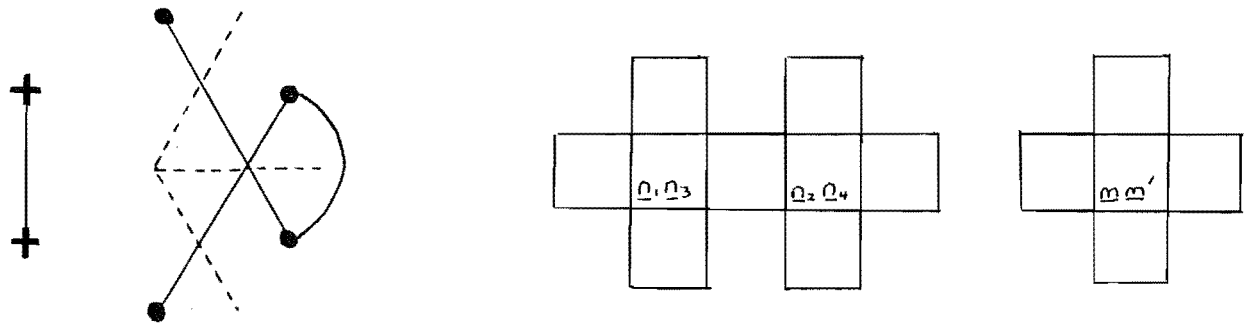

(a) (b)

Figure 3.5: (a) Classification polygon and (b) active plaquette picture for diagram with single overlap.

Crosses whose centres are separated by $\pm\mu\pm\nu$ share two even plaquettes as indicated by figures 3.6a and 3.6b. The common plaquettes are denoted by the two curved lines of figure 3.6a.

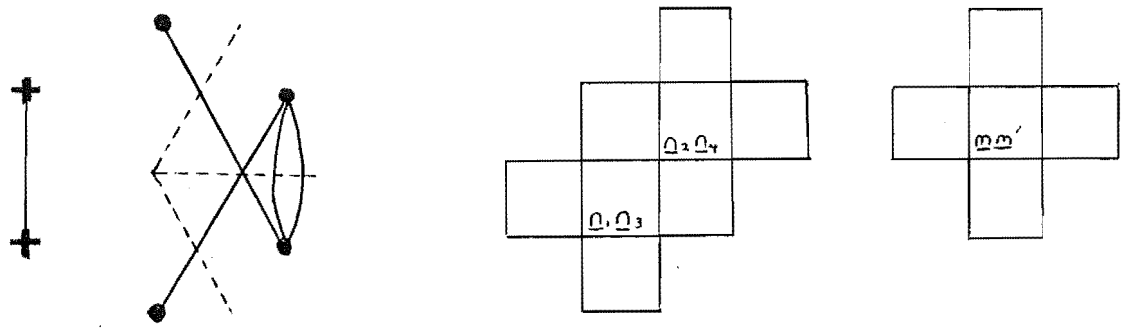

(a) (b)

Figure 3.6: (a) Classification polygon and (b) active plaquette picture for diagram with double overlap.

Figures 3.4, 3.5 and 3.6 illustrate only three of the types of diagram obtained by dressing the skeleton (no overlaps) diagram of figure 3.3. The other types involve more than one of the above types of overlap and all types have many constituent diagrams.

The topologically distinct polygonal classification diagrams each represent more than one matrix element since the corresponding active plaquettes may be placed at different lattice sites while still satisfying the constraints represented by the diagram. These equivalent contributions are collected by the counting factor as was seen in the example of the second order vacuum case

treated in the previous section. The different types of diagrams will in general have different counting factors. The corresponding active plaquette pictures provide a simple means of calculating these while avoiding the plethora of δ functions which appear in the constraints corresponding to equations (3.16), (3.24) etc. The near neighbours of a cross of even plaquettes centred on odd plaquette o are shown in figure 3.7. Crosses of active plaquettes centred on those marked c,s or d

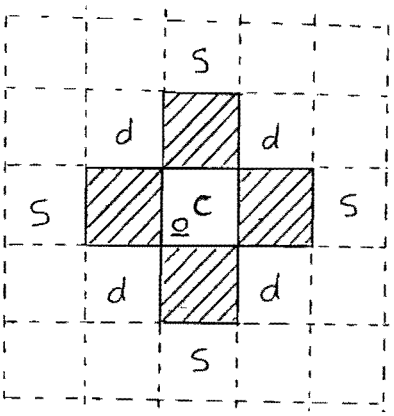

Figure 3.7: Near neighbours of plaquette o.

will coalesce or have single or double overlaps respectively.

Consider the counting factor for the diagram of figure 3.4 which has two separate crosses of active plaquettes. If one is centred on plaquette o then there are 1 + 4 + 4 = 9 forbidden locations for the second. Since o may be any odd plaquette there are thus N(N-9) possibilities. The factors of $\frac{1}{\sqrt{N}}$ associated with the initial and final states may be included in the counting factor to give $\frac{N(N-9)}{\sqrt{N}\ \sqrt{N}} = N-9$.

SEE ERRATA

When the diagram involves single and/or double overlaps the possibility of "rotational equivalents" occurs. Consider the diagram of figure 3.5a which is described by the active plaquette pictures of fig. 3.8 as well as figure 3.5b.

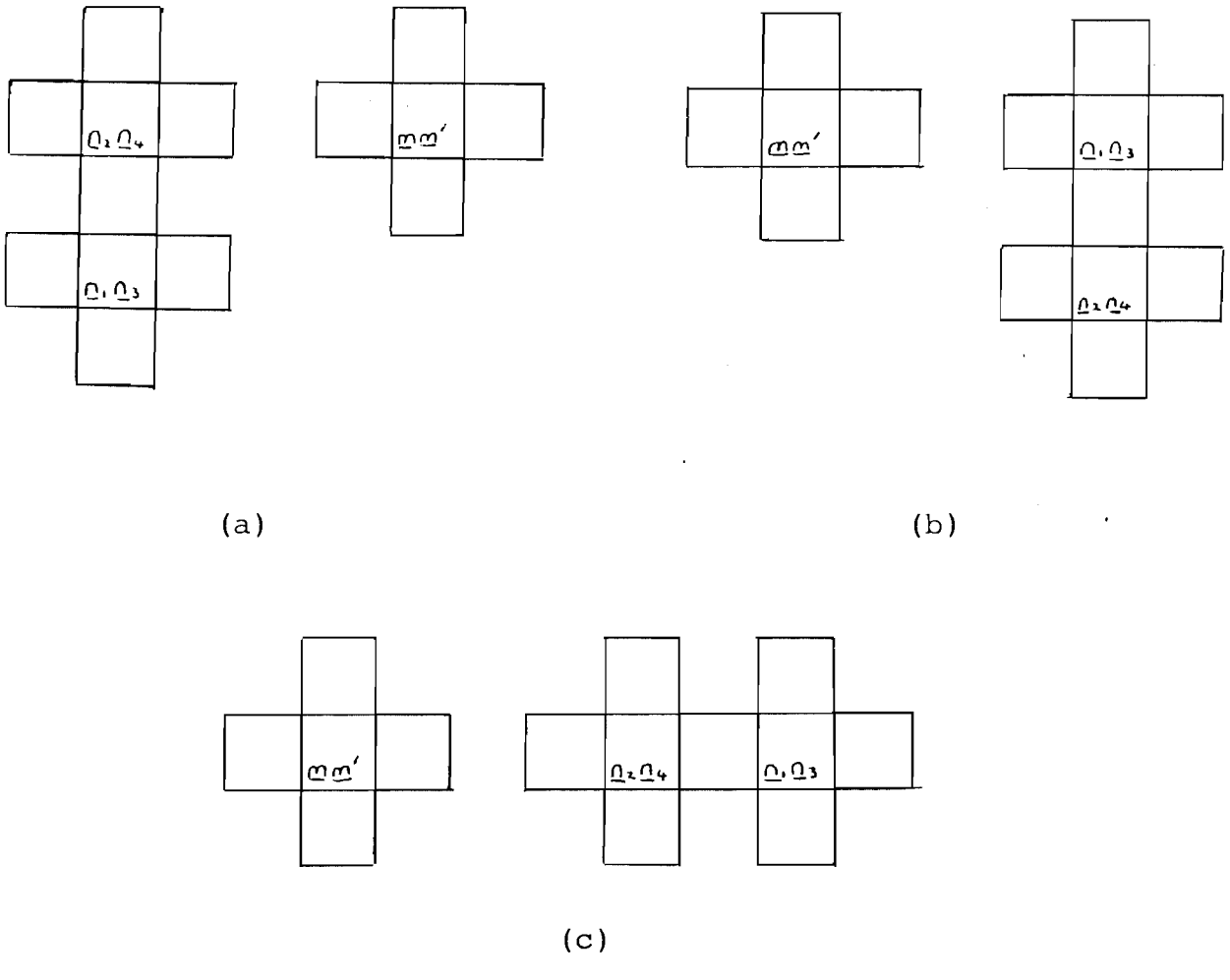

Figure 3.8: Rotational equivalents of figure 3.5b.

Although the four possibilities involve different sequences of the P,Q,R,S operators acting on particular active plaquettes the properties of tables 2.7 ensure that the corresponding matrix elements are equal. The two overlapped crosses have four common near neighbours, leaving N-14

possible centres for the third cross. When the rotational equivalents and $\frac{1}{\sqrt{N}}$ factors are included the counting factor for figure 3.5a becomes

$$\frac{4.N(N-14)}{\sqrt{N}\ \sqrt{N}} = 4(N-14).$$

Detailed examples of such rotated equivalents will be given in the next chapter.

Even at this extremely unsophisticated level these diagrams contain a great amount of information about the matrix elements they represent as is illustrated by the following examples of contributions to equation (3.23).

The diagram of figure (3.9) corresponds to a vanishing matrix element.

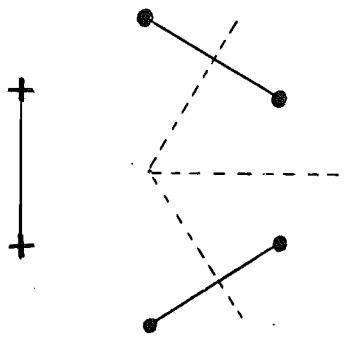

Figure 3.9: A vanishing matrix element.

The initial state, at the upper left, is a lower cross. As the vertices are traversed in a clockwise direction a second cross of excited plaquettes is added by $H'(\underline{n}_1)$ and the resulting state will pass through the projection operator Q_o associated with the dashed line representing

the first denominator. This second cross must be removed by $H'(\underline{n}_2)$ since the final state consists of a single lower cross at the same position as the initial one. This leaves only the initial lower cross at the second dashed line and, since Q_o projects out the initial state, the associated matrix element must vanish. Note that although this diagram does not contribute to equation (3.23) which represents the first term in equation (3.8e) it will contribute to the second term of equation (3.8e).

The matrix elements corresponding to the diagrams of figure 3.10 are equal. The diagram of figure (3.10b) is obtained from that of figure (3.10a) by reflection in the dashed line representing the second denominator

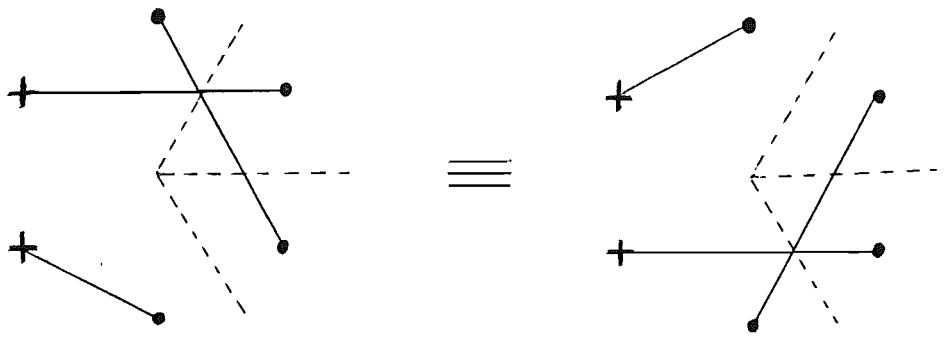

(a) (b)

Figure 3.10: (a) A diagram and (b) its reflection.

Traversing one in the usual clockwise direction is equivalent to traversing the other in an anti-clockwise direction. The matrix elements obtained by traversing

both in the same direction are Hermitian conjugates because of the Hermiticity of H'. The equality of these matrix elements follows from the fact that H' is also real.

Diagrams of the type shown in figure 3.11 are all zero.

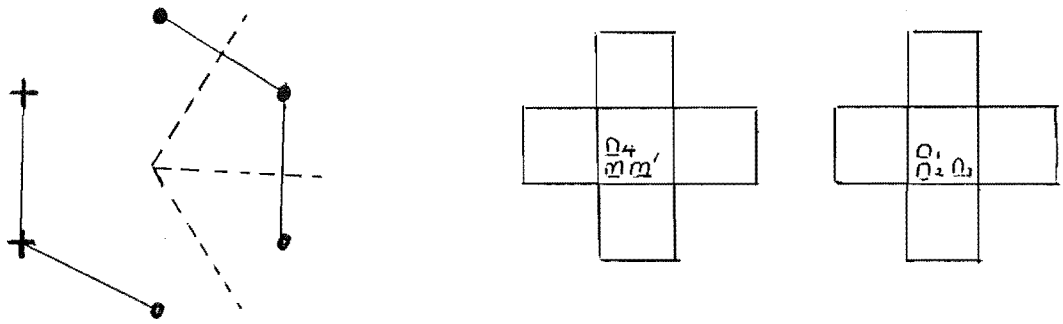

Figure 3.11: (a) Classification Polygon and (b) Active plaquette picture for a forbidden type.

Since there are no non-zero diagonal entries in tables (2.7) H' must act on a state an even number of times in order to have the possibility of returning to that state. This is clearly not consistent with figure 3.11 and all diagrams of this type are forbidden. All types corresponding to odd orders have been claimed to be forbidden by equation (3.12). This claim may be readily verified by considering each of the possible types in turn. An example of a third order diagram which gives zero contribution for the above reasons is shown in figure 3.12.

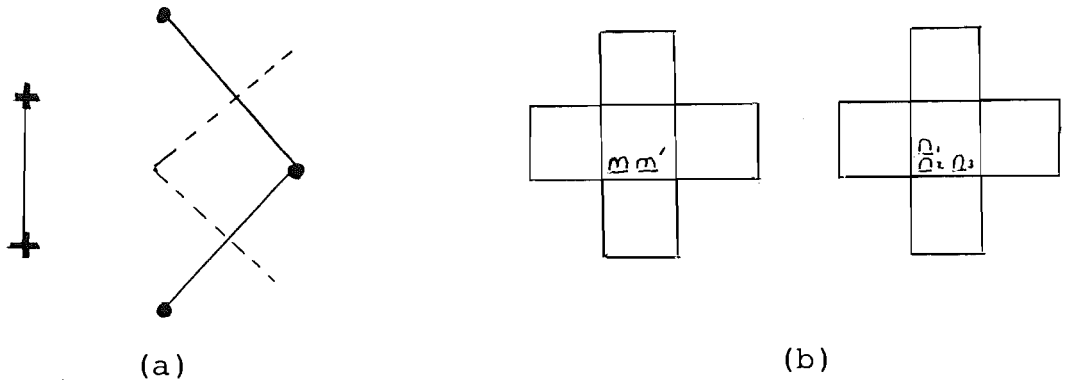

(a) (b)

Figure 3.12: (a) Classification polygon and
(b) active plaquette picture for forbidden third order diagram.

In this section it has been shown that the polygonal classification scheme and its associated active plaquette pictures may be used to specify the matrix elements contributing to equations (3.8). In the next section these specifications are used to evaluate the matrix elements.

3.5 EQUIVALENT PLAQUETTE METHOD FOR MATRIX ELEMENT EVALUATION

The polygonal classification scheme developed in the previous section allows the identification of the non-zero contributions to equations (3.8) and the evaluation of their counting factors. Once the active plaquettes have been specified the methods of section 3.3 may be used to describe the successive actions of the perturbation Hamiltonian on

each of them. The resulting expressions for the matrix elements are the counterparts of equation (3.17). Each time one of the operators of equation (2.40) acts on an active plaquette a summation over a new index is introduced and the expression for the energy denominators of the intermediate states is further complicated. This procedure rapidly becomes unwieldy for all but the simplest cases. In this section a closer examination of the properties of the perturbation Hamiltonian allows the definition of equivalent plaquettes. This allows the matrix elements of equations (3.8) to be evaluated in a more concise and computationally suitable manner.

The individual plaquette method of section 3.3 introduces sums like $\sum_{j=0}^{16} p_{ij}$, and the ε_j appear in the denominators. However tables 2.7 and 2.3 restrict the possible values of the coefficients p_{ij} etc to $\pm\rho_\pm$, $\pm\theta_\pm$ and the single plaquette energies ε_j to $\pm\sqrt{\lambda^2+16}$, $\pm\sqrt{\lambda^2+4}$, $\pm\lambda$. Recall the following properties of tables 2.7. Each row (column) has exactly two non-zero entries, corresponding to the initial state being connected by one of the operators of equation (2.40) to a state of negative energy, and a positive energy state whose energy has the same absolute value. Apart from some signs resulting from the choice of the set $\underline{Y}_i$ the non-zero entries in each row (column) consist of the non-ordered pairs (ρ_+,ρ_-) or (θ_+,θ_-). No coefficient occurs twice in any row (column) and no ρ coefficient occurs in the same row (column) as a θ.

The particular sign choices made when choosing the $\underline{Y}_i$ lead to a further feature, illustrated here by the

action of the operators of equation (2.40) on the state $\underline{Y}_1$:

$$\begin{aligned} P\underline{Y}_1 &= \rho_- \underline{Y}_2 + \rho_+ \underline{Y}_{12} \ , \\ Q\underline{Y}_1 &= \rho_- \underline{Y}_3 + \rho_+ \underline{Y}_{13} \ , \\ R\underline{Y}_1 &= \rho_- \underline{Y}_4 + \rho_+ \underline{Y}_{14} \ , \\ S\underline{Y}_1 &= \rho_- \underline{Y}_5 + \rho_+ \underline{Y}_{15} \ . \end{aligned} \tag{3.27}$$

Table 2.6 shows that $\varepsilon_j = \begin{cases} -\sqrt{\lambda^2+4} : & j = 2,3,4,5 \\ +\sqrt{\lambda^2+4} : & j = 12,13,14,15 \ . \end{cases}$ (3.28)

Specification of the energy of a state on the RHS of equation (3.27) thus determines the associated coefficient. Consider once again the example of the second order vacuum state term of equation (3.17) which is represented by the diagrams of figure 3.13.

(a) (b)

Figure 3.13: (a) Classification polygon and (b) active plaquette picture for 2nd order vacuum energy.

The possible intermediate states of the active plaquettes are determined by equations (3.27) and (3.28)

while the other N-4 even plaquettes remain in state $\underline{Y}_1$. The individual plaquette expression, equation (3.17), for the matrix element may be replaced by

$$\varepsilon^{(2)}_{|0>} = N \sum_{\alpha=0}^{1} \sum_{\beta=0}^{1} \sum_{\gamma=0}^{1} \sum_{\delta=0}^{1} \frac{\rho_+^{2(\alpha+\beta+\gamma+\delta)} \rho_-^{8-2(\alpha+\beta+\gamma+\delta)}}{-N\sqrt{\lambda^2+16} - [-(N-4)\sqrt{\lambda^2+16} + (\alpha+\beta+\gamma+\delta)\sqrt{\lambda^2+4} + (4-(\alpha+\beta+\gamma+\delta))(-\sqrt{\lambda^2+4})]} \tag{3.29}$$

where the sums over the plaquette indices a,b,c,d have been replaced by sums over the plaquette indices $\alpha,\beta,\gamma,\delta$, which take the value 0(1) if the plaquette is in the negative (positive) energy intermediate state. These indices occur only in the combination $\alpha+\beta+\gamma+\delta$ because of the similarity of equations (3.27), and the four active plaquettes to which they refer are said to be equivalent. This allows equation (3.29) to be written as

$$\varepsilon^{(2)}_{|0>} = N \sum_{\alpha=0}^{4} \frac{{}^4C_\alpha \, \rho_+^{2\alpha} \, \rho_-^{8-2\alpha}}{D(-4,4-2\alpha,0)} \quad , \tag{3.30}$$

where the energy denominators have been written in terms of the quantities

$$x = \sqrt{\lambda^2+16} \quad , \quad y = \sqrt{\lambda^2+4} \tag{3.31}$$

as

$$D(\alpha,\beta,\gamma) \equiv \alpha x + \beta y + \gamma\lambda. \tag{3.32}$$

The intermediate state is now specified by α, the number of active plaquettes of positive energy that it contains. The binomial factor ${}^4C_\alpha$ is introduced to count the number of ways the α positive energy plaquettes may be distributed

among the four active plaquettes. This is a much simpler expression than equation (3.17) and should lead to more efficient algorithms for the computation of the matrix elements.

The procedure for evaluating the matrix elements contributing to equations (3.8) for a given state and order will thus consist of the following steps:

(I) Using the polygonal classification scheme to determine the types of diagrams, their counting factors and constituent diagrams.

(II) Determination of the "clusters" of equivalent plaquettes for each diagram.

(III) Calculating the contribution of each cluster to the exponents of the coefficients $\rho_{\pm}$ and $\theta_{\pm}$ and to the overall sign of the expression for the matrix element. Each action of H' will introduce new summations and binomial coefficients.

(IV) Using the active plaquette composition of the intermediate states to obtain the energy denominators. The following diagrammatic method is a convenient means of implementing the above procedure.

Having specified a particular matrix element and evaluated its counting factor as described in section 3.4, the next step is the identification of the clusters of equivalent plaquettes involved. If one plaquette has initial, all intermediate, and final states whose energies are identical to those of another plaquette then the two are equivalent. The structure of tables (2.7) ensures that this occurs when the plaquettes are acted on by the

same sequence of $H'(\underline{n}_i)$, irrespective of which of the operators of equation (2.40) are involved. Each cluster of equivalent active plaquettes is represented by a series of boxes labelled by the appropriate energies. The boxes representing the initial state (upper left of polygon) are placed at the left and those representing the final state (lower left of polygon) at the right while between them are vertical dashed lines representing the operators $\frac{Q_o}{a}$. The vertical line of boxes at each of these represents the possible intermediate states for the active plaquettes.

The boxes representing the initial state are joined to those on their right by lines signifying the action of $H'(\underline{n})$ on their contents. A factor of 1 is associated with lines emanating from boxes not acted on by H' and factors of $\rho_\pm$ and $\theta_\pm$ with the remainder. The lines corresponding to each case are shown in figure 3.14.

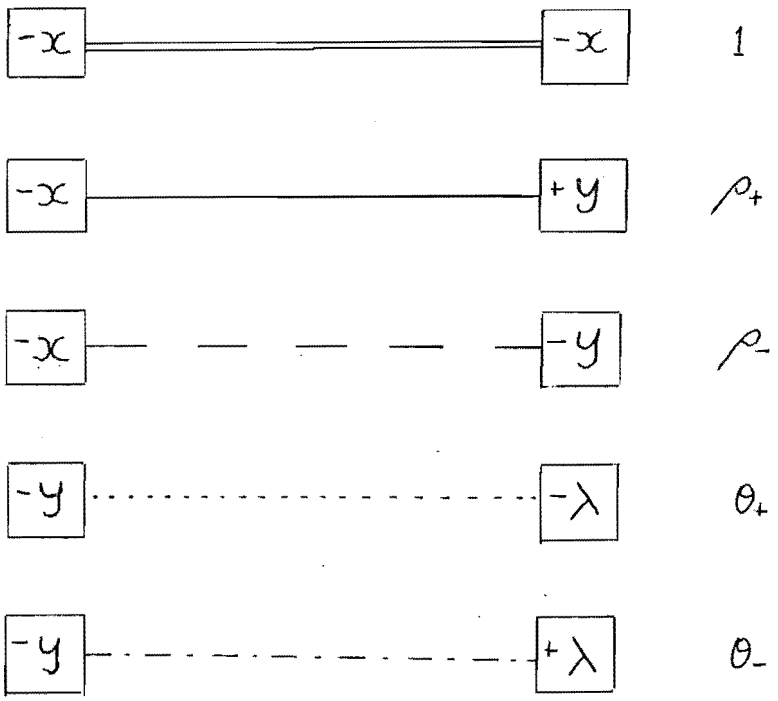

Figure 3.14: Lines representing action of perturbation Hamiltonian.

Since H' can connect a given state with two other states there will be two lines leaving each box whose contents are acted on by H'. Each line is labelled by an index recording the number of the plaquettes (represented by the box) that are making the transition represented by that particular line. The total of the indices on the lines entering a box from the left must be the same as the total on the lines leaving the box from the right. Each time the perturbation Hamiltonian acts on a box containing K equivalent plaquettes a new index η and a binomial factor ${}^{K}C_{\eta}$ are introduced. The indices associated with the different types of lines give the exponents of the coefficients $\rho_{\pm}$, $\theta_{\pm}$ in the expression for the matrix element. As an illustration consider the figure 3.15 which represents the expression, equation (3.30), for the second order vacuum diagram of figure (3.13).

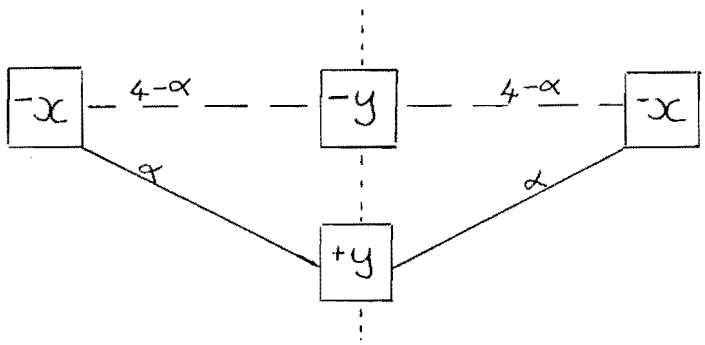

Figure 3.15: Diagrammatic representation of equation (3.30).

The leftmost box represents the four active plaquettes which are initially in the $\underline{Y}_1$ state with energy $-x = -\sqrt{\lambda^2+16}$. The action of H', described by equation 3.27, produces an intermediate state with α of these in the positive energy

states $\underline{Y}_{12}$, $\underline{Y}_{13}$, $\underline{Y}_{14}$, $\underline{Y}_{15}$ and the remaining $4-\alpha$ in the negative energy states $\underline{Y}_2$, $\underline{Y}_3$, $\underline{Y}_4$, $\underline{Y}_5$. The binomial factor ${}^4C_\alpha$ records the number of ways these α could have been chosen from the original four. The sum of the indices leaving the box corresponding to the initial state, entering (or leaving) those boxes representing the intermediate state, and entering the box for the final state is $(4-\alpha)+\alpha=4$. The exponent of the coefficient ρ_+, obtained by adding the indices on the solid lines is $\alpha+\alpha = 2\alpha$. Similarly the exponent of ρ_- is $(4-\alpha)+(4-\alpha) = 8-2\alpha$. There are no lines corresponding to $\theta_\pm$ coefficients. The energy denominator is obtained from the diagram by noting that the intermediate state has α plaquettes of energy $+y$, $(4-\alpha)$ of energy $-y$ and the remaining $(N-4)$ in $-x$. The denominator is therefore

$$-N_x - [-(N-4)x + \alpha y + (4-\alpha)(-y)] = D(-4,4-2\alpha,0).$$

The expression of equation (3.30) is obtained when this information is combined.

Extension of this method to higher orders and other states is straightforward. Now that the matrix elements may be evaluated the claims of rotational and reflectional equivalents made in the previous section may be verified.

Some lines will have associated with them minus signs which arise from tables (2.7). These contribute to the overall sign of the terms and are written in parentheses beside the lines other labels. Each plaquette in a cluster may of course be treated separately, in which case the minus signs may occur in different patterns depending on which of

the operators of equation (2.40) are involved. However it may be verified from tables 2.7 that although the signs corresponding to different members of a cluster may occur on different lines their combination is identical for each member. This means that the plaquette chosen to represent a cluster of equivalent active plaquettes is arbitrary and ensures that the rotational equivalents of section 3.4 are in fact equivalent.

The diagrams will, in general, involve more than one set of equivalent plaquettes, each of which gives rise to a "sub-diagram". The exponents of $\rho_{\pm}$, $\theta_{\pm}$ and the overall sign are obtained by simply adding the contributions from each of the sub-diagrams. The sum of the indices on lines entering or leaving the boxes on any vertical line is equal to the number of active plaquettes. The contribution of the active plaquettes to the energy of an intermediate state is found by recording the contents of all boxes on the appropriate vertical line and the indices of the lines entering them. Since all other even plaquettes are in state $\underline{Y}_1$ the intermediate state energy is known and the energy denominator may be calculated. Plaquettes represented by different sub-diagrams may have the same intermediate state energies. The method thus corresponds to the construction of an "exploded" energy level diagram for the active plaquettes. Each new index is summed over and a binomial coefficient is introduced.

Consider the diagram of figure 3.6 which contributes to the fourth order cross state. The active plaquette picture of figure 3.6b is reproduced in figure 3.16 to

show the four groups of equivalent plaquettes labelled by A,B,C,D.

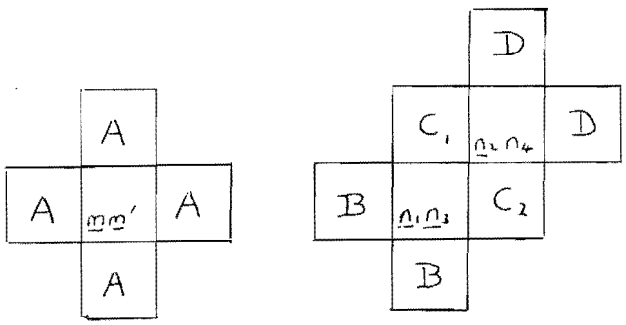

Figure 3.16: The equivalent plaquettes for the diagram of figure 3.6.

As an illustration of the above claim concerning signs the two equivalent plaquettes $C_1 + C_2$ will be treated individually. The diagram of figure 3.17 then represents the expression

$$4(N-12)\sum_{\alpha_1=0}^{1}\sum_{\beta_1=0}^{\alpha_1}\sum_{\gamma_1=0}^{1-\alpha_1}\sum_{\theta_1=0}^{\beta_1+\gamma_1}\sum_{\phi_1=0}^{1-\beta_1-\gamma_1}\sum_{\alpha_2=0}^{1}\sum_{\beta_2=0}^{\alpha_2}\sum_{\gamma_2=0}^{1-\alpha_2}\sum_{\theta_2=0}^{\beta_2+\gamma_2}\sum_{\phi_2=0}^{1-\beta_2-\gamma_2}\sum_{\eta=0}^{2}\sum_{\delta=0}^{2}$$

$$\cdot(-)^{\beta_1+\beta_2+\theta_1+\theta_2}\cdot {}^2C_\eta\cdot {}^2C_\delta\cdot \rho_+^{2(\eta+\delta)+\alpha_1+\alpha_2+\theta_1+\theta_2+\phi_1+\phi_2}$$

$$\cdot \rho_-^{12-2(\eta+\delta)-\alpha_1-\alpha_2-\theta_1-\theta_2-\phi_1-\phi_2}\cdot \theta_+^{4-2(\gamma_1+\gamma_2)-\alpha_1-\alpha_2+\theta_1+\theta_2-\phi_1-\phi_2}$$

$$\cdot \theta_-^{2(\gamma_1+\gamma_2)+\alpha_1+\alpha_2-\theta_1-\theta_2+\phi_1+\phi_2}$$

$$\cdot [D(-4,4-2(\delta+\theta_1+\theta_2+\phi_1+\phi_2),0)$$

$$D(-6,4-2(\eta+\delta),2-2(\beta_1+\beta_2+\gamma_1+\gamma_2))D(-4,4-2(\eta+\alpha_1+\alpha_2),0)]^{-1} \quad (3.33)$$

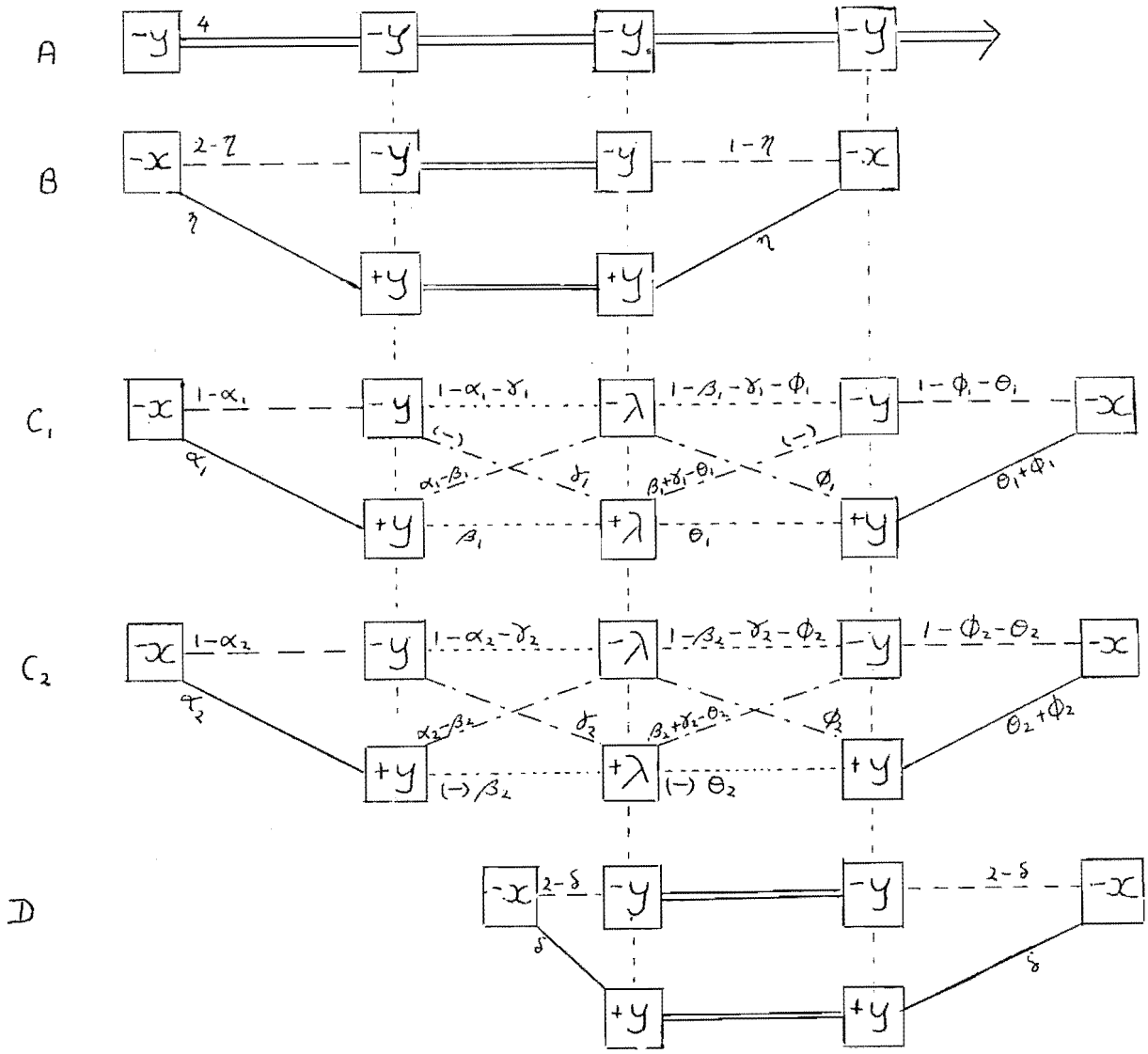

Figure 3.17: Diagrammatic representation of the expression for the matrix element corresponding to figure 3.6.

where the binomial coefficients whose values are unity have been omitted and the identification $(-)^{2\gamma_1+\beta_1+\beta_2-\theta_1+\theta_2} \equiv (-)^{\beta_1+\beta_2+\theta_1+\theta_2}$ has been made. If C_1 and C_2 are treated together the part of figure 3.17 referring to C_2 (C_1) is omitted and the labels $1-\alpha_1$ etc on the lines of the part

referring to $C_1(C_2)$ are replaced by $2-\alpha$ etc in which case equation (3.33) is replaced by

$$4(N-12)\sum_{\alpha=0}^{2}\sum_{\beta=0}^{\alpha}\sum_{\gamma=0}^{2-\alpha}\sum_{\theta=0}^{\beta+\gamma}\sum_{\phi=0}^{2-\beta-\gamma}\sum_{\eta=0}^{2}\sum_{\delta=0}^{2}(-)^{\beta+\theta}\,{}^{2}C_{\alpha}\,{}^{\alpha}C_{\beta}\,{}^{2-\alpha}C_{\gamma}\,{}^{\beta+\gamma}C_{\theta}\,{}^{2-\beta-\gamma}C_{\phi}\,{}^{2}C_{\eta}\,{}^{2}C_{\delta}$$

$$\rho_{+}^{2(\eta+\delta)+\alpha+\theta+\phi}\;\rho_{-}^{12-2(\eta+\delta)-\alpha-\theta-\phi}\;\theta_{+}^{4-2\gamma-\alpha+\theta-\phi}\;\theta_{-}^{2\gamma+\alpha-\theta+\phi}$$

$$[D(-4,4-2(\alpha+\eta),0)D(-6,4-2(\eta+\delta),2-2(\beta+\gamma))$$

$$D(-4,4-2(\delta+\theta+\phi),0)]^{-1}. \qquad (3.34)$$

It may be readily verified from tables 2.7 that the rotational equivalents of figure 3.6 give rise to only those two combinations of signs appearing in figure 3.17. The two possibilities give equal contributions so the rotational equivalents are indeed equivalent and may be included in the counting factor.

When a cluster of plaquettes is acted on by H' more than twice a nest of sums, whose indices are related, is produced. Larger nests occur as the order of terms in equation (3.8) increases. Some examples are given in table 3.1 where L is the number of plaquettes in the cluster. The expressions for all the contributions to equations (3.8) will contain combinations of the above sums. The computational advantage offered by the equivalent plaquette scheme is immediately apparent when the dependence of the number of terms in a nest of k sums on L is computed. The number of terms in the sums of table 3.1 is given in table 3.2.

No. H' actions	No. sums (k)	Nest Structure
0	-	-
1	-	-
2	1	$\sum_{\alpha=0}^{L}$
3	3	$\sum_{\alpha=0}^{L} \sum_{\beta=0}^{\alpha} \sum_{\gamma=0}^{L-\alpha}$
4	5	$\sum_{\alpha=0}^{L} \sum_{\beta=0}^{\alpha} \sum_{\gamma=0}^{L-\alpha} \sum_{\theta=0}^{\beta+\gamma} \sum_{\phi=0}^{L-\beta-\gamma}$

Table 3.1: Some types of nested sums occurring in matrix element evaluation.

k \ L	1	2	3	4	L
1	2	3	4	5	$L+1$
2	4	10	20	35	$\frac{1}{6}(L+1)(L+2)(L+3)$
3	8	34	104	259	$\frac{1}{30}(L+1)(L+2)(L+3)(L^2+4N+5)$

Table 3.2: Number of terms in some k-nested sums

The numbers of terms in equations (3.33) and (3.34) respectively are seen from table 3.2 to be 8 x 8 x 3 x 3 = 576 and 34 x 3 x 3 = 306 respectively, while if all the plaquettes had been treated individually the resulting expression would consist of 8 x 8 x 2 x 2 x 2 x 2 = 1024 terms.

The diagrams such as figures 3.15 and 3.17 may be interpreted as "exploded" energy level diagrams for the active plaquettes. The various parts of the diagram, each representing a cluster of equivalent plaquettes, may be superposed so that only one box of a given energy is present in each vertical line. As an example consider the diagrams whose classification polygons are given in figure (3.18). Figure 3.18b is the reflection of figure 3.18a in the line representing the central denominator so from section 3.4 they should represent equal matrix elements.

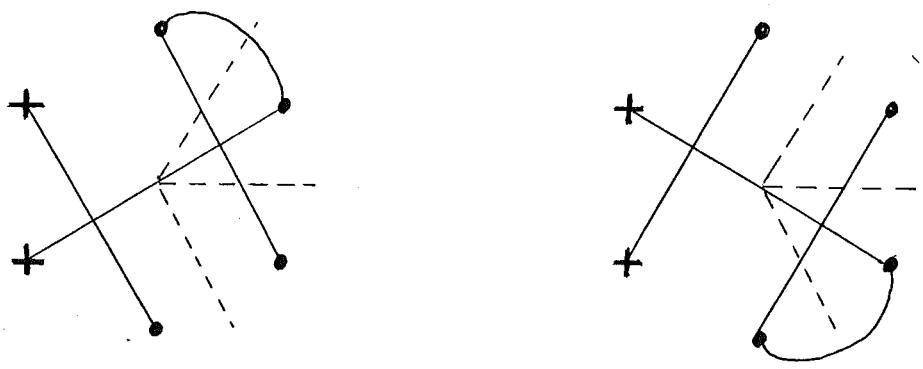

(a) (b)

Figure 3.18: (a) A fourth order cross state diagram and (b) its reflection.

The contributions from each sub-diagram may be superposed to give the energy level form of the diagram as indicated by figure 3.19. This form is more compact, but requires more careful construction (and a very sharp pencil!), and becomes somewhat cluttered for high orders. The different lines of figure 3.14 may all be replaced by solid lines since the coefficient associated with a particular line depends on the levels it connects and may be deduced from the slope of the line. The lines entering particular boxes may now arise from different sub-diagrams. Again the sum of the indices entering a box must be equal to the sum of those leaving it and the sum of the indices along any vertical line is equal to the number of active plaquettes.

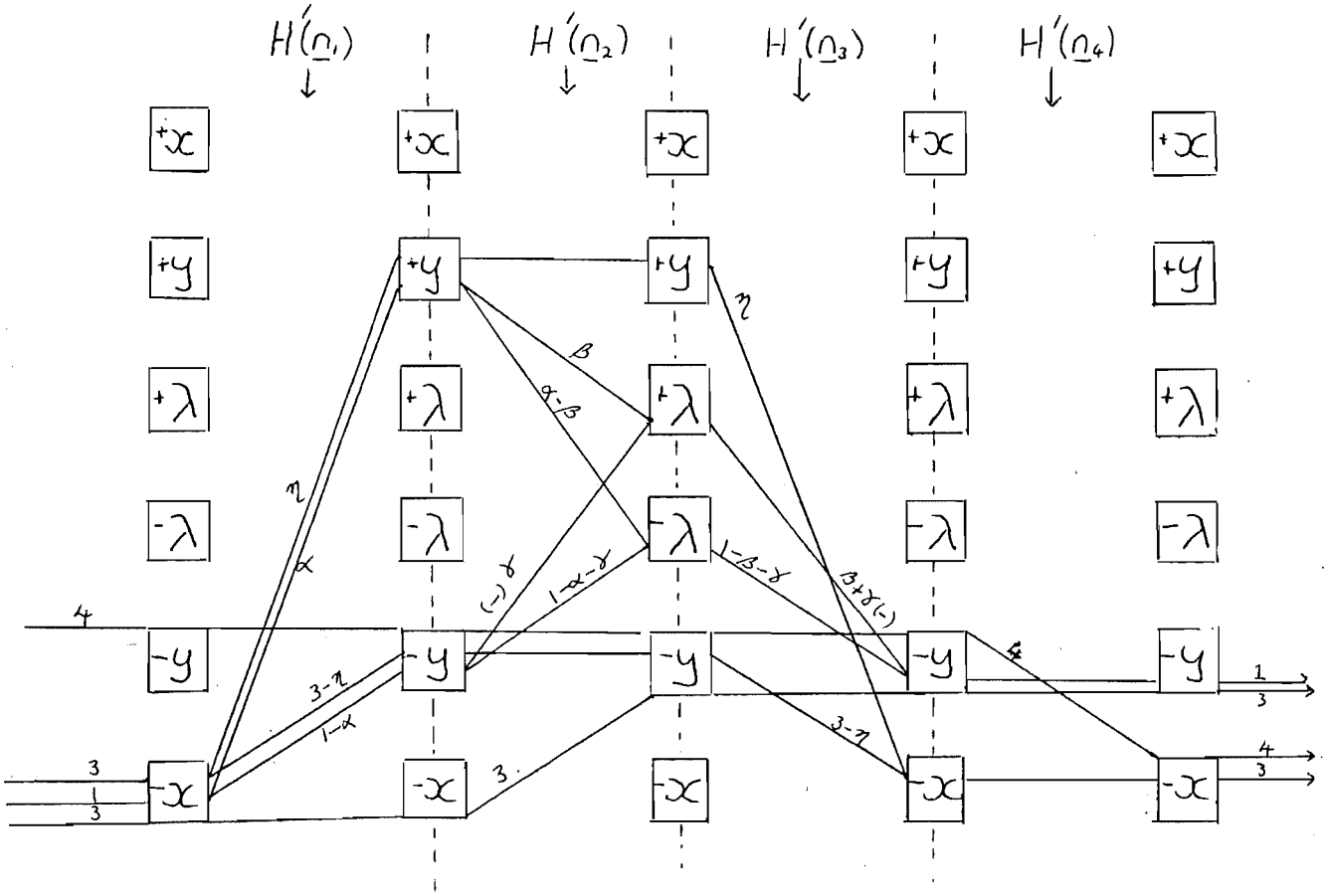

Figure 3.19: Energy level diagram for evaluating figure 3.18a.

The expression for the matrix element is

$$4(N-14)\sum_{\alpha=0}^{1}\sum_{\beta=0}^{\alpha}\sum_{\gamma=0}^{1-\alpha}\sum_{\eta=0}^{3}(-1)^{\beta}\,{}^{3}C_{\eta}\;\rho_{+}^{2\eta+\alpha}\;\rho_{-}^{14-2\eta-\alpha}\;\theta_{+}^{2-2\gamma-\alpha}\;\theta_{-}^{2\gamma+\alpha}$$

$$[D(-4,4-2(\alpha+\eta),0)\;D(-7,6-2\eta,1-2(\beta+\gamma))\;D(-4,4,0)]^{-1}. \tag{3.35}$$

The corresponding expression for the diagram of figure 3.18b is obtained by reflecting figure 3.19 in the vertical line representing the central denominator and evaluating it from left to right or, equivalently, by simply evaluating figure 3.19 from right to left. The result is equation (3.35) with the first and third denominators reversed, as would be expected from the Hermitian conjugation operation represented by the reflection, so the contribution to equation (3.8) from figure 3.18b may be included by simply doubling the counting factor for equation (3.35).

In this chapter a diagrammatic method for the enumeration and evaluation of the non-zero terms in the Brillouin-Wigner expansions for the energy of an arbitrary state has been developed. Each matrix element is specified by a diagram which describes it in terms of clusters of equivalent active plaquettes. This allows all intermediate states to be specified by the energies of their active plaquettes and leads to expressions for the matrix elements which are more suited to computation than their individual plaquette counterparts. There are some important differences between the series for the reformulated Hamiltonian of equation (2.41) and the conventional

Hamiltonian given by equation (2.27). Only even orders contribute to the series of equation (3.7) and the coefficients in this series are now functions of λ i.e. $\varepsilon_{|\psi>} \rightarrow \varepsilon^{(2k)}_{|\psi>}(\lambda)$. The λ-dependence of the $\varepsilon^{(k)}_{|\psi>}(\lambda)$ is introduced by the $\rho_{\pm}(\lambda), \theta_{\pm}(\lambda)$ coefficients in the numerator and by the $\varepsilon_i(\lambda)$ in the denominators. The methods of this chapter are obviously suitable for computer calculation. Chapter 7 deals with the way in which the methods of this chapter were mechanized.

CHAPTER 4

CALCULATION OF VACUUM ENERGY AND MASS GAP

The diagrammatic methods of the previous chapter allow the evaluation of the $\varepsilon^{(k)}_{|\Psi>}$ of equation (3.7) for any state $|\Psi>$. In this chapter these techniques will be applied to the $|0>$, $|+>$ and $|\Box>$ states. The (2+1)-dimensional Z(2) lattice gauge theory is known to undergo a second-order phase transition as does the (2+1)-dimensional Ising model to which it is related by a duality transformation (e.g. Wegner 1971, Kogut 1979b). The Hamiltonians for the two theories are related by

$$H(\text{(2+1)-dimensional Z(2) gauge; } \lambda) \equiv \lambda H^{I}(\text{(2+1)-dimensional Ising model; } \lambda^{-1}) \quad , \quad (4.1)$$

which means that the strong-coupling behaviour of the gauge model may be related to the weak-coupling behaviour of the spin model. The two models belong to the same universality class (Kadanoff 1976) and thus the behaviour of each in the region of the phase transition is described by the same set of critical indices (e.g. Fisher 1967, Kogut 1979b). Section 4.1 deals with the energy of the vacuum state, and the critical index for the specific heat is obtained. The mass gap, which is the energy difference between the first excited state and the vacuum

state, is the quantity which best indicates the onset of the phase transition in the Hamiltonian formulation of the theory. It is related to the reciprocal of the correlation length for the associated statistical mechanical system. The mass gaps for the two possible first excited states, the $|+\rangle$ and $|\square\rangle$ states, are studied in sections 4.2 and 4.3 respectively.

4.1 THE VACUUM ENERGY

The vacuum state is defined by equation (3.1). If the series of equation (3.7) is truncated after the fourth order the vacuum energy will be given by

$$E_{|0\rangle} = \varepsilon^{(0)}_{|0\rangle} + \lambda^2 \varepsilon^{(2)}_{|0\rangle} + \lambda^4 \varepsilon^{(4)}_{|0\rangle} \tag{4.2}$$

since there are no contributions from odd orders. The zero-order energy, given by equation (3.2), is

$$\varepsilon^{(0)}_{|0\rangle} = -Nx \quad . \tag{4.3}$$

The second-order correction is represented by the diagrams of figure 4.1.

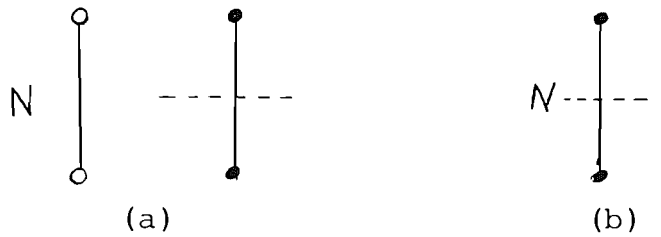

(a) (b)

Figure 4.1: (a) The second order vacuum correction and (b) its abbreviated form.

The initial and final states, denoted by the open circles of figure 4.1a, contain no excited plaquettes and are not connected to any other part of the diagram. The active plaquette structure of $\varepsilon^{(2)}_{|0>}$ may thus be represented by figure 4.1b in which the initial and final vacuum states are understood. The pth-order contributions to equation (3.7) may thus be represented by regular p-gons instead of the (p+2)-gons required for initial states containing excited plaquettes. The second-order correction, which was evaluated in the previous chapter, is

$$\varepsilon^{(2)}_{|0>} = N \sum_{\alpha=0}^{4} \frac{{}^{4}C_{\alpha}\rho_{+}^{2\alpha}\rho_{-}^{8-2\alpha}}{D(-4,\ 4-2\alpha,\ 0)} \quad . \tag{4.4}$$

The fourth-order vacuum energy correction is represented by the ten diagrams which, together with their counting factors, are given in figure 4.2.

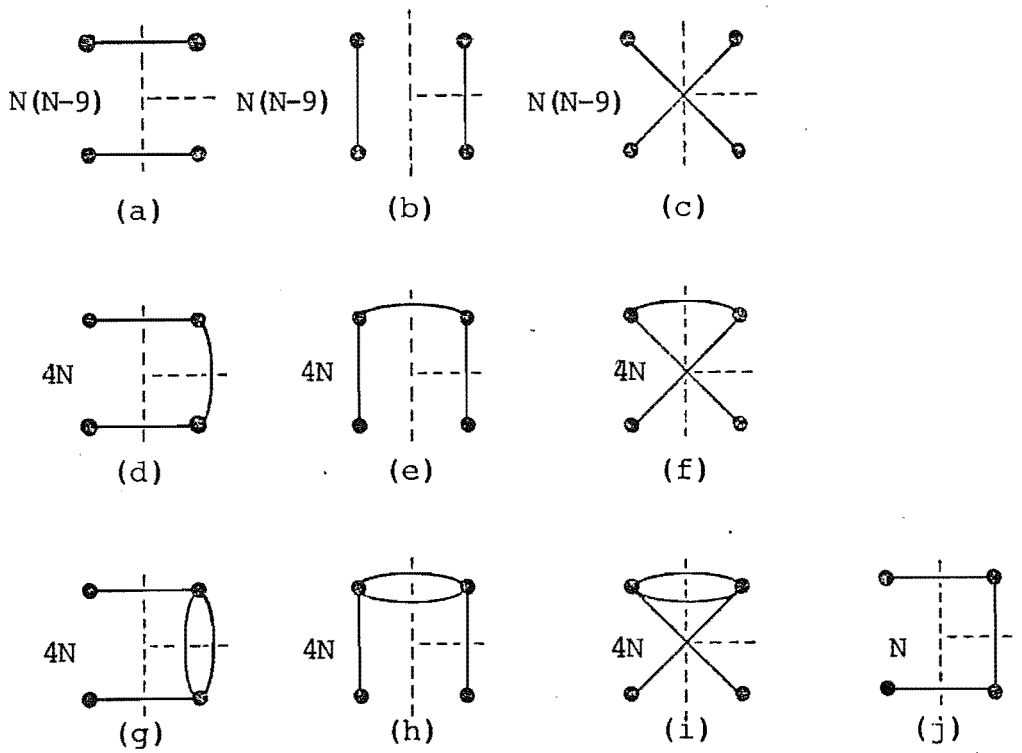

Figure 4.2: Diagrams representing $\varepsilon^{(4)}_{|0>}$.

The vacuum energy is an extensive quantity and thus depends on the size of the lattice. In order for the vacuum energy per plaquette, which is the lattice counterpart of the vacuum energy density, to be both finite and independent of the lattice size it must be of the form

$$\frac{E_{|0>}}{N} = K(\lambda) \quad , \tag{4.5}$$

where $K(\lambda)$ depends only upon λ. This means that all terms in equation (3.8) involving N to powers greater than one must cancel. The matrix elements represented by figure 4.2 involve terms proportional to N and N^2. The N^2 terms arise from the diagrams of figures 4.2(a),(b), and (c), which contribute to the first term of equation (3.8c), and from the product of two second order matrix elements, represented by figure 4.3, which contributes to the second term of equation (3.8c).

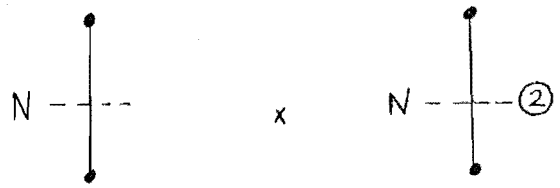

Figure 4.3: Product second-order contribution to $\varepsilon^{(4)}_{|0>}$.

The squared denominator which occurs in the second term of equation (3.8e) is denoted by the labelling of the dashed line representing the appropriate projector/denominator in figure 4.3 by the power to which the denominator is raised. The rules established in the previous chapter

require that the matrix element corresponding to figure 4.2a must vanish. The expressions for the matrix elements represented by figures 4.2b and 4.2c are obtained by the diagrammatic technique of section 3.5. They are

$$N(N-9)\ \text{ 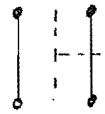 }\ = \frac{N(N-9)\sum_{\alpha=0}^{4}\sum_{\beta=0}^{4} {}^4C_\alpha\, {}^4C_\beta\, \rho_+^{2(\alpha+\beta)}\, \rho_-^{16-2(\alpha+\beta)}}{D^2(-4,4-2\alpha,0)\,D(-8,8-2(\alpha+\beta),0)} \tag{4.6}$$

and

$$N(N-9)\ \text{ 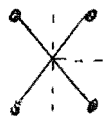 }\ = \frac{N(N-9)\sum_{\alpha=0}^{4}\sum_{\beta=0}^{4} {}^4C_\alpha\, {}^4C_\beta\, \rho_+^{2(\alpha+\beta)}\, \rho_-^{16-2(\alpha+\beta)}}{D(-4,4-2\alpha,0)\,D(-8,8-2(\alpha+\beta),0)\,D(-4,4-2\beta,0)} \tag{4.7}$$

which, when added together and expressed with a common denominator, give

$$N(N-9)\left[\text{ 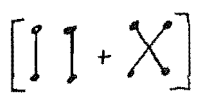 }\right] = \frac{N(N-9)\sum_{\alpha=0}^{4}\sum_{\beta=0}^{4} {}^4C_\alpha\, {}^4C_\beta\, \rho_+^{2(\alpha+\beta)}\, \rho_-^{16-2(\alpha+\beta)}}{D^2(-4,4-2\alpha,0)\,D(-4,4-2\beta,0)} \,. \tag{4.8}$$

It may be readily verified by the use of equation (4.4) that the N^2-dependence of equation (4.8) is equal to that of the product second-order term illustrated in figure 4.3. No other terms in equation (3.8e) contribute, since they are all products involving at least one matrix element of odd order. This means that the restriction of equation (4.5) is satisfied by equation (4.2).

The matrix elements represented by figures 4.1, 4.2, 4.3 were calculated, in double precision, on a Burroughs B6900 series computer. The coefficients of the series of equation (4.2), and the ratios of the corrections, are given, for several values of λ, in table 4.1. The vacuum energy to fourth order is plotted in figure 4.4.

λ	$\varepsilon^{(0)}_{\|0>}$	$\lambda^2\varepsilon^{(2)}_{\|0>}$	$\lambda^4\varepsilon^{(4)}_{\|0>}$	$\lambda^2\varepsilon^{(2)}/\varepsilon^{(0)}$	$\lambda^2\varepsilon^{(4)}/\varepsilon^{(2)}$
0	-4.0000	-	-	-	-
0.5	-4.0311	-0.0316	1.2284×10^{-4}	0.008	-0.004
1.0	-4.1231	-0.1302	1.9986×10^{-3}	0.03	-0.015
1.5	-4.2720	-0.3070	0.0103	0.07	-0.03
2.0	-4.4721	-0.5802	0.0332	0.13	-0.06
2.5	-4.7170	-0.9730	0.0813	0.21	-0.08
3.0	-5.0000	-1.5130	0.1654	0.30	-0.11
3.5	-5.3151	-2.2302	0.2907	0.42	-0.13
4.0	-5.6569	-3.1566	0.4497	0.56	-0.14
4.5	-6.0208	-4.3246	0.6106	0.72	-0.14
5.0	-6.4031	-5.7670	0.7046	0.90	-0.12

Table 4.1: The Vacuum Energy.

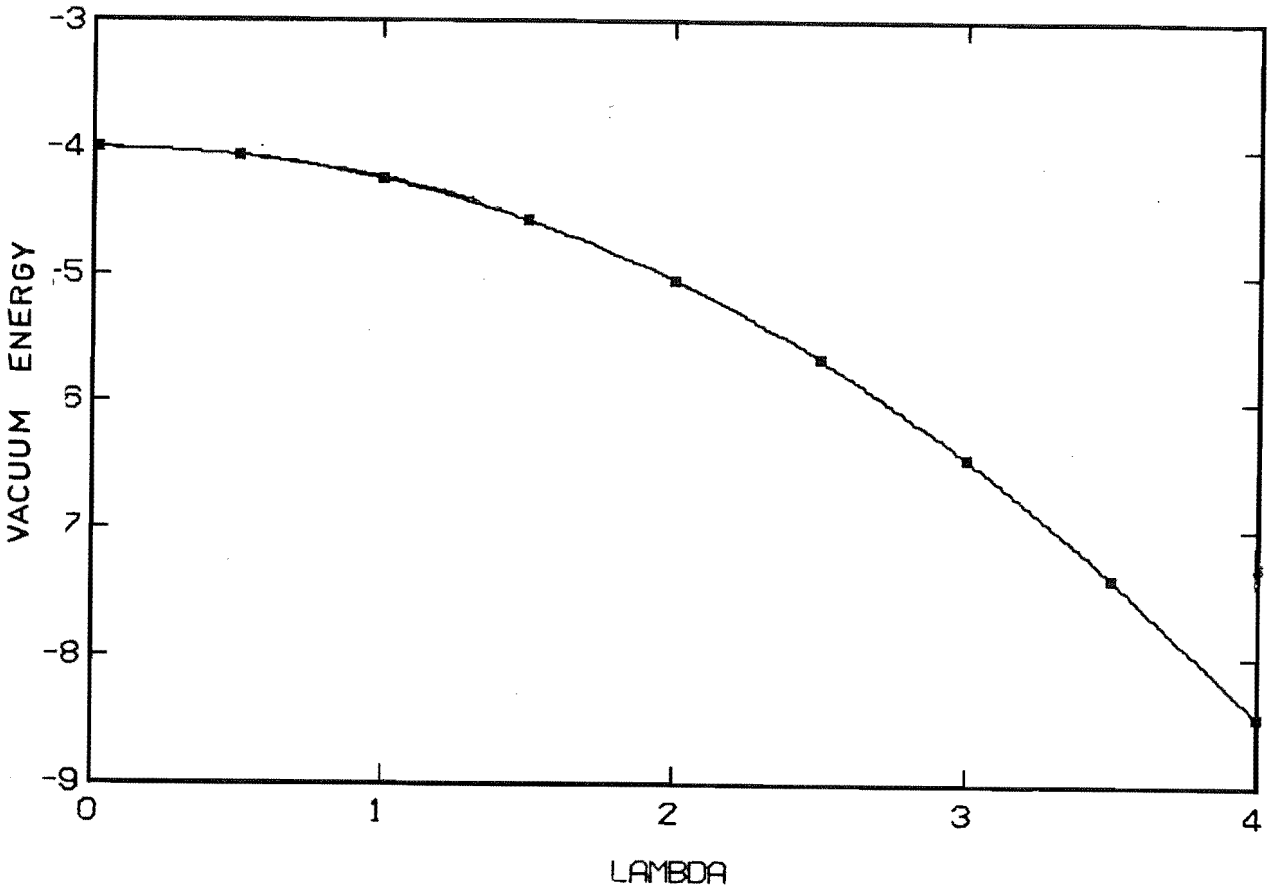

Figure 4.4: The Vacuum Energy.

This calculation must numerically satisfy the condition imposed by equation (4.5), namely that the terms $\propto N^2$ must vanish as indicated algebraically above, and must give identical results for any choice of active plaquette picture in the evaluation of the diagrams. These conditions were satisfied to the limit of the accuracy of double precision, (~23-25 significant figures), which suggests that roundoff errors are negligible.

The (2+1)-dimensional Ising model, which is dual to the Z(2) gauge theory, in the same number of dimensions, has been extensively studied (e.g. Fisher 1967) and is known to exhibit a second-order phase transition at the critical coupling $\lambda_c = 3.125$. The results of table 4.1 indicate that the series of equation (4.3) is convergent in this region. Following Hamer and Kogut (1979) the specific heat for the quantum Hamiltonian formulation of the Ising model is taken to be

$$C^I = - \frac{d^2 E^I_{|0>}}{dx^2} \quad . \tag{4.9}$$

The quantity $E^I_{|0>}$ is the ground state energy of the spin system and the coupling parameter X is analogous to the temperature. In the region of the second order phase transition the specific heat diverges according to

$$C^I \sim (x - x_c)^{-\alpha} \tag{4.10}$$

as x approaches its critical value from above. The specific heat critical index, α, for the (2+1)-dimensional

Ising model has the generally accepted value (Fisher, 1967) $\alpha = 0.125 \pm 0.015$.

Under the duality relation of equation (4.1) the large x properties of the Ising model are related to the small λ properties of the gauge system. In particular the behaviour of the specific heat for the gauge system, as λ increases towards its critical value, will also be generated by α. This may be verified by using equation (4.1) to write equation (4.9) in terms of quantities in the gauge system. The spectra of $H(\lambda)$ and $\lambda H^I(\lambda^{-1})$ are the same (Elitzur et al 1979, Fradkin and Susskind, 1978). Equation (4.1) relates their eigenvalues, or any linear combination of them. In particular the mass gaps and vacuum energies of the gauge system and the Ising model are related by

$$G(\lambda) = \lambda G^I(\lambda^{-1}) \tag{4.11}$$

and

$$E_{|0>}(\lambda) = \lambda E^I_{|0>}(\lambda^{-1}) \ . \tag{4.12}$$

by making the identification $x \equiv \lambda^{-1}$ and using equation (4.12) the specific heat of the Ising model may be written in terms of quantities of the gauge system as

$$\begin{aligned} C^I &= - \frac{d^2}{dx^2} \left(x \, E_{|0>}(\lambda) \right) \\ &= - \lambda^3 \frac{d^2 E_{|0>}(\lambda)}{d\lambda^2} \ . \end{aligned} \tag{4.13}$$

Near the phase transition the relation of equation (4.10)

becomes

$$- \lambda^3 \frac{d^2 E_{|0>}(\lambda)}{d\lambda^2} \sim (\lambda^{-1} - \lambda_c^{-1})^{-\alpha} \quad . \qquad (4.14)$$

Fitting the results to this expression, assuming $\lambda_c = 3.125$, gives the value $\alpha = 0.14 \pm 0.02$, which is in good agreement with that reported for the Ising model by Fisher (1967). The vacuum energy of figure 4.4 is similar in form to the results obtained by perturbative-variational methods (Banks and Zaks 1982) or renormalization group calculations (Horn and Yankielowicz, 1979). Note that figures 7a and 7b of the latter are incorrectly labelled. The calculation of the vacuum energy was repeated using the conventional strong-coupling expansion in order to allow detailed comparison with the present method.

The conventional strong-coupling expansion for the vacuum energy is obtained using the Hamiltonian of equation (2.27), which has eigenvectors defined by equation (2.29). Operators and states are then described in terms of the 4N links of the lattice instead of the N even plaquettes. The zero-order vacuum state is

$$|0>^{SC} = \otimes \prod_{\ell} |x\_>_{\ell} \qquad (4.14)$$

where $|x\_>$ is the negative energy eigenstate of σ_1 defined by equation (2.45). The perturbation Hamiltonian is a sum of terms which flip the spins around a single plaquette. No distinction is made between odd and even plaquettes. Only one intermediate state results from the action of the

perturbation H'_{SC} on an initial state, as indicated in section 2.2f, and the quantities $\varepsilon_{|\Psi>}$, defined by equations (3.7) and (3.8), do not depend on λ. The energy of an intermediate state depends on the number of flipped spins it contains. Each flipped spin is represented by a link state $|x_+>$, defined by equation (2.45), and contributes 2 units to the energy of the lattice state.

The polygonal classification scheme, and the associated active plaquette pictures, may be modified to describe the matrix elements of the conventional strong-coupling expansion. Plaquettes may have 0,1 or 4 common links. If the vertices of the polygon are interpreted as actions of H'_{SC} then the cases of 0 or 4 common links may be dealt with by retaining the convention that solid straight lines between vertices represent copunctual sites. The single curved line between two vertices, formerly used to indicate a common plaquette, is now interpreted as a single common link. The double curved lines between vertices are not required. Counting factors are obtained as in chapter 3.

The zero-order energy of the conventional strong-coupling vacuum state is

$$\varepsilon^{(0)}_{|0>SC} = -4N \,, \tag{4.15}$$

since each of the 4N links is in a link state with energy -1.

The second-order contribution arises from the diagram of figure 4.1. The corresponding active plaquette picture and counting factor are shown in figure 4.5. These should

be compared with their intermediate-coupling counterparts which are shown in figure 3.13.

Figure 4.5: Second order contribution to S.C. expansion for vacuum energy.

The only possible intermediate state has flipped spins on four links. The second order term is thus

$$\varepsilon^{(2)}_{|0>^{SC}} = -\frac{N\lambda^2}{4} \quad . \tag{4.16}$$

The fourth order contributions are presented in table 4.2. The product of second-order terms cancels the N^2-dependence of these terms.

The conventional strong-coupling expansion for the vacuum energy, to 4th order, is thus

$$-4N(1 + \frac{\lambda^2}{16} + \frac{\lambda^4}{3072}) \quad . \tag{4.17}$$

This series yields values for the vacuum energy which are in very close agreement with those obtained from equation (4.2). The conventional strong-coupling results are given, and compared with the intermediate coupling results, in table 4.3

The method developed in the preceding chapters gives results for the vacuum energy which are extremely close to those obtained from the conventional strong-coupling expansion. However the latter method is known to be less

Classification polygon	Active Plaquette Picture	Counting Factor	Diagram value
	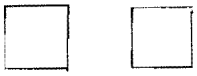	$4N^2-10N$	0
	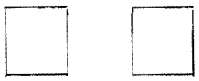	$4N^2-10N$	$-\frac{2N^2+N}{512}$
	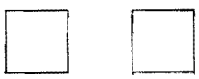	$4N^2-10N$	$-\frac{2N^2+5N}{512}$
		$8N$	0
		$8N$	$-\frac{N}{96}$
	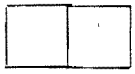	$8N$	$-\frac{N}{96}$
		N	0

Table 4.2: Fourth order contributions to the strong coupling expansion for the vacuum energy.

λ	$E_{\|0>}$	$E^{SC}_{\|0>}$	$\lambda^2\varepsilon^{(2)}_{SC}/\varepsilon^{(0)}_{SC}$	$\lambda^2\varepsilon^{(4)}_{SC}/\varepsilon^{(2)}_{SC}$
0	- 4.0000	- 4.0000	-	-
0.5	- 4.0626	- 4.0626	0.016	0.001
1.0	- 4.2513	- 4.2513	0.063	0.005
1.5	- 4.5687	- 4.5691	0.141	0.012
2.0	- 5.0191	- 5.0208	0.25	0.021
2.5	- 5.6087	- 5.6134	0.391	0.036
3.0	- 6.3476	- 6.3555	0.563	0.047
3.5	- 7.2546	- 7.2579	0.766	0.064
4.0	- 8.3638	- 8.3333	1.000	0.083
4.5	- 9.7348	- 9.5964	1.266	0.105
5.0	-11.4655	-11.0638	1.563	0.130

Table 4.3: Comparison with conventional strong-coupling method.

successful in the calculation of intensive quantities, such as the mass gap, than extensive quantities such as the vacuum energy. The present method uses zero-order states which are closer to the expected physical state of the system than those of the conventional strong-coupling expansion and should therefore provide a means of calculating both intensive and extensive quantities. The (2+1)-dimensional Z(2) lattice gauge theory and its dual, the Ising spin model, have been extensively studied and it is certain that series expansions for their vacua, in the strong and weak coupling regions respectively, are known. However the author is not aware of any publication in which the strong coupling series of equation (4.17) is calculated for the gauge theory.

4.2 THE CROSS STATE

In order to determine the mass gap the series of equation (3.7) must be evaluated for the first excited state, for which the lower cross state defined by equation (3.5) is a promising candidate. Although its zero-order energy is equal to that of the Y16 state, defined in equation (3.3), at $\lambda = 0$, it is the lower for all positive λ. The cross state represents the lowest-energy gauge-invariant excitation of an odd plaquette while the Y16 state is the corresponding even plaquette excitation. Odd and even plaquettes are treated differently in the present method and the zero-order energies of the two states are

different for non-zero λ. Since the $|+\rangle$ and $|\square\rangle$ states may be connected by the perturbation Hamiltonian the difference between their zero-order energies may appear in the energy denominators of equations (3.8). The convergence of the series of equation (3.7) may be poor if this difference remains small. The true first excited state of the system would then be a mixture of the two states. If the series for the cross state energy is also truncated after the fourth order terms to give

$$E_{|+\rangle} = \varepsilon^{(0)}_{|+\rangle} + \lambda^2 \varepsilon^{(2)}_{|+\rangle} + \lambda^4 \varepsilon^{(4)}_{|+\rangle} \quad , \tag{4.18}$$

the mass gap for the cross state becomes

$$G_{|+\rangle} = G^{(0)}_{|+\rangle} + \lambda^2 G^{(2)}_{|+\rangle} + \lambda^4 G^{(4)}_{|+\rangle}$$

$$= \varepsilon^{(0)}_{|+\rangle} - \varepsilon^{(0)}_{|0\rangle} + \lambda^2 (\varepsilon^{(2)}_{|+\rangle} - \varepsilon^{(2)}_{|0\rangle}) + \lambda^4 (\varepsilon^{(4)}_{|+\rangle} - \varepsilon^{(4)}_{|0\rangle}) \quad . \tag{4.19}$$

The mass gap is an intensive quantity, unlike the vacuum energy, and must therefore be independent of the number of plaquettes on the lattice.

The zero-order mass gap, given by equations (3.2) and (3.6) is

$$G^{(0)}_{|+\rangle} = 4(x-y) \quad . \tag{4.20}$$

This quantity decreases from a value of 8 at $\lambda = 0$ to zero as $\lambda \to \infty$ and does not depend on N.

The ten diagrams corresponding to $\varepsilon^{(2)}_{|+\rangle}$ are shown, with their counting factors, in figure 4.6.

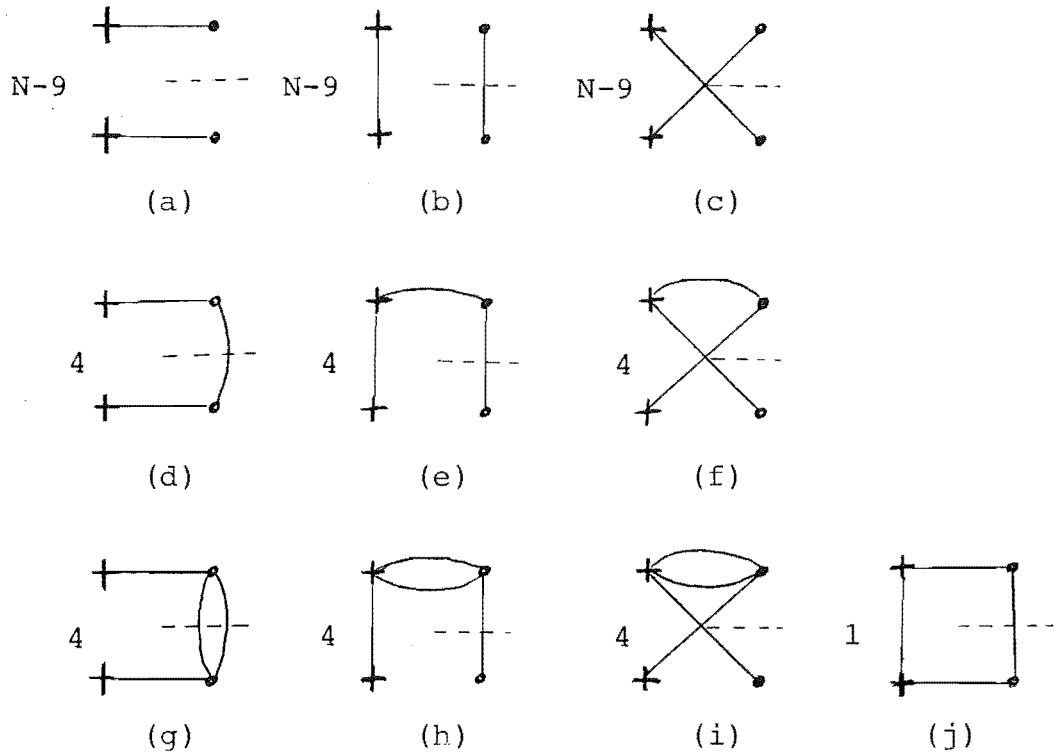

Figure 4.6: Second order cross state diagrams.

These diagrams are similar to those of figure 4.2, which contribute to the fourth order vacuum energy, but have only one projector/denominator and have excited plaquettes in the initial state. The N-dependent parts of the matrix elements represented by figures 4.6 a,b,c must equal the second order vacuum correction $\varepsilon^{(2)}_{|0>}$ if the mass gap is to be independent of N to fourth order. Evaluation of these diagrams shows that figures 4.6 a and 4.6 c correspond to equal and opposite matrix elements while the N-dependent part of figure 4.6 b is exactly equal to the second order vacuum energy correction of figure 4.1. The resulting second order mass gap is shown in figure 4.7 and leads to an estimated value for the critical coupling of $\lambda_c = 3.48 \pm 0.01$.

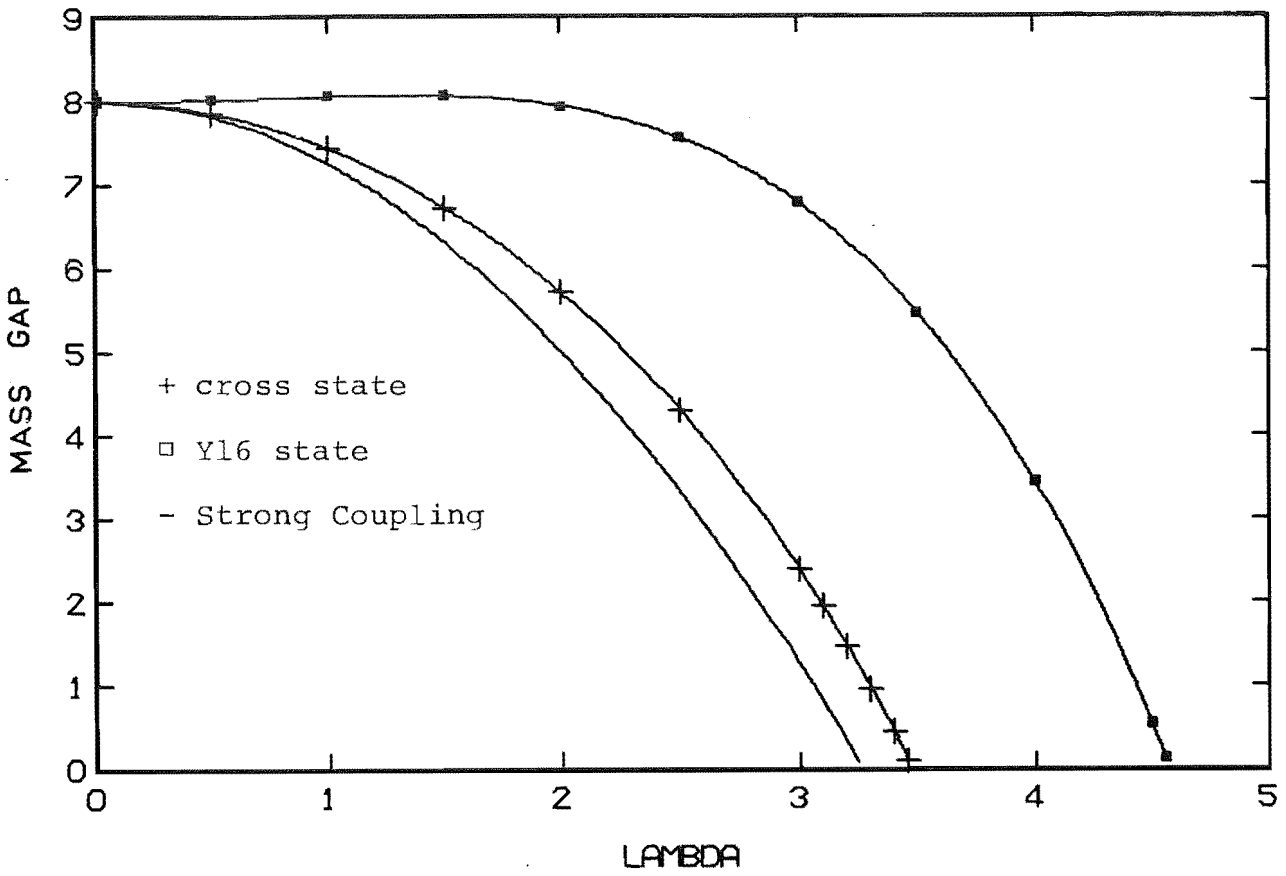

Figure 4.7: Second order mass gaps.

The fourth order correction $\varepsilon^{(4)}_{|+>}$ involves contributions from the 376 separate diagrams of Appendix A. These may be reduced to 237 by the rules developed in the previous chapter. Non-zero contributions to $\varepsilon^{(4)}_{|+>}$ arise from the first and second terms of equation (3.8e). When these are evaluated it is found that their N^2-dependent terms cancel internally and that their N-dependent terms are equal to those of the vacuum. Thus the mass gap is dependent of the lattice size to fourth order.

The terms of the series equation (4.15) for the mass gap are given, for several values of λ, in table 4.4.

λ	$G_{\|+>}$	$G^{(0)}_{\|+>}$	$\lambda^2 G^{(2)}_{\|+>}$	$\lambda^4 G^{(4)}_{\|+>}$	$\lambda^2 G^{(2)}_{\|+>}/G^{(0)}_{\|+>}$	$\lambda^2 G^{(4)}_{\|+>}/G^{(2)}_{\|+>}$
0.1	7.9923	7.9950	-8.3646×10^{-4}	-1.8517×10^{-3}	-1×10^{-4}	2.2
1	7.2427	7.5482	-0.1167	-0.1888	-0.15	1.6
2	4.7430	6.5748	-0.8639	-0.9677	-0.13	1.1
3	-1.6247	5.5778	-3.1847	-4.0178	-0.57	1.3

Table 4.4: The mass gap for the cross state.

The series fails to converge for any value of λ. Examination of the contributions from particular diagrams reveals the source of the problem. In some of the diagrams of figure 4.6 or Appendix A the initial state $|+>$ may be connected by the perturbation Hamiltonian to an intermediate state $|\square>$. The corresponding denominator is D(2,-4,0), which tends to zero as $\lambda \to 0$. In the strong coupling limit the $|+>$ ($|\square>$) state consists of four flipped spins on the links of a single odd (even) plaquette. The two states are thus degenerate in the strong coupling limit. As λ increases, the zero-order energies of the $|+>$ and $|\square>$ states fail to separate by a sufficient amount to make the denominators of the matrix elements large enough for the series to converge. The $|+>$ and $|\square>$ states are thus quasidegenerate and the first excited state will be a mixture of the two. Although the denominator D(2,-4,0) occurs in some of the second order terms it is always accompanied by powers of the "small" coefficients ρ_+ or θ_- in the numerator, which render it

harmless. Such compensating factors are not always present in the fourth order terms. The denominator D(2,-4,0) does not occur in the calculation of the vacuum energy.

4.3 THE Y16 STATE

The quasidegeneracy observed in the previous section implies that the Y16($|\square\rangle$) state, defined by equation (3.3), remains a candidate for the first excited state. However it is probable that the series of equations (3.7), which applies to a non-degenerate state, will fail to converge. The energy of the $|\square\rangle$ state, to fourth order, is

$$E_{|\square\rangle} = \varepsilon^{(0)}_{|\square\rangle} + \lambda^2\varepsilon^{(2)}_{|\square\rangle} + \lambda^4\varepsilon^{(4)}_{|\square\rangle} \tag{4.21}$$

and the corresponding mass gap is

$$\begin{aligned} G_{|\square\rangle} &= G^{(0)}_{|\square\rangle} + \lambda^2 G^{(2)}_{|\square\rangle} + \lambda^4 G^{(4)}_{|\square\rangle} \\ &= \varepsilon^{(0)}_{|\square\rangle} - \varepsilon^{(0)}_{|0\rangle} + \lambda^2(\varepsilon^{(2)}_{|\square\rangle} - \varepsilon^{(2)}_{|0\rangle}) \\ &\quad + \lambda^4(\varepsilon^{(4)}_{|\square\rangle} - \varepsilon^{(4)}_{|0\rangle}) \ . \end{aligned} \tag{4.22}$$

The zero-order mass gap is, from equations (3.2) and (3.4),

$$G^{(0)}_{|\square\rangle} = 2x. \tag{4.33}$$

The second order terms are represented by the three diagrams of figure 4.8.

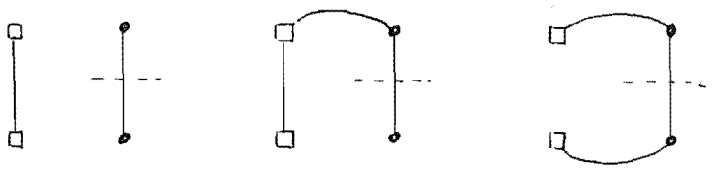

Figure 4.8: Second order contributions to $\varepsilon^{(2)}_{|\square>}$.

The resulting second order mass gap for the $|\square>$ state is shown, with the corresponding gap for the cross state, in figure 4.7. The estimated critical coupling is $\lambda_c = 4.57 \pm 0.01$.

The 99 fourth order diagrams contributing to $\varepsilon^{(4)}_{|\square>}$, given in Appendix A, may be reduced to 69 by the rules of chapter 3. Evaluation of these confirms the suspicion that the series of equation (4.22) does not converge for any λ. The results for several values of λ are given in table 4.5.

λ	$G_{\|\square>}$	$G^{(0)}_{\|\square>}$	$\lambda^2 G^{(2)}_{\|\square>}$	$\lambda^4 G^{(4)}_{\|\square>}$	$\lambda^2 G^{(2)}/G^{(0)}$	$\lambda^2 G^{(4)}/G^{(2)}$
0.1	8.0027	8.0025	-0.0017	0.0019	-2×10^{-4}	-1.1
1	8.2954	8.2462	-0.1877	0.2369	-0.02	-1.3
2	9.5646	8.9443	-1.0065	1.6268	-0.11	-1.6
3	22.3786	10.0000	-3.2064	15.5851	-0.32	-4.9

Table 4.5: The mass gap for the Y16 state.

Again the lack of convergence is due to the quasidegeneracy of the two low-energy states $|+\rangle$ and $|\square\rangle$. The initial $|\square\rangle$ state may be connected to the $|+\rangle$ state by the perturbation Hamiltonian, resulting in the appearance of the denominator $D(-2,4,0)$. As for the cross state the effects of this quasidegeneracy are hidden, since the small denominator is always accompanied by compensating factors in the numerator.

The conventional strong-coupling expansion may also be used to obtain a second order estimate of the mass gap. The zero order strong-coupling mass gap is

$$G^{(0)}_{|1\rangle^{SC}} = \varepsilon^{(0)}_{|1\rangle^{SC}} - \varepsilon^{(0)}_{|0\rangle^{SC}} = -4N+8 - (-4N) = 8. \qquad (4.24)$$

The first excited state, denoted by $|1\rangle^{SC}$, is the zero-momentum superposition of the 2N degenerate states consisting of a single plaquette of flipped spins. The procedure used to obtain the conventional strong-coupling vacuum energy yields the second order contributions ${}^{SC}\langle 1|H'_{SC}\frac{Q_o}{a}H'_{SC}|1\rangle^{SC}$ to the mass gap which are summarized in table 4.6.
The strong-coupling mass gap, to second order, is thus given by

$$G_{|1\rangle^{SC}} = 8\left(1 - \frac{3\lambda^2}{32}\right) \quad . \qquad (4.25)$$

This function is also plotted in figure 4.7. The quantity $G_{|1\rangle^{SC}}$ is independent of N, as required. The second-order estimate of the critical coupling is $\lambda_c = \frac{32}{3} = 3.266$.

Classification Polygon	active plaquette picture	counting factor	Diagram value
		2N-5	$\frac{2N-5}{8}$
	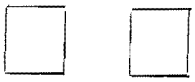	2N-5	$-\left(\frac{2N-5}{8}\right)$
	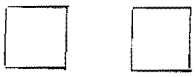	2N-5	$-\left(\frac{2N-5}{8}\right)$
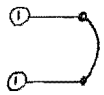		4	$\frac{1}{2}$
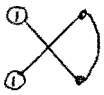		4	-1
	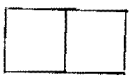	4	-1
		1	$\frac{1}{8}$

Table 4.6: Second order contributions to the conventional strong-coupling mass gap.

In this chapter the formulas of equations (3.7) and (3.8), which give perturbation series for the energies of non-degenerate states, have been applied to the vacuum, cross and Y16 states. The series for the vacuum energy has been calculated to fourth order. It has a satisfactory rate of convergence for values of λ ranging from zero to values beyond the critical point. The conventional strong coupling expansion has also been obtained and the two show good agreement. The series for the cross and Y16 states

fail to converge because of the quasidegeneracy of the two states. The energy of the first excited states, and hence the mass gap, must be calculated using quasidegenerate perturbation theory. The second order expression for the conventional strong-coupling mass gap has been obtained.

CHAPTER 5

QUASI-DEGENERATE PERTURBATION THEORY

The perturbation expansion for the energy of a non-degenerate state, given in equations (3.7) and (3.8), enabled the calculation of the vacuum energy in the previous chapter. This expansion failed to converge, for any value of λ, when applied to the calculation of the mass gap. The two gauge-invariant states of lowest energy, the $|+\rangle$ and $|\square\rangle$ states, were found to be quasi-degenerate. These two orthogonal states may be connected by the perturbation Hamiltonian. The difference between their zero-order energies depends on λ, and is small for small λ. Thus it is found that small denominators occur when the series of equation (3.7) is used to calculate the energy of either state and, as a result, the series does not converge. In this chapter methods for dealing with the problem of quasidegenerate states are presented and applied to the calculation of the mass gap.

In section 5.1 the Hamiltonian is modified to make the $|+\rangle$ and $|\square\rangle$ states exactly degenerate eigenstates of the zero order Hamiltonian. The resulting problem in degenerate perturbation theory is treated in section 5.2. The vacuum energy and mass gap are calculated in sections 5.3 and 5.4. The conventional strong-coupling expansion for the mass gap is obtained in section 5.5.

5.1 MODIFICATION OF THE HAMILTONIAN

In order to deal with the problem of quasi-degenerate states it is necessary (Messiah, 1962) to modify the definitions of the zero-order and perturbation Hamiltonians. The quasi-degenerate states are made exactly degenerate eigenstates of the zero-order Hamiltonian and the appropriate correction is made to the perturbation.

The zero-order single-plaquette Hamiltonian of equation (2.35) may be put in the form

$$h_o(\lambda) = \sum_i \varepsilon_i P_i^0 \quad , \tag{5.1}$$

where P_i^0 is the projector onto the subspace of the eigenvalue ε_i of $h_o(\lambda)$. This may be written in full as

$$h_o(\lambda) = +x|\underline{Y}_1><\underline{Y}_1| + y \sum_{i=2}^{5} |\underline{Y}_i><\underline{Y}_i| + \lambda \sum_{i=6}^{8} |\underline{Y}_i><\underline{Y}_i|$$

$$- \lambda \sum_{i=9}^{11} |\underline{Y}_i><\underline{Y}_i| - y \sum_{i=12}^{15} |\underline{Y}_i><\underline{Y}_i| - x|\underline{Y}_{16}><\underline{Y}_{16}| \quad , \tag{5.2}$$

where x,y are defined by 3.31.

The quasi-degeneracy is due to the fact that $\lim_{\lambda\to\infty} y = \frac{x}{2}$, which suggests that the $|+>$ and $|\square>$ may be made exactly degenerate by the replacement $y \to \frac{x}{2}$ in equation (5.2). This leads to the definition of the modified zero-order single-plaquette Hamiltonian

$$\tilde{h}_o(\lambda) = +x|\underline{Y}_1><\underline{Y}_1| + \frac{x}{2} \sum_{i=2}^{5} |\underline{Y}_i><\underline{Y}_i| + \lambda \sum_{i=6}^{8} |\underline{Y}_i><\underline{Y}_i|$$

$$- \lambda \sum_{i=9}^{11} |\underline{Y}_i><\underline{Y}_i| - \frac{x}{2} \sum_{i=12}^{15} |\underline{Y}_i><\underline{Y}_i| - x|\underline{Y}_{16}><\underline{Y}_{16}| \quad . \tag{5.3}$$

In order that the total Hamiltonian remain unchanged the perturbation Hamiltonian is modified by the addition of the term

$$\lambda\tilde{h}'(\lambda) = (y-\frac{x}{2}) \sum_{i=2}^{5} |\underline{Y}_i><\underline{Y}_i| + (\frac{x}{2}-y) \sum_{i=12}^{15} |\underline{Y}_i><\underline{Y}_i| \quad . \quad (5.4)$$

The lattice Hamiltonian, given in equation (2.35) now becomes

$$H = \tilde{H}_o(\lambda) + \lambda(H' + \tilde{H}')$$

$$= -\sum_{\underline{n} \text{ even}} \tilde{h}_o(\lambda) - \lambda[\sum_{\underline{n} \text{ odd}} H'(\underline{n}) + \sum_{\underline{n} \text{ even}} \tilde{H}'(\underline{n})] \quad . \quad (5.5)$$

The states defined in section 3.1 are eigenstates of the modified zero-order Hamiltonian and their zero-order energies are

$$\tilde{\varepsilon}^{(0)}_{|0>} = -Nx \quad ,$$

$$\tilde{\varepsilon}^{(0)}_{|\square>} = -(N-2)x \quad ,$$

and

$$\tilde{\varepsilon}^{(0)}_{|+>} = -(N-4)x - \frac{4x}{2} = -(N-2)x \quad .$$

The zero-order energies of the $|+>$ and $|\square>$ states are now equal.

The modification of the perturbation Hamiltonian will lead to quantities such as

$$M = \langle \Psi | H' \frac{Q_o}{a} \tilde{H}' \frac{Q_o}{a} \tilde{H}' \frac{Q_o}{a} H' | \Psi \rangle \qquad (5.7)$$

in the expansion for the energy of the excited state. These may be readily included in the diagrammatic methods of chapter three. The action of $H'(\underline{n})$ has been signified by "blobs" on the vertices of the classification polygons. This notation is retained, and the symbol "Ⓣ" is used to denote those vertices corresponding to the action of $\tilde{H}'(\underline{n})$. The classification polygon and active plaquette picture for a contribution to the quantity of equation (5.7) are shown in figure 5.1. The shaded plaquettes represent the

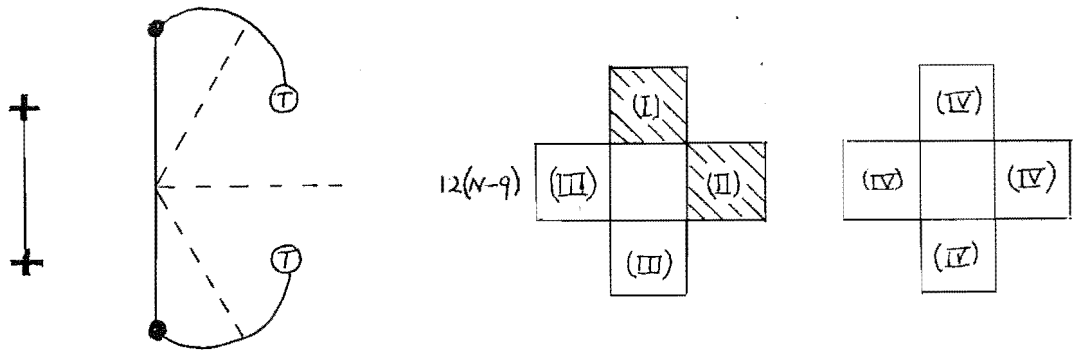

(a) (b)

Figure 5.1: (a) Classification polygon and (b) active plaquette picture for a diagram involving $\tilde{H}'$.

action of the operator $\tilde{H}'(\underline{n})$. Since the action of $\tilde{H}'(\underline{n})$ on a plaquette state is to multiply it by 0 or $\pm \frac{(y-\frac{x}{2})}{\lambda}$ its incorporation into the diagrammatic method for the evaluation of matrix elements is particularly simple. The boxes representing states connected by $\tilde{H}'$ are joined by horizontal lines, as are

any other states not acted on by H', with the addition of the symbol ±Ⓣ to indicate the appropriate multiplying factor. The energy level diagram for the evaluation of figure 5.1 is that of figure 5.2. The Roman numerals indicate the equivalent plaquettes of figure 5.1.

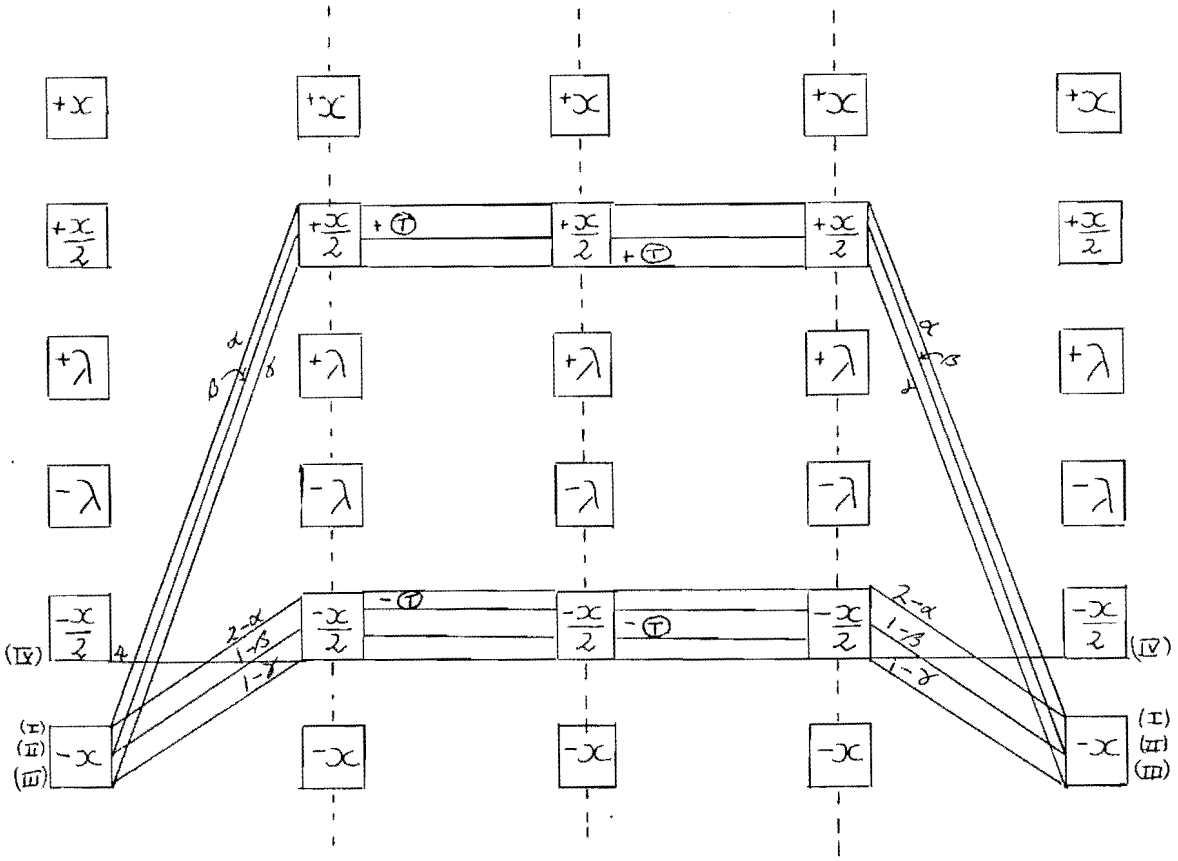

Figure 5.2: Diagram for the evaluation of figure 5.1.

The expression for the corresponding matrix element is

$$(y - \frac{x}{2})^2 \sum_{\alpha=0}^{2} \sum_{\beta=0}^{1} \sum_{\gamma=0}^{1} {}^2C_\alpha \, \rho_+^{2\alpha} \, \rho_-^{8-2\alpha}$$

$$\cdot \, [\tilde{D}(-4, 4-2(\alpha+\beta+\gamma), 0)]^{-3} \, . \qquad (5.8)$$

The denominator in this expression is defined by

$$\tilde{D}(\delta, \eta, \xi) \equiv \delta x + \eta\frac{x}{2} + \xi\lambda \equiv D(\delta + \frac{\eta}{2}, \, 0, \, \xi). \qquad (5.9)$$

The space spanned by the eigenvectors of $\tilde{H}_o$ contains a 2N-fold degenerate subspace spanned by the N degenerate $|+\rangle$ states and the N degenerate $|\square\rangle$ states. These symbols no longer denote the zero-momentum linear combinations of these states. In order to diagonalize the perturbation Hamiltonian within this subspace a suitable basis set must be constructed from these 2N states.

5.2 PERTURBATION EXPANSIONS FOR THE ENERGIES OF THE MODIFIED HAMILTONIAN

In the previous section the $|\square\rangle$ and $|+\rangle$ states, whose quasi-degeneracy was responsible for the non-convergence of the series of equation (3.7) for their energies, were made exactly degenerate under the modified zero-order Hamiltonian $\tilde{H}_o$. Following Messiah (1962) the following notation is introduced to describe the solution of the resulting problem in degenerate perturbation theory.

A g_a-fold degenerate eigen-energy of the unperturbed Hamiltonian is denoted by E_a^0, while P_o is the projector onto the corresponding subspace E_a^0. As $\lambda \to 0$ more than one eigen-energy

of the full Hamiltonian tends to E_a^0. These are denoted by E_α: $\alpha = 1,2 \ldots q$, and their degeneracies and subspaces by g_α: $\alpha = 1,2 \ldots q$ and $\mathcal{E}_\alpha$: $\alpha = 1,2 \ldots q$ respectively. The projector onto the space $\mathcal{E}_1 \oplus \mathcal{E}_2 \oplus \ldots \oplus \mathcal{E}_q$ is P, a continuous function of λ. These definitions imply the relations

$$g_1 + g_2 + \ldots + g_q = g_a \quad , \tag{5.10a}$$

$$\mathcal{E}_1 \oplus \mathcal{E}_2 \oplus \ldots \oplus \mathcal{E}_q \xrightarrow{\lambda \to 0} \mathcal{E}_a^0 \tag{5.10b}$$

and

$$P \xrightarrow{\lambda \to 0} P_o \quad . \tag{5.10c}$$

The usual method for obtaining the E_α perturbatively is that of Kato (1949). It is assumed that any vector of $\mathcal{E}_a$ is the projection in $\mathcal{E}_a$ of a well-defined vector in $\mathcal{E}_a^0$. The two spaces have the same dimension and the projectors P and P_o determine the corresponding vectors. Any eigenvector of H, the full Hamiltonian, in $\mathcal{E}_a$ may thus be written in the form

$$P|E_a^0\ \alpha\rangle \equiv PP_o|E_a^0\ \alpha\rangle \quad , \tag{5.11}$$

which satisfies the eigenvalue equation

$$HP|E_a^0\ \alpha\rangle = E_\alpha P|E_a^0\ \alpha\rangle \quad . \tag{5.12}$$

The projections of both sides of equation (5.12) into $\mathcal{E}_a^0$ must be equal. Thus, with the definitions

$$H_a = P_o H P P_o \tag{5.13a}$$

and

$$K_a = P_o P P_o \quad , \tag{5.13b}$$

equation (5.12) may be written as

$$H_a | E_a^0 \ \alpha> = E_\alpha K_a | E_a^0 \ \alpha> \ . \tag{5.14}$$

Both H_a and K_a are operators in E_a^0 and may be represented by series in λ (Messiah, 1962). This enables the solution of equation (5.14) for the E_α to any order in λ.

A similar method, due to Bloch (1958), was found to be more suitable for application to the present problem. This method makes use of the operator U, which is defined implicitly by the relations

$$P P_o = U K_a \tag{5.15a}$$

and

$$U P_o = U \ . \tag{5.15b}$$

The operator U may be written as the power series in λ

$$U = \sum_{n=0}^{\infty} \lambda^n U^{(n)} \quad . \tag{5.16}$$

The $U^{(n)}$ are given, in terms of the quantity

$$S^k = \begin{cases} 0 & k < 0 \\ -P_o & k = 0 \\ \dfrac{Q_o}{a^k} & k > 0 \end{cases} \tag{5.17}$$

introduced by Kato, by

$$U^{(n)} = \sum_{\{n\}} S^{k_1} V S^{k_2} V \ldots V S^{k_n} V P_o \quad . \tag{5.18}$$

The perturbation Hamiltonian, equal to $H' + \tilde{H}'$ in the present case, is denoted by V and the notation $\sum_{\{n\}}$ implies the summation over all sets of non-negative integers $k_1, k_2 \ldots k_n$ satisfying the relations

$$k_1 + k_2 + \ldots k_p \geqslant p : \quad p \in \{1, 2, \ldots, n-1\} \tag{5.19a}$$

and

$$k_1 + k_2 + \ldots + k_n = n \quad . \tag{5.19b}$$

The further relations

$$P_o U = P_o \tag{5.20a}$$

and

$$PU = U \tag{5.20b}$$

may be obtained with the aid of the above definitions. The operator U acts on a vector of E_a^0 to give the vector of E_a of which it is the projection in E_a^0. These definitions allow equation (5.14) to be written as

$$(P_o H U - E_\alpha) K_a | E_a^0 \; \alpha\rangle = 0 \quad . \tag{5.21}$$

This is an ordinary eigenvalue equation for the non-Hermitian operator

$$P_o H U \equiv H_a K_a^{-1} \tag{5.22}$$

of E_a^0 and the eigenvalues are the required energies. The corresponding eigenvectors are the $K_a | E_a^0 \; \alpha\rangle$, which are the

projections of the eigenvectors of H onto E_a^0.

The expansion of the operator $P_o H U$ as a series in λ is obtained by noting the relation

$$P_o H U = P_o(\tilde{H}_o + \lambda V)U = E_a^o P_o + \lambda P_o V U \tag{5.23}$$

and making use of equations (5.16) and (5.18). The first few terms are

$$P_o H U = E_a^o P_o + \lambda P_o V P_o + \lambda^2 P_o V \frac{Q_o}{a} V P_o$$

$$+ \lambda^3 [P_o V \frac{Q_o}{a} V \frac{Q_o}{a} V P_o - P_o V \frac{Q_o}{a^2} V P_o V P_o] + O(\lambda^4). \tag{5.24}$$

5.3 APPLICATION TO A NON-DEGENERATE STATE: RE-CALCULATION OF THE VACUUM ENERGY

(a) The Expansion

In the case of a non-degenerate state the spaces E_a and E_a^0 are one-dimensional and the energy of the state is given by

$$E_a = \langle E_a^0 | H U | E_a^0 \rangle$$

$$= \sum_{n=0}^{\infty} \lambda^n \beta(n) \quad , \tag{5.25}$$

where

$$\beta^{(n)} = \sum_{\{n-1\}} \langle E_a^0 | V S^{k_1} V S^{k_2} V \cdots V S^{k_n} | E_a^0 \rangle \ . \tag{5.26}$$

The vacuum is such a non-degenerate state. The Hamiltonian of equation (5.5), which has been modified to

make the $|+\rangle$ and $|\square\rangle$ states degenerate in zero-order, should yield values for the vacuum energy that are comparable to those obtained in the previous chapter. The substitution $V \rightarrow H' + \tilde{H}'$ in equation (5.26) allows the terms of the series of equation (5.25) to be identified. The resulting series is different from that arising from equation (3.7).

The zero-order energy is the same as that obtained in the previous chapter, namely

$$\beta^{(0)}_{|0\rangle} = -Nx \quad . \tag{5.27}$$

Higher order contributions will involve different combinations of H' and $\tilde{H}'$, many of which must vanish. The relations

$$\tilde{H}'|0\rangle = 0 \tag{5.28a}$$

and

$$\langle\Psi|\tilde{H}'Q_o = Q_o\tilde{H}'|\Psi\rangle = 0 \qquad \forall \qquad \Psi \quad , \tag{5.28b}$$

which follow from equation (5.4), assist in the identification of the non-zero contributions to equation (5.25). It is clear from the previous chapters that any terms involving odd numbers of H' operators must also vanish. The contributions, up to fifth order, are

$$\beta^{(1)}_{|0>} = 0 \ , \tag{5.29a}$$

$$\beta^{(2)}_{|0>} = \langle 0|H' \frac{Q_o}{a} H'|0> \ , \tag{5.29b}$$

$$\beta^{(3)}_{|0>} = \langle 0|H' \frac{Q_o}{a} \tilde{H}' \frac{Q_o}{a} H'|0> \ , \tag{5.29c}$$

$$\beta^{(4)}_{|0>} = \langle 0|H' \frac{Q_o}{a} H' \frac{Q_o}{a} H' \frac{Q_o}{a} H'|0> - \langle 0|H' \frac{Q_o}{a^2} H'P_oH' \frac{Q_o}{a} H'|0>$$

$$+ \langle 0|H' \frac{Q_o}{a} \tilde{H}' \frac{Q_o}{a} \tilde{H}' \frac{Q_o}{a} H'|0> \ , \tag{5.29d}$$

$$\beta^{(5)}_{|0>} = \langle 0|H' \frac{Q_o}{a} H' \frac{Q_o}{a} \tilde{H}' \frac{Q_o}{a} H' \frac{Q_o}{a} H'|0>$$

$$+ \langle 0|H' \frac{Q_o}{a} H' \frac{Q_o}{a} H' \frac{Q_o}{a} \tilde{H}' \frac{Q_o}{a} H'|0>$$

$$+ \langle 0|H' \frac{Q_o}{a} \tilde{H}' \frac{Q_o}{a} H' \frac{Q_o}{a} H' \frac{Q_o}{a} H'|0>$$

$$+ \langle 0|H' \frac{Q_o}{a} \tilde{H}' \frac{Q_o}{a} \tilde{H}' \frac{Q_o}{a} \tilde{H}' \frac{Q_o}{a} H'|0>$$

$$- \langle 0|H' \frac{Q_o}{a^2} H'P_oH' \frac{Q_o}{a} \tilde{H}' \frac{Q_o}{a} H'|0>$$

$$- \langle 0|H' \frac{Q_o}{a^2} \tilde{H}' \frac{Q_o}{a} H'P_oH' \frac{Q_o}{a} H'|0>$$

$$- \langle 0|H' \frac{Q_o}{a} \tilde{H}' \frac{Q_o}{a^2} H'P_oH' \frac{Q_o}{a} H'|0> \ . \tag{5.29e}$$

(b) Results for the Quasi-Degenerate Vacuum Energy

All the diagrams contributing to equations (5.29) were obtained from those of figures 4.1 and 4.2 using the computer program described in chapter seven. Those terms

of equations (5.29) containing the operator P_o contribute only N^2-dependent terms. The resulting "quasi-degenerate" vacuum energy is plotted, to fourth and fifth order, in figure 5.3. The values for several values of λ are given in table 5.1.

λ	$E^{(5)}_{\|0>}$	$E^{(4)}_{\|0>}$	$\lambda\beta^{(2)}/\beta^{(0)}$	$\lambda\beta^{(3)}/\beta^{(2)}$	$\lambda\beta^{(4)}/\beta^{(3)}$	$\lambda\beta^{(5)}/\beta^{(4)}$
0	-4	-4	-	-	-	-
0.1	-4.0025	-4.0025	3.1×10^{-4}	9.4×10^{-4}	-0.17	5.7×10^{-3}
0.5	-4.0626	-4.0626	7.7×10^{-3}	0.02	-0.13	0.16
1.0	-4.2515	-4.2521	0.03	0.08	-0.03	2.12
1.5	-4.5721	-4.5753	0.06	0.16	0.11	-0.67
2.0	-5.0402	-5.0438	0.10	0.25	0.28	-0.12
2.5	-5.6848	-5.6682	0.14	0.34	0.45	0.17
3.0	-6.5409	-6.4518	0.17	0.42	0.61	0.40
3.5	-7.6384	-7.3890	0.21	0.49	0.76	0.60
4.0	-8.9924	-8.4660	0.24	0.55	0.90	0.77

Table 5.1: Vacuum energy of the modified Hamiltonian.

The "standard" result obtained in the previous chapter is included for comparison. As expected the results from both methods are very similar.

Agreement between the two methods becomes worse as λ becomes large, reflecting the fact that the relation $\sqrt{\lambda^2+4} \cong \frac{\sqrt{\lambda^2+16}}{2}$ used to modify the Hamiltonian no longer gives a good description of the physical processes occurring. The series remains convergent over the range

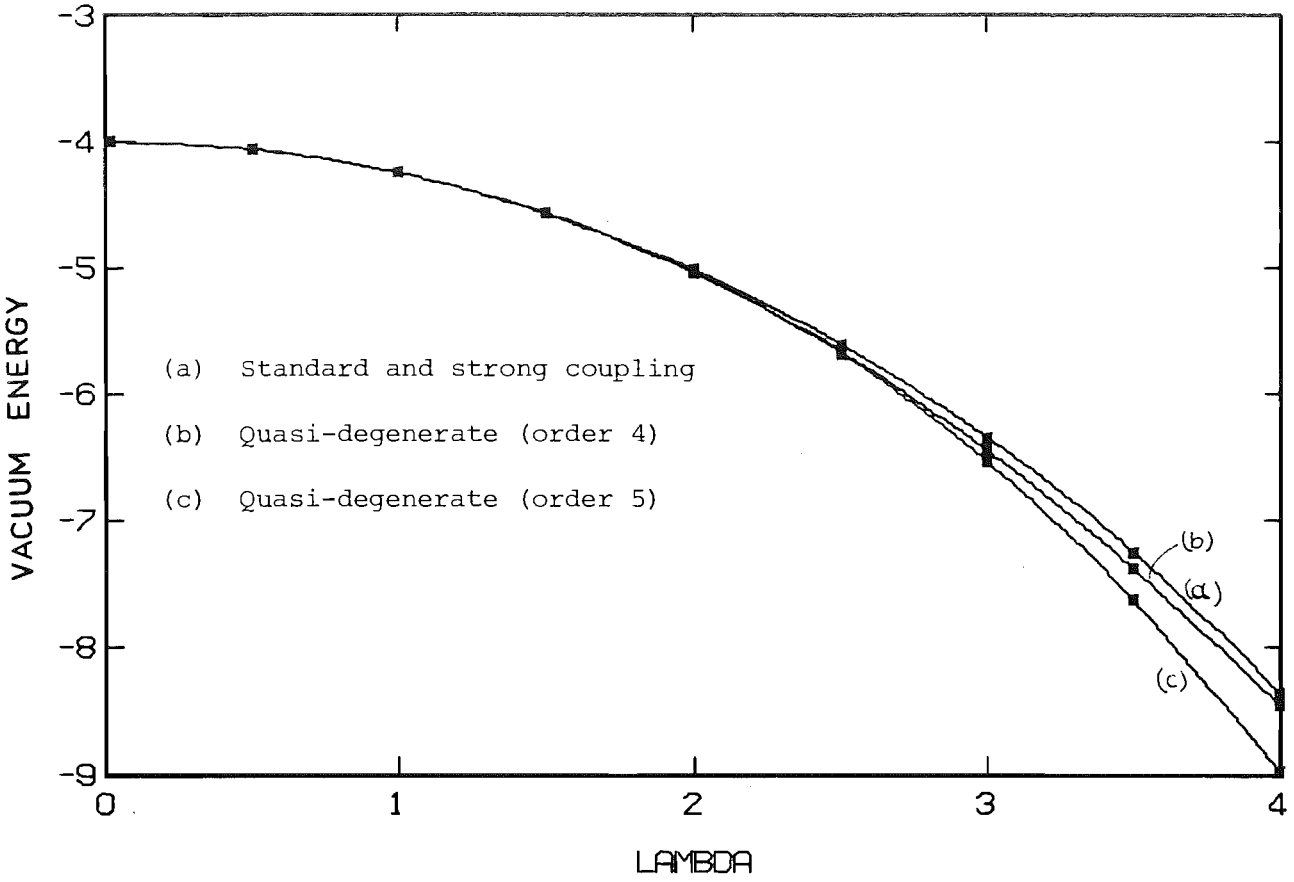

Figure 5.3: The vacuum energy.

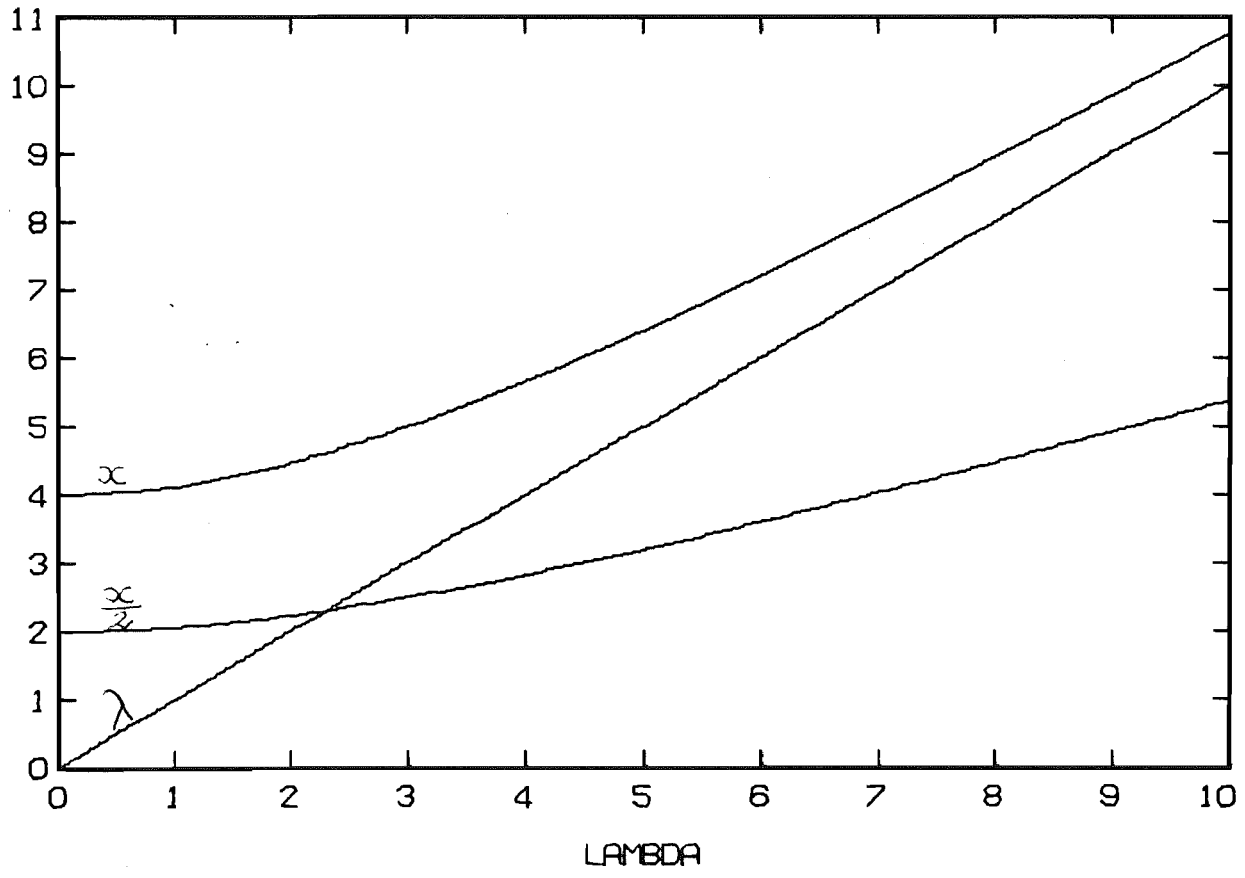

Figure 5.4 (+ve) Energy levels of $\tilde{h}_o(\lambda)$

of λ shown in figure 5.3. The energy levels of the modified zero-order single plaquette Hamiltonian $\tilde{h}_o(\lambda)$ are shown in figure 5.4. Vanishing denominators due to the "level crossing" of $\frac{x}{2}$ and λ, occuring at $\lambda = \sqrt{\frac{16}{3}}$, do not appear. Such denominators would be of the form $\pm D(-\alpha, 0, 2\alpha)$ and these do not occur in any of the diagrams under consideration. They would in fact correspond to intermediate states outside the gauge invariant sector.

(c) The Exactly Degenerate Model

In order to study the effects of the term which has been added to the perturbation, a system closely related to the present problem is considered. The Hamiltonian for the "exactly degenerate" model is defined to be

$$H_D = \tilde{H}_o(\lambda) + \lambda H' \ . \tag{5.30}$$

Although this model does not necessarily describe any known physical system it is a useful model to study as its energies, and other parameters, are within a perturbation of the corresponding quantities for the Z(2) lattice gauge theory. The energies of the exactly degenerate model may be calculated by the methods of the previous section. Note that the $|+\rangle$ and $|\square\rangle$ states are exactly degenerate eigenstates of the zero-order Hamiltonian of this model. The expansion for the vacuum energy of the exactly degenerate model is considerably simpler than that for the quasi-degenerate case given by equations (5.29). Only those terms

involving no $\tilde{H}'$ operators contribute and hence the expansion for the vacuum state of the completely degenerate state involves only even orders. The results are given, for several values of λ, in table 5.2. The vacuum states for the standard, quasi-degenerate and exactly degenerate cases are shown, to fourth order, in figure 5.5.

λ	$E_{\|0>}$	$\lambda^2\beta^{(2)}/\beta^{(0)}$	$\lambda^2\beta^{(4)}/\beta^{(2)}$
0	-4	-	-
0.1	-4.0025	3.1×10^{-4}	-1.6×10^{-4}
0.5	-4.0619	7.7×10^{-3}	-3.5×10^{-3}
1.0	-4.2413	0.03	-0.01
1.5	-4.5261	0.06	-0.01
2.0	-4.9061	0.10	4.0×10^{-3}
2.5	-5.3754	0.14	0.03
3.0	-5.9299	0.17	0.07
3.5	-6.5650	0.21	0.12
4.0	-7.2742	0.24	0.18

Table 5·2 Vacuum Energy of the Exactly Degenerate Model.

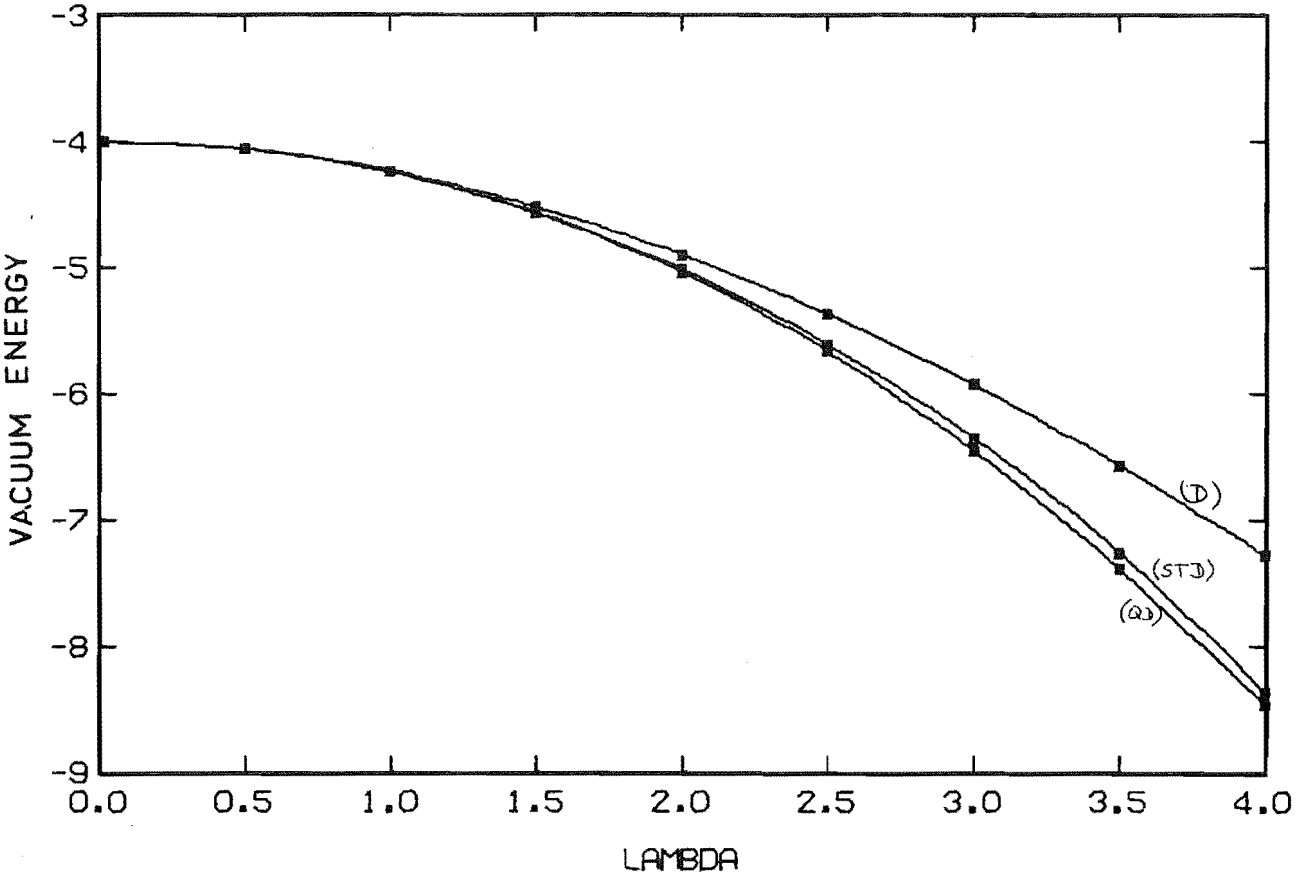

Figure 5.5: Comparison of vacuum energies for standard, (STD) quasi-degenerate (QD) and exactly degenerate (D) models.

5.4 QUASIDEGENERATE PERTURBATION THEORY CALCULATION OF THE MASS GAP

In the previous section the energy of the vacuum state of the modified Hamiltonian $H = H_o(\lambda) + \lambda(H' + \tilde{H}')$ was calculated using the formulation of perturbation theory developed by Bloch. In order to obtain the mass gap it is necessary to calculate the energy of the first excited state in the same way. This requires the solution of the eigenvalue problem of equation (5.21) in the 2N-dimensional space $\mathcal{E}_a^0$ spanned by the N $|+\rangle$ and N $|\square\rangle$ states.

To avoid confusion with the zero-momentum states of the previous chapter the symbols $|\square\rangle$ and $|+\rangle$ should now be interpreted as

$$|+\rangle \equiv |+(\underline{n})\rangle : \underline{n} \text{ odd} \tag{5.31a}$$

and

$$|\square\rangle \equiv |\square(\underline{n})\rangle : \underline{n} \text{ even} \quad . \tag{5.31b}$$

The basis vectors of $\mathcal{E}_a^0$ are then chosen to be the set

$$|E_a^0\ \underline{n}\rangle = \begin{cases} |+(\underline{n})\rangle\ , & \underline{n} \text{ odd} \\ |\square(\underline{n})\rangle\ , & \underline{n} \text{ even} \end{cases} \quad . \tag{5.32}$$

The projector onto $\mathcal{E}_a^0$ is then given by

$$\begin{aligned} P_o &= \sum_{\alpha} |E_a^0\ \underline{n}\rangle\langle E_a^0\ \underline{n}| \\ &= \sum_{\underline{n}\ \text{odd}} |+(\underline{n})\rangle\langle+(\underline{n})| + \sum_{\underline{n}\ \text{even}} |\square(\underline{n})\rangle\langle\square(\underline{n})| \\ &\equiv |+\rangle\langle+| + |\square\rangle\langle\square| \quad . \end{aligned} \tag{5.33}$$

The projector onto the complementary space is

$$Q_o = 1-P_o \ . \tag{5.34}$$

Equation (5.21) may be written, using equation (5.33), as

$$P_o H U (P_o+Q_o) K_a |E_a^0\ \underline{n}\rangle = E_{\underline{n}}\ K_a |E_a^0\ \underline{n}\rangle$$

$$\Rightarrow \sum_{\underline{n}'} P_o H U |E_a^0\ \underline{n}'\rangle\langle E_a^0\ \underline{n}'|K_a|E_a^0\ \underline{n}\rangle = E_{\underline{n}}\ K_a|E_a^0\ \underline{n}\rangle, \tag{5.35}$$

since $Q_o K_a = 0$. The energy of the first excited state is the lowest eigenvalue of this equation, which may be written in component form as

$$\sum_{\underline{n}''}\ \sum_{\underline{n}'}\ \sum_{\underline{n}} \langle E_a^0\ \underline{n}''|P_o H' U|E_a^0\ \underline{n}'\rangle\langle E_a^0\ \underline{n}'|K_a|E_a^0\ \underline{n}\rangle$$

$$= E_{\underline{n}} \sum_{\underline{n}''} \langle E_a^0\ \underline{n}''|K_a|E_a^0\ \underline{n}\rangle \ . \tag{5.36}$$

Recall that the matrix $P_o H' U$ is non-Hermitian. Since the N $|+\rangle$ states should be physically equivalent, as should the N $|\square\rangle$ states, it is expected that it should be possible to partition the problem of equation (5.36). If the $|E_a^0\ \underline{n}\rangle$ are ordered as suggested by figure 5.6 the expected partition is of the form

$$\begin{pmatrix} M_{++} & M_{+\square} \\ M_{\square+} & M_{\square\square} \end{pmatrix} \begin{pmatrix} \underline{a} \\ \underline{b} \end{pmatrix} = E_{\underline{n}} \begin{pmatrix} \underline{a} \\ \underline{b} \end{pmatrix} \ . \tag{5.37}$$

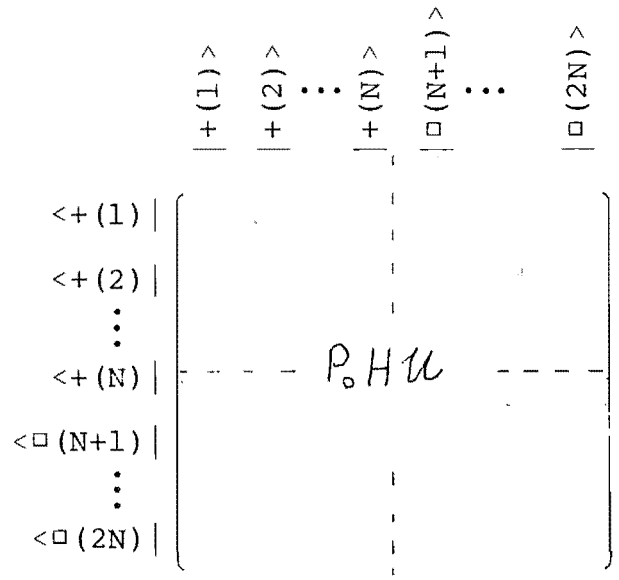

Figure 5.6: Ordering the $|E_a^0\ \underline{n}\rangle$ to partition the $P_o H\mathcal{U}$ matrix.

The submatrices M are N x N square matrices and the vectors $\underline{a}$ and $\underline{b}$ are N-dimensional. The study of small lattices shows that the rows of a submatrix are equivalent: the same elements occur but their order is different. This suggests that there exist solutions for which $a_i = a$ and $b_i = b$. If these solutions correspond to the lowest energy then the 2N-dimensional eigenvalue problem of equation (5.37) is reduced to a pair of simultaneous equations. It was verified that the minimum energy solutions for small finite lattices were of the above form. The nature of the

solution should not depend on the size of the lattice and hence, by induction, the lowest energy-solution for the infinite lattice should also be of this form. Each element is a series in λ whose terms may be specified and evaluated using the diagrammatic techniques introduced in chapter 3. The sums of the elements of any of the equivalent rows of the sub-matrices are denoted by

$$\Sigma_{\eta\kappa} \; : \; \eta,\kappa\in\{+,\square\} \; . \tag{5.38}$$

The $\Sigma_{\eta\kappa}$ may be written, using equations (5.16), (5.18) and (5.23) as

$$\begin{aligned}
\Sigma_{\eta\kappa} &= \langle\eta|P_o H U|\kappa\rangle \\
&= \langle\eta|P_o(\tilde{H}_o'(\lambda) + (H'+\tilde{H}'))(\sum_{\{n\}}\lambda^n U^{(n)})|\kappa\rangle \\
&= \langle\eta|\tilde{H}_o|\kappa\rangle + \lambda\langle\eta|(H'+\tilde{H}')|\kappa\rangle \\
&\quad + \lambda^2\langle\eta|(H'+\tilde{H}')\frac{Q_o}{a}(H'+\tilde{H}')|\kappa\rangle + O(\lambda^3) \; .
\end{aligned} \tag{5.39}$$

As in the case of equations (5.29) for the vacuum state, many of the possible terms do not contribute. In addition to the restriction of equation (5.28b) the relation

$$\langle\square|\tilde{H}' = \tilde{H}'|\square\rangle = 0 \tag{5.40}$$

follows from the definition of $\tilde{H}'$.

The non-zero terms contributing to the $\Sigma_{\eta K}$ are given in Appendix B.

The required energies may now be obtained by solving the equation

$$\begin{pmatrix} \Sigma_{++} & \Sigma_{+\square} \\ \Sigma_{\square+} & \Sigma_{\square\square} \end{pmatrix} \begin{pmatrix} a \\ b \end{pmatrix} = E \underline{n} \begin{pmatrix} a \\ b \end{pmatrix} \tag{5.41}$$

to obtain the eigenvalues

$$E_{\pm} = (\Sigma_{++} + \Sigma_{\square\square})/2 \pm \tfrac{1}{2}[(\Sigma_{++} - \Sigma_{\square\square})^2 + 4\Sigma_{+\square}\,\Sigma_{\square+}]^{\frac{1}{2}} . \tag{5.42}$$

The first excited state of the exactly degenerate model defined in the previous section may be calculated in exactly the same way. The corresponding series for the $\Sigma_{\eta K}$ consists of those terms of Appendix B that contain no $\tilde{H}'$ operators and are thus considerably simpler than those for the quasi-degenerate case.

All the required matrix elements may be obtained from those of the expression of equation (3.7) for the zero-momentum superpositions of the $|+\rangle$ and $|\square\rangle$ states. The construction of the additional diagrams and calculation of the energies $E_{\pm}$ was achieved using the computer program described in chapter seven. The mass gaps G_D and G_{QD}, for the exactly degenerate and quasi-degenerate cases respectively, were then obtained by subtracting the vacuum energy for the appropriate case.

The mass gap is required to be an intensive quantity for physical reasons, just as the vacuum energy is required

to be extensive. Some methods for the calculation of these quantities, such as the perturbative-variational scheme of Bessis and Villani (1975) which has recently been applied to the (2+1)-dimensional Z(2) lattice gauge theory by Banks and Zaks (1982), do not necessarily satisfy these physical requirements. All of the expansions used in the present work lead to extensive vacuum energies and intensive mass gaps.

In order to obtain an intensive mass gap using the Bloch formulation it is necessary to truncate the series for the $\Sigma_{\eta\kappa}$ appearing in equation (5.42) to different orders, depending on whether or not they are inside the square brackets of that equation. Those $\Sigma_{\eta\kappa}$ occurring outside the square brackets are truncated at order q while those inside are truncated so that the terms $(\Sigma_{++} - \Sigma_{\square\square})^2$ and $\Sigma_{+\square}\Sigma_{\square+}$ contain all terms up to order 2q. Since the gap resulting from the choice of either sign in equation (5.42) must be intensive it is clear that the quantity within the square brackets must be independent of N, while the N-dependence of the quantity outside the square brackets must be equal to that of the vacuum.

The present calculation was continued up to third order outside the square brackets and sixth order inside. Diagrams contributing to $\Sigma_{\eta\kappa}$ up to fifth order were required. The energies resulting from the choice of the minus sign in equation (5.42) were lower than those resulting from the choice of the plus sign and were therefore used in the calculation of the mass gap, which is denoted by $G^{(-)}_{|1>}$.

The results obtained for the mass gaps of the quasi-degenerate and exactly degenerate theories are given in tables 5.3 and 5.4, and plotted in figure 5.7. The series

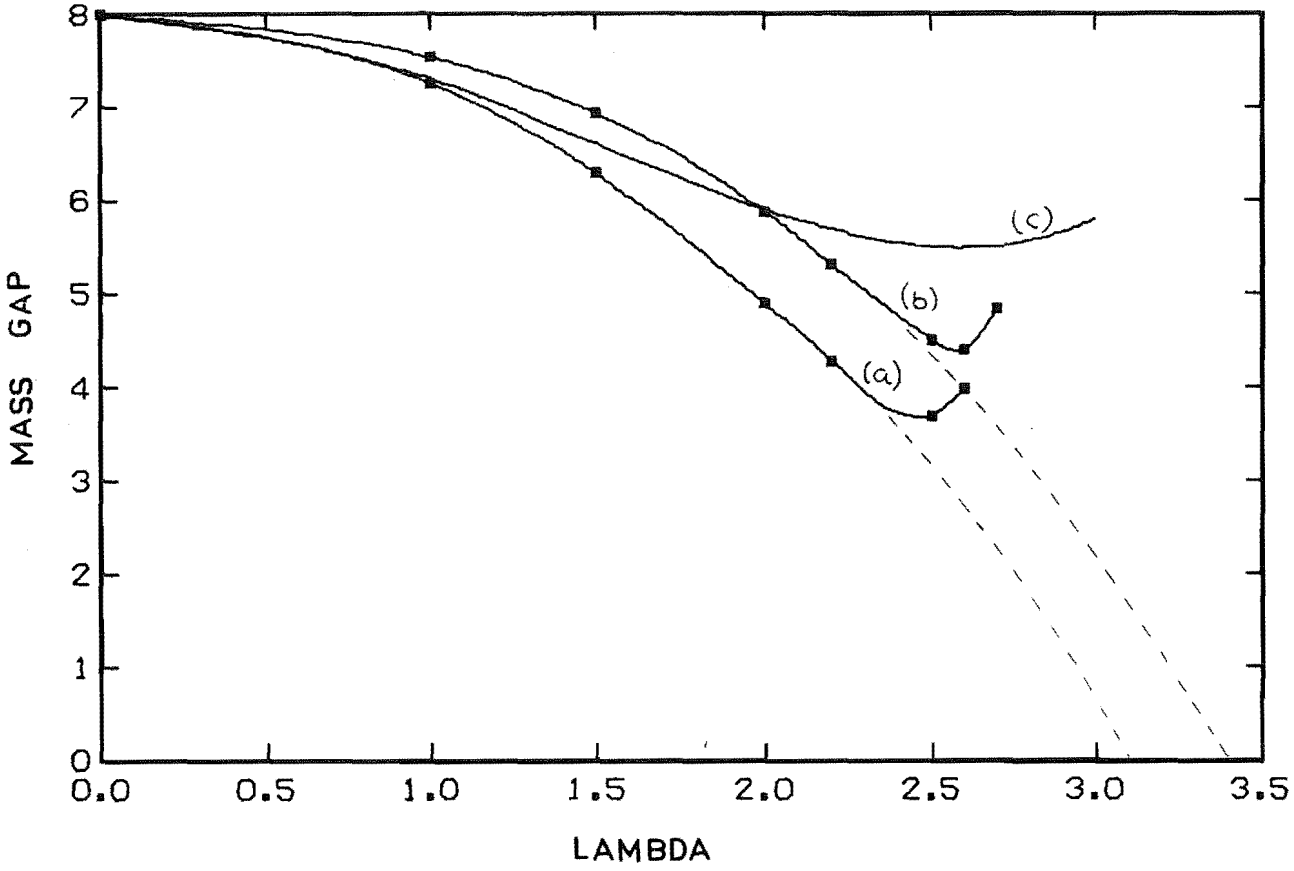

Figure 5.7: Mass gaps for (a) quasi-degenerate (b) exactly degenerate, (c) strong coupling (section 5.5) cases.

for the mass gaps in the Bloch formalism are not simple polynomials. In order to study the convergence of these series the quantities Δ_q are defined. The Δ_q are those terms added to the series for the mass gap when terms of order λ^q are added outside the square brackets of equation (5.42) and terms of order λ^{2q-1} and λ^{2q} are added inside them.

Before the critical coupling is reached the quantity inside the square brackets of equation (5.42) becomes negative, implying that the energy of the first excited state, and hence

λ	$G_{QD}^{(-)}$	Δ_1	Δ_2	Δ_3
0	8	0	0	0
1	7.2553	-0.9018	-0.0785	-0.0106
1.5	6.2857	-1.8288	-0.4653	0.0359
2	4.8913	-2.8943	-1.6253	0.4666
2.2	4.2804	-3.3395	-2.4316	0.9214
2.5	3.6974	-4.0166	-4.1164	2.3964
2.6	3.9758	-4.2436	-4.8205	3.4984
2.7	*	*	*	*
2.8	*	*	*	*
3	*	*	*	*

Table 5.3: Mass Gap for the Quasi-Degenerate Case

* denotes complex value for $G_{QD}^{(-)}$

λ	$G_{D}^{(-)}$	Δ_1	Δ_2	Δ_3
0	8	0	0	0
1	7.5372	-0.4287	-0.2810	0.0087
1.5	6.9317	-0.8257	-0.8104	0.0239
2	5.8767	-1.2325	-1.9433	0.1082
2.2	5.3105	-1.3879	-2.6814	0.2496
2.5	4.5028	-1.6088	-4.2205	0.8980
2.6	4.4037	-1.6788	-4.8689	1.4100
2.7	4.8331	-1.7470	-5.5930	2.5211
2.8	*	*	*	*
3	*	*	*	*

Table 5.4: Mass Gap for the Degenerate Case

*denotes complex value for $G_{D}^{(-)}$

the mass gap, is taking complex values. However it is clear from tables 5.3 and 5.4 that the series is failing to converge before this point is reached.

If those points for which $\left|\frac{\Delta_2}{\Delta_1}\right| > 1$ are ignored it is possible to extrapolate the $G^{(-)}_{|1>}(\lambda)$ curve to obtain the value

$$\lambda_c = 3.1 \pm 0.1 \quad ,$$

which is consistent with the generally accepted value of

$$\lambda_c = 3.125 \quad .$$

The duality relation of equation (4.11) relates the mass gaps of the gauge and Ising models. As λ increases towards λ_c the mass gap behaves as

$$G(\lambda) = \lambda G^I(\lambda^{-1}) \sim (\lambda^{-1} - \lambda_c^{-1})^{\nu}, \qquad (5.43)$$

where ν is the critical index for the mass gap. The result $\nu = 0.7 \pm 0.4$ is obtained from the estimated value of λ_c. The correlation length scaling hypothesis (e.g. Kogut 1979b) leads to the relation

$$\alpha = 2 - \nu d \quad , \qquad (5.44)$$

where d is the number of space-time dimensions, between the critical indices whose values have been estimated. Substitution of the value of α obtained in the previous chapter implies the value $\nu = 0.62 \pm 0.01$, which is consistent with that obtained above. The crudity of the extrapolation used to estimate the mass gap critical index suggests that this result should be treated with

caution. The accepted value for the Ising model (Fisher 1967) is

$$\nu = 9/14 \pm 0.0025 = 0.6429 \pm 0.0025 \quad .$$

The results for the degenerate case indicate that the ratio $|\Delta_2/\Delta_1|$ becomes greater than unity for lower values of λ than in the quasi-degenerate case. If points for which $\left|\frac{\Delta_2}{\Delta_1}\right| > 1$ are discarded the curve for the mass gap of the degenerate model may be (crudely) extrapolated to indicate that its critical point is in the region of 3.4 ± 0.2.

The values of the mass gap, $G^{(-)}_{|1>}$ obtained by including contributions from successive orders are shown in figure 5.8 for the quasi-degenerate case.

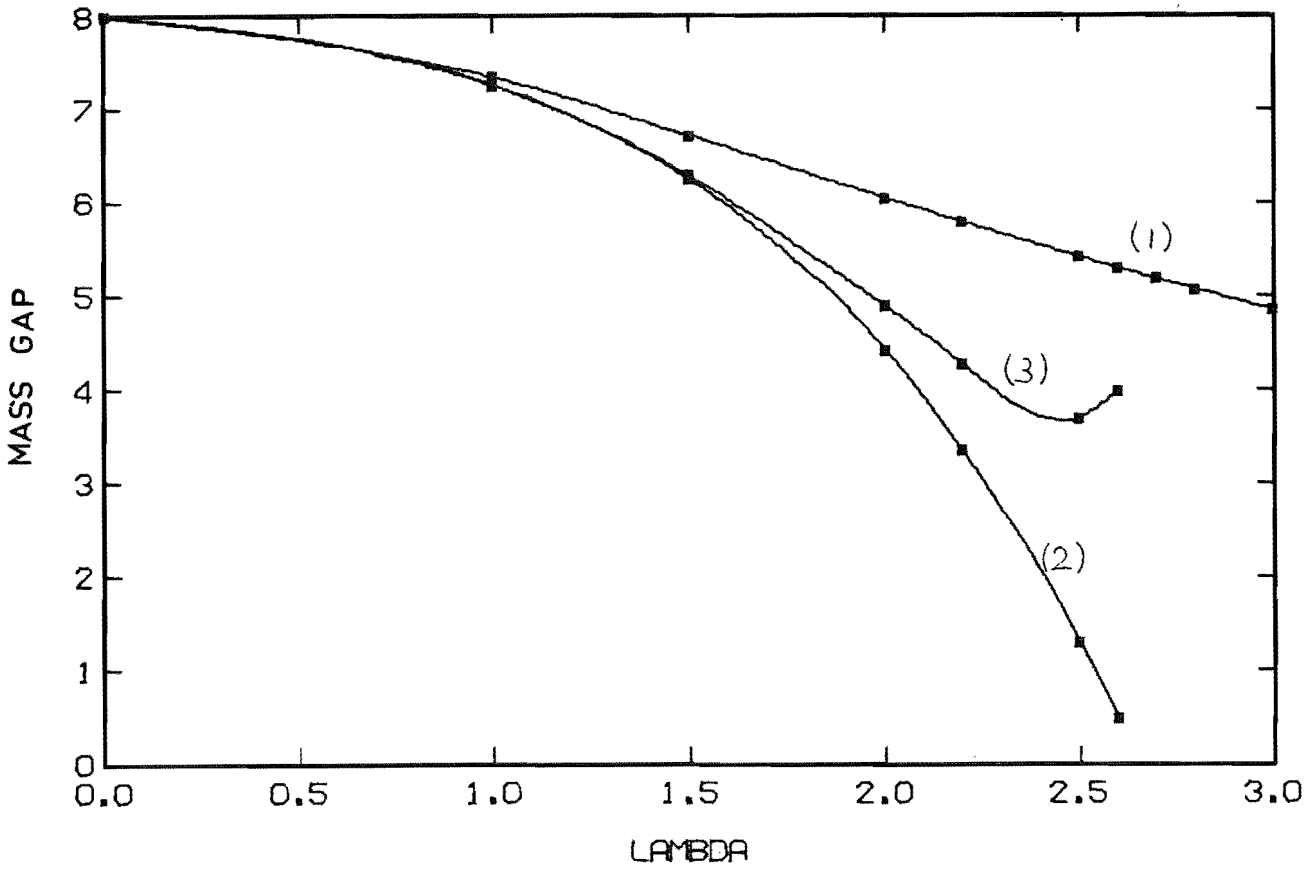

Figure 5.8: Successive values for $G^{(-)}_{|1>}$. The lines are labelled by the highest order of the terms inside the square brackets of equation (5.42).

It is probable that the performance of this series would improve if higher order terms were calculated. Since the zero-order term, 2x, is increasing with λ the lower order corrections must necessarily be large in order to achieve small values for the mass gap. The ratio $\left|\frac{\Delta_3}{\Delta_2}\right|$ remains less than unity for all the results obtained. If it is assumed that $|\Delta_4/\Delta_3| \simeq |\Delta_3/\Delta_2|$. Then it is quite possible that those points for which $\left|\frac{\Delta_2}{\Delta_1}\right| > 1$ will be corrected back to the extrapolated lines of figure 5.7 and that the problem of apparently complex mass gaps will not occur.

Values for the energy gap $G^{(+)}_{|1>}(\lambda)$, resulting from the choice of the plus sign in equation (5.42), were also obtained. Tables 5.5 and 5.6 give the results obtained for the quasidegenerate and degenerate cases respectively.

λ	$G^{(+)}_{QD}$	Δ_1	Δ_2	Δ_3
0	8	0	0	0
1	8.2238	0.2038	-0.3352	0.1090
1.5	8.4029	0.3728	-0.8860	0.3721
2	8.3029	0.5248	-1.7037	0.5376
2.2	8.0173	0.5768	-2.0847	0.3951
2.5	6.8289	0.6443	-2.6978	-0.5516
2.6	5.8284	0.6641	-2.9115	-1.4657
2.7	*	*	*	*
2.8	*	*	*	*
3	*	*	*	*

Table 5.5: Energy gap $G^{(+)}_{|1>}$ for the quasi-degenerate case.

λ	$G_D^{(+)}$	Δ_1	Δ_2	Δ_3
0	8	0	0	0
1	8.5415	0.4287	-0.1248	-0.0087
1.5	8.8049	0.8257	-0.5409	-0.0239
2	8.6829	1.2325	-1.3856	-0.1082
2.2	8.4334	1.3879	-1.8350	-0.2496
2.5	7.5511	1.6088	-2.5937	-0.8980
2.6	6.9472	1.6788	-2.8631	-1.4100
2.7	5.7391	1.7470	-3.1387	-2.5211
2.8	*	*	*	*
3	*	*	*	*

Table 5.6: Energy gap $G_{|1>}^{(+)}$ for the degenerate case.

The values of both $G_{|1>}^{(+)}$ and $G_{|1>}^{(-)}$ are plotted in figure 5.9 for both the quasi-degenerate and exactly degenerate cases. As in the case of $G_{|1>}^{(-)}$ it is found that $|\Delta_2/\Delta_1| > 1$ for some of the values of λ considered, but $|\Delta_3/\Delta_2|$ remains less than unity. The $G_{|1>}^{(+)}$ represent a low lying excited state. It is interesting to note that the curves of $G_{|1>}^{(+)}$ on figure 5.9 appear to turn downwards as λ increases, indicating that this state may also become massless at the critical point. If this is the case then the quantity inside the square brackets of equation (5.42) must approach zero near the critical point and the mass gap will be given by $(\Sigma_{++} + \Sigma_{\square\square})/2$. The relatively short series being used

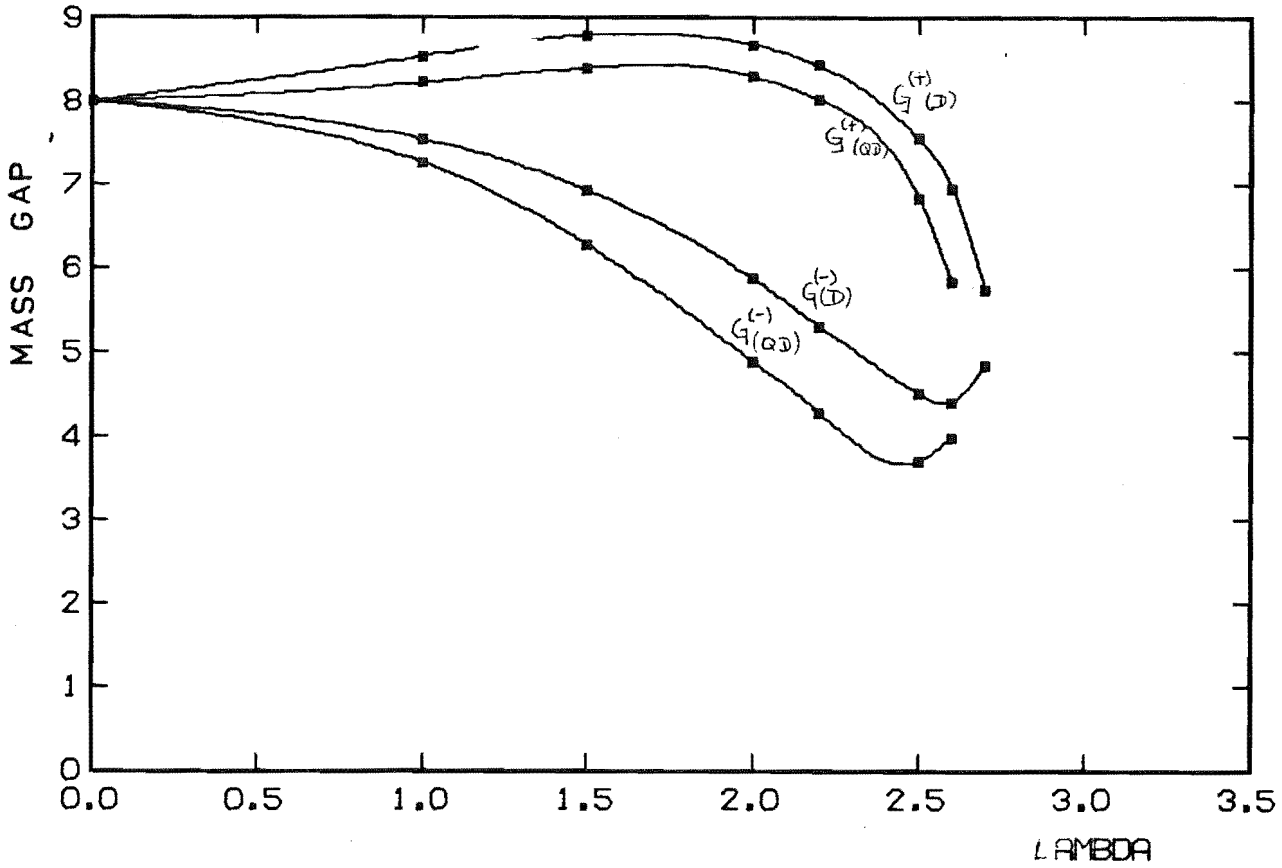

Figure 5.9: The quantities $G^{(+)}_{|1>}$ and $G^{(-)}_{|1>}$ for the quasi-degenerate and exactly degenerate cases.

in the present work were still behaving erratically in the region of the critical point. Retaining only the real part of the mass gap was thus of no assistance in further defining λ_c.

The requirements that the quantity $(\Sigma_{++}-\Sigma_{\square\square})^2 + 4\Sigma_{+\square}\Sigma_{\square+}$ be independent of N and that the N-dependence of the quantity $(\Sigma_{++} + \Sigma_{\square\square})/2$ be equal to that of the vacuum were satisfied numerically to machine accuracy for double precision. As well as fulfilling the requirement that the mass gap be intensive this result is an extremely important indicator of the integrity of the data used in its calculation. Diagrams whose counting factors do not involve N are also included in this result via terms such as $\Sigma_{+\square}\Sigma_{\square+}$. However there are still many diagrams which do not enter into the N-dependence calculation.

Since a single error is capable of drastically affecting the outcome of the calculation it is vital that further conditions, to be satisfied by these diagrams, be devised. The increasing complexity of the diagrams makes checking by hand-calculation impractical.

The required conditions arise as a natural consequence of the Bloch formulation, and the partitioning of the $P_o H U$ matrix, and its eigenvectors, defined by equation (5.37). As an example consider the diagrams corresponding to the quantity

$$A = \langle \square | H' \frac{Q_o}{a} H' \frac{Q_o}{a} H' \frac{Q_o}{a} H' \frac{Q_o}{a} H' | + \rangle \ , \qquad (5.45)$$

which contributes to the fifth order term of $\Sigma_{\square +}$. Those diagrams contributing to A which have no N-dependence are not included in the calculation of the overall N-dependence of the mass gap. However several other quantities such as

$$B = \langle \square | H' \frac{Q_o}{a^2} H' P_o H' \frac{Q_o}{a} H' \frac{Q_o}{a} H' | + \rangle, \qquad (5.46)$$

which also contributes to the fifth order term of $\Sigma_{\square +}$, are calculated from the same diagrams. Substitution of the definition of P_o, given by equation (5.33), allows this quantity to be expressed as

$$B \equiv \langle \square | H' \frac{Q_o}{a^2} H' | \square \rangle \langle \square | H' \frac{Q_o}{a} H' \frac{Q_o}{a} H' | + \rangle \ . \qquad (5.47)$$

This may now be calculated as the product of a second-order contribution to $\Sigma_{\square\square}$ and a third-order contribution to

$\Sigma_{\square+}$. Equalities such as that implied by equations (5.46) and (5.47) were devised for all the contributions to the mass gap. Those terms which could be expressed as products of lower order terms were calculated in that way, resulting in a considerable reduction in the amount of computation required. It is important to know that the results, favourable or otherwise, are in fact due to the method under consideration and not to incorrect data or computation. It is felt that the comprehensive system of checks available within the present method eliminates the need for the customary expressions of doubt (e.g. Munster, 1981), however light-hearted they may be.

Strong-coupling expansions for the mass gap have been obtained by other methods (e.g. Munster, 1981). Hamiltonian methods, such as the finite lattice approach to the gauge model (e.g. Irving and Thomas, 1982) or its dual spin system (e.g. Roomany and Wyld, 1980), frequently obtain results for the mass gap by scaling arguments. The latter authors stated that they were not aware of any previous treatment of the (2+1)-dimensional Ising model in the Hamiltonian formulation.

The conventional strong-coupling calculation of the mass gap was performed to fourth order. Banks and Sinclair (1981) report a similar calculation using a Hamiltonian differing from that of equation (2.27) by an irrelevant additive constant and an overall factor of ½. With the identifications $b_{oo} \equiv \varepsilon^{(0)}_{|1>SC}/2$ and $x \equiv \frac{\lambda}{2}$ their result agrees with that obtained in the next section.

5.5 CONVENTIONAL STRONG-COUPLING EXPANSION FOR THE MASS GAP

The conventional strong-coupling expansion for the mass gap of (2+1)-dimensional Z(2) lattice gauge theory in the Hamiltonian formulation was calculated to second order in chapter four. Odd orders do not contribute to this expansion so the next non-zero terms are the fourth-order corrections

$$\varepsilon^{(4)}_{|1>^{SC}} = {}^{SC}\langle 1|H'_{SC}\,\frac{Q_o}{a}\,H'_{SC}\,\frac{Q_o}{a}\,H'_{SC}\,\frac{Q_o}{a}\,H'_{SC}|1\rangle^{SC}$$

$$- {}^{SC}\langle 1|H'_{SC}\,\frac{Q_o}{a^2}\,H'_{SC}|1\rangle^{SC}\,{}^{SC}\langle 1|H'_{SC}\,\frac{Q_o}{a}\,H'_{SC}|1\rangle^{SC}. \quad (5.48)$$

The second term of equation (5.48) is constructed from the second-order diagrams of table 4.5 and its value is

$${}^{SC}\langle 1|H'_{SC}\,\frac{Q_o}{a^2}\,H'_{SC}|1\rangle^{SC}\;{}^{SC}\langle 1|H'_{SC}\,\frac{Q_o}{a}\,H'_{SC}|1\rangle^{SC}$$

$$= -\frac{(3N^2 + 20N + 33)}{128} \quad (5.49)$$

The types of diagrams contributing to the first term of equation (5.48) are shown in table 5.7. The active plaquette picture and counting factor is shown for each of the types and the total contribution from each type is also shown. Combination of these results and the second-order terms obtained in chapter four gives the expression

$$G_{|1>^{SC}} = 8\left(1 - \frac{3}{32}\,\lambda^2 + \frac{43}{6144}\,\lambda^4 + O(\lambda^6)\right). \quad (5.50)$$

Active plaquette picture	Counting Factor	Contribution to $\varepsilon^{(4)}_{\|1>^{SC}}$
□□□	$2(2N^2-15N+32)$	$\frac{3}{256}(-2N^2 + 15N - 31)$
□□□	$8(N-4)$	$\frac{1}{12}(-7N + 16)$
□□□	12	$-\frac{75}{64}$
□□	4	0
□	1	0

Table 5.7: Fourth order contributions to the conventional Strong-Coupling Mass Gap.

This series has a minimum at $\lambda \sim 2.6$ and clearly exhibits poor convergence in the region of the phase transition. Since the series may be oscillating the inclusion of higher order terms may improve its performance. Some values for the mass gap obtained using equation (5.50) are given in table 5.8 and plotted in figure 5.7 for comparison with the present method.

In this chapter the problem of quasi-degenerate perturbation theory was turned into a problem of degenerate perturbation theory by the modification of the definitions of the zero-order and perturbation Hamiltonians. The lowest-energy state of the resulting problem was examined using the formulation of perturbation theory due to Bloch. The vacuum energy calculated by this method agrees closely

λ	Strong-Coupling Mass Gap	$\lambda^2\varepsilon^{(4)}_{\|1>^{SC}}/\varepsilon^{(2)}_{\|1>^{SC}}$
0	8	-
0.5	7.81600	-0.019
1	7.30599	-0.075
1.5	6.59595	-0.168
2	5.89583	-0.299
2.5	5.49959	-0.467
3	5.78516	-0.672
3.5	7.21444	-0.915

Table 5.8: The Conventional Strong-Coupling Mass Gap.

with the results of the previous chapter, implying that the modification of the Hamiltonian does not affect the calculation of the energy of a non-degenerate state. The results for the mass gap are clearly superior to those obtained from the conventional strong-coupling series calculated in section 5.5. Although the present series fails to produce real values for the mass gap close to the critical point it is felt that the inclusion of higher order terms would result in considerable improvement.

Quasi-degenerate perturbation expansions have been applied to calculations in lattice gauge theory by other authors (e.g. Carroll and Kogut, 1979, Jones et al., 1979). The method of these authors differs from that of the present work in that it involves modification of the

projectors P_o and Q_o rather than the Hamiltonian itself. Attempts to apply their method to the present problem yielded a non-intensive mass gap and were abandoned.

CHAPTER 6

THE STRING TENSION

In the previous chapters the phase structure of the theory has been studied by examining the behaviour of the mass gap as λ is varied. Another quantity whose behaviour signals the onset of phase transitions is the string tension. In quantum chromodynamics (QCD) spatially separated quarks interact via narrow "flux tubes" or "strings". The string tension measures the way the strength of this interaction varies with the separation of the quarks. String theory is important in the theory of the structure of hadrons (e.g. Tassie 1979), which may be regarded as a number of quarks joined together by string "bits". The study of strings in Z(N) theories (e.g. Imachi and Yoneyama, 1980) is relevant to this work. The Z(N) groups are the centres of the proposed gauge groups for QCD and are thought (e.g. 't Hooft 1978) to control the phase structure of the theory.

Matter fields are not considered in the present work and the strings to be considered are the flux tubes connecting two unseen quarks at opposite ends of the (infinite) lattice. The energy of such a state may be calculated perturbatively. In the strong coupling limit the string consists of a line of L flipped spins joining the two "quarks". As higher order contributions to the string energy are included the string "thickens" or "vibrates".

The string tension may then be defined (e.g. Horn et al. 1979) as

$$T = \lim_{L\to\infty} \frac{E|\text{string}\rangle - E|0\rangle}{L} \quad . \tag{6.1}$$

Discontinuities or zeros of the string tension signify the occurrence of phase transitions.

The tension should not, in principle, depend on the orientation of the string. However the symmetries of the lattice theory are very restricted and the behaviour of strings parallel to one of the axes of the lattice differs from that of "off-axis" strings. These two cases are examined in sections 6.1 and 6.2 respectively. The observed "roughening" of the theory (e.g. Itzykson 1981) provides evidence for the recovery of rotational invariance in the continuum limit, where the lattice spacing vanishes (e.g. Kogut et al. 1981, Kogut and Sinclair 1981b).

6.1 THE AXIAL STRING

A string constructed from the links of the lattice is perfectly straight only if it follows one of the lattice directions μ,ν. The horizontal line of flipped spins shown in figure 6.1 is an example of such an axial string. This is the zero-order state for the conventional strong-coupling

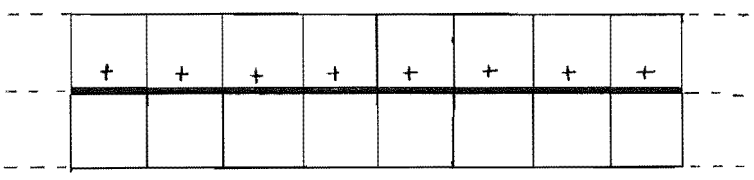

Figure 6.1: Horizontal axial string in the strong-coupling limit.

calculation of the string tension. The corresponding state in the present formulation is that of figure 6.2.

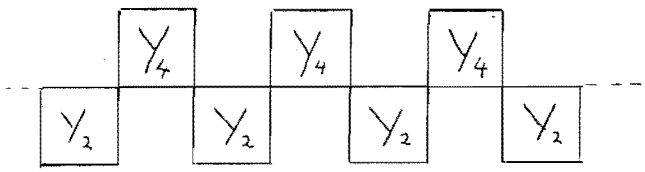

Figure 6.2: Horizontal string constructed from plaquette states.

The two states are identical in the strong-coupling limit. It may be confirmed from table 2.8 that the configuration of figure 6.2 is gauge invariant.

For non-zero λ it is clear, from tables 2.2 and 2.4, that this zero-order state incorporates configurations of the string which would not normally occur until higher orders in the strong-coupling expansion. An example is shown in figure 6.3. The zero-order state thus has non-zero thickness.

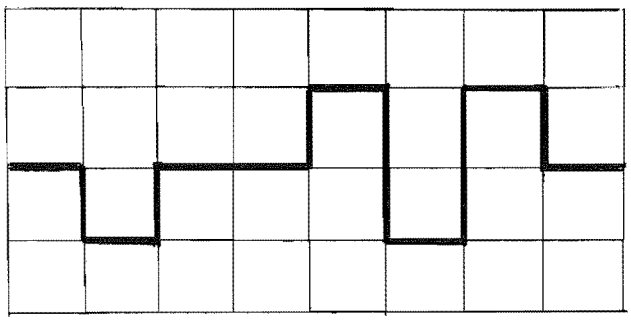

Figure 6.3: String configuration now included in the zero-order state.

The spatial lattice under consideration has N even and N odd plaquettes, and is assumed to be square. The number of plaquettes along a side, which is the length in lattice units of the horizontal string, is thus

$$L = \sqrt{2N} \quad . \tag{6.2}$$

The horizontal string state, denoted by $|\text{---}>$, is clearly L-fold degenerate and a zero momentum state is defined as in chapter three. This is not strictly necessary since no two degenerate horizontal string states may be connected in any finite order perturbation expansion. The series defined by equations (3.7) and (3.8) may be used to calculate the tension defined by equation (6.1). The resulting expression is

$$T_{|->} = T^{(0)}_{|->} + \lambda^2 T^{(2)}_{|->} + \lambda^4 T^{(4)}_{|->} + 0(\lambda^6) \tag{6.3a}$$

$$= \frac{\varepsilon^{(0)}_{|->} - \varepsilon^{(0)}_{|0>}}{L} + \lambda^2 \left(\frac{\varepsilon^{(2)}_{|->} - \varepsilon^{(2)}_{|0>}}{L} \right)$$

$$+ \lambda^4 \left(\frac{\varepsilon^{(4)}_{|->} + \varepsilon^{(4)}_{|0>}}{L} \right) + 0(\lambda^6) \, . \tag{6.3b}$$

No odd order terms contribute to the tension of the horizontal string.

The zero-order energy of the horizontal string is

$$\varepsilon^{(0)}_{|->} = -(N-L)x - Ly \tag{6.4}$$

and, using equation (4.3), the zero-order tension is

$$T^{(0)}_{|->} = x-y \quad . \tag{6.5}$$

The string tension, like the mass gap, is an intensive quantity and therefore does not depend on the lattice size.

In order to evaluate the higher order terms of equation (6.3) an extension of the diagrammatic methods of chapter three is used. The three contributions to the second order term

$$\varepsilon^{(2)}_{|\longrightarrow} = \langle\longrightarrow| H' \frac{Q_o}{a} H' |\longrightarrow\rangle \tag{6.6}$$

are shown, together with their corresponding counting factors and active plaquette pictures, in Table 6.1. A cross of active plaquettes may have one or three common plaquettes with the string, depending on whether the odd plaquette at its centre is on a hummock (case (b) of Table 6.1) or in a hollow (case (c)). Rather than introducing triple curved lines to describe this situation single curved lines, emanating from hummocks or hollows of the symbol (ζ) for the string state, are used.

There are 75 fourth order diagrams arising from the first term of equation (3.8e). The product terms participate only in the cancellation of the tension's dependence on the lattice size. Results are shown for several values of λ in Table 6.2 and are plotted in figure 6.4.

classification polygon	counting factor	active plaquette picture
(a) 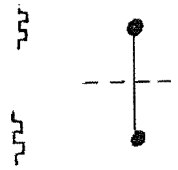	N-2L	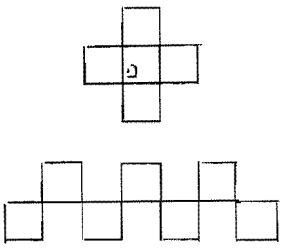
(b) 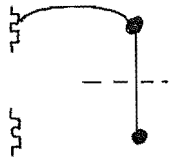	L	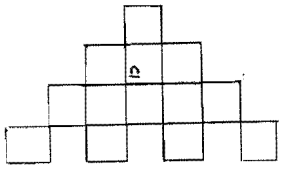
(c) 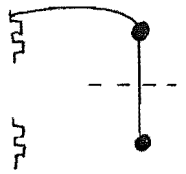	L	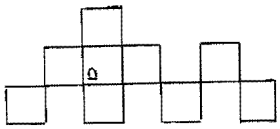

Table 6.1: Second order contributions to the horizontal string energy.

λ	Tension	$\lambda^2 T\|_{\rightarrow}^{(2)} / T\|_{\rightarrow}^{(0)}$	$\lambda^2 T\|_{\rightarrow}^{(4)} / T\|_{\rightarrow}^{(2)}$
0	2	-	-
0.5	1.9355	-0.02	-0.02
1	1.7119	-0.10	-0.04
1.5	1.1701	-0.32	0.07
1.75	0.6271	-0.52	0.22
1.9	0.1391	-0.68	0.34
2	-0.2821	-0.81	0.44

Table 6.2: Tension of the Horizontal string.

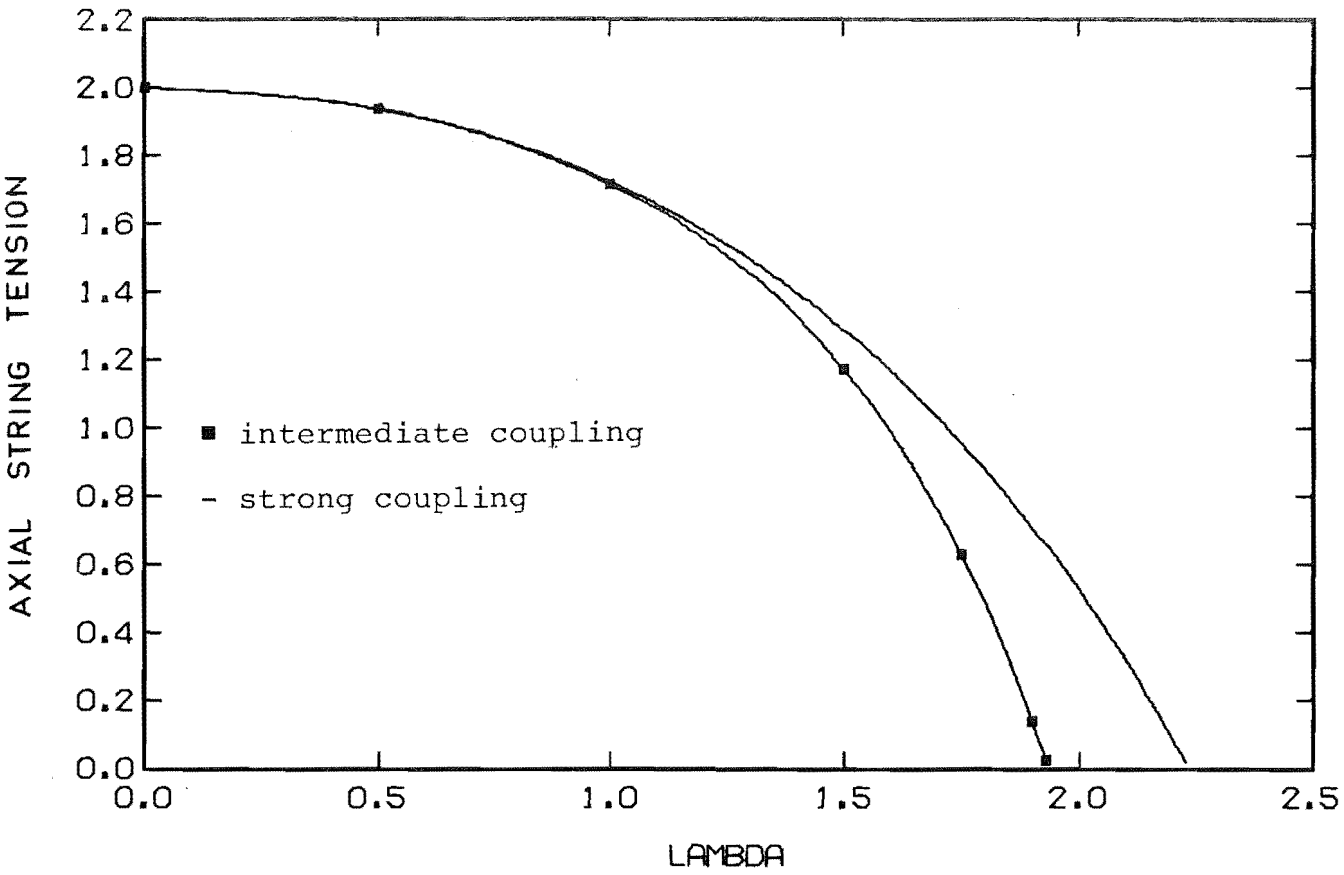

Figure 6.4: Tension of the horizontal string.

The string tension vanishes at $\lambda_R = 1.94 \pm 0.01$, considerably before the expected critical value $\lambda_c = 3.125$. The series appears to be converging satisfactorily in this region and both second and fourth order corrections are negative. Even if the higher order terms are of opposite sign it would appear that the tension will vanish for $\lambda < \lambda_c$.

It is currently believed (e.g. Itzykson et al 1980, Hasenfratz 1981) that lattice gauge theories undergo transitions

analogous to the surface roughening transitions known to occur in spin systems (Weeks et al 1973). As λ increases from the strong coupling limit the string begins to "thicken" or "vibrate" as the effect of the vacuum fluctuations becomes more important. An appropriate measure of this effect is the mean-square string width (Kogut and Sinclair 1981a). If this quantity diverges for some $\lambda_R < \lambda_C$ then the string excitations become massless and the string fluctuates wildly (Kogut et al. 1980). Kogut and Sinclair (1981a) have obtained series for the string width and estimated that the roughening transition occurs at $\lambda_R^{KS} = 1.36 \pm 0.10$.

Another method for estimating λ_R comes from the generalization of the solid-on-solid (SOS) model which was developed in the theory of crystal growth (e.g. Gilmer and Bennema 1972, Weeks and Gilmer 1979). This model may be related (Kogut and Sinclair 1981a) to the discrete Gaussian model in (1+1)-dimensions, which is identical to the planar model. The latter model has been studied by Hamer and Kogut (1979) using both the ratio method (e.g. Kogut 1979b) and Padé approximants (Baker, 1975). Their results suggests values $\lambda_R^{(r)} = 1.92$ and $\lambda_R^{(p)} = 1.94$ respectively. Hasenfratz (1981) reports values $\lambda_R^{(pert)} = 1.7$ and $\lambda_R^{(pm)} = 1.75 \pm 0.05$ from perturbation methods and relation to the planar model respectively.

The value of λ_R obtained in the present work is thus consistent with the occurrence of the roughening transition. This result is in the upper range of those quoted above but could be made more precise by the addition of higher order

terms. Both the second and fourth-order terms are negative, as are all the terms of the corresponding series for (3+1)-dimensions given by Kogut and Sinclair (1981a). Thus it is likely that higher-order terms will reduce the estimated value of λ_R.

The conventional strong-coupling series for the tension of the horizontal string has clearly been obtained by Kogut and Sinclair (1981a) who however give only the corresponding series in (3+1)-dimensions. The series for the case of (2+1)-dimensions is calculated below for comparison with the present method.

The zero-order string energy is given by

$$\varepsilon_{|\longrightarrow} = -4N+2L, \tag{6.7}$$

where $L = \sqrt{2N}$ as before. The zero-order tension is thus

$$T^{(0)}_{|\longrightarrow^{SC}} = \frac{\varepsilon^{(0)}_{|\longrightarrow^{SC}} - \varepsilon^{(0)}_{|0\rangle^{SC}}}{L} = 2 . \tag{6.8}$$

Two diagrams contribute to the second-order correction. Their active plaquette pictures, counting factors and values are given in table 6.3.

active plaquette picture	counting factor	value
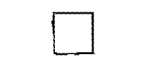	2(N-L)	(-N+L)/8
	2L	$-\frac{L}{2}$

Table 6.3: Second-order contributions to the conventional strong-coupling string energy.

The second order term is thus

$$T^{(2)}_{|\longrightarrow SC} = \frac{\varepsilon^{(2)}_{|\longrightarrow SC} - \varepsilon^{(2)}_{|0\rangle SC}}{L} = -\tfrac{1}{4} \ . \qquad (6.9)$$

The fourth order contributions are summarised in table 6.4.

active plaquette picture	counting factor	value
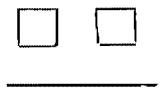	$2(2N^2-4NL-N+6L)$	$(-2N^2+4NL+N-6)/256$
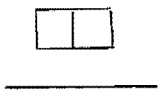	$2(4N-5L)$	$(-4N+5L)/192$
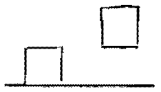	$2(2NL-4N-L)$	$3(-2NL+4N+L)/128$
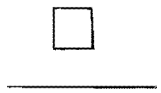	$N-2L$	0
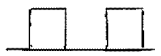	$8(N-L)$	$(-N+L)/8$
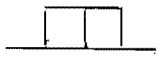	$4L$	$-\frac{L}{8}$
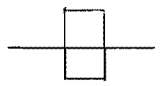	$2L$	$-\frac{L}{48}$
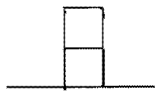	$2L$	$-\frac{9L}{256}$
	$2L$	0

Table 6.4: Fourth-order contributions to the conventional strong-coupling string energy.

The product second-order term has the value

$$SC_{\langle\!\!-\!\!|}\, H' \frac{Q_o}{a^2} H' |\!\!-\!\!\rangle SC \; SC_{\langle\!\!-\!\!|}\, H' \frac{Q_o}{a} H' |\!\!-\!\!\rangle SC$$

$$= -(N^2 + 4NL + 6N)/128 \,. \qquad (6.10)$$

Combining equation (6.10) with the results of table 6.4 and subtracting the fourth order vacuum correction obtained in chapter four gives

$$T^{(4)}_{|\!\!-\!\!\rangle SC} = -\frac{23}{768} \,. \qquad (6.11)$$

The conventional strong-coupling series for the tension of the horizontal string is thus

$$T_{|\!\!-\!\!\rangle SC} = 2 - \frac{\lambda^2}{4} - \frac{23\lambda^4}{768} \,. \qquad (6.12)$$

The values of this expression for several values of λ are given in table 6.5 and are plotted in figure 6.4.

λ	S.C. Tension	$\lambda^2\, T^{(2)}_{\|\!\!-\!\!\rangle SC} / T^{(0)}_{\|\!\!-\!\!\rangle SC}$	$\lambda^2\, T^{(4)}_{\|\!\!-\!\!\rangle SC} / T^{(2)}_{\|\!\!-\!\!\rangle SC}$
0	2	-	-
0.5	1.9356	-0.03	0.03
1.0	1.7201	-0.13	0.12
1.5	1.2859	-0.28	0.27
2.0	0.5208	-0.50	0.48
2.2366	0	-0.63	0.60

Table 6.5: The conventional strong coupling string tension.

This expansion also gives a vanishing tension, at $\lambda^{SC} = 2.2366$, at a value of λ less than λ_C. The ratio of the fourth order term to the second order term is significantly greater than for the present method, and λ_R^{SC} is further from the values reported by other authors.

6.2 THE OFF-AXIS STRING

The occurrence of the roughening transition at $\lambda_R < \lambda_C$, within the strong-coupling region, presents a potentially serious problem since the transitions of the bulk system, which contains no infinite length excitations, become inaccessible to strong and intermediate-coupling methods. Recent work (e.g. Kogut et al. 1981, Kogut and Sinclair 1981b) indicates that this problem may be resolved by considering diagonal, or off-axis strings. Such strings are "rough" for all values of λ (Kogut et al. 1981). This work has also provided further evidence for the restoration of rotational symmetry in the continuum limit, a necessary property if lattice gauge theories are to be capable of describing continuum physics but one which has not been rigorously established.

Two quarks at sites $\underline{n}_1$ and $\underline{n}_2$ will be joined by an off-axis string if their separation $\underline{\Delta}$ satisfies

$$\underline{\Delta} = \underline{n}_1 - \underline{n}_2 = q\mu + r\nu: \quad q,r \neq 0 \tag{6.13}$$

The sites may be joined by more than one off-axis string, each consisting of $|q| + |r|$ flipped spins. Some possible

paths are illustrated in figure 6.5. They correspond to the "diagonal" string, which lies at 45° to the lattice axes and has $|q| = |r|$.

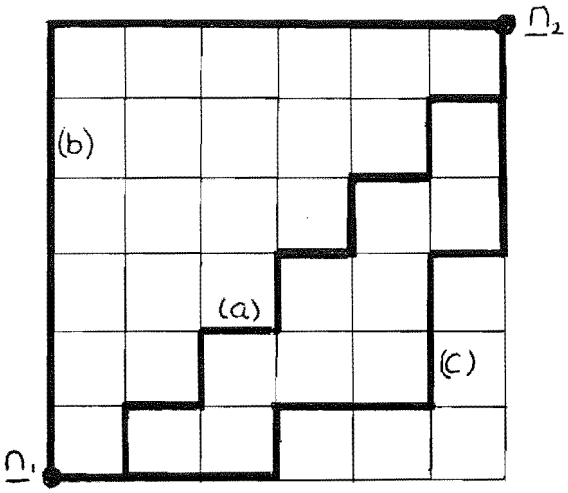

Figure 6.5: Some possible 12-link strings between $\underline{n}_1$ and $\underline{n}_2$

The number of possible strings of $|q| + |r|$ links connecting $\underline{n}_1$ and $\underline{n}_2$ is

$$N = \frac{(|q| + |r|)!}{|q|! \quad |r|!} \quad . \tag{6.14}$$

These all have the same energy in the conventional strong-coupling limit, since they all have the same number of links, and the calculation of the off-axis tension is an N-fold degenerate problem.

The state corresponding to the diagonal string in the present method is that of figure 6.6. This configuration is gauge-invariant. The zero-order term includes $2^{|q|}$ of the N paths with $|2q|$ links joining $\underline{n}_1$ and $\underline{n}_2$. These include path (a) of figure 6.5. The present method differs significantly from the conventional strong-coupling method in that the

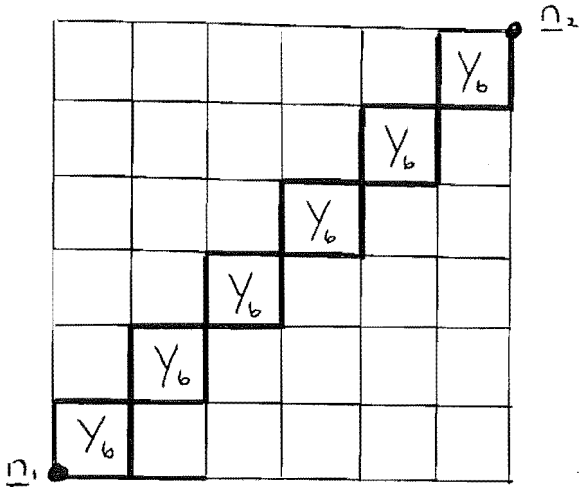

Figure 6.6: The diagonal string.

remaining $N-2|q|$ paths of $|2q|$ links correspond to states which are not degenerate with that of figure 6.6. The states corresponding to paths (b) and (c) of figure 6.5 are shown in figures 6.7 and 6.8 respectively.

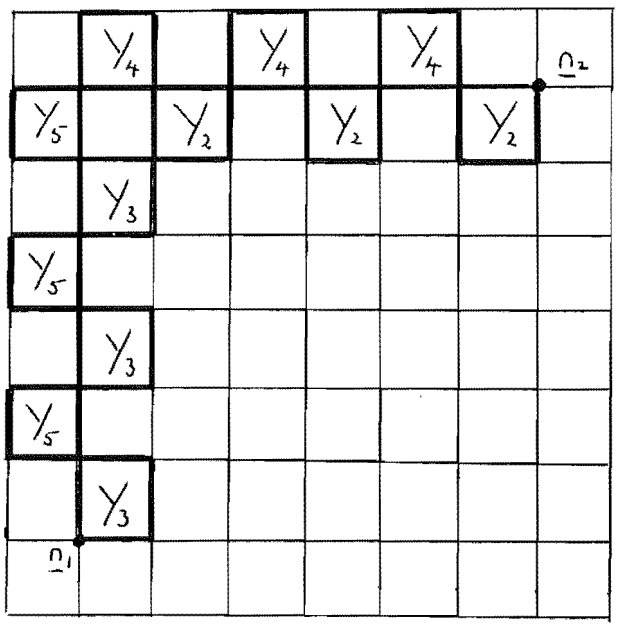

Figure 6.7: The string state corresponding to path (b) of figure 6.5.

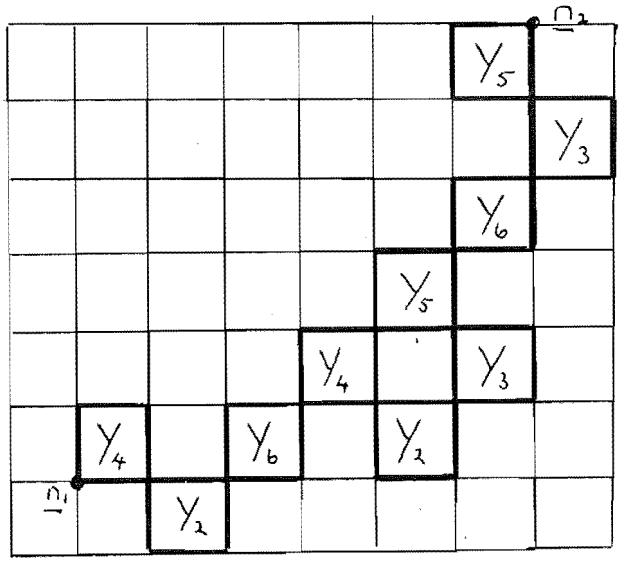

Figure 6.8: The string state corresponding to path (c) of figure 6.5.

These states also include contributions from states with more than $|2q|$ links. Both involve more excited even plaquettes than the state of figure 6.6.

If the effects of the quarks at $\underline{n}_1$ and $\underline{n}_2$ are ignored, the zero-order energies of these string states may be calculated as before. The values for the states of figures 6.6, 6.7 and 6.8 respectively are

$$\varepsilon^{(0)}_{(a)} = -Nx + 6(x-\lambda) \quad , \tag{6.15a}$$

$$\varepsilon^{(0)}_{(b)} = -Nx + 12(x-y) , \tag{6.15b}$$

$$\varepsilon^{(0)}_{(c)} = -Nx + 2(5x-4y-\lambda) \quad . \tag{6.15c}$$

The state of figure 6.6 has the lowest energy, while the energies of the other two states are greater by

$$\varepsilon^{(0)}_{(b)} - \varepsilon^{(0)}_{(a)} = 6(x - 2y + \lambda) \qquad (6.16a)$$

and

$$\varepsilon^{(0)}_{(c)} - \varepsilon^{(0)}_{(a)} = 4(x - 2y + \lambda) \quad . \qquad (6.16b)$$

Each of the N paths of $|2q|$ links joining $\underline{n}_1$ and $\underline{n}_2$ has a zero-order energy greater than $\varepsilon^{(0)}_{(a)}$ by a multiple of $(x-2y+\lambda)$. In the strong-coupling limit this quantity becomes zero and the N states are exactly degenerate. For non-zero values of λ the states separate. However they may remain quasi-degenerate if this separation is too small.

An infinitely long diagonal string may be defined, following the procedure for the horizontal string of section 6.1, by placing the two quarks at opposite corners of the lattice and joining them by L even plaquettes in state $\underline{Y}_6$. This is an infinite version of the state of figure 6.6 and is denoted by $|\,\lrcorner\!\!\lrcorner\,\rangle$. The length of this string is 2L lattice units and its zero-order energy is

$$\varepsilon^{(0)}_{|\,\lrcorner\!\!\lrcorner\,\rangle} = -Nx + L(x-\lambda) \quad . \qquad (6.17)$$

The translational degeneracy of this state may also be neglected for finite-order calculations. The zero order tension is thus

$$T^{(0)}_{|\,\lrcorner\!\!\lrcorner\,\rangle} = \frac{\varepsilon^{(0)}_{|\,\lrcorner\!\!\lrcorner\,\rangle} - \varepsilon^{(0)}_{|0\rangle}}{2L} = \frac{x-\lambda}{2} \quad , \qquad (6.18)$$

which is equal to the horizontal string tension $T^{(0)}_{|\longrightarrow\rangle}$ at $\lambda = 0$, as expected.

Higher order corrections may be calculated by the methods of the previous chapters. The two second-order contributions are shown in table 6.6.

Classification Polygon	Counting Factor	Active Plaquette Picture
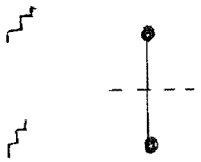	(N-2L)	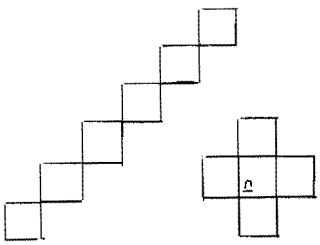
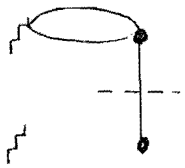	2L	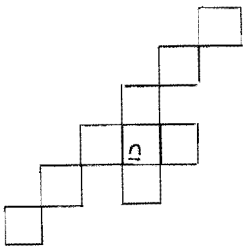

Table 6.6: Second order diagrams for the diagonal string.

The tension of the diagonal string was calculated to fourth order but, like the mass gap of chapter 4, failed to converge for any λ. This is due to the quasi-degeneracy of the $|\,\text{⌐¬}\,\rangle$ state and the infinite-length counterparts of such states as those of figures 6.7 and 6.8. These additional states consist of the diagonal string with one or more "deviations" such as those of figure 6.9.

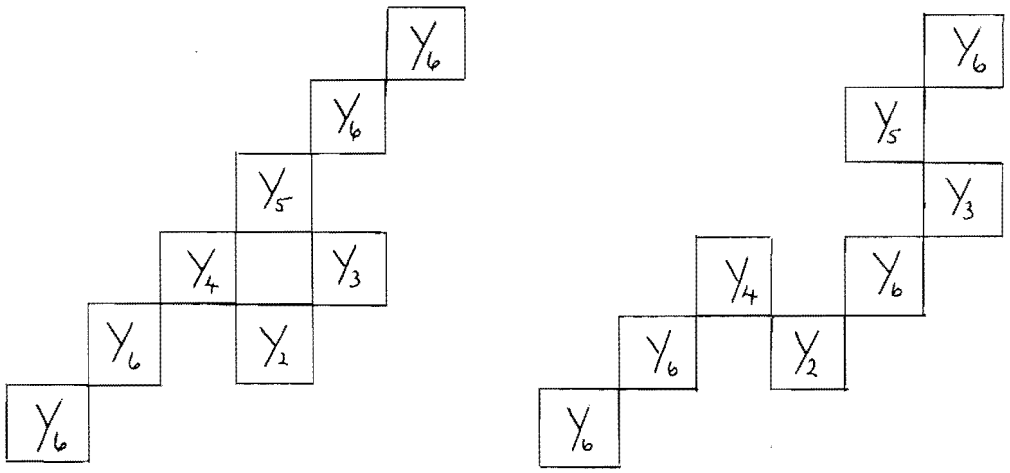

Figure 6.9: Possible deviations of the diagonal string.

The zero order energy of the states of figure 6.9(a) and (b) is $\varepsilon^{(0)}_{|\lrcorner^{\lrcorner}>} + 2(x-2y+\lambda)$, and that of an arbitrary deviant state is of the form AN + BL + C, where A,B and C are functions of λ. The term AN must be equal to the vacuum energy and the tension is thus of the form

$$T = \lim_{L\to\infty} \frac{BL+C}{L} \quad . \tag{6.19}$$

The value of C depends on the number of deviations in the original state, or set of (quasi-) degenerate states, and may be neglected if $C << L$.

In order to calculate the tension for the diagonal string quasi-degenerate perturbation methods, such as those used in chapter five, would be required. The possible strings would then be divided into those with "few" or "many"

deviations. Those with few deviations would then be made exactly degenerate by suitably modifying the Hamiltonian. The precise definition of "few" would probably depend on the order at which the calculation is truncated. This calculation would be considerably more complicated than that of the mass gap reported in the previous chapter.

CHAPTER 7

MECHANIZATION OF THE CALCULATION

The calculation of the mass gap, or the energy of a state, by the perturbative methods of the previous chapters may be reduced to the following basic steps:

(I) construction of the classification polygons for each order by the methods of section 3.4,

(II) use of the diagrammatic technique of section 3.5 to obtain expressions for the corresponding matrix elements,

(III) evaluation of these expressions to obtain a numerical value for each and (IV) combination of the results for each order to obtain the required energy or mass gap.

The procedures involved in these four steps are straightforward but the number of diagrams involved increases rapidly with the order of the calculation. The expressions for the matrix elements are, in all but the simplest cases, too complicated to be conveniently evaluated by hand. This means that the calculation becomes lengthy, and the possibility of introducing errors increases. Such errors would be extremely difficult to locate. The motivation for the construction of SISYPHUS (System Improving Speed Yet Preventing HUman Stupidity) was the desire to obtain results which could be calculated efficiently, with a minimum of human input, and which could be used with confidence.

The program is written in Burroughs Extended Algol and was implemented on the University of Canterbury's Burroughs 6700 series computer and (eventually) on its replacement, a 6900 series machine. The text is available from the author. There are four main procedures, each of which performs one of the four steps in the calculation. The program is designed for interactive use.

The core of the problem is the third step, in which the expressions for the matrix elements are evaluated. These expressions vary considerably in complexity and all involve nested summations over a number of indices. Each term in the summation consists of a sign, a product of binomial coefficients, powers of the coefficients $\rho_{\pm}, \theta_{\pm}$, and energy denominators, all of which depend on the indices. The number of summations in the expression for a particular diagram depends on the number of groups of active plaquettes, and the number of terms in each summation is related to the number of equivalent active plaquettes in each group. It is known from chapter three that these summations occur in particular combinations depending on the particular sequences of the operators of equation (2.40) which act on a given group of active plaquettes. These are the k-sums of table 3.1.

It is convenient to introduce a "standard order" for the sums in which the smaller nests are innermost as indicated in figure 7.1.

$$\underbrace{\Sigma\Sigma\Sigma\Sigma\Sigma\ \Sigma\Sigma\Sigma\Sigma\Sigma\ \cdots}_{5\text{- sums}}\ \underbrace{\Sigma\Sigma\Sigma\ \Sigma\Sigma\Sigma\ \cdots}_{3\text{-sums}}\ \underbrace{\Sigma\Sigma\Sigma}_{1\text{-sums}}$$

Figure 7.1: Standard order for summations

It is clear from table 3.2 that the number of terms in a k-sum depends only on L, the upper limit of its outermost index. The limits of the summations are functions of the indices as may be seen from table 3.1. In order to obtain the possible index configurations for an arbitrary combination of k-sums in standard order it is only necessary to specify the number of k-sums for each k and the value of L for each. The term corresponding to each index configuration may then be evaluated.

Often it is necessary to evaluate the same matrix elements with different combinations of the projectors P_o and Q_o, and energy denominators with different exponents. It was shown in section 3.5 that the expressions for a diagram and its reflection differ only in the order of their denominators. When the denominators occur with different exponents, as is the case in the Bloch formalism, it is necessary to "undo" the operation of combining such diagrams. It is also necessary to specify whether the energies of the zero-order Hamiltonian correspond to the standard ($y = \sqrt{\lambda^2+4}$) or quasidegenerate ($y = \frac{x}{2}$) case. The pointer constructs of the Algol language allow these details, as well as other information, to be specified implicitly as parts of the names of the input and output

files. This reduces the number of commands required to run the program and enables considerable versatility in the interaction of the four main procedures.

Once the diagram values have been obtained it is necessary to combine them in the appropriate manner to obtain the required energy or mass gap. The procedure whose function is to calculate these quantities accepts commands consisting of the titles of files containing diagram values and a direction to add their contents to, or subtract them from, one of the $\varepsilon^{(i)}_{|\psi>}$ or one of the $\Sigma^{(i)}_{\square\square}$. Quantities involving products of matrix elements, such as

$$<\Psi|H' \frac{Q_o}{a^2} H'|\Psi><\Psi|H' \frac{Q_o}{a} H'|\Psi> \quad ,$$

may be readily obtained. Optional features include an explicit check on the N-dependence of the calculation and the ability to record the contribution from each file in a log file or access results previously recorded.

The need for rapid, error-free production of the expressions for the matrix elements corresponding to a large number of diagrams led to the mechanization of this step. The input to this procedure is the description of one of the possible active plaquette pictures associated with each classification polygon. The initial state, sequence of even plaquette operators, and final state are specified for a representative of each group of active plaquettes. The even plaquette operators are the P,Q,R,S operators defined by equation (2.40), the identity

and $\tilde{H}'$. This information, together with a knowledge of tables 2.7, allows the corresponding expression to be constructed. The resulting summations are in standard order and the output is of the form of a data file which may be accessed by the procedure for diagram evaluation. The effects of reflecting the classification polygon or rotating the active plaquette picture may be readily observed.

All the diagrams required for the calculations of the preceding chapters may be evaluated by these methods. However it is possible to further reduce the number of diagrams which need to be described, and thus also the possibility of error, by obtaining the diagrams of a given order directly from those of the preceding order. Diagrams of order q+1 are regular (q+3)-gons and are obtained from those of order q, represented by regular (q+2)-gons, by the addition of a vertex, representing the action of H' or $\tilde{H}'$, and a projector/denominator. The additional vertex may possibly be connected to the remainder of the diagram in more than one way so any diagram of order q may give rise to more than one diagram of order q+1.

Consider the diagrams of figure 7.2(a),(b),(c),(d) which contribute to

$$\langle + | H'(\underline{n}_2) \frac{Q_o}{a} H'(\underline{n}_1) | + \rangle \quad ,$$

$$\langle + | H'(\underline{n}_3) \frac{Q_o}{a} \tilde{H}'(\underline{n}_2) \frac{Q_o}{a} H'(\underline{n}_1) | + \rangle \quad ,$$

$$\langle \square | H'(\underline{n}_3) \frac{Q_o}{a} H'(\underline{n}_2) \frac{Q_o}{a} H'(\underline{n}_1) | + \rangle$$

and

$$\langle \square | H'(\underline{n}_5) \frac{Q_o}{a} H'(\underline{n}_4) \frac{Q_o}{a} \tilde{H}'(\underline{n}_3) \frac{Q_o}{a} \tilde{H}'(\underline{n}_2) \frac{Q_o}{a} H'(\underline{n}_1) | + \rangle$$

respectively. The diagram of figure 7.2(b) is obtained from that of figure 7.2(a) by the addition of a vertex

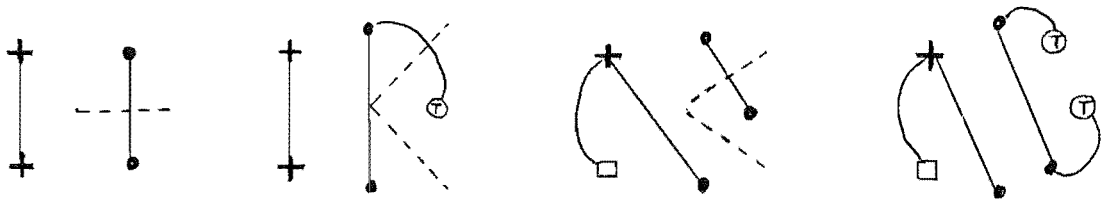

Figure 7.2: A second order diagram and higher order diagrams obtained from it.

representing $\tilde{H}'(\underline{n}_2)$ and an additional projector/denominator. The final cross state of figure 7.2(a) may be replaced by a Y16 state with the addition of a vertex $H'(\underline{n}_3)$ and a projector/denominator to give the diagram of figure 7.3(c). These operations may be performed consecutively. The addition of two $\tilde{H}'$ vertices, one final H' vertex and three projector/denominators leads to fifth order diagrams of which figure 7.2(d) is an example. All the diagrams required for the calculations of previous chapters may be obtained in this way from the second and fourth order vacuum, cross and Y16 diagrams of figures 4.1, 4.2, 4.6, 4.8 and Appendix A.

The procedure used in this operation manipulates the sequences of plaquette operators specifying particular diagrams to produce those corresponding to each of the diagrams resulting from the addition of the specified vertex and projector/denominator combination. When a vertex

corresponding to H' is added it is necessary to separate those diagrams which have been combined using the reflection principle of chapter three since they will, in general, lead to different higher order diagrams. All the required diagrams may be generated from those of chapter four by the addition of vertices which correspond to the insertion into a matrix element of the operator $\frac{Q_o}{a}\tilde{H}'$ or the replacement of $<+|H'$ by $<\square|H'\frac{Q_o}{a}H'$. In order to perform calculations to higher order than those of the present work it would be desirable to be able to insert combinations of vertices corresponding to $\frac{Q_o}{a}H'$ and hence obtain the diagrams of arbitrary order.

There are a number of features of the program whose functions are to warn of any inconsistencies which may result from incorrect data or improper use of the program commands. These include such things as plaquette operator sequences which cannot connect the specified states. The requirements that the vacuum energy must be linear in N and that the mass gap be independent of N provide a means of checking that the correct values have been obtained for many of the diagrams. Diagrams which have no dependence on N may contribute to the N-dependence of the mass gap if they occur in the product terms of the expansion. In practice these requirements were satisfied to the limit of machine accuracy. The Bloch formulation allows a further check on the diagram values. A term such as $<+|H'\frac{Q_o}{a^2}H'\,P_o\,H'\frac{Q_o}{a}H'|+>$, which contributes to Σ_{++}, may be written as

$$\langle +|H' \frac{Q_o}{a^2} H'|+\rangle\langle +|H' \frac{Q_o}{a} H'|+\rangle$$

when the expression of equation (5.33) is substituted for P_o. The result may thus be calculated from the fourth order diagrams of Appendix A, or as a product of the second order diagrams of figure 4.6 The equivalence of these and other expressions was also confirmed to the limit of machine accuracy. Each section of the program has satisfied all the required conditions. It is believed that the aim of obtaining the required results accurately, efficiently and with the minimum of human involvement has been fulfilled.

CHAPTER 8

APPLICATIONS AND EXTENSIONS

In this chapter several applications and extensions of the intermediate-coupling expansion are considered. In section 8.1 a family of (2+1)-dimensional Z(2) lattice gauge models with inhomogeneous coupling strengths is studied. These models arise naturally within the framework of the present method and are a valuable tool for the study of the isotropic-coupling model considered in the previous chapters.

The zero-order problem of the (2+1)-dimensional Z(3) lattice group theory on a triangular lattice is the subject of section 8.2. The extensions of the intermediate-coupling expansion to continuous gauge groups and (3+1)-dimensions are the subjects of sections 8.3 and 8.4 respectively.

8.1 INHOMOGENEOUS-COUPLING MODELS

The inhomogeneous-coupling models defined by equation (2.43) arise when λ_o, the value of the coupling strength parameter associated with the odd plaquette terms in the Hamiltonian, is allowed to differ from λ_e, the corresponding value for the even plaquette terms. This inhomogeneity of space should be distinguished from the anisotropy used in the development of the Hamiltonian formulation of lattice gauge theory, which was described in chapter 2. In that case the coupling strength for

plaquettes involving time links was allowed to differ from that of all the purely spatial plaquettes. The theory which has been studied in the previous chapters is recovered when $\lambda_o=\lambda_e=\lambda$.

Those terms involving λ_e are included in the zero-order Hamiltonian $H_o(\lambda_e)$, which has been solved exactly, and those involving λ_o have been considered as a perturbation. The series of equation (3.7) for the energy of an arbitrary state $|\Psi>$ may thus be interpreted as

$$E_{|\Psi>} = \overset{(0)}{\varepsilon}(\lambda_e) + \lambda_o \overset{(2)}{\varepsilon}(\lambda_e) + \lambda_o^2 \overset{(2)}{\varepsilon}(\lambda_e) + \lambda_o^3 \overset{(3)}{\varepsilon}(\lambda_e) + \ldots \tag{8.1}$$

This series may also be calculated using the computer program described in the previous chapter.

The inhomogeneous-coupling models may be studied in their own right. Although their properties are not directly related to those of any known physical system they may nevertheless be calculated, and the models have their own phase structure. The smooth manner in which the homogeneous-coupling model, which is of physical significance, is recovered as $\lambda_o \to \lambda_e$ is of considerable interest. For a given value of λ_e there exists a range of values of λ_o for which the series of equation (8.1) is convergent. Even if, as was the case for the mass gap calculations of chapter four, the series does not converge for any $\lambda=\lambda_o=\lambda_e$, the properties of the inhomogeneous-coupling models for which the series do converge may be extrapolated to this limit.

As an example of the use of these models consider the case of the horizontal string tension, which was calculated in chapter six. The series of equation (6.3) for the string tension can be evaluated for different combinations of λ_o and λ_e. The results of this procedure are shown in figure 8.1.

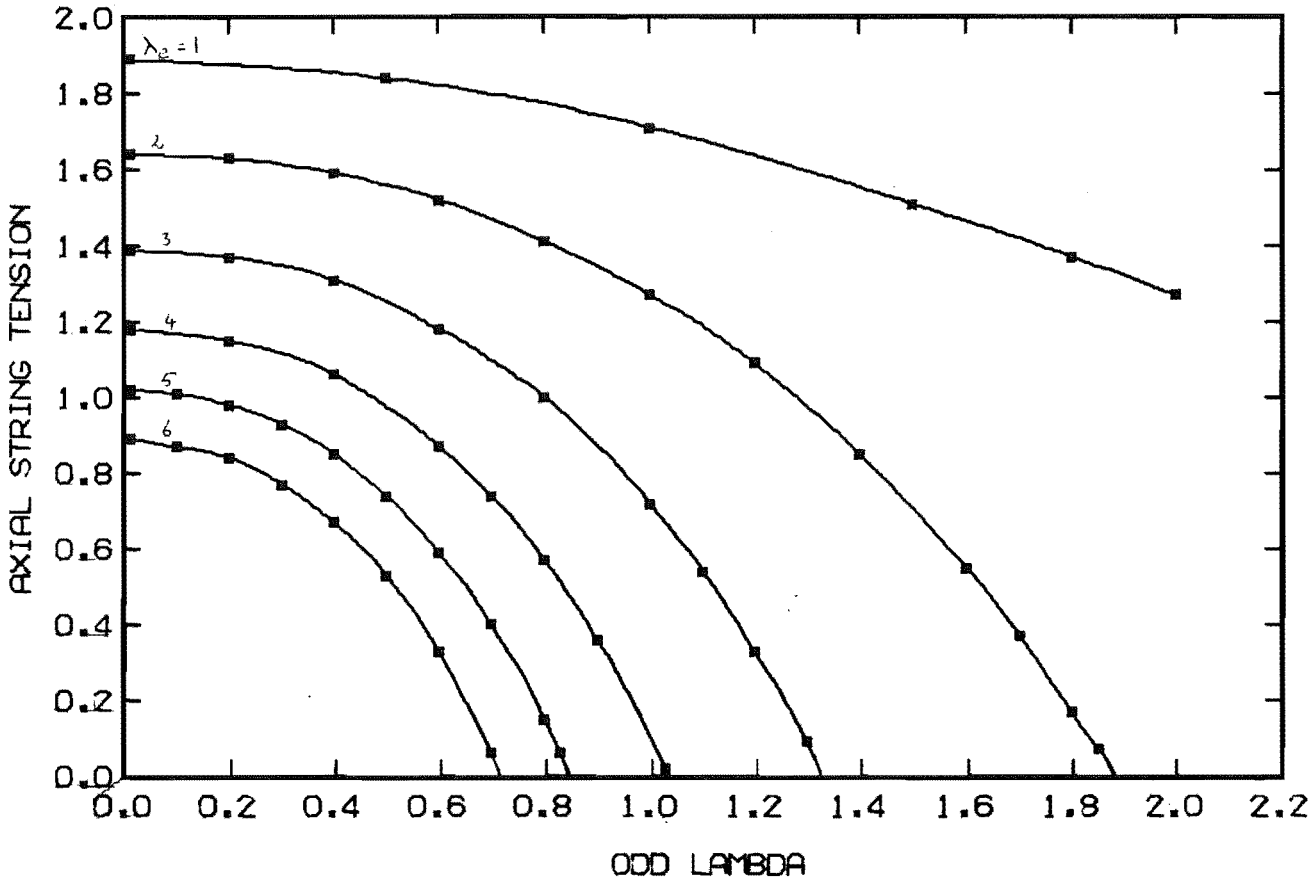

Figure 8.1: Horizontal string tension of the inhomogeneous-coupling model. Lines of constant even plaquette coupling strength are shown.

As the value of λ_e is increased the value of λ_o for which the tension vanishes decreases.

The terms "odd" and "even" have no physical significance: they merely distinguish two sets of plaquettes, each of which includes all the links of the lattice. The zero-order Hamiltonian could have been written entirely in terms of odd plaquettes, with the even plaquette terms being treated as a perturbation, without altering the results of the previous chapters. Physical quantities, such as the string tension, should be unaffected by the interchange of the values of λ_o and λ_e.

Consider the results shown in table 8.1.

λ_e	λ_o	Tension	$\lambda_o^2 T^{(2)}(\lambda_e) / T^{(0)}(\lambda_e)$	$\lambda_o^2 T^{(4)}(\lambda_e) / T^{(2)}(\lambda_e)$
1	3	0.8035	-0.87	-0.34
1	2	1.2686	-0.39	-0.15
2	1	1.2729	-0.20	0.11
3	1	0.7192	-0.38	0.27

Table 8.1: Some values for the string tension of the homogeneous-coupling model.

The two values of the tension for which $\lambda_o\lambda_e=2$ agree to three significant figures while those for which $\lambda_o\lambda_e=3$ show much poorer agreement. Truncated expansions, such as that used to calculate the string tension, perform best for small values of the perturbation parameter. The convergence of the series for the string tension becomes worse as either λ_o or λ_e increases while the other remains constant. This

behaviour is indicated by the results of Table 8.1. Thus, although physical quantities should remain invariant under the interchange of λ_o and λ_e, the use of truncated series means that the choice which minimizes the perturbation parameter will give the most reliable results. This invariance, which is suggested by purely physical arguments, suggests that quantities such as the tension should take constant values along hyperbolic trajectories satisfying

$$\lambda_o\lambda_e = \text{Const}, \tag{8.2}$$

which are symmetrical about the line $\lambda_o=\lambda_e$.

Contours of constant string tension, obtained from the results shown in figure 8.1, are plotted in figure 8.2. The line $\lambda_o=\lambda_e$ is also shown. Points marked by crosses were calculated using the series for the string tension, while their reflections in the line $\lambda_o=\lambda_e$ are denoted by shaded squares. The contours are symmetric about the line $\lambda_o=\lambda_e$, which they cross at right angles. They may be expected to become closer to hyperbolae as higher order terms are included in the series for the tension. The $T_{|->}=0$ contour cuts the line $\lambda_o=\lambda_e$ at $\lambda_o=\lambda_e=\lambda_R$, and the result of chapter six is recovered. Other values of λ_o and λ_e which correspond to the onset of the roughening transition may be obtained from figure 8.2.

The study of the horizontal string tension of the inhomogeneous-coupling model provided no additional information about the homogeneous-coupling case considered in the previous chapters. Consider now the mass gap $G_{|+>}$,

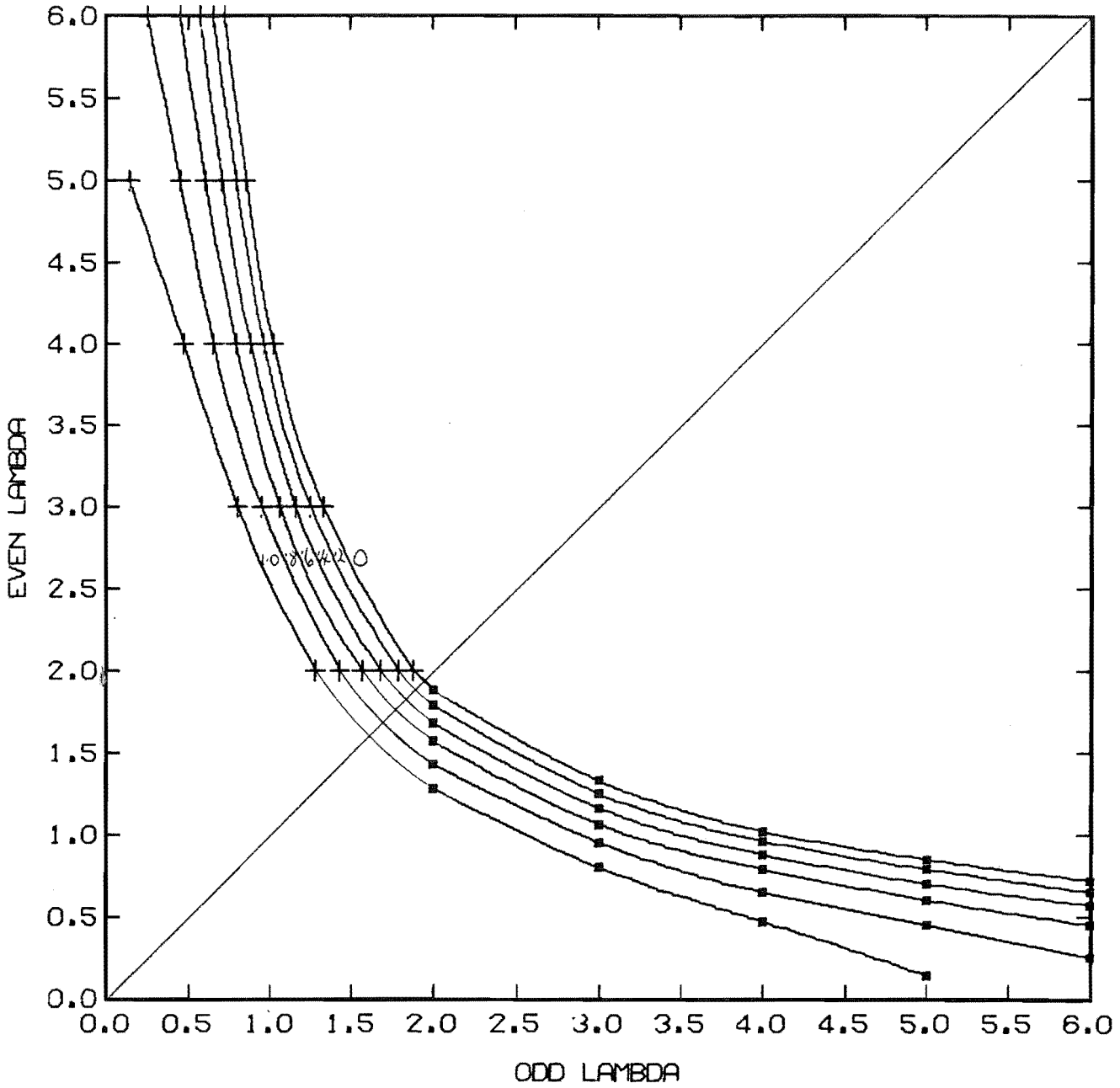

Figure 8.2: Contours of constant string tension for the inhomogeneous-coupling model. The lines are labelled by the value of the tension. Symbols are explained in the text.

defined for the homogeneous-coupling model by equation (4.19). The calculation of this quantity for the homogeneous-coupling case, which was reported in chapter 4, failed bacause of the large terms resulting from the

quasi-degeneracy of the $|+\rangle$ and $|\square\rangle$ states. In the inhomogeneous-coupling model the denominator $\pm D(2,-4,0)$, which is the source of these large terms, depends only on λ_e. For a given value of λ_e, the series for the mass gap will always converge for some values of λ_o, where $\lambda_o<\lambda_e$. If the contour of zero mass gap can be established then the value of λ_c for the homogeneous-coupling model may be deduced. The mass gap for several values of λ_e is plotted in figure 8.3

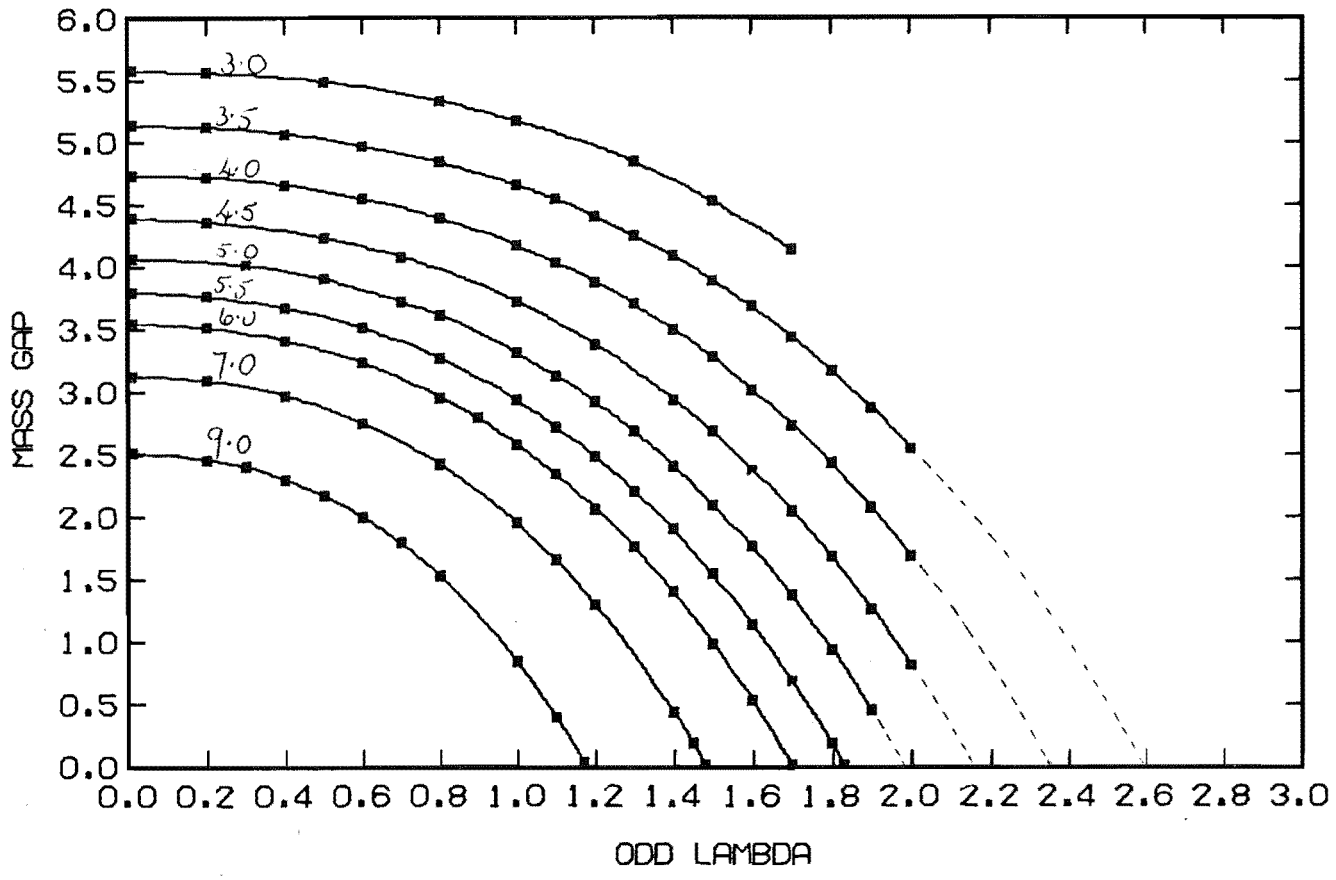

Figure 8.3: The mass gap for the inhomogeneous-coupling model. The lines are labelled by λ_e.

The solid lines of figure 8.3 end where the convergence of the series has deteriorated such that the absolute value of the fourth-order term is equal to half that of the second order term. The broken lines are extrapolations of the solid lines. In order to obtain the contours of constant mass gap the invariance of that quantity under interchange of λ_o and λ_e is invoked since no values for $\lambda_o \geqslant \lambda_e$ may be directly calculated. The contours are plotted in figure 8.4. Of the points for which $\lambda_o<\lambda_e$, those marked by crosses are directly calculable, while the remainder, which are marked by squares, are obtained from the extrapolated lines of figure 8.3. The points corresponding to $\lambda_o>\lambda_e$ are obtained by reflection in the line $\lambda_o=\lambda_e$, which is also shown. The broken lines represent curves interpolated through these points. The contour of zero mass gap cuts the line $\lambda_o=\lambda_e$ at $\lambda_c=3.0\pm0.1$. This result is close to the accepted result of 3.125 and was obtained with considerably less calculation than was required for the complete quasi-degenerate calculation of the mass gap which was described in chapter 5.

The inhomogeneous-coupling model thus constitutes a powerful tool for the determination of the homogeneous-coupling model's phase diagram. The latter case is recovered smoothly from the former and no additional phase transitions are introduced. If the inhomogeneous-coupling model can be solved in some region R of the λ_o-λ_e plane then its properties may be extrapolated smoothly to the homogeneous-coupling case.

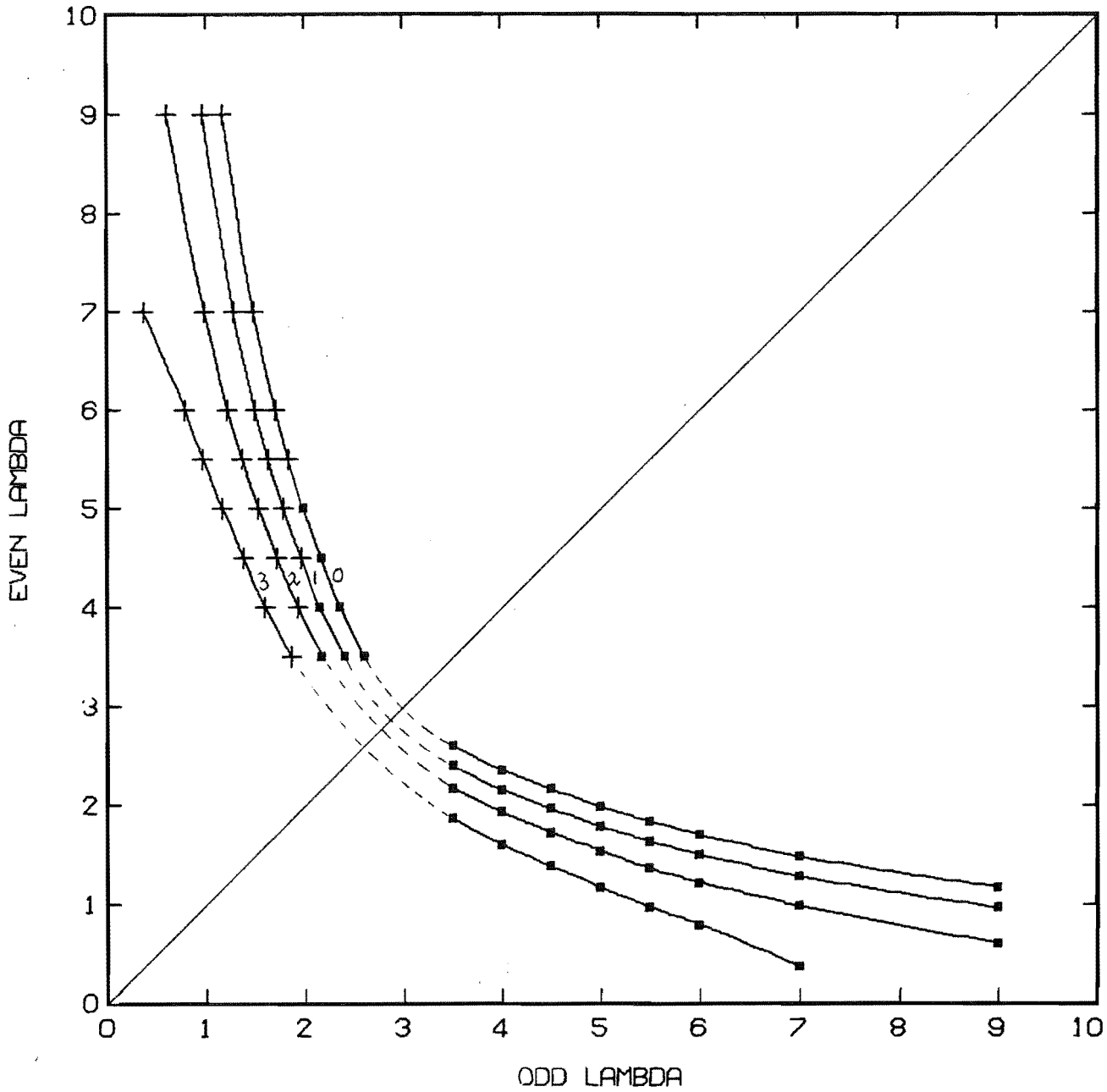

Figure 8.4: Contours of constant mass gap for the inhomogeneous model. The lines are labelled by the mass gap value. The symbols are explained in the text.

This extrapolation only yields useful quantitative results if R contains points which are reasonably close to the line $\lambda_o=\lambda_e$. In the case of the quantities $G_{|\square>}$ and

$G^{(\pm)}_{|1>}$, defined by equations (4.22) and (5.42) respectively, R is very small and includes no points where these mass gaps vanish. This is because the zero-order terms in both cases increase as λ_e increases and, for $\lambda_o \leqslant \lambda_e$ the radius of convergence is reached before this effect is overcome by the higher order terms. Similarly the inhomogeneous-coupling model is of limited use in the case of the diagonal string. The order of the quasi-degeneracy of that state is considerably greater than that of the mass gap. Even though the zero-order tension of the diagonal string decreases as λ_e increases the higher order terms cannot overcome the effects of this quasi-degeneracy for any non-zero λ_o. Consequently the tension does not vanish and the radius of convergence of the series for the tension remains too small even for the extrapolation of useful results.

8.2 Z(3) LATTICE GAUGE THEORY ON A TRIANGULAR SPATIAL LATTICE.

In this section the direct product vector method of solution of the zero-order problem, which was introduced in chapter 2, is extended to the case of the gauge group Z(3). The degrees of freedom, which reside on the links, are elements of Z(3) and may be represented by the unimodular complex numbers $1, e^{i\pm 2\pi/3}$.

The solution of the single-plaquette zero-order problem requires the diagonalization of a matrix whose dimension is the number of elements of the group raised to

the power of the number of links per plaquette. Thus the Z(3) theory on a square lattice would present an 81×81 dimensional problem which is considerably larger than the corresponding 16×16 problem for the Z(2) case. The formulation of the problem on a triangular lattice reduces the dimension of the single-plaquette zero-order problem to 27.

The sites of the two-dimensional triangular spatial lattice shown in figure 8.5 are specified, as before, by

$$\underline{n} \equiv (n_1,n_2) = n_1\mu+n_2\nu. \qquad (8.3)$$

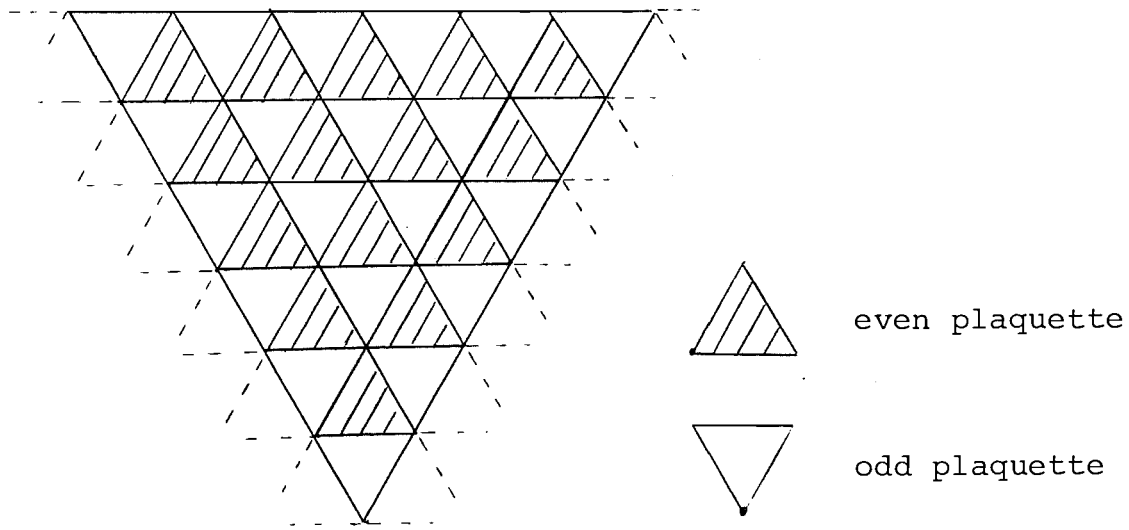

Figure 8.5: The triangular spatial lattice.

As in the case of the square lattice the set of plaquettes is divided into odd and even subsets. This division is indicated in figure 8.5. An even plaquette may be specified by the site at its lower left vertex and an odd plaquette by that at its lowest vertex.

The Hamiltonian, written in terms of link operators P and Q which obey the Z(N) algebra of equations 2.20 for N=3, is that of equation (2.18). These operators, in the representation of equations (2.24) are given in equation (2.26) and repeated below for convenience.

$$P = \begin{pmatrix} 0 & 0 & 1 \\ 1 & 0 & 0 \\ 0 & 1 & 0 \end{pmatrix}, \quad Q = \begin{pmatrix} 1 & 0 & 0 \\ 0 & e^{i2\pi/3} & 0 \\ 0 & 0 & e^{i4\pi/3} \end{pmatrix}$$

The plaquette terms now represent the product of the Q operators around a triangular plaquette, e.g., for an even plaquette

$$Q_{\underline{p}} = \bigotimes_{\underline{\ell}\varepsilon\underline{p}} \pi \; Q(\underline{\ell}) = Q(\underline{p},\mu) \otimes Q(\underline{p}+\mu,\nu-\mu) \otimes Q(\underline{p}+\nu,-\nu). \quad (8.4)$$

Following the procedure of section 2.2 the link terms of the Hamiltonian are associated with the even plaquettes. All the even plaquette terms are then included in the zero-order Hamiltonian and the odd plaquette terms are treated as a perturbation. The resulting Hamiltonian, in generic form, is $H = \sum_{\underline{p}_{even}} h_o(\lambda) + \lambda \sum_{p_{odd}} h'$

$$= -\frac{1}{2} \sum_{p_{even}} [(P+P^+)\otimes I\otimes I + I\otimes(P+P^+)\otimes I + I\otimes I\otimes(P+P^+) + \lambda(Q_p+Q_p^+)]$$

$$- \frac{\lambda}{2} \sum_{p_{odd}} (Q_p+Q_p^+) \; . \quad (8.5)$$

The eigenvectors of P and Q are denoted by $\underline{x}_i$ and $\underline{y}_i$ respectively. The eigenvalue equation for P may be written

$$P\underline{x}_i = \omega_{ij}\underline{x}_j \quad , \tag{8.6}$$

with

$$\omega = \begin{pmatrix} 1 & 0 & 0 \\ 0 & \delta & 0 \\ 0 & 0 & \delta^2 \end{pmatrix} \tag{8.7}$$

and

$$\delta = e^{i2\pi/3} \quad . \tag{8.8}$$

The non-zero components of ω are the eigenvalues $\omega_i=\omega_{ii}$, and the corresponding eigenvectors are

$$\underline{x}_1 = \begin{pmatrix} 1 \\ 1 \\ 1 \end{pmatrix} \quad , \quad \underline{x}_2 = \begin{pmatrix} 1 \\ \delta^2 \\ \delta \end{pmatrix} \quad , \quad \underline{x}_3 \begin{pmatrix} 1 \\ \delta \\ \delta^2 \end{pmatrix} \quad . \tag{8.9}$$

The $\underline{x}_i$ are not orthogonal: eigenvectors corresponding to distinct eigenvalues must be orthogonal but $\omega_3=\omega_2^*$. The eigenvalue equation for P^+ is

$$P^+\underline{x}_i = \omega_i^* \underline{x}_i \quad . \tag{8.10}$$

Thus the $\underline{x}_i$ are also eigenvectors of P^+, but correspond to different eigenvalues.

The eigenvalues of $(P+P^+)$ must be real. From equations (8.6) and (8.10) it is clear that the $\underline{x}_i$ are also eigenvectors of $(P+P^+)$ with real eigenvalues 2,-1,-1. Three real, orthogonal eigenvectors of $(P+P^+)$,

$$\underline{z}_1 = \underline{x}_1 = \begin{pmatrix} 1 \\ 1 \\ 1 \end{pmatrix} \quad , \quad z_2 = 2\mathrm{Re}(\delta\underline{x}_2) = \begin{pmatrix} 1 \\ -2 \\ 1 \end{pmatrix} \quad , \quad z_3 = \frac{2}{\sqrt{3}}\mathrm{Im}(\delta\underline{x}_2) = \begin{pmatrix} 1 \\ 0 \\ -1 \end{pmatrix} \tag{8.11}$$

may be defined.

Similarly the eigenvalues and eigenvectors of Q satisfy

$$Q\,\underline{y}_i = \mu_{ij}\,\underline{y}_j \ , \tag{8.12}$$

where
$$\mu = \begin{pmatrix} 1 & 0 & 0 \\ 0 & \delta & 0 \\ 0 & 0 & \delta^2 \end{pmatrix} \tag{8.13}$$

and the corresponding real orthogonal eigenvectors are

$$\underline{y}_1 = \begin{pmatrix} 1 \\ 0 \\ 0 \end{pmatrix} \ , \quad \underline{y}_2 = \begin{pmatrix} 0 \\ 1 \\ 0 \end{pmatrix} , \quad \underline{y}_3 = \begin{pmatrix} 0 \\ 0 \\ 1 \end{pmatrix} \quad . \tag{8.14}$$

These are also eigenvectors of Q^+ with eigenvalues $\mu_i^* = \mu_{ii}^*$.

The $\underline{x}_i$ and $\underline{y}_i$ are related by

$$\underline{x}_i = \beta_{ij}\,\underline{y}_j \tag{8.15}$$

with
$$\beta = \begin{pmatrix} 1 & 1 & 1 \\ 1 & \delta^2 & \delta \\ 1 & \delta & \delta^2 \end{pmatrix} \tag{8.16}$$

and
$$\beta^{-1} = \frac{1}{3}\,\beta^+ \quad . \tag{8.17}$$

these are the Z(3) counterparts of equations (2.52) and (2.53). The relation

$$\beta\mu\beta^{-1} = P \ , \tag{8.18}$$

which corresponds to equation (2.54), will also be required.

The eigenvalues and eigenvectors of the zero-order Hamiltonian are the solutions of

$$h_o(\lambda)\ \underline{V} = \Omega\underline{V} \tag{8.19}$$

where

$$h_o(\lambda) = -\frac{1}{2}[(P+P^+)\otimes I\otimes I + I\otimes(P+P^+)\otimes I + I\otimes I\otimes(P+P^+) + \lambda Q\otimes Q\otimes Q + Q^+\otimes Q^+\otimes Q^+]. \quad (8.20)$$

Following the method of chapter 2 eigenvectors of the form

$$\underline{V} = \Gamma_{ijk}(\underline{x}_i\otimes\underline{x}_j\otimes\underline{x}_k) \quad (8.21)$$

are sought. The L.H.S. of equation (8.19) then becomes

$$h_o(\lambda)\underline{V} = -\frac{1}{2}\Gamma_{ijk}[(P+P^+)\underline{x}_i\otimes\underline{x}_j\otimes\underline{x}_k + \underline{x}_i\otimes(P+P^+)\underline{x}_j\otimes\underline{x}_k + \underline{x}_i\otimes\underline{x}_j\otimes(P+P^+)\underline{x}_k + Q\underline{x}_i\otimes Q\underline{x}_i\otimes Q\underline{x}_k + Q^+\underline{x}_i\otimes Q^+\underline{x}_j\otimes Q^+\underline{x}_k] \quad . \quad (8.22)$$

The action of Q on the $\underline{x}_i$ is, using equation (8.15), given by

$$Q\underline{x}_{i'} = (\beta\mu\beta^{-1})_{i'i}\,\underline{x}_i = (P)_{ii'}\underline{x}_{i'} \quad . \quad (8.23)$$

Similarly

$$Q^+\underline{x}_i = (P^+)_{i'i}\,\underline{x}_i \quad . \quad (8.24)$$

Equating the coefficients of any choice of ijk in the eigenvalue equation for $h_o(\lambda)$ then gives

$$-\frac{1}{2}[\Gamma_{ijk}(\omega_i+\omega_i^*+\omega_j+\omega_j^*+\omega_k+\omega_k^*) + 2\Omega\Gamma_{ijk} + \lambda\Gamma_{i'j'k'}\,P_{i'i}P_{j'j}P_{k'k} + \Gamma_{i'j'k'}\,P^+_{i'i}P^+_{i'i}P^+_{j'j}P^+_{k'k}] = 0 \quad (8.25)$$

Define the quantity $\Sigma_{ijk} = (\omega_i+\omega_i^*+\omega_j+\omega_j^*+\omega_k+\omega_k^*) = 2\mathrm{Re}(\omega_i+\omega_j+\omega_k)$. (8.26)

Also define the "bar" operation on indices such that

$$P_{i'i} \equiv \delta_{\bar{i}i} \quad , \quad P^{+}_{i'i} \equiv \delta_{\bar{\bar{i}}i} \tag{8.27}$$

The action of this operation is summarized in table 8.2.

i	$\bar{i}$	$\bar{\bar{i}}$
1	2	3
2	3	1
3	1	2

Table 8.2: Action of the "bar" operation on indices.

The three-index operator S is then defined such that

$$S(ijk) = \overline{ijk}. \tag{8.28}$$

The operators S, S^2 and $S^3 \equiv E$ form a representation of Z(3). Equation (8.25) may now be written

$$(\zeta_E + 2\Omega)\Gamma_E + \lambda(\Gamma_S + \Gamma_{S^2}) = 0 \quad . \tag{8.29}$$

Operating on this equation with S and S^2 leads to two further equations which, together with equation (8.29) may be written in matrix form as

$$\begin{pmatrix} \zeta_E+2\Omega & \lambda & \lambda \\ \lambda & \zeta_S+2\Omega & \lambda \\ \lambda & \lambda & \zeta_{S^2}+2\Omega \end{pmatrix} \begin{pmatrix} \Gamma_E \\ \Gamma_S \\ \Gamma_{S^2} \end{pmatrix} = 0 \, . \tag{8.30}$$

The eigenvalues Ω are then given by the solutions of the characteristic equation

$$8\Omega^3+4\Omega^2(\Sigma_E+\Sigma_S+\Sigma_{S^2})+2\Omega(\Sigma_E\Sigma_S+\Sigma_E\Sigma_{S^2}+\Sigma_S\Sigma_{S^2}-3\lambda^2) + \Sigma_E\Sigma_S\Sigma_{S^2}$$

$$-\lambda^2(\Sigma_E+\Sigma_S+\Sigma_{S^2}-2\lambda) = 0 \quad . \qquad (8.31)$$

This equation may be simplified considerably by noting that

$$\Sigma_E+\Sigma_S+\Sigma_{S^2} \equiv 0 \quad . \qquad (8.32)$$

The possible values of $\Sigma_E\Sigma_S$ and Σ_{S^2} are summarised in table 8.3 The coefficients of equation (8.31) are invariant under permutations of the index choices given in the table.

ijk	permutations	Σ_E	Σ_S	Σ_{S^2}
111	1	6	-3	-3
112	3	3	-3	0
113	3	3	0	-3
122	3	0	-3	3
123	6	0	0	0
133	3	0	3	-3
222	1	-3	-3	6
223	3	-3	0	3
233	3	-3	3	0
333	1	-3	6	-3

Table 8.3: Possible values of the Σ.

Examination of these values shows that there are only three distinct equations for Ω, namely

$$8\Omega^3 - 6(9+\lambda^2)\Omega + (54+2\lambda^3) = 0 , \qquad (8.33a)$$

$$8\Omega^3 - 6(3+\lambda^2)\Omega + 2\lambda^3 = 0 , \qquad (8.33b)$$

$$8\Omega^3 - 6\lambda^2\Omega + 2\lambda^3 = 0 . \qquad (8.33c)$$

The solutions are

$$\Omega_a^{(\ell)} = -\sqrt{\lambda^2+9}\ \mathrm{Cos}\left(\frac{\theta_1+2\ell\pi}{3}\right) : \ell=0,1,2 \qquad (8.34a)$$

$$\Omega_b^{(\ell)} = -\sqrt{\lambda^2+3}\ \mathrm{Cos}\left(\frac{\theta_2+2\ell\pi}{3}\right) : \ell=0,1,2 \qquad (8.34b)$$

$$\Omega_c^{(\ell)} = -\lambda\ \mathrm{Cos}\ \frac{2\ell\pi}{3} : \ell=0,1,2 \qquad (8.34c)$$

where

$$\theta_1 = \mathrm{Cos}^{-1}\left(\frac{(\lambda^3+27)}{(\lambda^3+9)^{3/2}}\right) \qquad (8.35a)$$

$$\theta_2 = \mathrm{Cos}^{-1}\left(\frac{\lambda^3}{(\lambda^2+3)^{3/2}}\right) . \qquad (8.35b)$$

These solutions, together with their degeneracies are summarized in table 8.4 and plotted in figure 8.6.

Eigenvalue	Degeneracy	S.C. Limit
$\Omega_a^{(0)}$	1	-3
$\Omega_b^{(0)}$	-6	$-\frac{3}{2}$
$\Omega_c^{(0)}$	2	0
$\Omega_b^{(2)}$	6	0
$\Omega_c^{(2)}$	2	0
$\Omega_c^{(1)}$	2	0
$\Omega_a^{(2)}$	1	$\frac{3}{2}$
$\Omega_b^{(1)}$	6	$\frac{3}{2}$
$\Omega_a^{(1)}$	1	$\frac{3}{2}$

Table 8.4: The zero-order single plaquette energies for Z(3) on a triangular lattice.

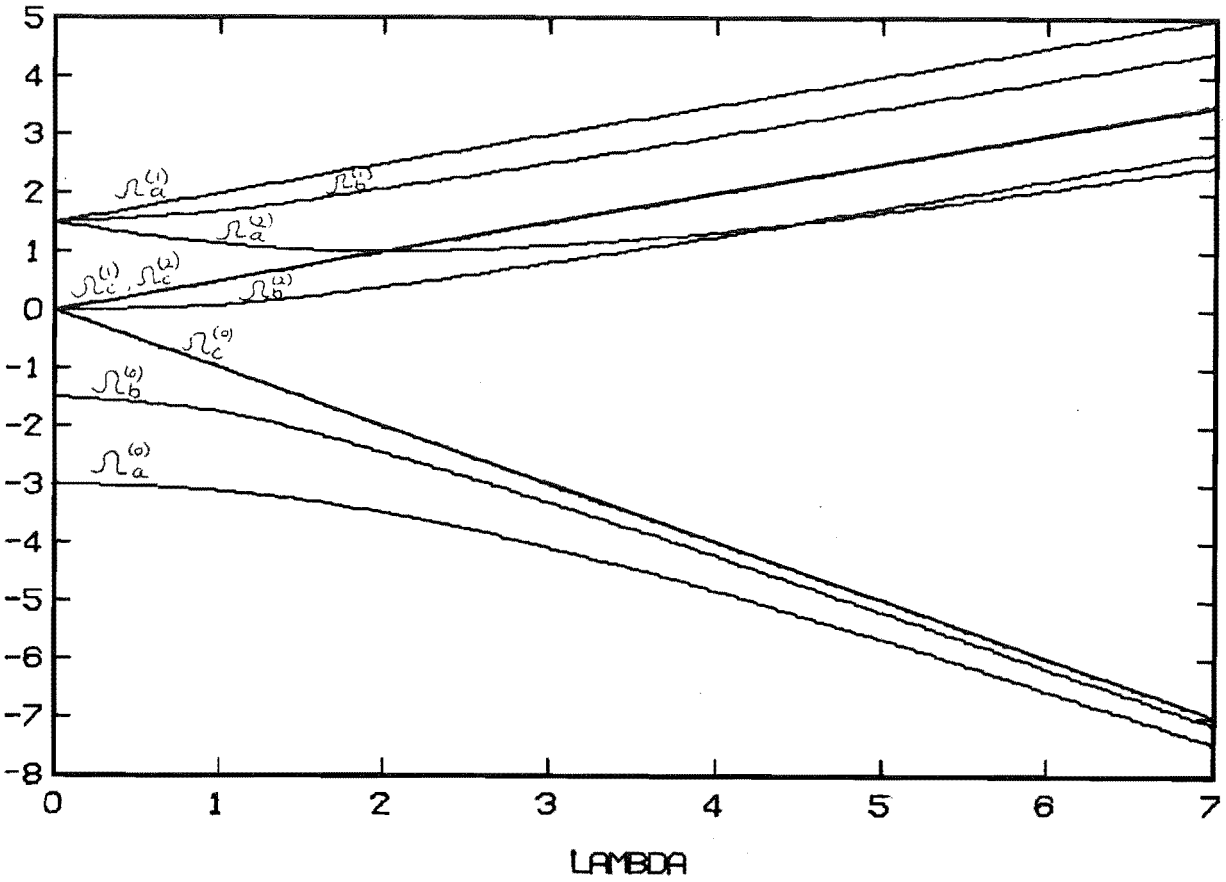

Figure 6: The zero-order single plaquette energies for Z(3) on a triangular lattice.

The components of the eigenvectors are then given by equation (8.30). The treatment of the perturbation term follows that of chapter 2: the action of the perturbation on a single odd plaquette is expressed in terms of the three neighbouring even plaquettes. Note that the quasi-degeneracy of single, odd and even plaquette excitations occurs here also. The counterpart of the $|+\rangle$ state, representing an excited odd plaquette, is the $|\text{人}\rangle$ state of figure 8.7a and the $|\Delta\rangle$ state, shown in figure 8.7b, corresponds to the $|\square\rangle$.

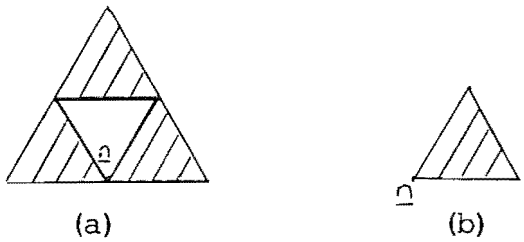

Figure 8.7: Low energy excited states of (a) odd and (b) even plaquette.

At the strong-coupling limit $\lambda=0$ these states consist of three excited even plaquettes of energy $-\frac{3}{2}$ and a single excited plaquette of energy $+\frac{3}{2}$ respectively while in the vacuum state all even plaquettes have energy -3. Thus

$$\epsilon^{(0)}_{|\Lambda>} = \epsilon^{(0)}_{|\Delta>} = -3N + 9/2 \quad . \tag{8.36}$$

8.3 APPLICATION TO CONTINUOUS GAUGE GROUPS

The definitions of the sets of even and odd plaquettes are independent of the properties of the gauge group. A zero-order Hamiltonian including all even plaquette terms may be constructed from the full Hamiltonian of equation (2.15). The exact solution of the zero-order problem in this case requires the diagonalization of an infinite-dimensional matrix but approximate solutions may be obtained.

The intermediate-coupling method is currently being applied to the (2+1)-dimensional U(1) lattice gauge theory (Bimler, 1982). Initial results are encouraging,

and suggest that the problem of quasi-degenerate excited states is not as severe in this case. The degrees of freedom of the U(1) theory are, in the fundamental representation, matrices of the form

$$U(\underline{\ell}) = e^{i\theta(\underline{\ell})} \quad . \tag{8.37}$$

The link terms of the Hamiltonian consist of the operator $\frac{\partial^2}{\partial\theta^2}$, the Casimir operator for U(1).

Gauge-invariant variational solutions of the zero-order single-plaquette problem of the form

$$\begin{aligned} |\psi(\underline{p})> &= \sum_{m=-\infty}^{\infty} |\psi(\underline{p}),m> \\ &= \sum_{m=-\infty}^{\infty} \Gamma_m \, e^{im[\theta(\underline{p},\mu) + (\underline{p}+\mu,\nu)+\theta(\underline{p}+\mu+\nu,-\mu)+\theta(\underline{p}+\nu,-\nu)]} \end{aligned} \tag{8.38}$$

are sought. These include contributions from higher representations of U(1). The matrix corresponding to equation (8.30), although infinite, is tridiagonal and contains a row for each value of m. If the summation over m is restricted to $|m| \leqslant m_{max}$ then the eigenvalues and eigenvectors are readily obtained. In practice the value $m_{max} = 4$ is found to be sufficient.

The action of the perturbation term on the zero-order states is calculated as in the Z(2) case. The four coefficients $\rho\pm,\theta\pm$ are replaced by a series depending on m. This series may also be truncated without significant loss of accuracy.

8.4 EXTENSION TO (3+1)-DIMENSIONS

The zero-order Hamiltonian of the intermediate-coupling expansion is defined on a set of even plaquettes, which include all the links of the lattice. In the case of (2+1)-dimensions it has been shown that the resulting zero-order problem may be decomposed into a sum of independent terms, each of which involves the degrees of freedom of a single even plaquette.

Consider now the case of (3+1)-dimensions. It might be expected that in this case the Hamiltonian could be decomposed into independent terms involving elementary cubes on the lattice.

A possible arrangement of odd and even cubes is the "body-centred" configuration, shown in figure 8.8, in which the even cubes have common vertices but no common edges or faces. Note that, although only one quarter of the cubes of the lattice are even, half of the plaquettes are covered by their faces. Each cube may be labelled by its "lower left front" vertex. A zero-order Hamiltonian, which includes all of the link terms and half of the plaquette terms, may thus be defined in terms of the independent even cubes of figure 8.8. There are 12 links on an even cube. In the Z(2) model each of these may be in one of the 2 states and the zero-order problem may be reduced to one of $2^{12}=4096$ dimensions. Further decomposition is not possible since each link of an even cube is shared by two of its faces.

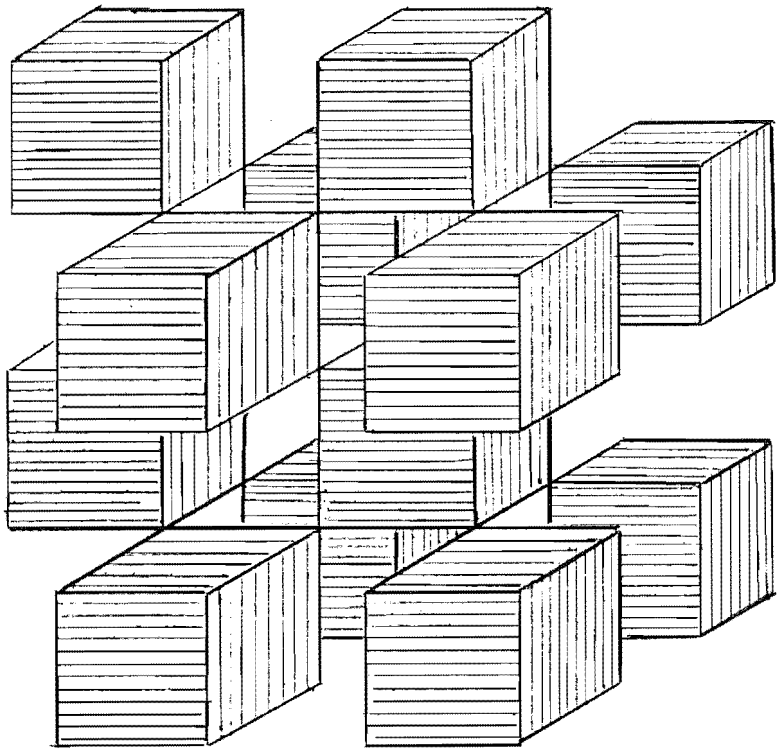

Figure 8.8: The "body-centred" arrangement of cubes.

Another possible choice of odd and even plaquettes has been suggested by Bimler (1982). Six links, and hence six plaquettes, are associated with each site of the lattice. A "cluster" of three even plaquettes, including one plaquette parallel to each plane of the lattice, may be defined at any site $\underline{n}$ as shown in figure 8.9a. An "inverted cluster" may be defined at $\underline{n}$ by inverting the cluster through the site $\underline{n}$, as shown in figure 8.9b.

The sites specifying the even cubes of figure 8.8 may be regarded as forming two interlocking simple cubic

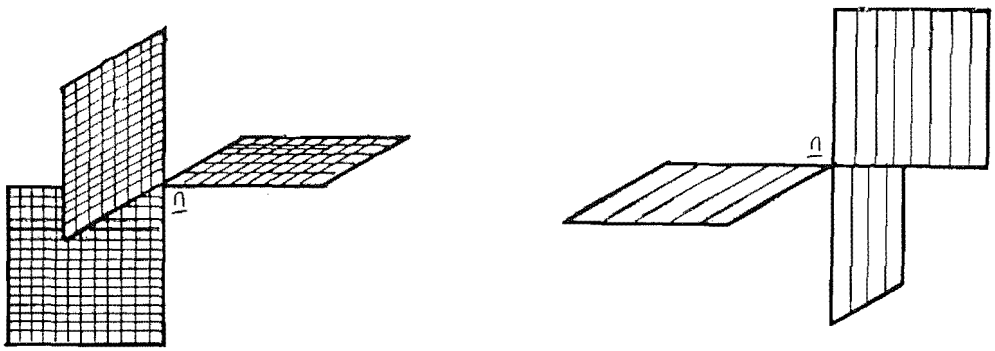

Figure 8.9: (a) Cluster and (b) inverted cluster at site n.

structures, and accordingly may be labelled by "A" or "B". An arrangement consisting of a cluster at each "A" site and an inverted cluster at each "B" site is shown in figure 8.10.

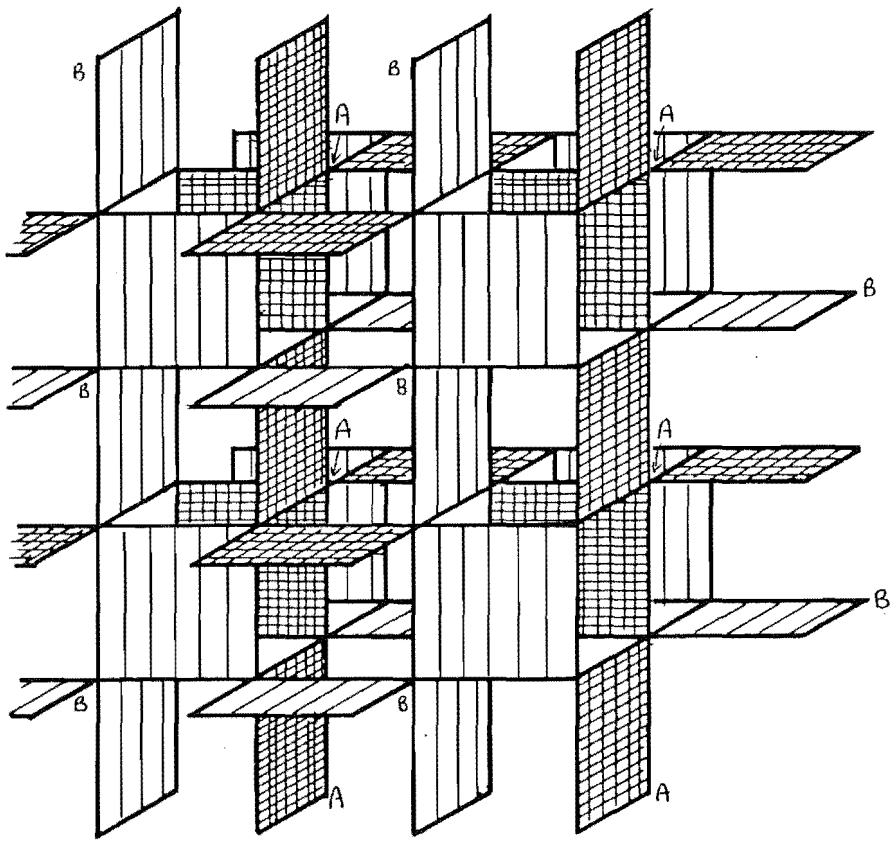

Figure 8.10: Covering all the links with clusters and inverted clusters.

All of the links of the lattice are included, but only one quarter of the plaquettes are even. No two A or B clusters have any common plaquettes or links. The corresponding zero-order Hamiltonian for the intermediate-coupling expansion may thus be reduced to independent even plaquette terms, involving only a $2^4=16$ dimensional problem for the Z(2) model.

The importance of the choice of the most suitable sets of even and odd plaquettes to the ultimate tractability of the zero-order problem is clearly illustrated by the above examples. Although the (3+1)-dimensional problem is more complicated than the (2+1)-dimensional case the techniques involved are the same: the zero-order problem includes all but the odd plaquette terms of the Hamiltonian, which are treated as a perturbation. The diagrammatic techniques introduced in chapter 3 would be applicable, requiring only modification to describe the relative orientations of plaquettes in 3 spatial dimensions.

CHAPTER 9

CONCLUSION

An intermediate-coupling expansion for the Hamiltonian formulation of lattice gauge theory has been developed. The expansion is applicable to both finite and continuous gauge groups, and provides an alternative to the conventional strong-coupling expansion. Two complementary subsets of the set of plaquettes of the lattice are identified. These are the sets of even and odd plaquettes. In two space dimensions the even and odd plaquettes are like the black and white squares of a chess board. Each subset includes all the links.

Each term of the Hamiltonian is associated with an even or odd plaquette. The link terms are associated with even plaquettes. The zero-order Hamiltonian of the intermediate-coupling expansion includes all the terms associated with even plaquettes. The resulting zero-order problem may be separated, and its solutions may be expressed in terms of independent single even plaquette states. The odd plaquettes terms are then treated as a perturbation.

The solutions of the zero-order problem are identical to those of the conventional strong-coupling expansion in the strong-coupling limit $\lambda \to 0$. For all intermediate values of λ the zero-order solutions include some of the quantum fluctuation effects and thus describe

the physical state of the system more completely than their strong-coupling counterparts do.

The single-plaquette zero-order problem, for all values of λ, has been solved exactly for the Z(2) and Z(3) models. The corresponding zero-order problems for models with continuous gauge groups, which are of interest in QCD, are more complicated, but variational solutions may be obtained. Exact single-plaquette solutions for U(1), SU(2) and SU(3) have been given by Robson and Webber (1980). These authors consider only gauge-invariant single-plaquette states. However the solutions of the single-plaquette zero-order problem for the intermediate-coupling expansion include some states in the gauge-invariant sector and others in the non-gauge-invariant sector. In the case of the (2+1)-dimensional Z(2) model only two of the sixteen single-plaquette states were gauge-invariant. In the intermediate-coupling expansion the gauge-invariant states of the infinite lattice are expressed as products of single-(even) plaquette states. The single-plaquette states from both sectors are required to describe all the gauge-invariant lattice states. The perturbative treatment of the odd plaquette terms of the Hamiltonian introduces gauge-invariant intermediate states which are constructed from non-gauge invariant single-plaquette states, even if the initial state consists of only gauge invariant single-plaquette states. This was also demonstrated in the case of the Z(2) model. Bimler (1982) has obtained single-plaquette solutions, belonging

to both the gauge-invariant and non-gauge-invariant sectors for the U(1) model. The gauge-invariant solutions agree with those of Robson and Webber. However in order to extend these single-plaquette solutions to the infinite lattice, via the intermediate-coupling expansion, the single-plaquette states for both sectors are required.

The intermediate-coupling expansion for the energy of a state is a more complicated function of λ than the corresponding strong-coupling expansion, which is a polynomial in λ. Discontinuities in quantities such as the mass gap and string tension, or their derivatives, will not be reproduced by truncated polynomials. The terms of the intermediate-coupling expansion also depend on λ through the coefficients in their numerators ($\rho_{\pm}$ and $\theta_{\pm}$ for the Z(2) model) and through their energy denominators. A truncated series of terms with more complicated dependence on λ should thus better represent the behaviour of quantities such as the mass gap. It is interesting to note that the coefficients $\rho_{\pm}$, plotted in figure 2.7, have broad minima in the region of λ_c. It would be necessary to perform detailed studies of a number of models with other gauge groups in order to demonstrate any significant correlation between these quantities.

A diagrammatic method for the enumeration of the terms of the expansion has been presented and, in the case of the Z(2) model, used for their evaluation. The diagrams are suitable for construction and evaluation by computer and this process has been described.

The example of (2+1)-dimensional Z(2) lattice gauge theory has been examined in detail. The vacuum energy density has been calculated and, assuming the accepted value of λ_c, the specific heat critical index α is estimated. In order to calculate the mass gap a form of degenerate perturbation theory due to Bloch was used to overcome the difficulty of quasi-degenerate excited states. These corresponded to excitations of single, odd or even plaquettes. The critical index ν for the mass gap was estimated. The values obtained for α and ν were consistent with the prediction of the correlation length scaling hypothesis.

The intermediate-coupling expansion was also used to calculate the tension of (horizontal) on-axis strings. The results indicated the occurrence of a roughening transition. Off-axis, or diagonal strings were also considered. The high degeneracy of such states in the strong-coupling expansion is partially lifted. The separation of the resulting states, which depends on λ, remains small and the states are quasi-degenerate. The calculation of the off-axis string tension in the Hamiltonian formulation of lattice gauge theory presents an extremely complicated problem and the intermediate-coupling expansion may prove to be useful in this case.

Strong-coupling expansions for the vacuum energy, the mass gap and the axial string tension have been obtained. In the case of the vacuum energy, an extensive quantity involving global excitations, the strong-coupling and

intermediate-coupling expansions are in close agreement. However in the calculation of the mass gap and string tension, both intensive quantities involving local excitations, the performance of the intermediate-coupling expansion was superior.

A class of models with inhomogeneous coupling strengths has been examined. These arise naturally within the framework of the intermediate-coupling expansion and include the homogeneous-coupling models as a special case. The inhomogeneous-coupling models provide a valuable tool for the study of the corresponding homogeneous-coupling models.

The application of the intermediate-coupling model to other gauge groups and (3+1)-dimensions has been indicated. The expansion is also suitable for application to a number of other areas of lattice gauge theory. Real space renormalization group techniques (e.g. Horn and Yankielowicz, 1979) provide an example. This would involve the relation of the single plaquette states to those describing larger lattice surfaces. Another potentially fruitful application would be the study of finite lattice systems. The fact that its perturbation Hamiltonian consists of only half of the plaquette terms of the full Hamiltonian may make the intermediate-coupling expansion useful in that case. Finite lattices with periodic boundary conditions proved valuable for analyzing the degeneracy of the mass gap, as was reported in chapter 5.

The intermediate-coupling expansion provides an

alternative to the conventional strong-coupling expansion for calculations in lattice gauge theory. It has been successfully tested in the case of the (2+1)-dimensional Z(2) model, where its performance is superior to conventional strong-coupling expansions of the same order. The expansion is of general applicability and it is hoped that it will prove to be useful in the solution of current problems.

A paper based upon the material presented in this thesis is to be submitted to Nuclear Physics B[FS] (Moreau et al. 1982).

APPENDIX A

FOURTH-ORDER CLASSIFICATION POLYGONS

The classification polygons for the fourth order diagrams of the cross and Y16 states are given. All of the diagrams required for the quasi-degenerate calculations of chapter five may be obtained from these, and the second-order diagrams given in chapter four, by the computer program described in chapter seven. The dashed lines representing the three projector/denominator operators have been omitted.

Counting Factor: 1
No. of Diagrams: 1

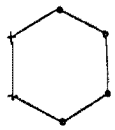

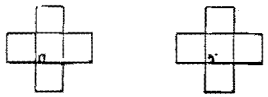

Counting Factor: N-9
No. of Diagrams: 15

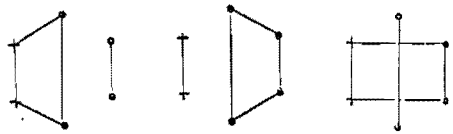

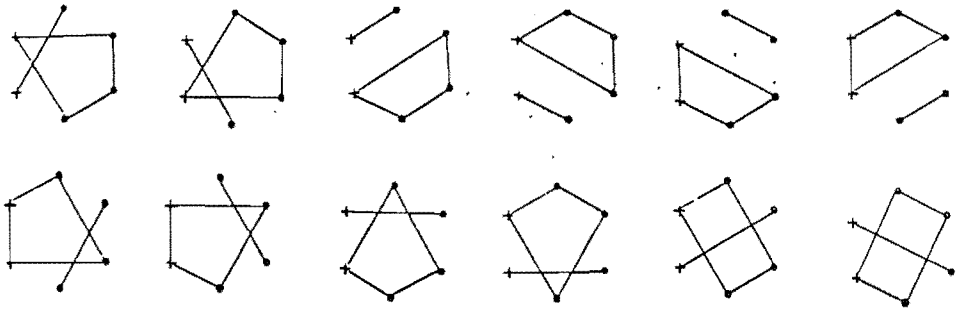

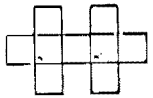

Counting Factor: 4
No. of Diagrams: 15

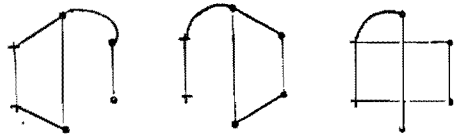

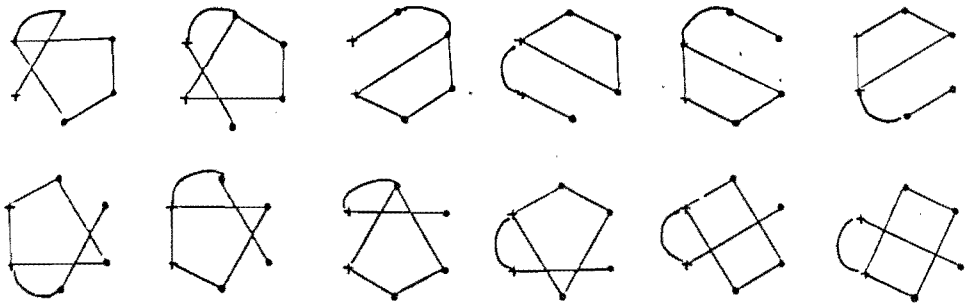

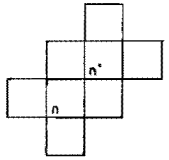

Counting Factor: 4
No. of Diagrams: 15

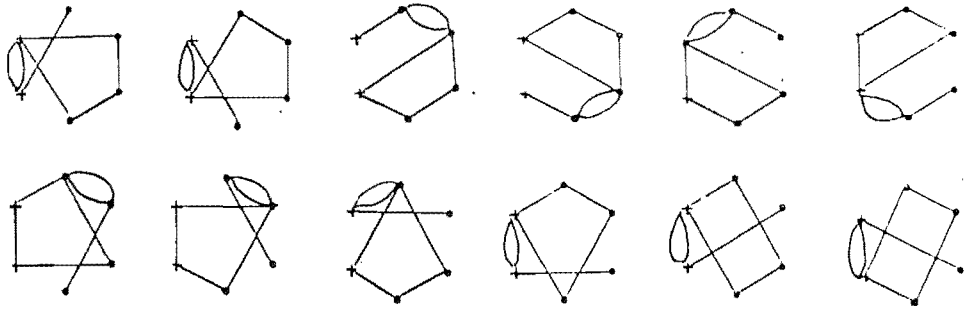

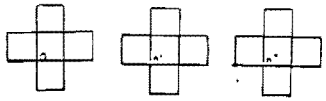

Counting Factor: $N^2-27N+194$
No. of Diagrams: 15

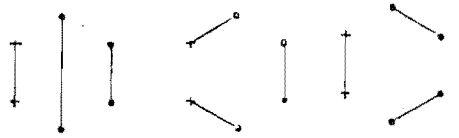

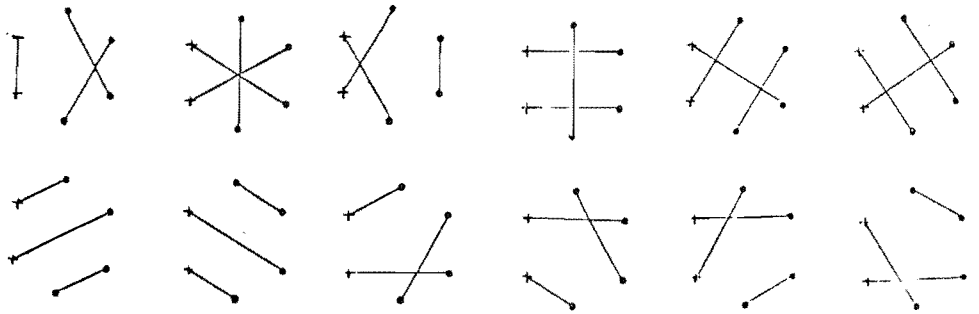

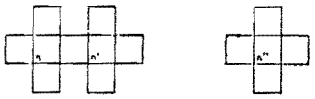

Counting Factor: 4(N-14)
No. of Diagrams: 45

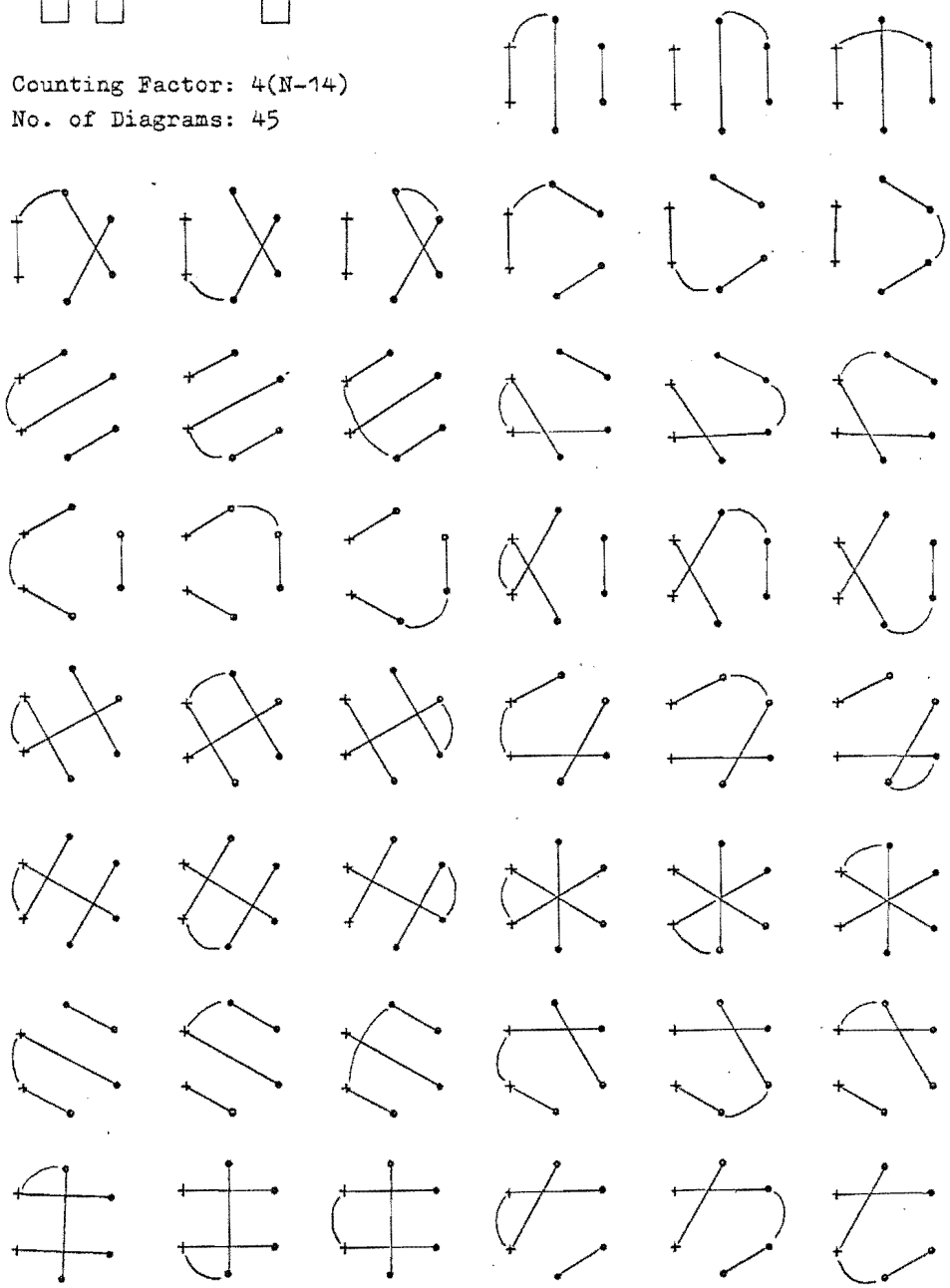

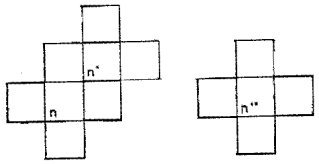

Counting Factor: 4(N-12)
No. of Diagrams: 45

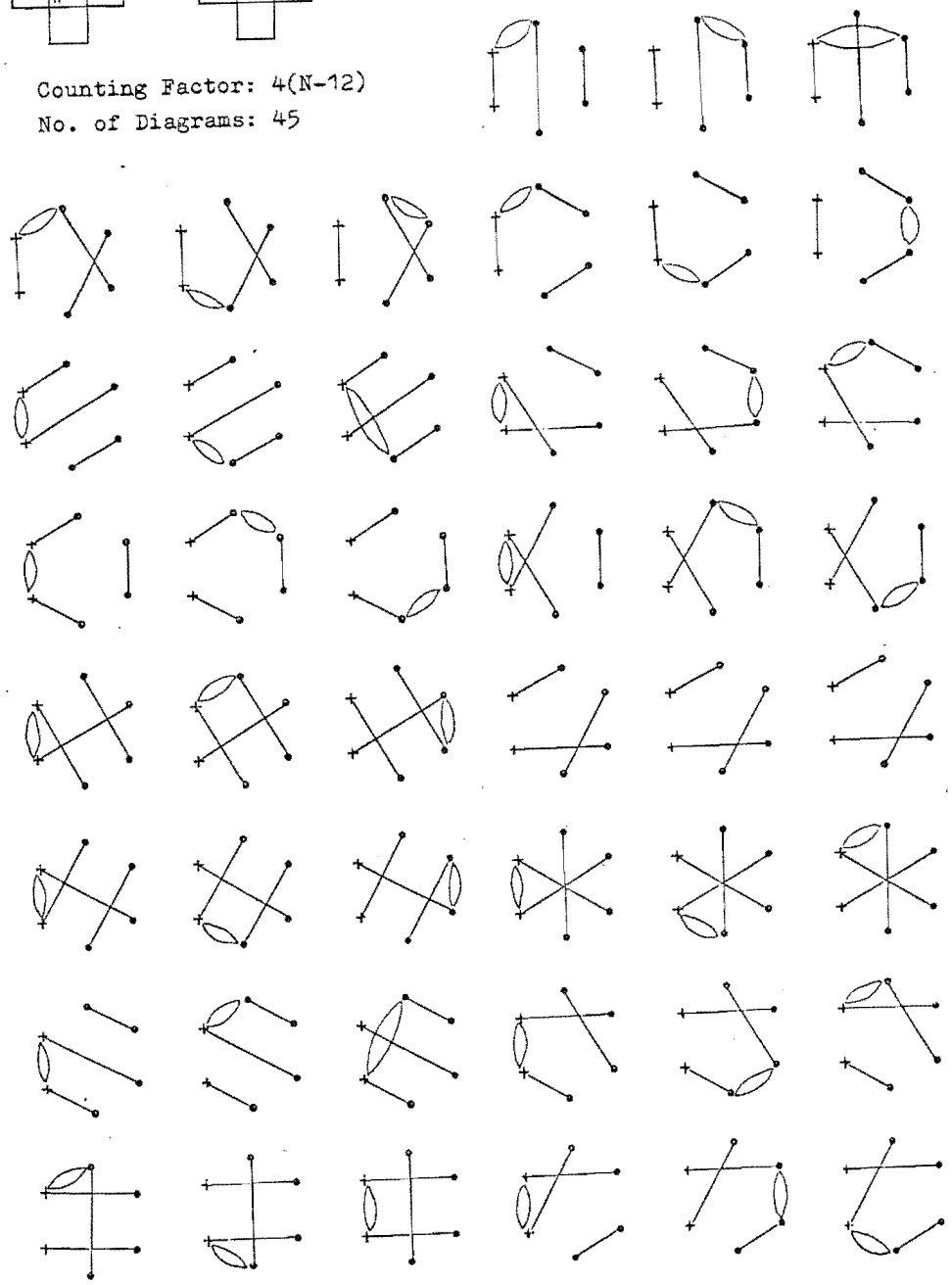

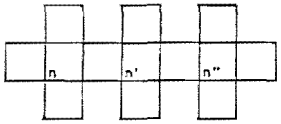

Counting Factor: 12
No. of Diagrams: 45

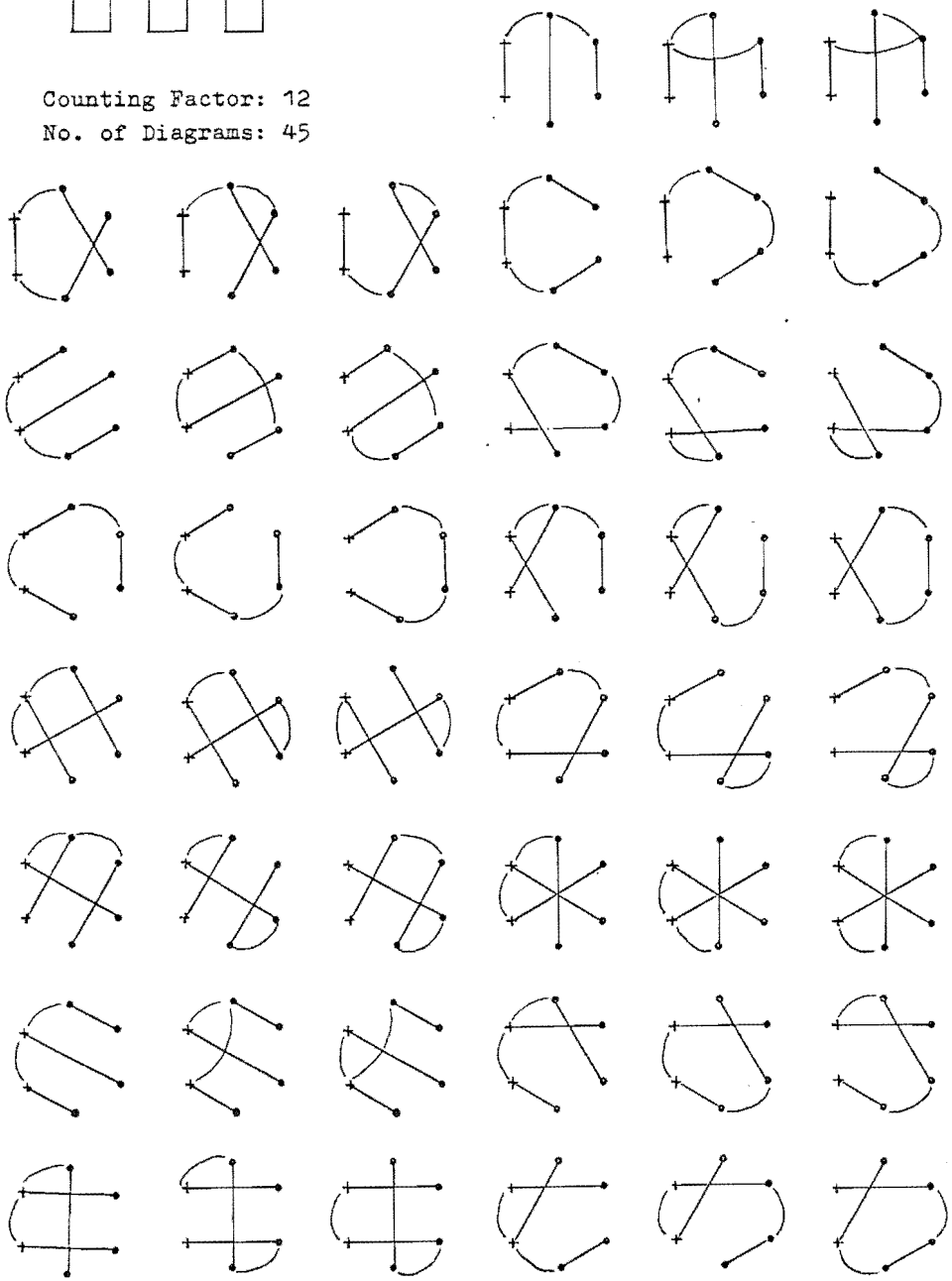

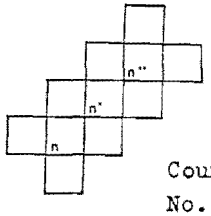

Counting Factor: 4
No. of Diagrams: 45

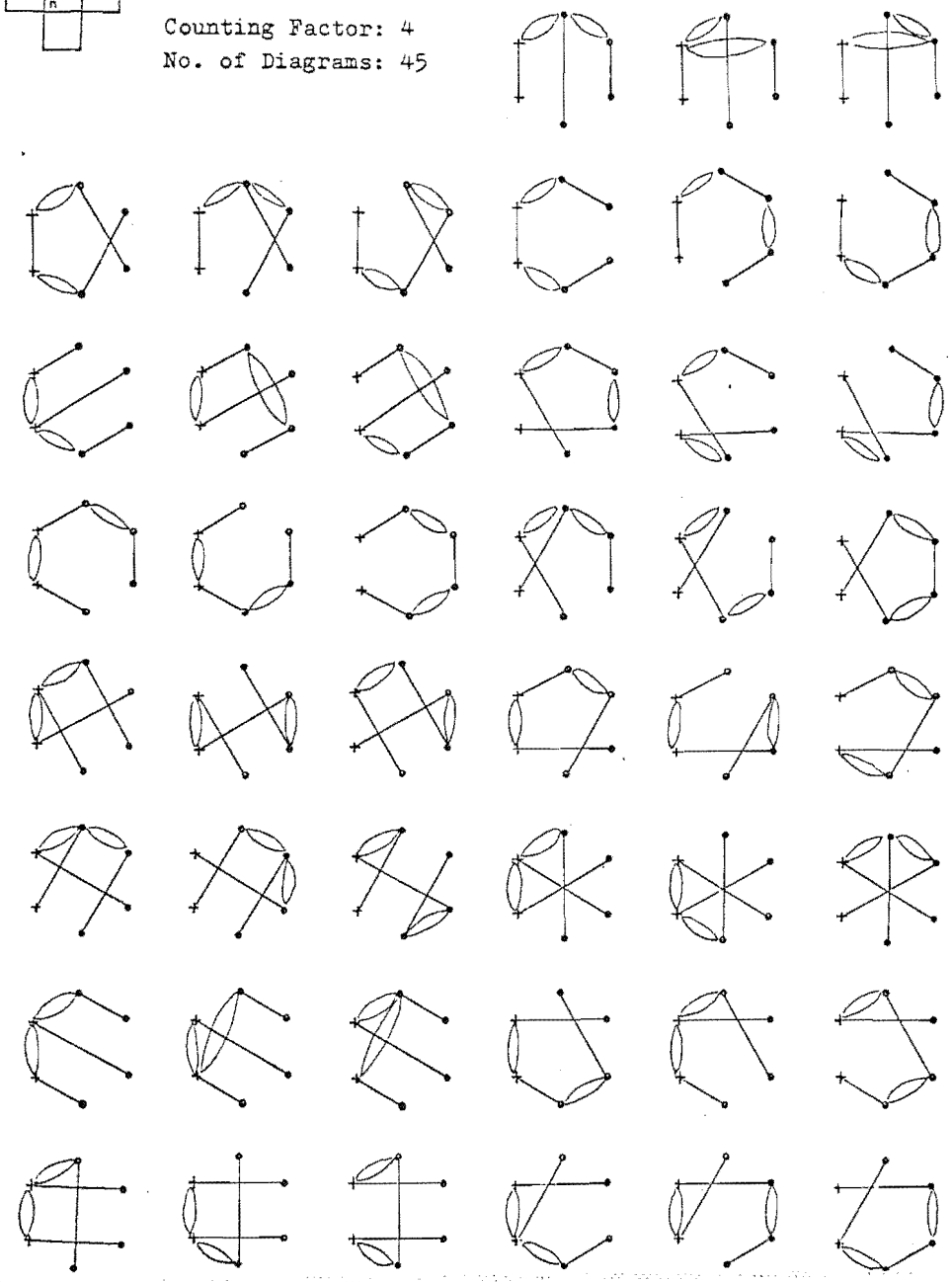

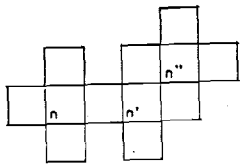

Counting Factor: 8
No. of Diagrams: 90

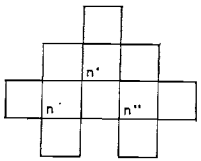

Counting Factor: 8
No. of Diagrams: 45

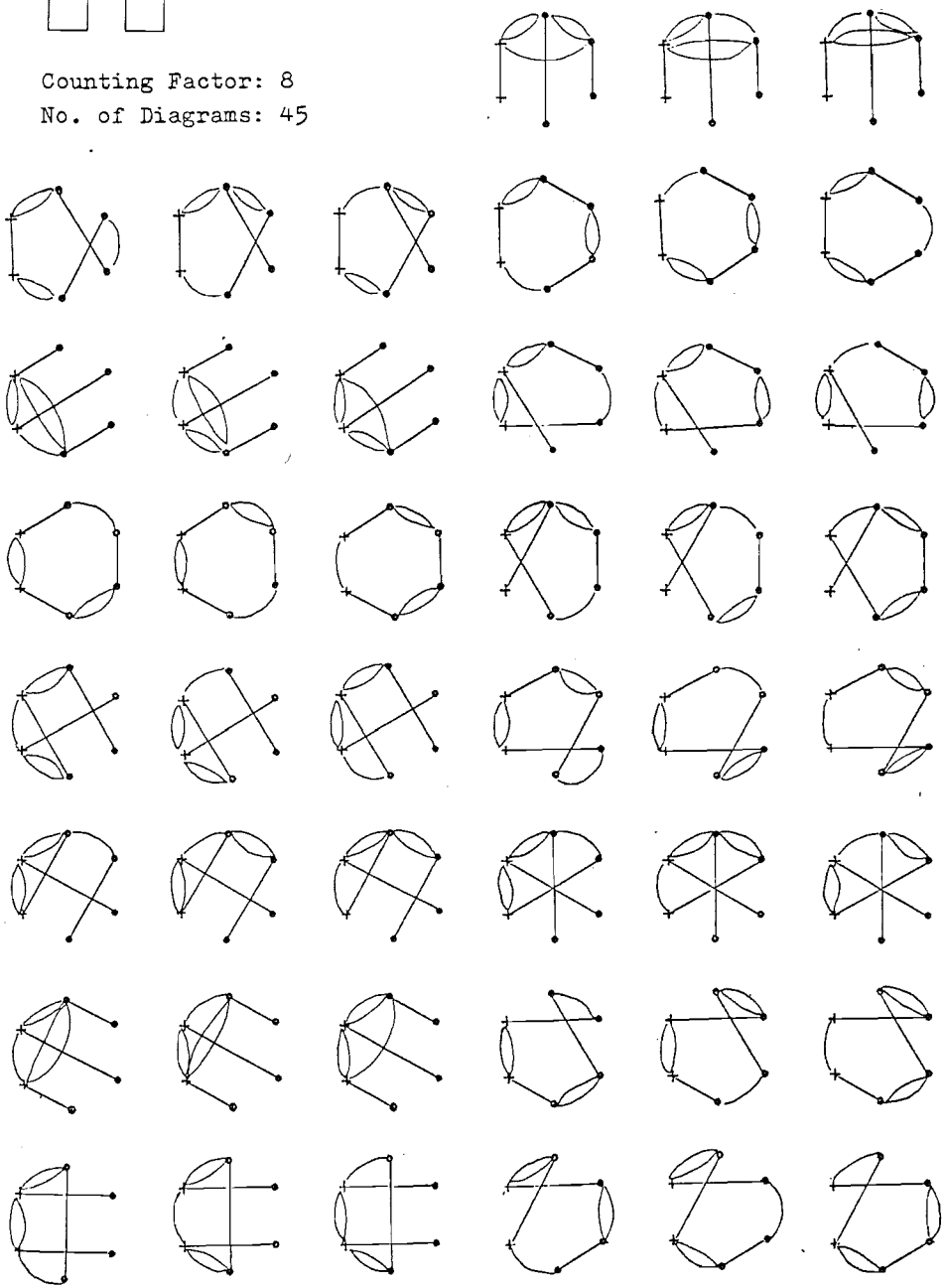

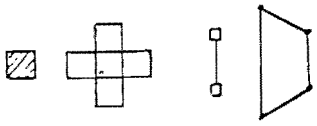

Counting Factor:N-4

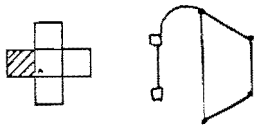

Counting Factor: 4

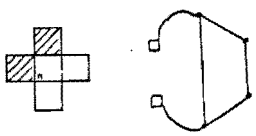

Counting Factor:12

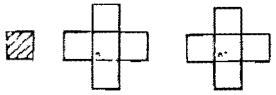

Counting Factor:N^2-17N+72
No. of Diagrams:3

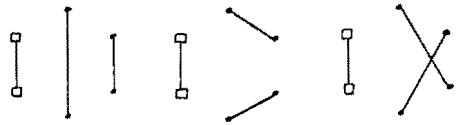

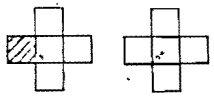

Counting Factor:4(N-9)
No. of Diagrams:6

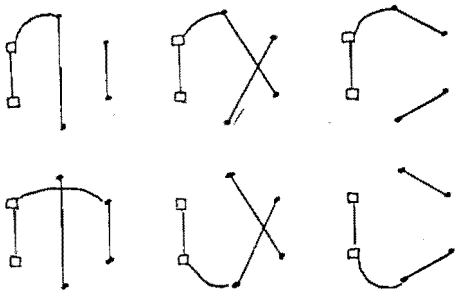

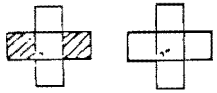

Counting Factor:12(N-9)
No. of Diagrams:6

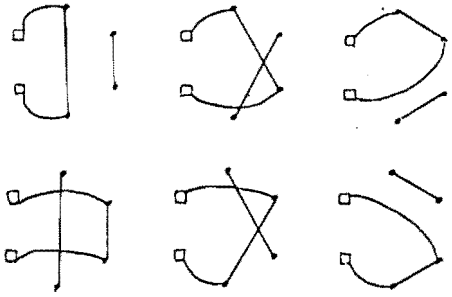

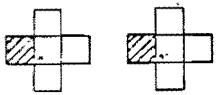

Counting Factor:16(N-9)
No. of Diagrams:6

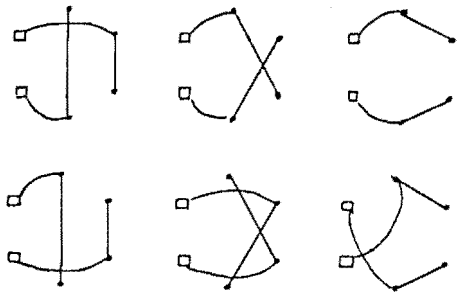

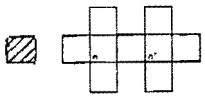

Counting Factor:4(N-7)
No. of Diagrams:3

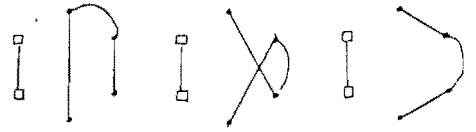

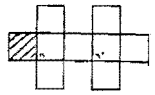

Counting Factor:12
No. of Diagrams:6

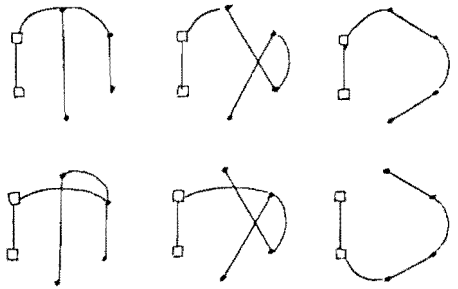

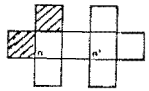

Counting Factor:24
No. of Diagrams:6

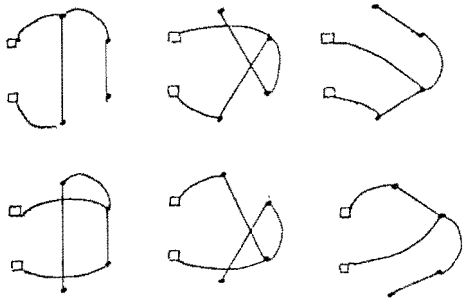

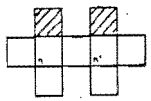

Counting Factor:36
No. of Diagrams:6

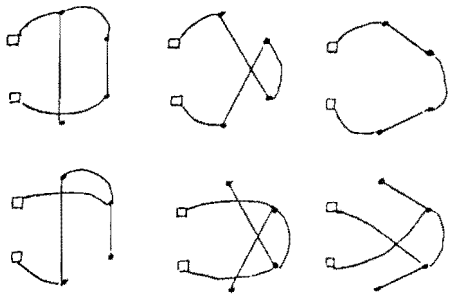

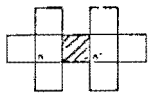

Counting Factor:4
No. of Diagrams:3

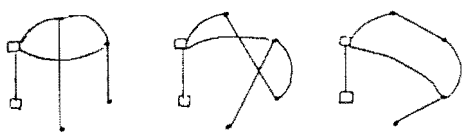

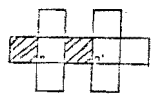

Counting Factor:12
No. of Diagrams:12

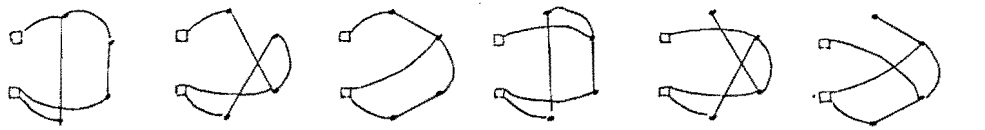

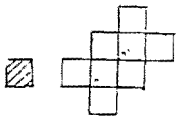

Counting Factor:4(N-6)
No. of Diagrams:3

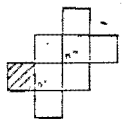

Counting Factor:8
No. of Diagrams:6

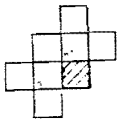

Counting Factor:8
No. of Diagrams:3

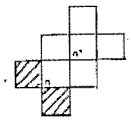

Counting Factor:8
No. of Diagrams:6

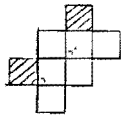

Counting Factor:16
No. of Diagrams:6

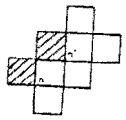

Counting Factor:32
No. of Diagrams:12

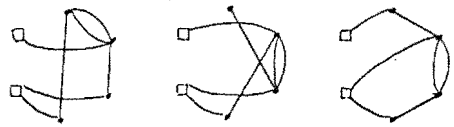

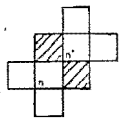

Counting Factor:8
No. of Diagrams:3

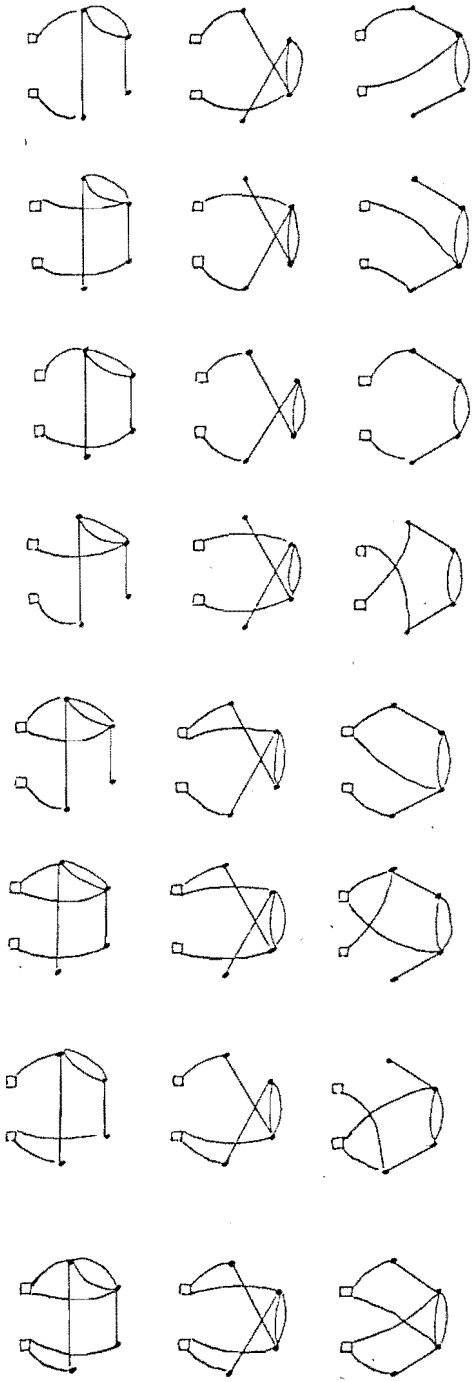

APPENDIX B

NON-ZERO CONTRIBUTIONS TO $\Sigma_{\eta\kappa}$

The sums of the elements of any row of the sub-matrices $M_{\eta\kappa}$ occurring in equation (5.37) are denoted by the $\Sigma_{\eta\kappa}$ which are defined by equation (5.39). Many of the possible terms vanish because of the restrictions of equations (5.28b) and (5.40): those which do not are listed below up to fifth order. The quantity S^k is defined in equation (5.17).

(I) Σ_{++}

zero order: $\langle + | H_o | + \rangle$

1st order: $\langle + | \tilde{H}' | + \rangle$

2nd order: $\langle + | H' \, S^1 \, H' | + \rangle$

3rd order: $\langle + | H' \, S^1 \, \tilde{H}' \, S^1 \, H' | + \rangle - \langle + | H' \, S^2 \, H' \, S^0 \, \tilde{H}' | + \rangle$

4th order: $\langle + | H' \, S^{k_1} H' \, S^{k_2} \, H' \, S^{k_3} | + \rangle (k_1 k_2 k_3) \in \{(111),(120),(210),(201),(300)\}$

$+ \langle + | H' \, S^3 \, H' \, S^0 \, \tilde{H}' \, S^0 \, \tilde{H}' | + \rangle + \langle + | H' \, S^1 \, \tilde{H}' \, S^2 \, H' S^0 \, \tilde{H}' | + \rangle$

$+ \langle + | H' \, S^2 \, \tilde{H}' \, S^1 \, H' \, S^0 \, \tilde{H}' | + \rangle + \langle + | H' \, S^1 \, \tilde{H}' \, S^1 \, \tilde{H}' \, S^1 \, H' | + \rangle$

5th order: $\langle + | H' \, S^{k_1} \, H' \, S^{k_2} \, H' S^{k_3} \, H' S^{k_4} \, \tilde{H}' | + \rangle$

$(k_1 k_2 k_3 k_4) \in \{(1120),(1210),(2110),(2200),(2020),(1300),(3100),$

$(3010),(4000)\}$

$$+\langle+|H'\ S^{k_1}\ H'\ S^{k_2}\ H'\ S^{k_3}\ \tilde{H}'\ S^{k_4}\ H'|+\rangle$$

$$(k_1k_2k_3k_4)\in\{(1111),(2011)\}$$

$$+\langle+|H'\ S^{k_1}\ H'\ S^{k_2}\ \tilde{H}'\ S^{k_3}\ H'\ S^{k_4}\ H'|+\rangle$$

$$(k_1k_2k_3k_4)\in\{(1111),(1120),(1210),(2110),(3001),(4000)\}$$

$$+\langle+|H'\ S^{4}\ H'S^{0}\ \tilde{H}'S^{0}\ \tilde{H}'\ S^{0}\ \tilde{H}'|+\rangle$$

$$+\langle+|H'\ S^{k_1}\ \tilde{H}'\ S^{k_2}\ H'\ S^{k_3}\ H'\ S^{k_4}\ H'|+\rangle$$

$$(k_1k_2k_3k_4)\in\{(1111),(1120),(1210),(2110),(1201),(2101),$$

$$(2200),(1300),(3100)\}$$

$$+\langle+|H'\ S^{k_1}\ \tilde{H}'S^{k_2}\ H'S^{k_3}\ \tilde{H}'\ S^{k_4}\ \tilde{H}'|+\rangle$$

$$(k_1k_2k_3k_4)\in\{(2200),(1300),(3100)\}$$

$$+\langle+|H'\ S^{k_1}\ \tilde{H}'\ S^{k_2}\ \tilde{H}'S^{k_3}\ H'S^{k_4}\ \tilde{H}'|+\rangle$$

$$(k_1k_2k_3k_4)\in\{(1120),(1210),(2110)\}$$

$$+\langle+|H'\ S^{1}\ \tilde{H}'\ S^{1}\ \tilde{H}'\ S^{1}\ \tilde{H}'\ S^{1}\ H'|+\rangle\ .$$

(II) $\Sigma_{\square\square}$

zero order: $\langle\square|H_o|\square\rangle$

1st order: 0

2nd order: $\langle\square|H'\ S^{1}\ H'|\square\rangle$

3rd order: $\langle\square|H'\ S^{k_1}\ \tilde{H}'\ S^{k_2}\ H'|\square\rangle \quad (k_1k_2) \in \{(11),(20)\}$

4th order: $\langle\square|H'\ S^{k_1}\ H'\ S^{k_2}\ H'\ S^{k_3}\ H'|\square\rangle$

$$(k_1k_2k_3)\in\{(111),(120),(201),(210),(300)\}$$

$$+\langle\square|H'\ S^{1}\ \tilde{H}'\ S^{1}\ \tilde{H}'\ S^{1}\ H'|\square\rangle$$

5th order: $\langle\square|H' S^{k_1} H' S^{k_2} H' S^{k_3} \tilde{H}' S^{k_4} H'|\square\rangle$

$(k_1k_2k_3k_4)\varepsilon\{(1111),(2011),(2200),(1300),(3100),(4000)\}$

$+\langle\square|H' S^{k_1} H' S^{k_2} \tilde{H}' S^{k_3} H' S^{k_4} H'|\square\rangle$

$(k_1k_2k_3k_4)\varepsilon\{(1111),(1120),(1210),(2110)\}$

$+\langle\square|H' S^{k_1} \tilde{H}' S^{k_2} H' S^{k_3} H' S^{k_4} H'|\square\rangle$

$(k_1k_2k_3k_4)\varepsilon\{(1111),(1120),(1210),(2110),(1201),(2200),(2101),$

$(1300),(3100)\}$

$+\langle\square|H' S^{1} \tilde{H}' S^{1} \tilde{H}' S^{1} \tilde{H}' S^{1} \tilde{H}'|\square\rangle$

(III) $\Sigma_{+\square}$

zero order: 0

1st order: $\langle+|H'|\square\rangle$

2nd order: 0

3rd order: $\langle+|H' S^{k_1} H' S^{k_2} H'|\square\rangle$ $(k_1k_2) \varepsilon \{(11),(20)\}$

4th order: $\langle+|H' S^{k_1} H' S^{k_2} \tilde{H}' S^{k_3} H'|\square\rangle$

$(k_1k_2k_3)\varepsilon\{(111),(300)\}$

$\langle+|H' S^{k_1} \tilde{H}' S^{k_2} H' S^{k_3} H'|\square\rangle$

$(k_1k_2k_3)\varepsilon\{(111),(120),(210)\}$

5th order: $\langle+|H' S^{k_1} H' S^{k_2} H' S^{k_3} H' S^{k_4} H'|\ \rangle$

$(k_1k_2k_3k_4)\varepsilon\{(1111),(1120),(1210),(1201),(2110),(2101),$

$(2011),(2200),(2020),(1300),(3100),(3010),(3001),(4000)\}$

$+\langle+|H' S^{k_1} H' S^{k_2} \tilde{H}' S^{k_3} \tilde{H}' S^{k_4} H'|\square\rangle$

$(k_1k_2k_3k_4)\varepsilon\{(1111),(4000)\}$

$$+\langle +|H'\,S^{k_1}\,\widetilde{H}'\,S^{k_2}\,H'\,S^{k_3}\,\widetilde{H}'\,S^{k_4}\,H'|\square\rangle$$

$$(k_1k_2k_3k_4)\varepsilon\{(1111),(2200),(1300),(3100)\}$$

$$+\langle +|H'\,S^{k_1}\,\tilde{H}'\,S^{k_2}\,\tilde{H}'\,S^{k_3}\,H'\,S^{k_4}\,H'|\square\rangle$$

$$(k_1k_2k_3k_4)\varepsilon\{(1111),(1120),(1210),(2110)\}$$

(IV) $\Sigma_{\square+}$

zero order: 0

1st order: $\langle\square|H'|+\rangle$

2nd order: 0

3rd order: $\langle\square|H'\,S^{k_1}\,H'\,S^{k_2}\,H'|+\rangle \quad (k_1k_2)\varepsilon\{(11),(20)\}$

4th order: $\langle\square|H'\,S^{k_1}\,H'\,S^{k_2}\,H'\,S^{k_3}\tilde{H}'|+\rangle$

$$(k_1k_2k_3)\varepsilon\,\{(120),(210),(300)\}$$

$$+\langle\square|H'\,S^{1}\,H'\,S^{1}\,\tilde{H}'\,S^{1}\,H'|+\rangle$$

$$+\langle\square|H'\,S^{k_1}\,\tilde{H}'\,S^{k_2}\,H'\,S^{k_3}\,H'|+\rangle$$

$$(k_1k_2k_3)\varepsilon\{(111),(120),(210)\}$$

5th order: $\langle\square|H'\,S^{k_1}\,H'\,S^{k_2}\,H'\,S^{k_3}\,H'\,S^{k_4}\,H'|+\rangle$

$$(k_1k_2k_3k_4)\varepsilon\{(1111),(1200),(1210),(1201),(2110),(2101),$$

$$(2011),(2200),(2020),(1300),(3100),(3010),(3001),(4000)\}$$

$$+\langle\square|H'\,S^{k_1}\,H'\,S^{k_2}\,H'\,S^{k_3}\,\widetilde{H}'\,S^{k_4}\,\widetilde{H}'|+\rangle$$

$$(k_1k_2k_3k_4)\varepsilon\{(2200),(1300),(3100),(4000)\}$$

$$+\langle\square|H'\,S^{k_1}\,H'\,S^{k_2}\,\tilde{H}'\,S^{k_3}\,H'\,S^{k_4}\,\tilde{H}'|+\rangle$$

$$(k_1k_2k_3k_4)\varepsilon\{(1120),(1210),(2110)\}$$

$$+\langle\square|H'\,S^{1}\,H'\,S^{1}\,\tilde{H}'\,S^{1}\,\tilde{H}'\,S^{1}\,H'|+\rangle$$

$$+\langle\Box|H'\ S^{k_1}\ \widetilde{H}'\ S^{k_2}\ H'\ S^{k_3}\ H'\ S^{k_4}\ \widetilde{H}'|+\rangle$$

$$(k_1k_2k_3k_4)\varepsilon\{(1120),(1210),(2110),(2200),(1300),(3100)\}$$

$$+\langle\Box|H'\ S^{1}\ \tilde{H}'\ S^{1}\ H'\ S^{1}\ \tilde{H}'\ S^{1}\ H'|+\rangle$$

$$+\langle\Box|H'\ S^{k_1}\ \widetilde{H}'\ S^{k_2}\ \widetilde{H}'\ S^{k_3}\ H'\ S^{k_4}\ H'|+\rangle$$

$$(k_1k_2k_3k_4)\varepsilon\{(1111),(1120),(1210),(2110)\}.$$

REFERENCES

Baker G.A. 1975 "Essentials of Padé approximants". (Academic Press).

Balian R., Drouffe J.M. and Itzykson C. 1975 Phys.Rev. D11 2104.

Bander M. 1981 Phys. Reports 75C 205.

Banks J.L. and Sinclair D.K. 1981 Phys. Rev. D23 2962.

Banks T., Raby S., Susskind L., Kogut J.B., Jones D.R.T., Sharbach P.N. and Sinclair D.K. 1977 Phys. Rev. D15 1111.

Banks, T. and Zaks A. 1982 Nucl. Phys. B200 [FS4] 391.

Baym G. 1969 "Lectures on Quantum Mechanics" (W.A. Benjamin, New York).

Bessis J. and Villani M. 1975 J. Math. Phys. 16 462.

Bimler D. 1982 University of Canterbury Ph.D. Thesis (in progress).

Bloch C. 1958 Nucl. Phys. 6 329.

Callan C., Dashen R. and Gross F. 1978 Phys. Rev. D17 2717.

Carroll A. and Kogut J.B. 1979 Phys. Rev. D19 2429.

Close F.E. 1976 in "Fundamentals of Quark Models", eds. Barbour I.M. and Davies A.T. (SUSSP, Edinburgh).

Domb C.S. and Green M. 1972 "Phase Transitions and Physical Phenomena". (Academic, London).

Drouffe J.M. and Itzykson C. 1978 Phys. Reports 38C 133.

Elitzur S., Pearson R.B., Shigemitsu J. 1979 Phys. Rev. D19 3698.

Ellis J. 1977 in "Weak and Electromagnetic Interactions at High Energy", eds Balian R. and Llewellyn-Smith C.S. (North-Holland, Amsterdam).

Fisher M.E. 1967 Rep. Prog. Phys. 30 615.

Fradkin E. and Suskind L. 1978 Phys. Rev. D17 2637.

Fritzsch H., Gell-Mann M. and Leutwyler H. 1974 Phys. Lett. 47B 365.

Fritzsch H. 1981 Physica Scripta 24 847.

Gilmer G.H. and Bennema P. 1972 J. Appl. Phys. 43 1347.

Hamer C.J. 1982 Lectures delivered at University of Melbourne Summer School in Physics.

Hamer C.J. and Barber M.N. 1981 J. Phys. A.14 241.

Hamer C.J. and Kogut J.B. 1979 Phys. Rev. B20 3859.

Hasenfratz P. 1981 Physics Scripta 23 978.

1982 CERN Preprint TH-3349.

Horn D., Weinstein M., and Yankielowicz S. 1979 Phys. Rev. D19 3715.

Horn D., and Yankielowicz S. 1979 Nucl. Phys. B161 533.

Ichinose I. 1982 Tokyo Inst. Tech. Preprint TIT/HEP - 72.

Imachi M. and Yoneyama H. 1980 Prog. Theor. Phys. 63 1738.

Irving A.C. and Thomas A. 1982 Nucl. Phys. B200 [FS4] 424.

Itzykson C. 1976 Phys. Reports 23C 237.

1981 Physics Scripta 24 854.

Itzykson C., Peskin M.E. and Zuber J.B. 1980 Phys. Lett. 95B 249.

Jones D.R.T., Kenway R.D., Kogut J.B. and Sinclair D.K. 1979 Nucl. Phys. B158 102.

Kadanoff L.P. 1976 in "Phase Transitions and Critical Phenomena" Vol. 5a eds. Domb C. and Green M.S. (Academic, London).
1977 Rev. Mod. Phys. 49 267.

Kalotas T. 1980 Private communication.

Kato T. 1949 Prog. Theor. Phys. 4 514.

Kogut J.B. 1976 in "Many Degrees of Freedon in Particle Theory" ed. Satz H. (Plenum, New York).
1979a University of Illinois at Urbana-Champaign. Preprint ILL-(TH)-79-21.
1979b Rev. Mod. Phys. 51 659.

Kogut J.B., Pearson R.B., Shigemitsu J. and Sinclair D.K. 1980 Phys. Rev. D22 2447.

Kogut J.B. and Sinclair D.K. 1981a Phys. Rev. D23, 2962.
1981b Phys. Rev. D24 1610.

Kogut J.B., Sinclair D.K., Pearson R.B., Richardson J.L. and Shigemitsu J. 1981 Phys. Rev. D23 2945.

Kogut J.B., Sinclair D.K. and Suskind L. 1976 Nucl. Phys. B114 199.

Kogut J.B. and Suskind L. 1975 Phys. Rev. D11 395.

Mack G. 1980 in "Recent Developments in Gauge Theories" ed. 't Hooft G. et al. (Plenum, New York).

Manton N.S. 1980 Phys. Lett. 96B 328.

Marciano W. and Pagels H. 1978 Phys. Reports 36C 137.

Marinelli M. and Morpurgo G. 1982 Phys. Reports 85C 161.

Martin P.P. 1982 University of Southampton preprint SHEP 81/82 1 (to appear in Nucl. Phys. B).

Messiah A. 1962 "Quantum Mechanics" Vol. 2 (North-Holland, Amsterdam).

Moreau W.R., Churcher N.I. and Kalotas T. 1982 In preparation. (To be submitted to Nucl. Phys. B.).

Munster G. 1981 Nucl. Phys. B190 [FSI] 439.

Omero C. 1982 Phys. Lett. 110B 265.

Politzer H.D. 1974 Phys. Reports 14C 129.

Robson D. and Webber D.M. 1980 Z. Physik C7 53.

Roomany H.H. and Wyld H.W. 1980 Phys. Rev. D21 3341.

Schiff L.I. 1953 Phys. Rev. 92 766.

Schultz T.D., Mattis D.C. and Lieb E.H. 1964 Rev. Mod. Phys. 36 856.

Stanley H.E. 1971 "Introduction to Phase Transitions and Critical Phenomena" (Oxford University Press).

Susskind L. 1976 in "Fundamentals of Quark Models". Edinburgh. Barbour I.M. and Davies A.T. (SUSSP Ed.)

1977 in "Weak and Electromagnetic Interactions at High Energy" eds Balian R. and Llewellyn-Smith C.S. (North-Holland, Amsterdam).

Tassie L.J. 1979 "An Introduction to the String Theory of Hadrons". Lectures at A.N.U. (reported by Burdon C.J.).

't Hooft G. 1974 Nucl. Phys. B72 461.

1978 Nucl. Phys. B138 1.

Turban L. 1981 J. Physique 42 793.

Weeks J.D. and Gilmer G.H. 1979 in Advances in Chemical Physics 40, eds Prigogine I. and Rice S.A. (Wiley, New York).

Weeks J.D., Gilmer G.H. and Leary H.J. 1973 Phys. Rev. Lett. 31 549.

Weinstein M. 1977 in "Particles and Fields" eds
Boal D.H. and Kamal A.N. (Plenum, New York).

Wegner F. 1971 J. Math. Phys. 12 2259.

Wilson K.G. 1974 Phys. Rev. D10 2445.

Wilson K.G. and Kogut J.B. 1974 Phys. Reports 12C 75.

Yang C.N. and Mills R.L. 1954 Phys. Rev. 96 1605.